HUMAN PYROGLUTAMYL PEPTIDASES AND THEIR INVOLVEMENT IN ALZHEIMERS DISEASE

Submitted by

Justyna Słonka

to the University of Exeter as a thesis for the degree of Doctor of Philosophy in Biosciences
(November 2011)

I certify that all material in this thesis which is not my own work has been identified and that no material has previously been submitted and approved for the award of a degree by this or any other University.

Signature: ……

Acknowledgments

I would like to thank my supervisor, Prof. Jenny Littlechild for her support, guidance and encouragement during this project.

I also wish to thank Dr Janet Holley and Prof. Nick Gutowski from Peninsula Medical School for their time, advice and teaching me techniques of AD immunostaining.

I should also acknowledge the OPPF-UK team, particularly Dr Ray Owens and Dr Jo Nettleship for their help during a study on PcpII expression.

I would like to thank everyone in Biocat for their help and special thanks should be given to Halina, Rita, Nick and Vahid for being the best friends in the world.

Lastly, I would like to thank my beloved husband for his constant support and love.

Abstract

The N-terminally pyroglutamyl-modified β-amyloid (Aβ) peptides are found in abundance in the pathological Alzheimer disease (AD) brain deposits. Such modification not only increases the hydrophobic properties of a given molecule, but also plays a protecting role against proteolytic degradation. This project involved the study of the human type I and type II pyroglutamyl peptidases and their involvement in Aβ processing in AD.

Human PcpI has been successfully overexpressed in *Escherichia coli* strain and purified to homogeneity. The protein displayed significant instability *in vitro*. To overcome this problem a number of methods were employed such as screening for an optimal protein expression system and buffer composition, site-directed mutagenesis and chemical modification of selected surface residues. This resulted in the selection of the HEPPS buffer system as providing the most stabilising conditions for human PcpI. Improvement in the protein stability enabled initial crystallisation experiments and the identification of favourable conditions for crystal production. Further optimization of this process is needed in order to obtain good quality crystals which are required for structural study.

The study on human PcpII involved an extensive screening for optimal expression conditions in bacterial, baculovirus/insect and mammalian systems. The truncated PcpII isoform PcpII/S62-H1024, which lacks the N-terminal transmembrane domain, was successfully expressed and secreted from the HEK 293T cell line using three different pOPIN-based constructs. Moreover, homology modelling of human PcpII catalytic domain was performed, which helped to gain an insight into the three-dimensional structure of the protein and its mode of substrate binding.

Lastly, immunohistochemical staining of the human AD brain tissue sections was performed to compare the level and distribution of PcpI and PcpII enzymes between diseased and control cases. The results confirmed that the neurodegenerative conditions lead to the increased synthesis of both enzymes in the cortical AD tissues. Additionally PcpI was shown to be able to participate in the degradation of pGlu-modified Aβ peptides.

List of content

List of figures

List of tables

Abbreviations

Å	Angstrom, 10^{-10}m
aa	amino acids
Aβ	Amyloid β
AβpGlu3	Amyloid β peptide with pyroglutamyl residue at the position 3
AβpGlu11	Amyloid β peptide with pyroglutamyl residue at the position 11
ABC	Dimethylamine-Borane Complex
ACh	Acetylcholine
AD	Alzheimer's Disease
AMC	7-amino-4-methylcoumarin
APP	Amyloid Precursor Protein
APS	Ammonium Persulfate
BACE	β-site APP cleaving enzyme
β-Me	β-mercaptoethanol
Bis-Tris propane	1,3-Bis[tris(hydroxymethyl)methylamino]propane
bp	base pair
BSA	Bovine Serum Albumin
cDNA	complementary DNA
CHES	2-(N-Cyclohexylamino)ethane sulfonic acid
CMV	Cytomegalovirus, constitutive promoter
CNS	Central Nervous System
CtA	mutated isoform of pyroglutamyl peptidase type I with the all non-catalytic cysteines replaced by alanines
Da	Dalton
DAB	3,3′-diaminobenzidine tetrahydrochloride
ddH_2O	double distilled water
DMEM	Dulbecco's Modified Eagle's Medium
DMF	Dimethylformamide
DMSO	Dimethyl Sulfoxide
DS	Down's Syndrome
DTNB	5,5′-dithiobis-(2-nitrobenzoic acid)
DTT	Dithiothreitol
EDTA	Ethylenediaminetetraacetic acid, chelating agent

ER	endoplasmic reticulum
ExPASy	Expert Protein Analysis System, biochemical server
FAD	Familial Alzheimer's Disease
FCS	Foetal Calf Serum
HEK	Human Embryonic Kidney cells
HEPES	N-(2-Hydroxyethyl)piperazine-N′-(2-ethanesulfonic acid)
HEPPS	N-(2-Hydroxyethyl)piperazine-N′-(3-propanesulfonic acid)
HRP	Horseradish Peroxidase
i.d.	internal diameter
Ig	Immunoglobulin
IHC	Immunohistochemistry
IPTG	Isopropyl β-D-1-thiogalactopyranoside
LB	Luria-Bertani broth
L-pGlu-AMC	L-pyroglutamyl-7-amido-4-methylcoumarin
MCI	Mild Cognitive Impairment
MRI	Magnetic Resonance Imaging
MES	2-(N-morpholino)ethanesulfonic acid
MOPS	3-(N-morpholino)propanesulfonic acid
NDSB	Non-Detergent Sulfobetaine
NFTs	Neurofibrillary Tangles
NT	Neuropil Threads
OD	Optical Density
OPPF	Oxford Protein Production Facility
PAGE	Polyacrylamide Gel Electrophoresis
Pcp	Pyrrolidone carboxyl peptidase, Pyroglutamyl peptidase, EC 3.4.19.3
PcpIIFL	full-length pyroglutamyl peptidase type II
PCR	Polymerase Chain Reaction
PDB	Protein Data Bank
pGlu	pyroglutamyl
PHFs	paired helical filaments
PIPES	piperazine-1,4-bis(2-ethanesulfonic acid)
PMSF	Phenylmethylsulfonyl fluoride
PSEN	Presenilin

psi	pound-force per square inch, unit of pressure, = 14.696 atmosphere (atm)
QC	glutaminyl cyclase
RFU	Relative Fluorescence Unit
RMSD	root mean square deviation
rpm	revolutions per minute, unit of angular velocity
SAD	Sporadic Alzheimer's Disease
SDS	Sodium Dodecyl Sulfate
***Sf*9**	*Spodoptera frugiperda* insect cell line
SFs	straight filaments
SOC	Super Optimal broth with Catabolite repression, SOB medium with added glucose, bacterial growth medium
SV40	Simian vacuolating virus 40, constitutive promoter
T7	T7 bacteriophage
TAE	Tris-acetate-EDTA
TEMED	N,N,N′,N′-Tetramethylethylenediamine
TNG	Trans-Golgi Network
TRH	Thyrotropin-releasing hormone
TRHDE	Thyrotropin-releasing hormone-degrading ectoenzyme, Pyroglutamyl peptidase type II (PcpII), EC 3.4.19.6
Tris-HCl	Trishydroxymethylaminomethane hydrochloride
U	Enzyme unit, U is the amount of the enzyme that catalyzes the conversion of 1 micromole of substrate per minute
VE-*Sf*9	vankyrin-enhanced *Spodoptera frugiperda* insect cell line
v/v	volume/volume
w/v	weight/volume
X-gal	5-bromo-4-chloro-3-indolyl-β-D-galacto-pyranoside

Chapter 1 – Introduction

1.1. Introduction to Alzheimer's disease

1.1.1. Disease of 20th century

Twentieth century brought rapid advances in medicine and an increase in the awareness of the beneficial aspects of a hygienic lifestyle, nutrition and prophylaxis. Modern diagnostic services and intensive research focused on drug discovery and medical treatments, which significantly contributed to human health and longevity. In the industrialized countries the average life expectancy has nearly doubled over the 20th century from 40-45 years to 78 years for both males and females (Kinsella, 1992). Extended life time is undoubtedly a priceless value, but unfortunately it has also some negative consequences, such as prevalence of different diseases and ailments characteristic for the older age. One of leading death causes is Alzheimer's disease (AD) considered to be the most common type of dementia and often referred as a disease of the 20th century (Blennow *et al.*, 2006). Current estimations show that there are around 37 million people living with dementia worldwide with the number increasing to 66 million by 2030 (ADI, 2010). AD accounts for 50-80% of dementia cases in developed countries and it is reported to be a source of massive economic burden (Alzheimer's Association, 2010). The disease is often associated with ageing and it affects around 12% of people at the age of 65 and then the number increases exponentially with women being more likely to develop AD and other dementia types (Kawas and Corrada, 2006). Alzheimer's with lesser frequency is also diagnosed in younger individuals before the age of 65 and therefore it is differentiated as a late-onset (sporadic) and early-onset (familial, FAD) type (Seltzer and Sherwin, 1983). Both forms may have distinct aetiology (1.1.4.1) and display varied clinical features (Seltzer and Sherwin, 1983; Koedam *et al.*, 2010). AD sufferers struggle with progressive decline in cognitive functions, memory impairment, problems with speech and understanding, changes in mood and personality as well as difficulties in basic activities of daily living which finally leads to a complete loss of functional independence. After diagnosis the clinical duration of the disease takes on average 8 to 10 years (Bird, 2008).

1.1.2. Pathology of Alzheimer's

The disease was named after psychiatrist Alois Alzheimer, who aptly associated unusual changes in the brain anatomy with aggressive dementia symptoms in one of his patients (Alzheimer, 1907). Alzheimer performed post-mortem brain tissue examination, which revealed common symptoms of the disease such as brain atrophy, thick neurofibrillary tangles, minute cortical senile plaques and disintegrated neuronal cells (Alzheimer, 1907). These structural abnormalities are widespread throughout the neocortical and sub-cortical grey matter, hippocampus and amygdala regions (Winkler *et al.*, 1998; Murdoch, 2010). Brain neuropathological lesions and processes have become indicative of AD and constitute the basis of diagnostic criteria.

1.1.2.1. Changes to AD brain

Accurate diagnosis of Alzheimer's sometimes may be problematic because some neuropathological lesions and processes are similar for a diseased and cognitively normal ageing brain (Bancher *et al.*, 1989; Munoz and Feldman, 2000; Guillozet *et al.*, 2003). One of those common features is whole-brain shrinkage (figure 1.1) which accelerates in later adulthood by an average of 0.2% to 0.7% per year in healthy elderly patients (Scahill *et al.*, 2003; Enzinger *et al.*, 2005) and from 1% to 4% per year in AD patients (Wang *et al.*, 2002a; Schott *et al.*, 2005). Higher brain atrophy rate is related to an increased risk of dementia as a result of progressive loss of neurons and supporting cells. This phenomenon is thought to be in direct relationship with neurofibrillary pathology affecting cellular functioning (1.1.2.2) or as a result of not fully understood cellular events leading to apoptotic cell death (Stadelmann *et al.*, 1999; Raina *et al.*, 2001; Zhao *et al.*, 2003). Neuronal deterioration is thought to start years before the symptoms of dementia occur and in the AD case it was observed to be the most prominent in limbic system areas such as the medial temporal lobe and neocortex (Mungas *et al.*, 2002; Karas *et al.*, 2004). These areas are particularly sensitive as the temporal lobe is a home for the hippocampus, which is the region essential for short- and long-memory function as well as spatial navigation and behaviour. The neocortex is involved in control of conscious thought, language, motor functions and sensory perception (figure 1.1).

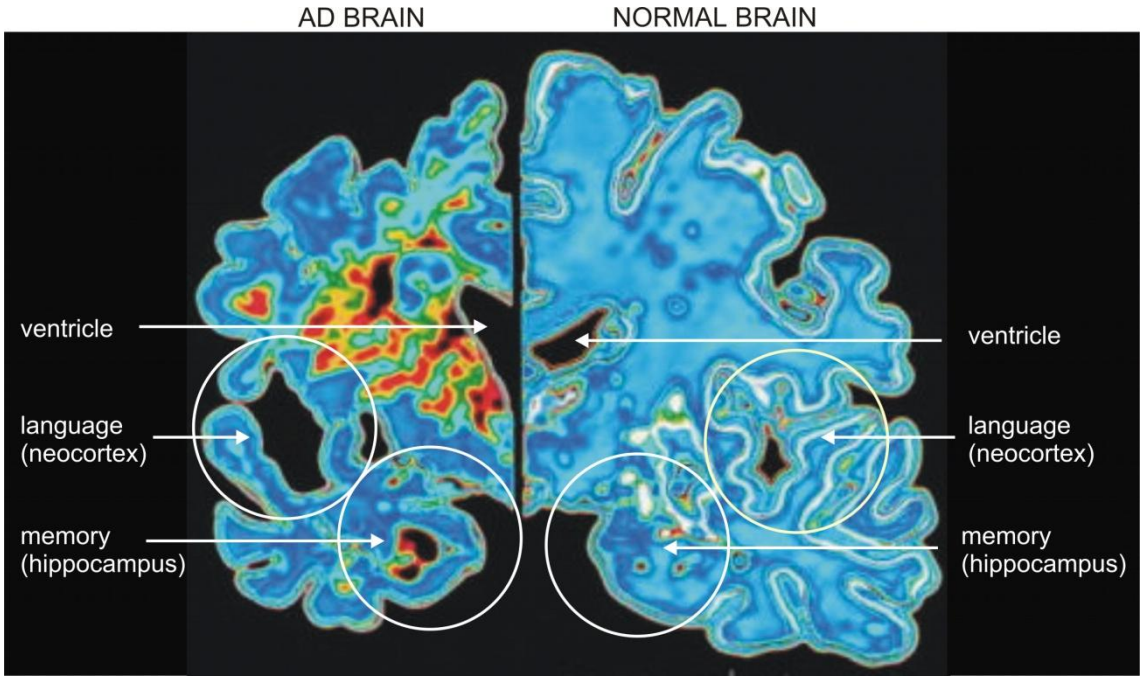

Figure 1.1. Juxtaposition of Alzheimer's disease vs. normal brain. Graphical comparison of a vertical slice of an Alzheimer's (left) and a vertical slice of a normal brain (right). The AD brain displays severe atrophy and surface folding due to neuronal degradation. Massive ventricular enlargement can be observed as large holes in the brain cross-section. Structural damage mainly affects cortical and hippocampal areas which are involved in memory, language and behavioural control. Taken from www.sciencephoto.com.

Neuronal loss in the pathological brain has rather a focal character and in advanced disease stages can reach even 90% of the normal nerve cell population (Gomez-Isla *et al.*, 1996). AD brain, due to general shrinkage, has been found to be underweight comparing to healthy one and could weigh less than 1 kg (Murdoch, 2010). An important pathological phenomenon observable in the early AD phase is an enlargement of the ventricular system containing the cerebrospinal fluid (figure 1.1) (Thompson *et al.*, 2004). This occurs not only in AD but also in other disorders like schizophrenia, mild cognitive impairment, HIV/AIDS as well as to some extent in normal ageing brain (Thompson *et al.*, 2004; Styner *et al.*, 2005; Thompson *et al.*, 2006).

Determination of AD predisposition on the basis of observable brain changes is still challenging, however recent discoveries seem to be extremely promising on this subject. It has been reported that very subtle cortical thinning may be a premorbid biomarker of AD and can be shown in asymptomatic patients even 10 years before the appearance of severe neurodegeneration using magnetic resonance imaging (MRI) (Dickerson *et al.*, 2011). MRI could be also applied to analyze hippocampal and entorhinal cortex morphology or degeneration of basal forebrain in people with mild cognitive impairment (MCI) or early dementia symptoms (Teipel *et al.*, 2005; Devanand *et al.*, 2007). Moreover, ventricles volume is evaluated using MRI and is strongly related to the changes in the surrounding structures. This correlation is considered to be indicative for AD tissue deterioration and can provide measures for the assessment of the disease progression and therapy effectiveness (Thal *et al.*, 2006; Carmichael *et al.*, 2007). Aforementioned examination methods seem particularly worth further improvement considering that the diagnosis of AD is usually given too late to counteract already advanced neuropathological changes.

1.1.2.2. Neurofibrillary tangles (NFTs)

Specific features accepted as diagnostic criteria in AD determination are known as senile plaques (1.1.2.3) and NFTs (figure 1.2). Other often observed findings are dystrophic neurites called neuropil threads (NTs) (figure 1.2). Interestingly, both neuritic plaques and NFTs can also be observed in young patients with Down syndrome (DS) and in marginal amounts in cognitively healthy individuals (Bancher *et al.*, 1989; Cork, 1990; Davis *et al.*, 1999; Guillozet *et al.*, 2003). The changes are thought to be a natural consequence of ageing and may be responsible for mild memory disturbance. Therefore, the level of morphological changes and brain distribution of these abnormalities are a sign of pathology and determine the stage of AD (Braak and Braak, 1991).

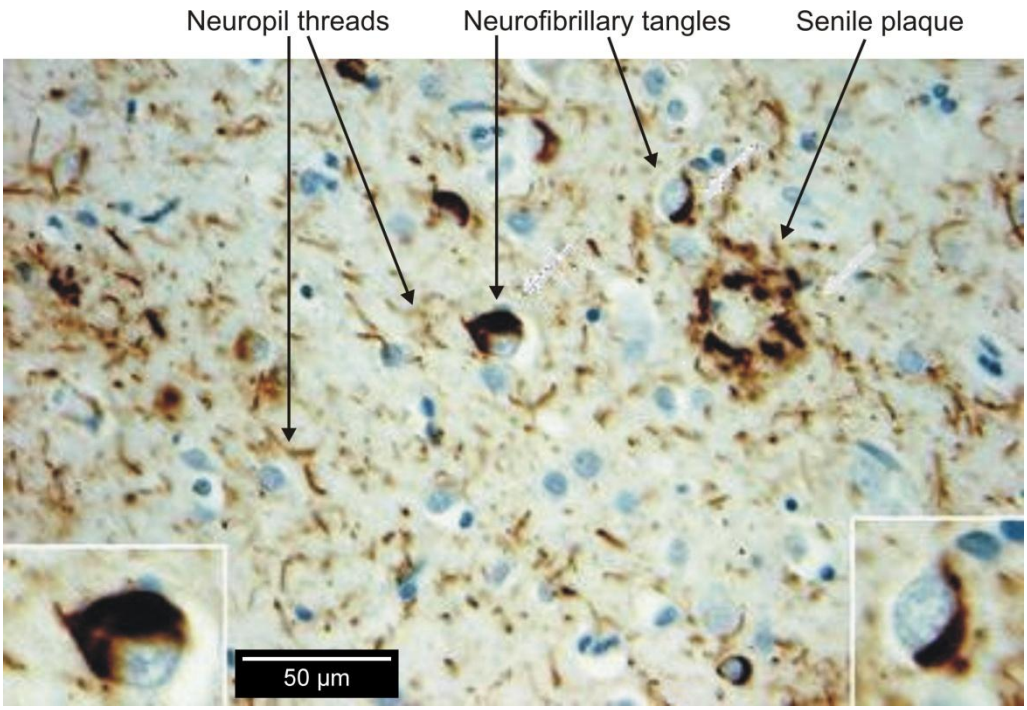

Figure 1.2. Senile plaques, neuropil threads (NTs) and neurofibrillary tangles (NFTs) in AD middle frontal gyrus. The image shows the result of the immunostaining of the tau protein revealing its accumulation within neuronal cytoplasm, dendrites (NTs) and in the senile plaque halo. Two degenerated neurons containing NFTs are enlarged in the bottom insets. Taken from (Munoz *et al.*, 2007).

Progressive deposition of the space-occupying NFTs is considered to be a major cause of nerve cells death during AD and other neurodegenerative disorders called tauopathies (Gomez-Isla *et al.*, 1997; Tolnay and Probst, 1999). The tangles are the aggregates of abnormally hyperphosphorylated tau (P-tau) protein located within the neuronal cytoplasm (Bancher *et al.*, 1989). Tau is a natural mediator that stimulates and supports the assembly of tubulin in microtubules creating the cellular cytoskeleton. If it is aberrantly phosphorylated, it dissociates from the microtubuli and sequesters normal tau along with the other microtubule associated proteins (Alonso *et al.*, 1997). This leads to disintegration of cellular scaffolding and compromises associated biological processes as well as complex axonal transport and structure. P-tau molecules self-assemble into paired helical filaments (PHFs) or straight filaments (SFs) (Iqbal *et al.*, 1986). PHFs and SFs further accumulate forming NFTs or processes, such as NTs and dystrophic neurites (Trojanowski and Lee, 1995). Tau was first isolated from AD tangles in 1974 and identified as a microtubule-associated protein in 1986 (Iqbal *et al.*,

1974; Grundke-Iqbal *et al.*, 1986). The protein exists in nine isoforms as a result of an alternative splicing (Goedert *et al.*, 1989). The level of transcripts encoding the isoforms is comparable in normal and AD brain tissues and all of the variants are incorporated into NFTs.

The reason for an abnormal tau hyperphosphorylation, as many other aspects of Alzheimer's, remains unknown. The level of phosphorylation is three- to four-fold higher in AD than in a healthy control brain (Iqbal *et al.*, 2010). So far, a few enzymes have been considered to be involved in this modification e.g. glycogen synthase kinase-3 (GSK-3) which may be up-regulated in AD by an unknown mechanism (Imahori *et al.*, 1998). Moreover, GSK-3 can be induced by amyloid β peptides (Aβ, 1.1.3) triggering a P-tau increase in embryonic rat hippocampus (Imahori and Uchida, 1997). Other disregulation observed in AD relates to the cleaved form of protein phosphatase 2B (PP2B) the level of which can be three-fold higher than in control brain tissues (Qian *et al.*, 2011). Studies show that P-tau also antagonizes neuronal apoptosis through inhibition of β-catenin phosphorylation, a protein naturally participating in programmed cell-death (Li *et al.*, 2007). This may explain why AD neurons containing NFTs rather go through a degeneration process than apoptotic death. The resulting neuronal loss preferentially affects brain areas involved in memory creation and storage such as the hippocampus or basal forebrain (Munoz and Feldman, 2000). The latter is a home for the cholinergic system producing acetylcholine (ACh), an important neurotransmitter in the central and peripheral nervous system, which is involved in numerous physiological processes. The counteraction of ACh deficiency is currently one of the main treatment strategies in mild and moderate AD cases (1.1.4.2).

Severe neuronal death, common in AD, has been initially directly related to the number of tangles (Cras *et al.*, 1995). Later findings revealed that nerve cells loss is correlated but also far exceeds the level of formed NFTs (Gomez-Isla *et al.*, 1997; Kril *et al.*, 2002). Moreover, the density threshold of tangles above which one can determine the case with significant neuronal depletion has been estimated for 5/mm^2 (Grignon *et al.*, 1998). In the late AD stage, after cell death released NFTs convert to less condensed extracellular tangles that increases their immunoreactivity for astroglial proteins (Yamaguchi *et al.*, 1987). NFT protein constituents undergo modifications and probable cross-linking which make them resistant to proteolysis and which prevents their removal from the brain environment (Cras *et al.*, 1995). Besides, deposition of P-tau in the extracellular space stimulates an increase of intraneuronal calcium level and

consequent cell death (Gomez-Ramos *et al.*, 2008). Lastly, P-tau mediates aggregation of α-synuclein in the form of Lewy bodies, found particularly in individuals with familial and sporadic types of AD as well as in DS patients with AD (Lippa *et al.*, 1999; Hamilton, 2000; Popescu *et al.*, 2004). This observation is one of many examples of aberrant protein fibrillization in synergistic mode and represents an important subject for further research (Giasson *et al.*, 2003). Pre-filament tau is considered as an interesting target in immunotherapy of Alzheimer's and tauopathies (Kayed and Jackson, 2009).

1.1.2.3. Senile plaques and congophilic angiopathy

The most prominent feature of AD is extracellular accumulation of amyloid β (Aβ) peptides in the form of insoluble fibrillary deposits. Limited Aβs deposition also occurs in healthy ageing individuals, but in AD as well as in DS the process is particularly elevated and leads to acute pathology (Cork, 1990; Davis *et al.*, 1999). Aβ is a product of complex proteolytic processing of amyloid precursor protein (APP) naturally found in many tissues (1.1.3.1) (Kang *et al.*, 1987). Abnormal build-up is considered to be a result of an imbalance in synthesis and clearance of the peptides (Mawuenyega *et al.*, 2010). Increased extracellular concentration of Aβ peptides leads to their aggregation in brain parenchyma and vessels in the form of plaques and cerebrovascular angiopathy, respectively (Duyckaerts *et al.*, 2009).

Senile plaques are lesions preferentially found in grey matter and have been first mentioned by Blocq and Marinesco and later associated with dementia by Alzheimer (Blocq and Marinesco, 1892; Alzheimer, 1907). They are primarily composed of an Aβ core, associated molecules, dystrophic neuronal processes and reactive microglia (Dickson, 1997). The crucial part of the plaque is its amyloid core of diverse Aβ peptides (1.1.3) making abnormal, insoluble fibrillary structure (Castano *et al.*, 1995). Some characteristic ultrastructural abnormalities can be identified within surrounding dilated neurites that include PHFs, enlarged lysosomes and mitochondria (Selkoe, 2001). Neuritic plaques are often enveloped by reactive astrocytes and with some of their processes reaching the amyloid core (Selkoe, 2001). Importantly, astrocytes are partially responsible for persistence of AD as they suppress efficient phagocytosis of senile plaques by microglia (DeWitt *et al.*, 1998). It was also discovered that senile

plaques contain free cholesterol and apolipoprotein E (ApoE) – a cholesterol transporter, which implies that they may be significant in AD progression (Namba *et al.*, 1991; Panchal *et al.*, 2010). Aβ peptides accumulate also in a form of diffuse plaques displaying amorphous structure and lack of the compacted amyloid centre of the classical neuritic plaques. They have no or very little associated molecules and deteriorated neurites. ApoE is co-localized with diffuse plaques and probably binds the N-terminal parts of Aβs as they display negative immunoreactivity (Uchihara *et al.*, 1996; Thal *et al.*, 2005). Moreover, the majority of ApoE-positive Aβ deposits were noticed in individuals carrying *apoϵ4* allele, which is one of the main risk factors in AD (1.1.4.1) (Thal *et al.*, 2005). Large representation of these lesions in cognitively normal subjects led to the conclusion that their toxic influence may be indirect or negligent (Delaere *et al.*, 1990; Dickson *et al.*, 1992). There are also suggestions that Aβ aggregation into diffuse/dense core plaques is a protective mechanism for removing excess soluble but highly neurotoxic Aβ monomers and oligomers (Poduslo *et al.*, 2010). It is not known for how long diffuse plaques remain in this state, but they are considered being indicative of a preclinical AD stage. Many studies have tried to answer the question if diffuse plaques evolve to a neuritic state and which is their mechanism of formation (Dickson *et al.*, 1992; Braak and Braak, 1997; D'Andrea *et al.*, 2004). Exclusive association of the agglomerates of glial cells with senile plaques led to conclusion that microglia may participate in maturation of diffuse plaques to a neuritic state (Mackenzie *et al.*, 1995). On the other hand it is hypothesised that different amyloid plaques rather originate by distinctive mechanisms explaining their varied structure and content (D'Andrea *et al.*, 2004). Popular dogma states that progressive extracellular amyloid deposition initiates plaque creation, however growing evidence indicates their origin from cerebral blood vessels, neurons, Purkinje cell dendritic processes and astrocytes (Miyakawa *et al.*, 1982; D'Andrea *et al.*, 2001; D'Andrea and Nagele, 2002; Wang *et al.*, 2002b; Nagele *et al.*, 2003). An interesting proposal for plaque origin involves neuronal death, when lysis of the cell filled with Aβs results in the deposition of its content in the brain or plaques initiated by astrocytic lysis (D'Andrea *et al.*, 2001; D'Andrea and Nagele, 2002; Nagele *et al.*, 2003). The question of the existence of unique plaque species may be backed by their distinguished morphologies and may be correlated with different dementia types.

Pathological AD plaques vary in density and compaction state. The usual spherical size of plaques is 10-160 μm in cross-sectional diameter and they are generally abundant in the association and limbic cortices (Armstrong *et al.*, 1991; Dickson, 1997). It is difficult to estimate the period of time necessary to develop mature plaques, but possibly the whole process can take years and starts long before the actual onset of the disease. Interestingly, in normal ageing brains the density of senile plaques have been found to stabilize after limited period of accumulation (Mackenzie, 1994). Therefore morphological changes within the plaques rather than their amount seem to be decisive for their pathological action.

Aβs deposition in cerebral vessels is also a common feature of advanced ageing and AD brain known as cerebral amyloid (congophilic) angiopathy (CAA). Amyloid presence is most prominent in arteries and rarely in veins of the cerebral cortex and the leptomeninges (Pezzini *et al.*, 2009). It has been observed that the distribution of CAA and Aβ plaques is correlated (Thal *et al.*, 2002; Thal *et al.*, 2008). However, there is a difference in Aβ content of both abnormalities, as the less soluble Aβ42 is generally found within brain parenchyma plaques, whereas the more soluble Aβ40 predominates in CAA (1.1.3) (Weller *et al.*, 2009). ApoE is co-localized with Aβ of those two distinct deposits and again in the case of CAA ApoE *ε4* genotype together with ageing is considered as a major risk factor (Love *et al.*, 2009; Weller *et al.*, 2009).

Positron emission tomography (PET) – one of the neuroimaging techniques – is found to be useful in determination of the brain amyloid pathophysiology *in vivo* (Nordberg, 1996; Nordberg *et al.*, 2010). This is particularly promising as so far amyloid deposits and other AD brain hallmarks have not been discovered until *post mortem* examination. Currently PET is a subject of an intensive development in order to improve its usefulness in the early diagnosis, monitoring and evaluation of anti-amyloid treatment in AD (Nordberg *et al.*, 2010).

1.1.3. β-amyloid peptides (Aβs)

1.1.3.1. APP processing and synthesis of Aβ peptides

APP is a large protein of 770 amino acids (aa) and 87 kDa with a single membrane-spanning domain close to its C-terminal end (Kang *et al.*, 1987). The gene encoding APP is located on chromosome 21 and yields three distinct isoforms APP695 (695 aa), APP751 (751 aa) and APP770 (770 aa) (Goate *et al.*, 1991). APP695 is predominantly expressed in nerve cells, whereas two other isoforms are functioning in most tissues and contain an additional 56 aa Kunitz Protease Inhibitor (KPI) domain (Rohan de Silva *et al.*, 1997). The splicing of APP RNA transcripts can be deregulated in AD and shifted towards the production of KPI-containing isoforms APP751 and APP770 (Menendez-Gonzalez *et al.*, 2005). This modification was found to be triggered by the deregulation of neuronal calcium homeostasis and associated long-time activation of the extrasynaptic N-methyl-D-aspartate receptor (NMDAR) which finally leads to high increase in neuronal production of Aβ (Waxman and Lynch, 2005; Bordji *et al.*, 2010). Although APP has been the subject of extended research regarding its involvement in AD, determination of its function in a cell is still unclear. APP is believed to play an important role in a few physiological processes, such as synaptogenesis or neuronal growth, adhesion and mobility (Moya *et al.*, 1994; Small *et al.*, 1999; Soba *et al.*, 2005). It could also be involved in copper homeostasis and reduction of oxidative stress as well as cell signalling and apoptosis (Barnham *et al.*, 2003; Chen, 2004). The conception of the regulatory role of APP in the neuronal copper homeostasis has been supported by the observation that the copper level in cerebral cortex significantly elevates in transgenic knockout mice and decreases in brain cells over-expressing APP (White *et al.*, 1999; Maynard *et al.*, 2002). APP is a type I transmembrane glycoprotein and a few reports based on the structural data suggest that it may function as a cell surface receptor interacting with a range of biomolecules including Aβ as potential ligands (Lorenzo *et al.*, 2000; Lu *et al.*, 2003). It has been reported that the protein is produced in the endoplasmic reticulum (ER) and its highest concentration is found in the trans-Golgi-network (TGN) of neurons (Greenfield *et al.*, 1999). From there APP can be shipped in post-TGN secretion vesicles to the cell surface where it is proteolytically metabolized or may be re-internalized and degraded

following the endosomal/lysosomal pathway (Sisodia, 1992; Caporaso *et al.*, 1994; Koo and Squazzo, 1994).

APP is processed *via* a set of proteases yielding different end products through non-amyloidogenic or amyloidogenic pathways (figure 1.3). In the first step of the non-amyloidogenic processing, APP is digested by α-secretase in the plasma membrane (Sisodia, 1992). This liberates a large soluble fragment known as sAPPα, but precludes generation of Aβ as the enzyme cuts within the Aβ sequence (between K16 and L17) (Sisodia, 1992). The α-secretase was identified as a membrane-bound zinc metalloproteinase and probably is a member of a disintegrin and metalloproteinase (ADAM) family (Sisodia, 1992; Roberts *et al.*, 1994; Buxbaum *et al.*, 1998). sAPPα has been considered to play a significant role in neuronal protection, as it is shown to be very potent against Aβ toxicity, excitotoxicity and glucose deprivation and helps in sustaining ion homeostasis in hippocampal tissue (Furukawa *et al.*, 1996; Mattson, 1997). It also participates in an early developmental stage of the central nervous system (CNS) and in control of proliferation of neural stem cells (Ohsawa *et al.*, 1999; Caille *et al.*, 2004). Interesting observations have been made in APP deficient mice, where sole expression of sAPPα successfully rescued appeared abnormalities, implying that sAPPα represents an essential part of physiological function of APP (Ring *et al.*, 2007). The α-secretase activity is dramatically reduced in platelets, cerebrospinal fluid and the temporal cortex of AD patients that correlates with diminished levels of sAPPα and may contribute to the disease pathology (Colciaghi *et al.*, 2002; Tyler *et al.*, 2002).

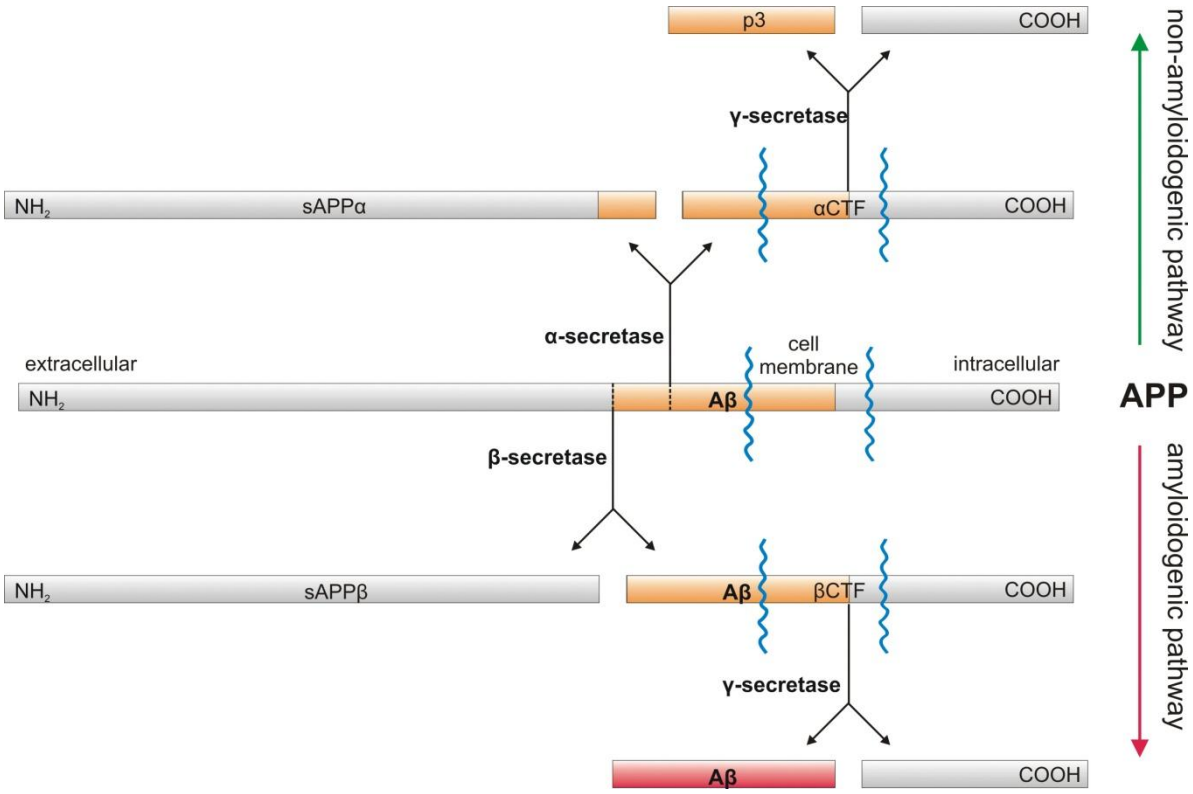

Figure 1.3. Schematic diagram of APP processing by α- β- and γ-secretase. Subsequent α- and γ-cleavage releases sAPPα and p3 fragments, whereas alternative β- and γ-cleavage yields sAPPβ and Aβ peptides.

An alternative APP cleavage is made by β-secretase which is the first step of the amyloidogenic pathway (figure 1.3). Potential activity of the enzyme was identified in a range of proteases such as BACE1 (β-site APP cleaving enzyme), BACE2 or cathepsin B (Vassar *et al.*, 1999; Solans *et al.*, 2000; Hook *et al.*, 2005). Among them BACE1, which is a type1 transmembrane protein (also known as memapsin 2 or aspartyl protease 2 (Asp2)) is the most efficient in and has been best analyzed so far, therefore it is referred as the major β-secretase (Sinha *et al.*, 1999; Vassar *et al.*, 1999). BACE1 proteolysis of APP takes place *via* the endosomal/lysosomal pathway, but also the potential involvement of ER and the Golgi apparatus has been reported (Koo and Squazzo, 1994; Haass *et al.*, 1995; Chyung *et al.*, 1997). The cleavage at the position 1 of the Aβ sequence leads to liberation of soluble ectodomain sAPPβ (Vassar *et al.*, 1999). sAPPβ is shorter from sAPPα only by the C-terminal Aβ(1-16) region, but this difference makes sAPPβ a mediator in nerve cell death and axon pruning in contrast to

the neuroprotective status of sAPPα (Nikolaev *et al.*, 2009). Contribution of BACE1 to AD pathology may be significant as the protease activity has been found to be seriously elevated in diseased brain areas and the enzyme itself is considered as a rate-limiting step in neurotoxic Aβ synthesis (Cai *et al.*, 2001; Yang *et al.*, 2003; Johnston *et al.*, 2005). On the other hand, deficiency of BACE1 in AD model mice prevents memory deficits, cholinergic dysfunction or neuronal atrophy and suppresses generation of Aβ peptides (Luo *et al.*, 2001; Ohno *et al.*, 2004; Ohno *et al.*, 2007). BACE2 is a homologue of BACE1, but it is expressed at significantly lower level in neurons (Bennett *et al.*, 2000). Moreover, the BACE2 predominant cleavage site of APP is localized near to the α-secretase site and this protease due to gene location, is suggested to be potentially involved in Aβ accumulation in DS (Solans *et al.*, 2000; Yan *et al.*, 2001).

Apart from soluble ectodomains, α- and β-secretase APP processing generates membrane-bound C-terminal fragments of αCTF (C83) and βCTF (C99), respectively, which are further cut by γ-secretase (figure 1.3). The cleavage of αCTF yields a p3 fragment of unknown function, whereas the γ-cleavage of βCTF releases a range of Aβ peptides – mostly Aβ(1-40) and Aβ(1-42) (Selkoe, 2001). The Aβ fragment is located within an extracellular membrane interface, where the first 28 amino acid residues are outside of the cell and the remaining residues reside within the membrane, which probably defines Aβ structural properties (1.1.3.3) (Kang *et al.*, 1987). γ-secretase is a high molecular weight transmembrane complex including presenilin 1 (PSEN1) and presenilin 2 (PSEN2), mutations of which have been found causative in the majority of FAD cases (1.1.4.1) (Selkoe, 2001). Interestingly, γ-secretase may also mediate additional ζ-cleavage yielding Aβ46 and ε-cleavage yielding Aβ49, which implies a yet to be studied, sequential mode of final APP proteolysis (Weidemann *et al.*, 2002; Zhao *et al.*, 2004; Zhao *et al.*, 2007).

1.1.3.2. Function and neurotoxic effect of Aβ peptides

Production of Aβs most likely occurs in subcellular compartments such as the ER and Golgi body or the endosome/lysosome complex (Koo and Squazzo, 1994; Greenfield *et al.*, 1999). Aβs are later secreted out of the cell in exosomes or may be re-internalized for degradation (Rajendran *et al.*, 2006; Mohamed and Posse de Chaves, 2011). The peptides were originally identified and purified from meningovascular amyloid deposits of AD brains and nearly a decade later they were confirmed as a major component of the plaques (Glenner and Wong, 1984; Miller *et al.*, 1993). This implied the conception of Aβs as abnormal and toxic species exclusively produced in demented and aged brains. However, a discovery of soluble Aβs in normal cultured cells and body fluids confirmed their constant synthesis and physiological function (Seubert *et al.*, 1992; Haass *et al.*, 1993; Selkoe, 1993; Ghiso *et al.*, 1997). There are reports stating that low levels of Aβ positively modulate synaptic neurotransmission and potassium ion channel work, may rescue neuronal cell death or enhance memory and learning (Plant *et al.*, 2003; Plant *et al.*, 2006; Puzzo *et al.*, 2008; Morley *et al.*, 2010). Moreover, an example of the *Caenorhabditis elegans* transgenic model was used to show that intracellular Aβ aggregates can entrap excess free copper and support a detoxification process in muscle cells (Minniti *et al.*, 2009). It is yet to be investigated whether this binding occurs in human peripheral cells.

The aspect of Aβ clearance is of much interest as it is considered to be affected in AD pathology. The peptides can be normally degraded by enzymes, such as neprilysin or insulin degrading enzyme (IDE) (Yasojima *et al.*, 2001; Behl *et al.*, 2009). Other possible ways include the removal from the brain parenchyma with interstitial fluid, interaction with P-glycoprotein helping to cross the blood-brain barrier or uptake by perivascular macrophages and microglia (Yazawa *et al.*, 2001; Cirrito *et al.*, 2005). Recent data show that statins – cholesterol lowering drugs – are promising stimulators of microglia-mediated degradation of extracellular Aβ (Tamboli *et al.*, 2010).

Neurotoxic action of Aβs has been identified as a result of their overproduction and assembly leading to substantial dysfunction of nerve cells, their eventual loss and general brain pathology (Wisniewski *et al.*, 1997; Selkoe, 2001). In diseased brain Aβs are found in soluble monomeric or oligomeric forms as well as in insoluble fibrillary aggregates further developing into amyloid plaques (1.1.2.3). There are hypotheses that

the severe neurotoxic effect of Aβ comes from its soluble oligomers, as they are thought to disturb structural integrity of the cell membrane and to enhance Aβs uptake into the cytosol (Kim *et al.*, 2003; Willliams *et al.*, 2011). Aβ could form ion channel-like structures that were shown to facilitate transport through the membrane and destabilize calcium homeostasis (Mattson *et al.*, 1992; Lin *et al.*, 2001). Studies consider that a few functional domains can be distinguished within the Aβ sequence, such as:

- KLVFFAEDV – Aβ(16-24) and IIGLMVGGVV – Aβ(31-40) involved in fibril formation, β-strand propensity (Danielsson *et al.*, 2006),
- HHQK – Aβ(13-16) – suppresses activation and interaction of microglia with Aβ; sulfate-binding region for sulfated proteoglycans found in senile plaques (Giulian *et al.*, 1998),
- HH – Aβ(13-14) – neuronal binding (Poduslo *et al.*, 2010) and metal coordination (together with H6) (Minicozzi *et al.*, 2008),
- GSNKGAIIGLM – Aβ(25-35) – biologically active fragment of Aβ, neurotoxic (Hughes *et al.*, 2000),
- VFF – Aβ(18-20) – amnestic effect, affects learning and memory (Flood *et al.*, 1994)
- IIGL – Aβ(31-34) – binds to the cell surface (Laskay *et al.*, 1997).

Identification of these essential Aβ fragments has been proven to be an important step towards designing of effective peptide antagonists, which could block physiological effects of Aβ species (Tjernberg *et al.*, 1996; Laskay *et al.*, 1997; Harkany *et al.*, 1999; Gordon *et al.*, 2001).

Intracellularly, Aβs probably form fibrils affecting a variety of organelle functions that causes alterations in synaptic transmission and neuronal damage. Dead nerve cells are the basis for the production of neuritic plaques characterized by a fibrillar amyloid core (1.1.2.3). It is proposed that an alternative protective mechanism occurs, where a large amount of extracellular soluble monomers and oligomers as well as ultimately insoluble protofibrils and fibrils assemble to form diffuse/dense core plaques (1.1.2.3) (Poduslo *et al.*, 2010).

One of the severe neurotoxic effects of Aβ species is the generation of intense oxidative stress in AD brain. Experimental evidence suggests that Aβ induces excessive production of reactive oxygen species (ROS) and peroxidative injury of membrane lipids, proteins and other cell constituents (Butterfield and Boyd-Kimball, 2004; Cetin and Dincer, 2007). It has been shown that oligomeric Aβ complex displays metalloenzyme-like activity as it shows high affinity for copper binding and catalyzes reduction of Cu(II) to Cu(I) liberating H_2O_2 (Opazo *et al.*, 2002). Aβ-catalyzed production of H_2O_2 employs biological reducing agents which negatively affects the brain environment redox state and contributes to the neurotoxicity of Aβs. There are also suggestions that ROS may play a role in Aβ-mediated vascular constriction affecting cerebral circulation (Niwa *et al.*, 2001).

The role of cholesterol is also a subject of extended study in relation to AD pathology. Aβ prevents its binding to ApoE and low-density lipoprotein that results in increased cholesterol levels in the extracellular space that was proven to be toxic for neurons (Yao and Papadopoulos, 2002). Interestingly, cholesterol binds to Aβ at the site cleaved by α-secretase, which may imply inhibition of α-cleavage in APP (Yao and Papadopoulos, 2002).

1.1.3.3. Modifications of Aβ peptides

Amyloidogenic γ-cleavage of APP yields two main C-terminally varied species Aβ(x-40) and Aβ(x-42) (figure 1.4) (Selkoe, 2001). Aβ(1-42) presents only about 10% of the produced Aβ pool, however two additional C-terminal residues – Ile41 and Ala42 – make it more hydrophobic and prone for *in vitro* oligomerization and fibril assembly compared to Aβ(1-40) (Burdick *et al.*, 1992; Jarrett *et al.*, 1993; Kim and Hecht, 2005). It seems that Aβ peptides ending at the position 42 or 43 generally can act as nuclei and trigger amyloidogenesis of more soluble Aβ40 peptides. An interesting proposal of a potential neuroprotective role of Aβ(1-40) came after the observation of its inhibiting action on Aβ deposition in a transgenic mouse model, which is opposite to the longer peptide (Kim *et al.*, 2007). The increasing Aβ42/Aβ40 ratio and elevated plasma levels of Aβ42 are common in FAD that suggests a crucial role of this longer peptide in the disease pathogenesis (Borchelt *et al.*, 1996; Scheuner *et al.*, 1996; Mayeux *et al.*, 1999).

In fact, the majority of the plaque core of Aβs is represented by the species of Aβ(x-42) organized in a fibrillary form (Jarrett *et al.*, 1993).

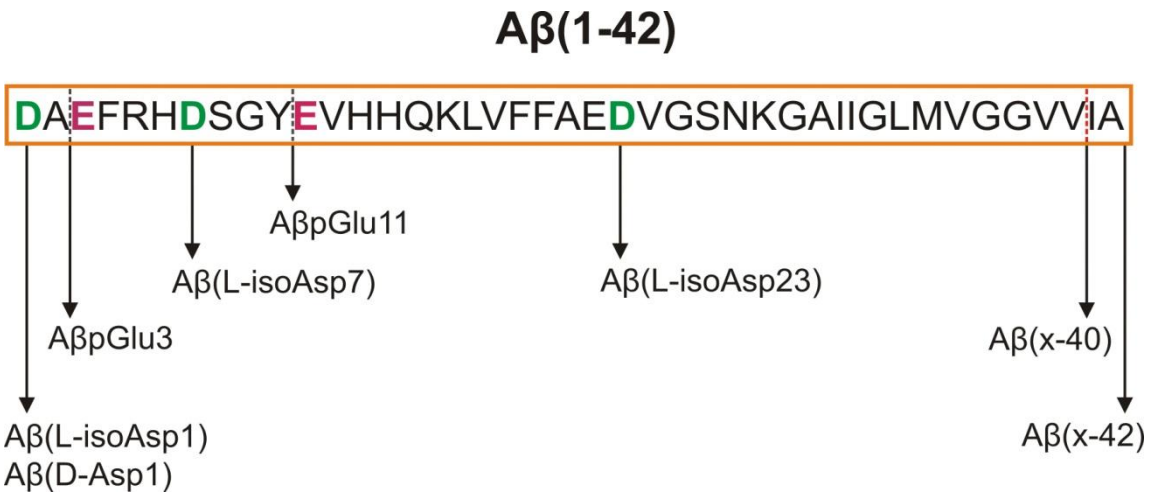

Figure 1.4. Sequence of Aβ(1-42) with marked N- and C-terminal truncations and modifications. Major modifications affect aspartic residues Asp1, Asp7 and Asp23 (racemisation or isomerisation) as well as glutamic residues Glu3 and Glu11 (cyclisation to pyroglutamyl form). Different γ-secretase truncation at the C-terminus results mostly in generation of Aβ peptides ending at the position 40 and 42.

Apart from the C-terminal heterogeneity (Aβ39 – Aβ43), Aβs display a variety of N-terminal modifications (figure 1.4), such as racemisation or isomerisation of Asp1, Asp7 and Asp23 residues, or cyclisation of Glu3 and Glu11 into the pyroglutamyl form (AβpGlu3 and AβpGlu11, respectively) (Jarrett *et al.*, 1993; Shimizu *et al.*, 2000). In 1998 Hosoda and co-workers reported the results of the quantification of plaque core peptides derived from the AD and DS frontal cortex formic acid extracts using the ELISA method (Hosoda *et al.*, 1998). The majority of these were represented by AβpGlu(3-42), Aβ(1-42) and Aβ(2-42) but also the small amounts of the L-isoaspartate isomers of Aβ – Aβ(1-42/L-isoAsp1) and Aβ(1-42/L-isoAsp7). Multiple studies have confirmed that AβpGlu(3-42) is the most prominent N-terminal Aβ variant in amyloid plaques, reaching 50-80% depending on the site of deposition (Saido *et al.*, 1995; Saido *et al.*, 1996; Hosoda *et al.*, 1998; Harigaya *et al.*, 2000). The level of AβpGlu(11-42), in turn, is particularly elevated in some FAD cases with identified PSEN1 mutations

(Russo *et al.*, 2000). pGlu-containing Aβ forms are believed to play a crucial role in initiation of neuropathogenic diseases. AβpGlu(3-42) deposition was observed to be dominant and precede deposition of Aβ(1-40/42) in DS patients and resulting plaques exhibit equivalent or higher density (Saido *et al.*, 1995). In addition, AβpGlu(3-40) and AβpGlu(3-42) were found to be strongly neurotoxic as they interact with the plasma membrane of cultured neurons and glial cells and significantly resist degradation by cultured astrocytes (Russo *et al.*, 2002). Intracellular occurrence of N-terminally truncated Aβs correlates with neuronal loss in the hippocampus of the transgenic mouse model (Casas *et al.*, 2004). Another fact, suggesting the neuropathological role of pGlu-modified Aβ peptides in AD, is their absence in brains of cognitively normal elderly patients with, nonetheless, observed accumulation of Aβ1-40 and Aβ1-42 (Piccini *et al.*, 2005). In diseased brain, intraneuronal accumulation of AβpGlu(3-40/42) was observed to progress continuously whereas the density of the full-length Aβ peptides is declining with age (Wirths *et al.*, 2010). This concludes that the full-length Aβs are N-terminally modified with the progression of the disease.

The mechanism of production of pyroglutamated Aβs remains poorly understood. One of the striking questions is the generation of free N-terminal Glu3 and Glu11 residues that are required for this reaction. Interesting experimental data show that the Swedish mutant APP (K670N/M671L) (1.1.4.1) can be processed by BACE1 *in vitro* in a pH-dependent manner (Sidera *et al.*, 2002). In acidic environment (pH 5) APP is cut at both β_1-site and β_2-site yielding Aβ starting with Asp1 and Glu11, respectively. BACE1 was localized in acidic TGN compartments so it has been suggested that β_2-site cleavage also occurs there (Huse *et al.*, 2000; Sidera *et al.*, 2002). Contrary to that, β_1-site cleavage is exclusive in neutral and basic pH, characteristic for the ER and early Golgi body (Sidera *et al.*, 2002). These data indicate that cellular localisation of APP may have profound effects on the production of Aβ species. Report by Creemers *et al.* (2000) shows that β_2-cleavage at Glu11 is a function of BACE1 expression level and it can be subsequent to the cleavage at Asp1 (Creemers *et al.*, 2001). Glu3, in turn, may only become available after the Asp1 and Ala2 removal by exopeptidases, such as aminopeptidase A (APA) or N (APN)-like types (Sevalle *et al.*, 2009). The isomeric form of Asp1 could be removed by a range of dipeptidyl peptidases or acylamino acid-releasing enzyme (Bohme *et al.*, 2008). An interesting alternative mechanism of the generation of the free Glu3 N-terminus was proposed by Drew group, which considers the involvement of Cu^{2+} (Drew *et al.*, 2010). It is possible that Aβ-coordinated

Cu^{2+} polarises the carbonyl moiety between Ala2 and Glu3 promoting subsequent amide hydrolysis and peptide bond cleavage which finally results in the generation of truncated Aβ(3-40/42) species (Drew *et al.*, 2010). Another important finding was reported by Kuda and co-workers (1997) stating significantly lower activity of plasma glutamyl aminopeptidase in sporadic AD brains comparing to age-matched controls (Kuda *et al.*, 1997). It seems to be clear that this reduction could limit the rate of Aβ catabolism and facilitate pyroglutamyl formation and finally accumulation of AβpGlu(3-40/42) in pathological brain. Early suggestions that pyroglutamyl and aspartate Aβ variants are the result of post-translational modification of Aβ(1-40/42) raised from the observation of constantly produced full-length Aβs in cerebrospinal fluid and cultured cells (Selkoe, 1993). The levels of racemised AβAsp1 forms, AβpGlu3 or AβpGlu11 remain essentially constant and independent that led to the conclusion that N-terminal conversions precede aggregation, otherwise their quantity would be proportional (Saido *et al.*, 1996). Aβ aggregates exist in solid state, as they need to be solubilised with formic acid, and this state may also slow and impair any structural modifications (Saido *et al.*, 1996). A recent report presented glutaminyl cyclase (QC) as being able to catalyze the conversion of Aβ(3-42) to AβpGlu(3-42) after APP processing and is thought to be favoured in the acidic environment of endosomal vesicles (Cynis *et al.*, 2008). However, it is unclear whether the cyclisation occurs inside the cell, or only later, after the Aβ peptide has been secreted. Interestingly, the enzyme removing Asp1, APA, is a metallo-ectopeptidase, which suggests that Aβ proteolysis may begin in the extracellular space (Sevalle *et al.*, 2009). This nonetheless does not preclude the possibility that truncated Aβ could be turned back into the cell and undergo further processing.

N-terminal pyroglutamyl modification serves as a protection against the action of aminopeptidases with the exception of pyroglutamyl peptidases (1.2). Proteolytic degradation of both AβpGlu3 and AβpGlu11 may be only initialized by pyroglutamyl specific protease as has been confirmed in previous enzymological studies (Armentrout and Doolittle, 1969; Barrett and McDonald, 1986). Therefore, pGlu protection contributes to the prolonged *in vivo* survival of Aβ peptides which increases their chances for aggregation (Saido *et al.*, 1996). Experimental data confirmed that Aβs contain structural regions potentially responsible for their conformational properties (Danielsson *et al.*, 2006; Tomaselli *et al.*, 2006). It was demonstrated that the large N-terminal fragment of Aβ 1-15 consists of helical regions, whereas fragments of 16-24

and 31-40/42 have β-sheet forming propensities and are separated by another disordered region 25-30 (Danielsson *et al.*, 2006). Therefore, a loss of 2 or 10 initial residues in case of AβpGlu3 and AβpGlu11, respectively, may significantly reduce helical propensity and accelerate the aggregation. Modification of full-length Aβ to AβpGlu3 results in a deficit of 3 charges (2 negative and 1 positive one) and 1 hydrophobic residue, and an increase by 1 polar residue in the N-terminus (D'Arrigo *et al.*, 2009). Conversion of full-length Aβ to AβpGlu11, in turn brings a deficit of 6 charges (4 negative and 2 positive ones) as well as a loss of 2 hydrophobic and 3 polar residues (D'Arrigo *et al.*, 2009). The resulting reduction in charge repulsion and the fact that the central hydrophobic part remains unaltered, makes the truncated and pyroglutamated peptides able to stabilize β-sheet conformation and hydrophobic intermolecular interactions that may initialize further Aβ assembly (D'Arrigo *et al.*, 2009; Schlenzig *et al.*, 2009). Organization of full-length Aβ fibrils, similarly to other amyloid fibrils, display a cross-β pattern, where individual β-strands are vertically orientated in relation to the fibrillar axis (Kirschner *et al.*, 1986). The peptide N-terminus in unmodified Aβ aggregates is shown to be structurally disordered and solvent-accessible (Balbach *et al.*, 2002; Petkova *et al.*, 2002). It has been proposed that the introduction of pGlu could induce structural changes stiffening the N-terminal part of the peptides (Schlenzig *et al.*, 2009). These rearrangements along with diminished solvent exposure could constrain the N-terminal disordered state, as it was observed in some pGlu-containing proteins (Liao *et al.*, 2003; Arnold *et al.*, 2006). Interestingly, the aggregation kinetics of AβpGlu3 is higher than that of AβpGlu11 which indicates the contribution of the longer N-terminal fragment in faster aggregation (D'Arrigo *et al.*, 2009). The rate of initial aggregation of pGlu variants can be up to 250-fold accelerated in comparison to that of full-length Aβs, so it has been suggested that they may act as seeding agents driving oligomerization and fibrillization processes of the other Aβ species (He and Barrow, 1999; Schilling *et al.*, 2006; D'Arrigo *et al.*, 2009). Moreover, the levels of the pyroglutamyl Aβs that terminate at position 42 in plaques are higher than those terminating at 40, and the longer form has also a greater aggregation rate (Iwatsubo *et al.*, 1996; Hosoda *et al.*, 1998; He and Barrow, 1999). Studies indicate that the differences in hydrophobicity of AβpGlu(3-42) and Aβ(1-42) are minimal, however at equimolar quantities the former aggregates more rapidly than the latter one (Kuo *et al.*, 1997). In the same study Aβ(1-42) was shown to be the most polar peptide succeeded by Aβ(1-42/L-isoAsp) variants, AβpGlu(3-42) and the most hydrophobic fragment Aβ(17-42) (Kuo *et al.*, 1997). The special role of AβpGlu(3-42) was manifested through

the observation that it can inhibit the formation of full-length peptides in fibrils (Quist *et al.*, 2005; D'Arrigo *et al.*, 2009). This may in turn favour (toxic for neurons) pre-fibrillar aggregation of Aβs that is also believed to influence the progression of AD (D'Arrigo *et al.*, 2009). It seems to be obvious that the production of modified Aβs such as AβpGlu(3-40/42) and AβpGlu(11-40/42) have pronounced effect on faster aggregation and generation of neurotoxic amyloid species found in AD and DS brains. Interestingly, inherited neurodegenerative disorders, such as familial British dementia (FBD) and familial Danish dementia (FDD) also are characterized by amorphous and fibrillar deposits consisting mainly of pGlu-modified amyloid peptides – ABri or ADan, respectively that are not related to Aβ (Schlenzig *et al.*, 2009). The pyroglutamyl residue is particularly dangerous as it prevents proteolytic degradation and clearance of these neurotoxic products from diseased brain.

1.1.4. Aetiology and treatment strategy of AD

AD has been a matter of intensive study for many decades but nonetheless its ultimate cause still remains unknown. The major problem lies in the clinical heterogeneity of AD and relative inability to determine the onset of the disorder. A further complication is a resemblance of AD symptoms to a few other conditions e.g. diffuse Lewy body dementia, Parkinson's and Huntington disease, Pick's disease, vascular and frontotemporal dementia (Rogan and Lippa, 2002; Lautenschlager and Martins, 2005; von Bernhardi *et al.*, 2010). All of them, for example, exhibit progressive and irreversible degeneration of brain cells. So far, many risk factors, such as genetic mutations, physiological disturbances or environmental agents have been analyzed and became a foundation for development of therapeutic strategies for AD treatment.

1.1.4.1. Factors behind AD pathogenesis

The genetic basis of Alzheimer's has been widely studied since the identification of several gene mutations and genotype predispositions underlying some cases of the disease. The majority of early-onset dominantly inherited AD cases are known to be associated with mutations in APP, PSEN1 or PSEN2 genes (Sandbrink *et al.*, 1996).

Many APP point mutations have been identified and associated with AD e.g. Swedish – (K670N/M671L) (Mullan *et al.*, 1992), London – V717I (Goate *et al.*, 1991), Dutch – E693Q (Levy *et al.*, 1990) or Flemish – A692G (Hendriks *et al.*, 1992). These mutations increase selective β-cleavage of APP and overproduction of Aβ(x-42/43) or promote its faster aggregation. APP mis-metabolism as a key initiating event and the subsequent amyloid deposition is the basis of the amyloid cascade hypothesis, a leading theory explaining AD pathogenesis (Hardy and Allsop, 1991; Hardy and Selkoe, 2002). Mutations in genes encoding PSEN1 and PSEN2 also result in increased extracellular concentration of Aβ42 and are thought to account for the majority of early-onset, dominantly inherited FAD cases (Sandbrink *et al.*, 1996; Scheuner *et al.*, 1996).

Discovery of ApoE within senile plaques raised an interest in its association with AD (Namba *et al.*, 1991). This protein plays an important role in lipid transport and patients carrying *ε4* allele of the *apoε* gene are frequent within those affected by late-onset familial AD (Strittmatter *et al.*, 1993). On the contrary those possessing allele *ε2* are potentially protected from the disease (Bickeboller *et al.*, 1997). This relationship has been considered to be associated with ApoE isoform-dependent efflux of cholesterol and other lipids from cultured neurons and astrocytes, with ApoE2 functioning significantly better as the acceptor (Michikawa *et al.*, 2000). A recent report also links regulation of synthesis and clearance of Aβs with ApoE isoform prevalence (Castellano *et al.*, 2011).

One of the potential risk factors, although still not well understood, is a microbial infection that can elicit neuropathological disorders. Currently, several important pathogens induce infections that appear to be related to sporadic AD and cognitive decline. There are reports suggesting the contribution of the organisms, such as *Herpes simplex* virus type 1 (HSV1) (Wozniak *et al.*, 2009), *Chlamydophila pneumoniae* (Hammond *et al.*, 2010), *Helicobacter pylori*, spirochete, picornavirus or Borna disease virus to the AD pathophysiology. Infection with HSV1 is very common and affects many people with the symptoms known as cold sores. Recent discoveries strongly link HSV1 presence with pathogenic changes in the Alzheimer's brain. It has been shown that infection of neuronal and glial cell cultures with the virus triggers intracellular accumulation of Aβ(1-40) and Aβ(1-42), and brain deposition of Aβ(1-42) (Wozniak *et al.*, 2007). Interestingly, in the later study HSV1 DNA was detected within 90% and associated with 72% of amyloid plaques (Wozniak *et al.*, 2009). This shows the strong relationship between the virus and AD pathophysiology. Aforementioned findings

determine the HSV1 virus as a one of the initiators of senile plaques formation and point to the application of antiviral agents in disease treatment. Antigens of the other pathogen, *C. pneumoniae*, have been immunohistochemically detected in neurons, neuroglia, endothelial and peri-endothelial cells (Hammond *et al.*, 2010). Surprisingly, there was also strong immunoreactivity of the pathogen in extracellular areas of the frontal and temporal cortices of the AD brain. Moreover, the appearance of *C. pneumoniae* is co-localised with amyloid deposits and NFTs in the studied regions of the brain. One may assume that the chronic or frequent infections could be considered as a potential risk factor in sporadic AD and an early preventative action seems to be very important. However, the idea of the pathogenic aetiology of Alzheimer's needs further scientific evidence and study.

The contribution of metal ions towards neurological disorders is also being debated (Budimir, 2011; Chen *et al.*, 2011). Most important biometals, Zn^{2+}, Cu^{2+}, and Fe^{3+}, for example may act as seeding factors for amyloidogenesis as they are found abundant in Aβ plaques (Bush *et al.*, 1994; Stoltenberg *et al.*, 2007). A recent report also suggests the contribution of iron to Aβs toxicity as it was shown to hinder the transition of the peptides from unstructured to ordered cross-β conformation (Liu *et al.*, 2011). The nonphysiological metal, aluminium, is observed to localize at high concentrations in Aβ deposits, although its causative role in neuropathogenesis is still being questioned (Drago *et al.*, 2008). Interestingly, accumulation of Aβs can be inhibited by a Cu/Zn-selective chelator (clioquinol) both *in vitro* and in a transgenic mouse brain *in vivo* (Cherny *et al.*, 2001). This indicates that copper also promotes Aβ aggregation. Moreover, metal ion imbalance is thought to be associated with oxidative stress, another potential cause of AD (1.1.3.2) (Budimir, 2011).

1.1.4.2. Potential therapeutic strategies

Rigorous studies are currently being carried out to develop effective ways to stop β-amyloid overproduction, enhance its clearance and aggregation blockage.

Therapeutic strategies leading to decrease of Aβ concentration are mainly focused on inhibition of APP cleavage by two proteases, β- and γ-secretase releasing Aβ peptide (Vassar, 2002). For example, oestrogen was found to reduce the neuronal Aβ level by stimulation of the APP α-secretase cleavage and thus preclude Aβ generation (Xu *et al.*,

1998; Greenfield *et al.*, 2002). Similarly, testosterone is believed to decrease the level and activity of β- and γ-secretases, to lower plaque formation and can have a positive influence on cognitive functions (Gouras *et al.*, 2000; Ghosh and Thakur, 2008; McAllister *et al.*, 2010). One of the proposed approaches towards AD is also application of the four-drug cocktail treatment consisting of nonsteroidal anti-inflammatory drugs (NSAIDs), cholesterol-lowering drugs (statins) combined with β- and γ-secretase inhibitors, which effectively reduces the synthesis of Aβs in cultured cells (Asai *et al.*, 2010). Particularly β-secretase is a prime drug target as its level is significantly elevated in the AD affected brain regions (Yang *et al.*, 2003; Johnston *et al.*, 2005). However, the viability of the protease as a therapeutic object is questioned since many, other than APP, physiologically important substrates have been identified (reviewed in (Vassar *et al.*, 2009). Moreover, BACE1 knock-out mice have very low life expectancy and exhibit severe physiological abnormalities (Dominguez *et al.*, 2005; Hu *et al.*, 2006). Lastly, inhibition of pyroglutamyl forming enzyme, QC, results in reduction of the AβpGlu(3-42) level, decreased plaque formation and gliosis as well as the improvement of cognitive functions in the mouse model that makes the enzyme an interesting therapeutic target (Schilling *et al.*, 2008b).

Immunotherapy is another area of research shown to be promising in decreasing the level of amyloid deposits and hyperphosphorylated tau in APP transgenic mouse models (Wilcock *et al.*, 2009). Furthermore, evidenced reductions in neuronal loss and cognitive decline as well as full reversion of memory deficit have been observed. Preclinical studies indicate that the best effects of Aβ immunotherapy might be achieved if it is applied before the disease onset or in its very earliest stages (Lemere and Masliah, 2010). Constantly improved diagnostic methods are invaluable for identification of presymptomatic, at risk individuals who might particularly benefit from early vaccination to prevent AD. There is also a need for natural mobilization of the immune system. One such interesting example is the observation of immune stimulation of macrophages by the form of vitamin D_3 in combination with curcumin (Fiala, 2010).

Significant attempts have been made to develop strategy preventing Aβ fibrillization and deposition (Wisniewski and Sadowski, 2008). In a number of studies Aβ homologues have been proven efficient in disrupting β-sheet conformation (Hilbich *et al.*, 1992; Soto *et al.*, 1998; Sigurdsson *et al.*, 2000). These β-sheet breakers are particularly advantageous as they target only the abnormal conformation of Aβ and do

not affect the normal function of the soluble Aβ peptides. A similar concept is found to reverse protein disorders caused by prions (Soto *et al.*, 2000). The promising therapeutic means represent N-methylated peptides (meptides) that are examples of specially designed peptide aggregation inhibitors and are also able to block β-sheet formation (Kokkoni *et al.*, 2006). An intriguing concept using the metal-chelating property of Aβ has been found effective in order to prevent peptide aggregation. A binuclear Ru(II)−Pt(II) complex and Pt(II)-based compounds bind to Aβ42 and effectively inhibit its abnormal assembly (Barnham *et al.*, 2008; Kumar *et al.*, 2010). Another approach utilizes inhibitors of pathological chaperones, a group of proteins that were found to enhance conformational assembly of Aβ to fibrils by increasing their β-sheet content that stabilizes their abnormal structure (Wisniewski and Sadowski, 2008). Key examples linked to AD Aβ aggregation include ApoE4, α1-antichymotrypsin and C1q complement factor (Ma *et al.*, 1994; Sanan *et al.*, 1994; Wisniewski *et al.*, 1994; Boyett *et al.*, 2003). There is also a wide interest in a potent antioxidant, resveratrol, as a beneficial compound in reducing the risk of AD. Indeed, this polyphenol has been observed to directly bind to Aβ42, attenuate cytotoxicity of Aβ42 oligomers and interfere in its fibril assembly (Feng *et al.*, 2009).

One of the earliest propositions for AD origin was the cholinergic hypothesis (Francis *et al.*, 1999). It assumes that the disease is caused by the brain when the deficit of the ACh and ACh-synthesizing enzyme, choline acetyltransferase (ChAT) as well as related loss of cholinergic neurons. ACh is crucial for memory formation, reasoning and information processing. The majority of the drugs treating mild and moderate AD symptoms are cholinesterase inhibitors and aim to counteract ACh deficit (Birks, 2006). Apart from ACh also other neurotransmitters, such as noradrenalin, serotonin and somatostatin are observed to be unusually low in AD and DS (Mann and Yates, 1986).

Numerous AD treatment and prevention strategies are a matter of study and development nowadays, but unfortunately nothing has been proven to stop the disease so far (Selkoe, 2001). In high income countries the key strategy is to increase the awareness of the disease, promote prophylactic care and early diagnosis of dementia.

1.2. Pyroglutamyl peptidases

1.2.1. General characteristics

Pyroglutamyl peptidase also known as pyrrolidone carboxyl peptidase (Pcp) is an enzyme hydrolytically removing the N-terminal pyroglutamyl residue (pGlu) from peptides or proteins (figure 1.5) and is classified as an ω-exopeptidase displaying specificity for L-pGlu-L-amino acid optical isomers (Doolittle and Armentrout, 1968; Uliana and Doolittle, 1969). Pcp has also been referred to by many other names such as pyroglutamate (pyroglutamyl) aminopeptidase, L-pyroglutamyl peptide hydrolase, pyrrolidonecarboxylate (pyrrolidonecarboxylyl) peptidase, 5-oxoprolyl peptidase or PYRase (Cummins and O'Connor, 1998).

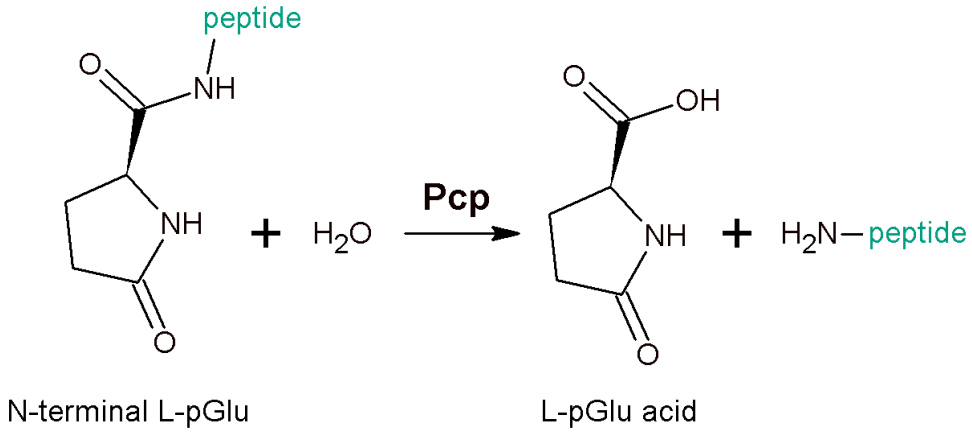

Figure 1.5. The hydrolytic removal of the N-terminal L-pGlu residue catalysed by Pcp. The enzymatic reaction liberates pyroglutamic acid (L-pGlu acid) and the peptide remnant with a free NH_2- terminus.

Pcp activity has been observed in a number of prokaryotic and eukaryotic organisms (1.2.3 and 1.2.4) (Haitinger, 1882; Doolittle and Armentrout, 1968). Moreover, in mammalian tissues it exists in three distinct enzymatic forms: Pcp type I (EC 3.4.19.3), Pcp type II (EC 3.4.19.6) and serum thyroliberinase (EC 3.4.19.-) (Cummins and O'Connor, 1998).

1.2.2. Role of the pyroglutamyl group

Pyroglutamic acid (pGlu), also known as pyrrolidone carboxylic acid (PCA) or 5-oxo-L-proline, is a product of glutamic acid dehydration (Haitinger, 1882). It can also be obtained from glutamine, various glutamate esters and diesters or γ-glutamyl derivatives (Sanger *et al.*, 1955; Winstead and Wold, 1964; Orlowski and Meister, 1971). Biologically N-terminal pGlu formation is a result of post-translational cyclisation of glutamyl or the glutaminyl residue catalysed by glutaminyl cyclase (QC) (Schilling *et al.*, 2003). Substrate specificity of QC is pH-dependent where conversion of Gln to pGlu is favoured at pH 8.0 whereas optimal pH for the conversion of Glu is 6.0 (figure 1.6) (Schilling *et al.*, 2004).

There are also reports on the spontaneous generation of free pyroglutamyl acid. For example, glutamine can non-enzymatically degrade to pyroglutamyl acid and ammonia during incubation at 37ºC in phosphate or bicarbonate buffer or in cell culture media (Gilbert *et al.*, 1949; Tritsch and Moore, 1962). Free pGlu has also been observed to be generated from glutamic acid under specific culture conditions (78ºC and pH 3.0) (Park *et al.*, 2001). Although spontaneous cyclisation of the N-terminal glutamyl or glutaminyl residue *in vivo* has not been experimentally supported, recent data suggest that this could occur in some gluten peptides (Monsuur *et al.*, 2006). There is also no evidence so far regarding the catalytic attachment of the pGlu residue to a peptide N-terminus.

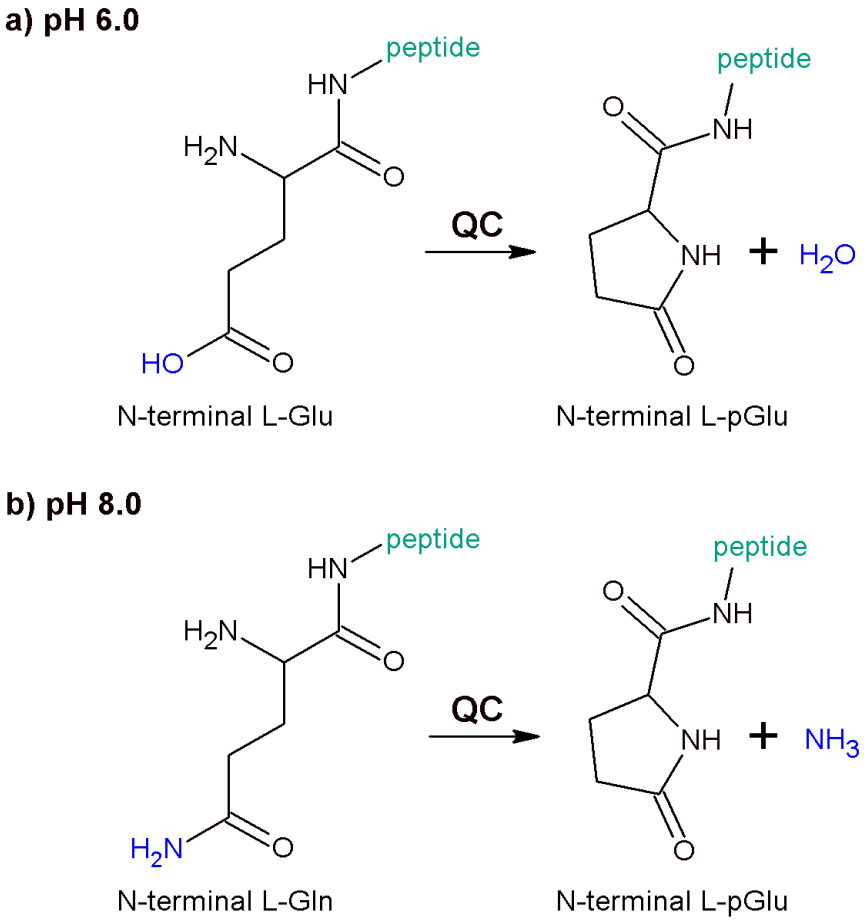

Figure 1.6. The formation of the N-terminal pGlu residue catalysed by glutaminyl cyclase (QC). Under mild acidic conditions QC is able to catalyse the cyclisation of glutamyl group to pGlu (a), whereas in the basic pH range the enzyme favours the glutaminyl group as a substrate (b) (Schilling *et al.*, 2004).

The physiological role of free or N-terminal pGlu has been established in many aspects of cellular life. In *Pseudomonas fluorescens* pGlu was found to act as an inductor of the *pcp* gene expression (Le Saux and Robert-Baudouy, 1997). Studies showed that pGlu inhibits the growth of extremophiles e.g. hyperthermophilic archaeon *Sulfolobus solfataricus* in conditions of high temperature and low pH (Park *et al.*, 2001; Park *et al.*, 2003). On the other hand it can stimulate the growth of organisms living at low temperature and neutral pH (Park *et al.*, 2003). The inhibitory action of pGlu was also detected *in vitro* with hamster tumour cultured cells or on (Na^+-K^+) ATPase of the small intestine microvilli (Escobedo and Cravioto, 1973; Goetz *et al.*, 1973). The pGlu is physiologically metabolised to L-glutamic acid by 5-oxoprolinase as a step in the

γ-glutamyl cycle (Van der Werf *et al.*, 1971). In body, elevated levels of pGlu (5-oxoproline) are hallmarks of organic acid disorders such as 5-oxoprolinuria (pyroglutamic aciduria) and hawkinsinuria (Bachmann *et al.*, 1994). The increase has recently been observed in blood plasma samples of individuals with gastric cancer or in urine of malnourished rats (Wu *et al.*, 2010; Yu *et al.*, 2011). Prolonged pGlu accumulation triggers oxidative stress, causes protein oxidation and production of reactive species as well as was shown to impair non-enzymatic antioxidant action, energy production and lipid synthesis in cultured rat brain tissues (Silva *et al.*, 2001; Pederzolli *et al.*, 2007). In Huntington's disease patients diminished level of striatum pGlu is followed by its increase in the plasma (Uhlhaas and Lange, 1988).

The presence of the N-terminal pGlu group often plays a protecting role and its removal biologically activates or deactivates a given molecule. This modification can be found in many physiological peptides and proteins such as thyrotropin-releasing hormone (TRH), luteinizing hormone-releasing hormone (LHRH), neurotensin, gastrin, anorexigenic peptide, vasoactive peptide or fibrinopeptide B (reviewed in (Cummins and O'Connor, 1998). Other examples include snake venoms physalaemin (Anastasi *et al.*, 1964) eledoisin (Anastasi and Erspamer, 1963) and bradykinin-potentiating peptides (Hayashi and Camargo, 2005), honeybee antibacterial hymenoptaecin (Casteels *et al.*, 1993) phytotoxins (de Lamotte *et al.*, 2007) or light and heavy chains of immunoglobulin (Doolittle and Armentrout, 1968). TRH, LHRH or neurotensin represent a group called neuropeptides, which are derived from the central and peripheral nervous system and play an important role in modulation of functions of various cell types (Peillon *et al.*, 1991; Rozengurt, 2002). They are directly involved in cell signalling that is crucial for cellular metabolism, growth and differentiation. Neuropeptides consist of 3 to 40 amino acids in length and their biological activity is physiologically regulated by neuropeptidases, generally found on the neuronal cell surface (Isaac *et al.*, 2009). It is clear then that disturbances of their enzymatic activity consequently affect biochemical pathways. The example of neuropeptidase is Pcp type II (PcpII) which catalyzes degradation of TRH by the removal of the N-terminal pGlu group (figure 1.7) (Cummins and O'Connor, 1998). The function of PcpII and inactivation of TRH are further discussed in section 1.2.4.2

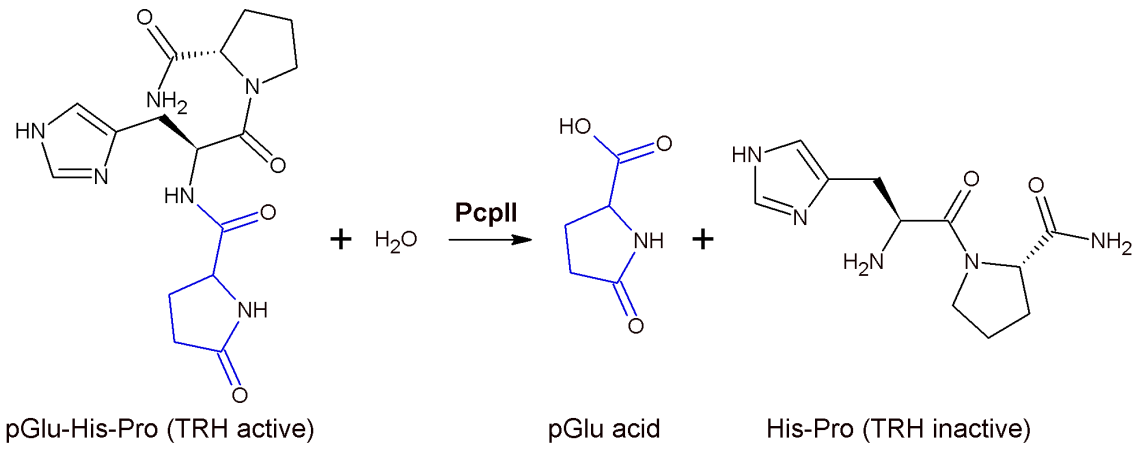

Figure 1.7. The hydrolytic removal of the N-terminal L-pGlu of TRH catalysed by PcpII. The reaction yields inactive TRH and free pyroglutamic acid.

In the case of TRH, the pyroglutamyl residue was shown to play an important structural role as the lactam ring carbonyl of the pGlu moiety interacts with the tyrosyl residue of the TRH receptor (Perlman *et al.*, 1994). Interestingly, it has been demonstrated that any structural alterations in the pGlu ring negatively affect hormonal efficiency and receptor binding ability (Hinkle and Tashjian, 1973).

Pharmacologically pGlu has become very popular since it is a natural component of human skin and its salts are found applicable in cosmetology mainly due to moisturising benefits (Lin *et al.*, 1995; Marty, 2002; Oshimura *et al.*, 2007). Moreover, administration of D,L-pGlu arginine salts prevents both electroconvulsive shock and scopolamine-induced amnesia in rats as well as improves cognitive properties (Spignoli *et al.*, 1987). Application of synthetic pGlu modifications to therapeutic peptides is beneficial for prolongation of their half-life in body. Such an example is pGlu-containing glucose-dependent insulinotropic polypeptide (GIP), gastric inhibitory polypeptide or glucagon-like peptides which are resistant to degradation by dipeptidyl peptidase IV (O'Harte *et al.*, 2002; Green *et al.*, 2004; Irwin *et al.*, 2005). On the other hand, presence of pGlu may also be a problem. For example, therapeutic administration of glutamine to the gastrointestinal tract may be difficult due to possible conversion to pGlu, therefore the N-terminal amino acid modifications, such as Gly-Glu are used to overcome this problem (Jiang *et al.*, 2006). Similarly, derivatization of the N-terminal pGlu group was shown to be effective protection against drug degradation by Pcps

(Moss and Bundgaard, 1992). Importantly, in several neurodegenerative disorders pGlu peptides are believed to initialize the formation of toxic deposits and therefore contribute to the pathogenesis (Saido, 2000). In Alzheimer's pGlu modification is found in Aβ peptides as a result of cyclisation of glutamic residues at the position 3 and 11. This increases the hydrophobic properties of the peptides triggering their aggregation that contributes to the disease progression and is discussed in detail in section 1.1.3.3.

1.2.3. Prokaryotic pyroglutamyl peptidases

Pcp activity was first discovered in *P. fluorescens* in 1968 and has since been reported and characterised in a variety of bacterial, plant and animal sources (Doolittle and Armentrout, 1968; Cummins and O'Connor, 1998). Biochemical studies resulted in this group of enzymes to be subdivided into two classes –type I and type II. The type I Pcps (PcpI) are cysteine proteases expressed both in prokaryotic and eukaryotic organisms, whereas type II Pcps (PcpII) are large zinc metallopeptidases and so far have been found in mammalian cells only (Cummins and O'Connor, 1998). PcpII are furthered described in section 1.2.4.2.

Bacterial and archaeal Pcps have been most extensively studied. This has resulted in the observation that they have high sequence and structural similarity. They all function intracellularly in either a dimeric or tetrameric form with an average subunit molecular mass of 25 kDa and an average polypeptide chain length of 215 aa. Amino acid sequence alignment shows up to 40% identity between respective bacterial and archaeal Pcps and up to 76% in the most conserved segments (Cummins and O'Connor, 1998). Moreover, there are no significant similarities to other known proteins (Awade *et al.*, 1994). Analysis of *Bacillus subtilis*, *Streptococcus pyogenes* or *P. fluorescens* genomes revealed that the *pcp* gene is present in a single copy and low transcript levels imply poor mRNA stability or weak protein synthesis (Awade *et al.*, 1992a; Cleuziat *et al.*, 1992; Gonzales and Robert-Baudouy, 1994). There is also suggestion of a possible bacterial mechanism controlling the enzyme expression, which may be supported by the identification of putative ferric uptake regulator (FUR) binding site within the *P. fluorescens pcp* gene promoter (Le Saux and Robert-Baudouy, 1997). Moreover, the same study demonstrated that Pcp synthesis is induced by pGlu acid and down-regulated by iron. As yet, not much is known about the exact physiological role

of prokaryotic Pcp. Some suggestions have been made, pointing to a possible involvement of the enzyme in protein maturation and degradation, as well as in detoxification of the bacterial cell cytoplasm form of pGlu peptides (Awade *et al.*, 1994). Exogenous pGlu-peptide could also be degraded in order to get essential nutrients. However, these suggestions are not conclusive and need further evidence since numerous bacterial strains, such as *Escherichia coli* show a lack of Pcp activity (Mulczyk and Szewczuk, 1970).

Despite the identification of enzymatic activity in a variety of organisms, to date structural information has been gained only from bacterial and archaeal Pcp homologues. All Pcp members with characterized protein structure along with source organisms and Protein Data Bank (PDB, www.pdb.org) accession codes are listed in table 1.1.

SOURCE ORGANISM		PDB ID	REFERENCE
bacteria	*Bacillus anthracis*	3LAC	unpublished
	Staphylococcus aureus	3GIU	unpublished
	Thermus thermophilus	2EBJ	unpublished
	Bacillus amyloliquefaciens	1AUG	(Odagaki *et al.*, 1999)
archea	*Pyrococcus horikoshii*	1IU8	(Sokabe *et al.*, 2002)
	Pyrococcus furiosus	1IOF	(Tanaka *et al.*, 2001)
	Thermococcus litoralis	1A2Z	(Singleton *et al.*, 1999)

Table 1.1. List of bacterial and archaeal Pcp homologues with known protein structure. These prokaryotic peptidases are the only source of structural information concerning Pcps so far.

Structural comparison of Pcp homologues shows the high similarity with minor differences which, however, are thought to be responsible for their individual biochemical properties. A study shows that the enzymes from hyperthermophile archaeal sources exhibit higher catalytic activity and elevated protein thermostability than their mesophilic counterparts (Ogasahara *et al.*, 2001). For example, Pcp from *Bacillus amyloliquefaciens* denatures at around 50ºC, whereas the *P. furiosus* counterpart and its oxidized form denature at 105ºC and 115ºC, respectively (Kabashima *et al.*, 2001; Ogasahara *et al.*, 2001).

One of the first solved Pcp structures was archaeal enzyme from *Thermococcus litoralis*, which has been determined to a resolution of 1.7 Å (PDB 1A2Z) (Singleton *et al.*, 1999). The native Pcp exists as a homotetramer of 96 kDa with overall dimensions of 78 Å x 65 Å x 52 Å and possesses a 222 point symmetry (figure 1.8). The centre of the *T. litoralis* enzyme is hydrophobic and contains a unique motif consisted of four β-hairpins, one from each monomer. One of the β-strands in each hairpin is build by amino acid residues Phe-Phe-Leu-Leu at positions 179 to 182 in the sequence. This highly hydrophobic insertion has been considered as a feature that may contribute to protein thermostability, however it has not been found in other thermophilic Pcp homologues.

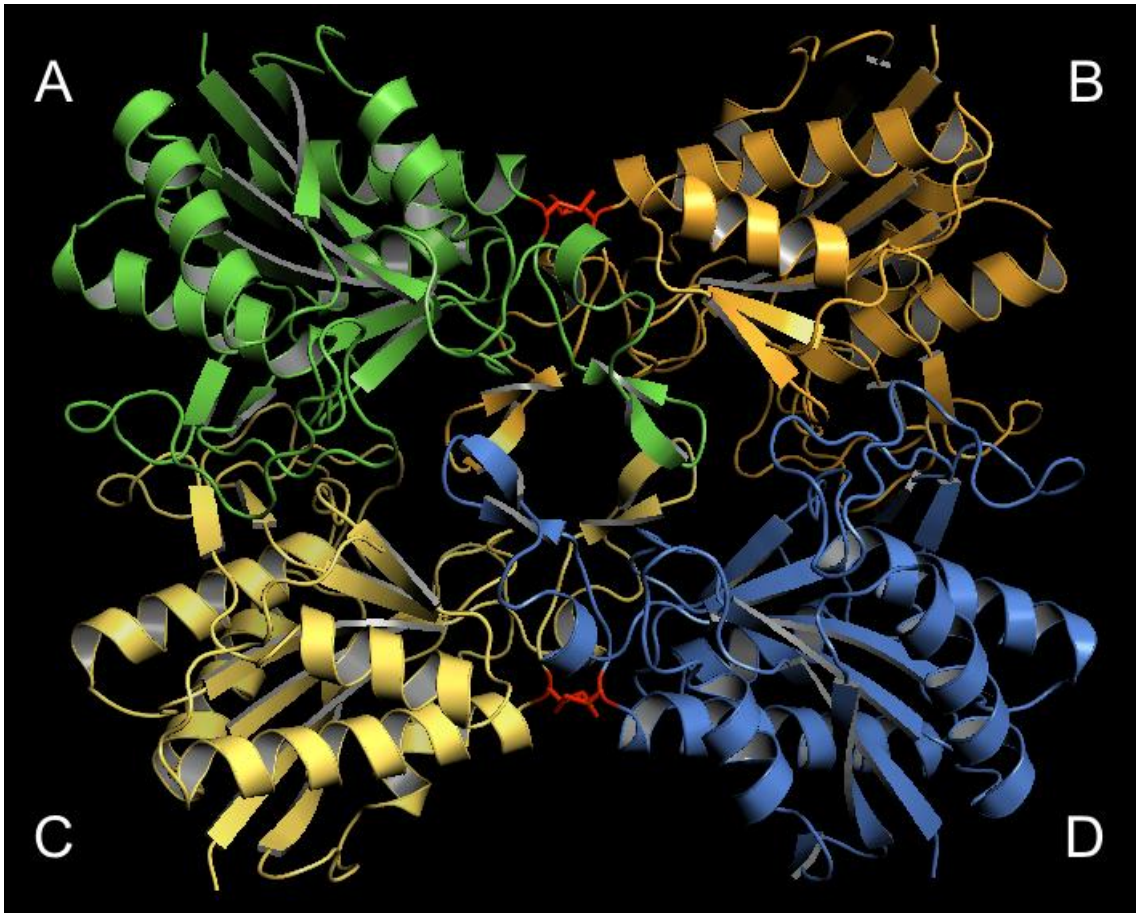

Figure 1.8. Cartoon diagram representing the Pcp homotetramer form *T. litoralis* (PDB 1A2Z). Each one of the subunits is labelled and shown in different colour. The disulfide bond between subunits A and B or C and D is coloured in red. The unique hydrophobic core in the centre of the tetramer is created by four β-hairpins from each monomer and is thought to significantly contribute to protein stability (Singleton *et al.*, 1999).

The other factor that may enhance protein stability is the presence of inter-subunit (A-B and C-D) disulfide bridges between Cys190 residues, which has been observed to remain intact even under strongly reducing conditions (Singleton *et al.*, 1999). Apart from *T. litoralis* this interaction appears only in Pcp from *P. furiosus* and is generally uncommon in intracellular enzymes (Tanaka *et al.*, 2001). Interestingly, mutagenesis of corresponding Ser185 to cysteine in *B. amyloliquefaciens* enzyme and consequent creation of inter-subunit disulfide bridge also greatly increased its thermal stability (Kabashima *et al.*, 2001).

The fact that known hyperthermophilic Pcps differ by some small but important structural features led to the conclusion that the origin of high stability does not arise from a single factor. In individual proteins enhanced thermostability is considered to be a result of increased hydrophobic or ionic interactions, stable secondary structure, improved hydrogen bonding, favourable packing and advanced oligomerization or their combination (Kumar *et al.*, 2000; Trivedi *et al.*, 2006).

Each 24 kDa *T. litoralis* Pcp monomer consists of 220 amino acid residues creating polypeptide chain folded into a single, 'comma-shaped' α/β domain with dimensions 40 Å x 36 Å x 23 Å. All of the Pcp structures characterized so far share common tertiary organization of the monomer, comprised of a seven-stranded β-sheet centre twisted by ~90º and surrounded by five α-helices. Structural secondary elements of the *T. litoralis* Pcp monomer with α-helices and β-strands sequentially labelled α_1-α_5 and β_A-β_K, respectively, are presented in figure 1.9.

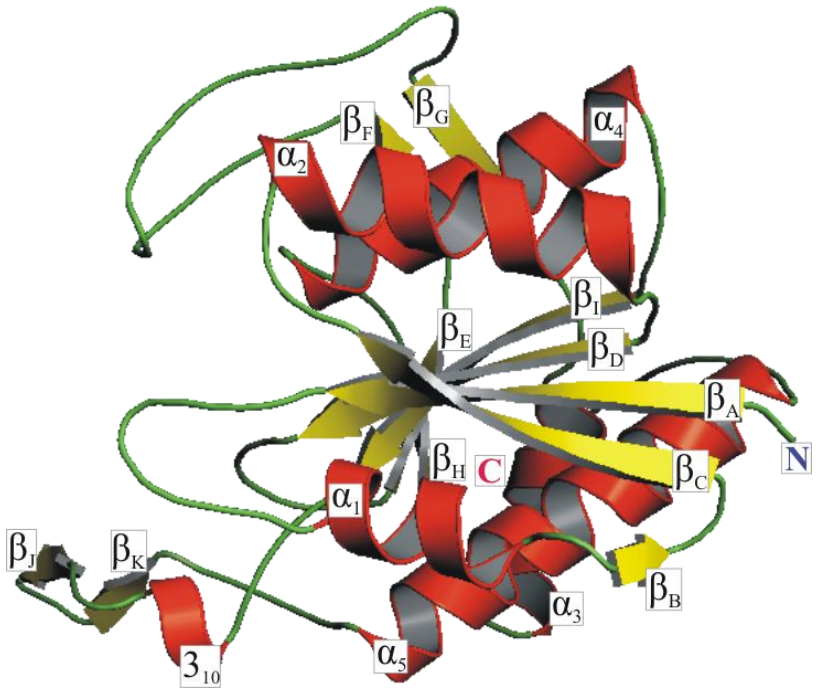

Figure 1.9. Cartoon representation of the Pcp monomer from *T. litoralis* . Secondary structure elements are sequentially labelled α_1-α_5, 3_{10} and β_A-β_K, respectively. Polypeptide N-terminus is marked as N (blue) and C-terminus is marked as C (red). A fragment between strands β_E and β_G creates small 'insertion' subdomain.

A subunit fragment between strands β_E and β_G (from residues 70 to 138) forms small 'insertion' subdomain (Singleton *et al.*, 1999). This constitutes one face of the Pcp monomer formed by long disordered loop and a double-stranded (β_F and β_G) anti-parallel β-sheet. Another significant structural fragment is two-stranded (β_J and β_K) anti-parallel β-sheet proceeded by a short 3_{10} helix which participates in the formation of the tetrameric hydrophobic centre. Both aforementioned substructures also are involved in hydrophobic interactions between respective protein subunits. The most disordered part of the polypeptide chain is its C-terminus, which is a long loop after α_5 helix running back towards the β-sheet centre.

Sequential conservation throughout Pcps and mutational analysis led to suggestions that the Cys-His-Glu triad is involved in the catalytic mechanism (Yoshimoto *et al.*, 1993; Awade *et al.*, 1994). In *T.litoralis* Pcp the catalytic triad – Glu80, Cys143 and His167 – occupies a hydrophobic pocket and is distributed on the central β-sheet and one of the α-helices (figure 1.10). The catalytic cysteine resides on the N-terminus of helix α_4 in opposition to His167 and Glu80 located on β_I and β_E, respectively. The Sγ of Cys143 makes a hydrogen bond of 3.46 Å in length with the Nε of His167. The other His167 nitrogen – Nδ is hydrogen-bonded to the Glu80 Oε with a distance of 2.86 Å. This suggests the role of Glu80 in stabilization and proper orientation of His167 imidazolium ring.

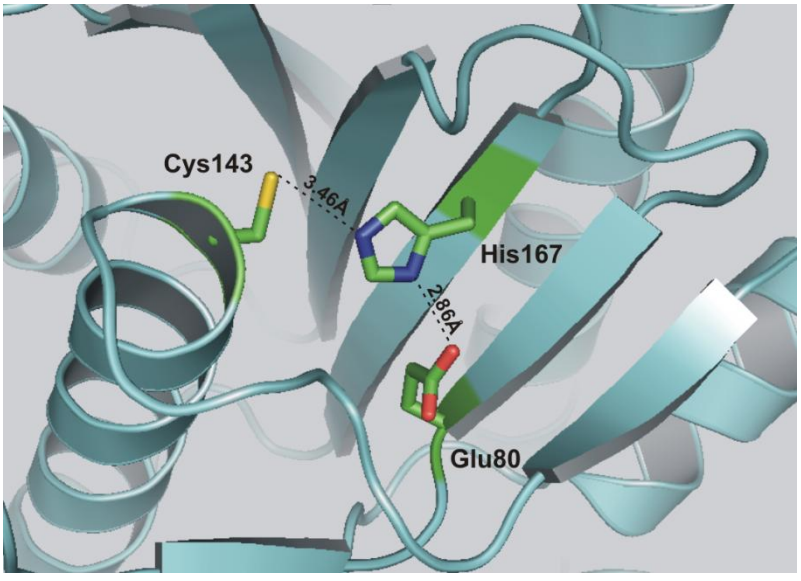

Figure 1.10. A diagram representing active site residues of *T. litoralis* Pcp. Proposed catalytic triad – Glu80, Cys143 and His167 are presented in stick mode and distances between them are shown in angstroms (Å) (Singleton *et al.*, 1999).

Analysis of the crystal structure of Pcp from *B. amyloliquefaciens* revealed that its active site contains a hydrophobic S1 binding pocket suitable to accommodate the pyroglutamyl residue (Ito *et al.*, 2001). This pocket has also been seen in *T. litoralis* enzyme and is lined with well conserved hydrophobic residues Phe9, Phe12, Val44, Ile91, Tyr141 and Leu143. There is no other defined main chain substrate-binding areas apart from this, which may explain the broad enzyme substrate specificity (Ito *et al.*, 2001). Co-crystallization of the *Bacillus* Pcp with the transition state analogue inhibitor 5-oxo-pyrrolidine-2-carbaldehyde has enabled the analysis of the mechanism of substrate recognition by the enzyme active centre (Ito *et al.*, 2001). In the structure, the pyrrolidone ring of the inhibitor has been located in the hydrophobic pocket composed of Phe10, Phe13, Thr45, Ile92, Phe142 and Val143 whereas the inhibitor has been seen to make two hydrogen bonds with the main chain of the enzyme (main chain71:O···H-N:Inhibitor and Gln71:N-H···OE:Inhibitor). Interestingly, the pyrrolidone ring of the inhibitor and the benzene rings of three Phe residues of the pocket appear to be almost parallel and they play a crucial role in proper nesting of the substrate. A large movement of Phe142 was observed in the crystal structure with bound inhibitor when compared to the unbound form and, together with Phe13, both residues were proposed to be involved in an induced fit mechanism. Multiple sequence alignments show that three phenylalanines (Phe10, Phe13 and Phe142 – *B. amyloliquefaciens* Pcp numbering) are conserved in all Pcp sequences with rare replacements of Phe13 and Phe142 by Tyr residues in some enzymes (Ito *et al.*, 2001). This replacement however may not be meaningful as Phe142Tyr mutagenesis experiments in *B. amyloliquefaciens* Pcp resulted in no change of kinetic performance of the enzyme. The conservation of Gln71 is not high, but it is the main chain that is involved in hydrogen bonding with the substrate, which suggests that the residue type may not be important.

Pcp type I enzymes have been assigned to C15 family, which is a single member of the CF clan of cysteine peptidases (Rawlings *et al.*, 2010). The primary and tertiary structure of PcpI shows no discernable similarity to any other peptidase in the family; hence it is associated with the separate clan CF.

Cysteine peptidases represent a separate class of enzymes, which have been identified in variety of organisms and are distinguished by their characteristic catalytic mechanism and active site. The hydrolytic pathway of cysteine peptidase is shown in figure 1.11. In the active site the cysteine thiolate is stabilized by the nitrogen of the neighbouring histidine imidazolium ring. In some cysteine peptidases containing catalytic triad, the imidazolium ring is orientated by the third residue such as asparagine, aspartate or glutamate, which helps to charge one of its nitrogen atoms. There are many of the enzymes however, which possess only Cys-His dyad. In the first step of catalytic pathway, the cysteine thiolate carries out the nucleophilic attack on the carbonyl moiety of the peptide bond. This results in the formation of a tetrahedral transition state and subsequent release of the acyl-enzyme thioester intermediate and amine product. In a second step the thioester intermediate is attacked by a water molecule which leads to the formation of second tetrahedral intermediate and finally the liberation of carboxylic acid product and regeneration of free enzyme. It is worth noting that serine peptidases display similar catalytic mechanism as cysteine peptidases, but in former enzymes it is based instead on an active site serine residue, where its hydroxyl oxygen functions as a nucleophile.

The cysteine thiol group is very reactive and can form complexes with metal ions or be rapidly oxidised that can result in the creation of disulfide bonds or higher oxidation states such as sulfenic, sulfinic, and sulfonic acids. In order to prevent this occuring, type I Pcps strictly require a thiol-reducing agent such as β-mercaptoethanol or dithiothreitol (DTT) to maintain catalytic activity (Prasad, 1987). Consequently, many sulfhydryl-blocking reagents, such as N-ethylmaleimide or 2-iodoacetamide, display strong inhibitory effect towards this class of cysteine peptidases (Bauer and Kleinkauf, 1980; Cummins and O'Connor, 1996).

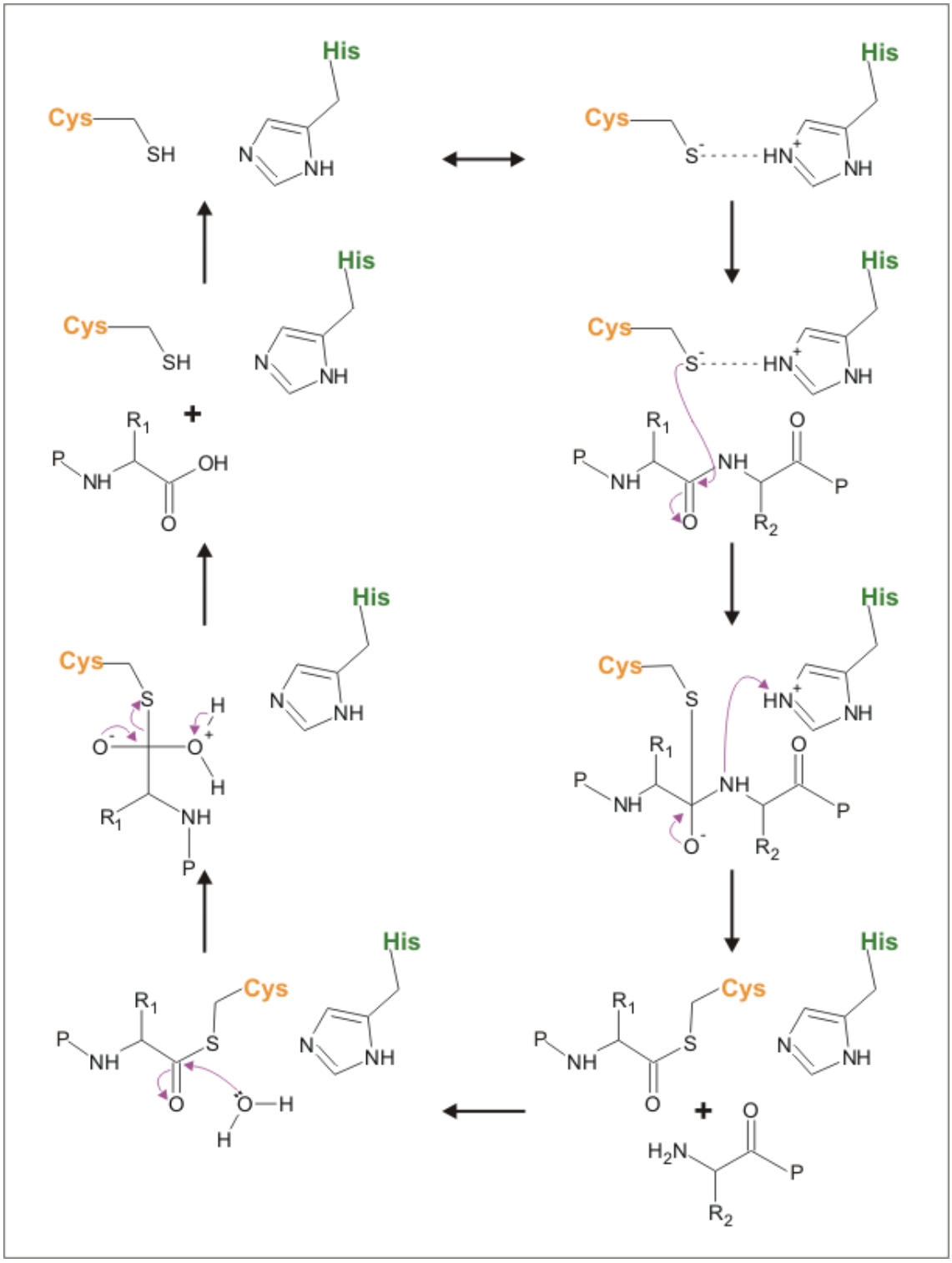

Figure 1.11. The catalytic mechanism of cysteine peptidase with the Cys-His dyad. Nucleophilic attack of thiolate on the carbonyl group of the peptide bond results in the formation of a thioester acyl-enzyme intermediate. In the subsequent step the thioester is hydrolysed, which leads to the release of carboxylic acid product and regeneration of the catalytic centre.

A particular feature of PcpI enzymes is their broad substrate specificity regarding the amino acid following the N-terminal pGlu with the exception when the second position is occupied by a proline residue (Mudge and Fellows, 1973; Browne and O'Cuinn, 1983). The only exemption from this rule is the Pcp isolated from *Klebsiella cloacae*, which is able to hydrolyse the pGlu-Pro bond (Kwiatkowska *et al.*, 1974). Moreover, this homologue is associated with a particulate fraction, unlike the Pcps from other sources which have been shown to be soluble proteins (Kwiatkowska *et al.*, 1974; Tsuru *et al.*, 1978; Awade *et al.*, 1992a; Awade *et al.*, 1992b). Studies showed that prokaryotic Pcps can process a variety of biologically active peptides as well as synthetic substrates such as pGlu-*p*-nitroanalide or pGlu-β-naphtylamide (pGlu-βNA) (Cummins and O'Connor, 1998). Despite that, the enzyme is very sensitive to even minor alterations in the pGlu structure, which may significantly impair its ability to hydrolyse the peptide bond (Capecchi and Loudon, 1985). This finding is believed to be potentially useful in the development of pro-drugs resistant to Pcp degradation.

Although Pcps exhibit no discernible structural similarity to any member of cysteine protease family, they do, however, resemble other enzyme classes in terms of fold or topological features. One example is carboxypeptidase A from *Bos taurus* (PBD 2CTB) which was observed to display significant homology to *T. litoralis* Pcp (Singleton *et al.*, 1999). Superimposition of both structures results in 2.0 Å root mean square deviation (RMSD) between their Cα atom positions over 100 out of 220 Pcp residues. Moreover, the location of the catalytic residues is almost identical and the position of catalytic zinc ion in carboxypeptidase A is only 1.2 Å away from Cys143-Sγ in Pcp. The other enzyme that also exhibits structural similarity is *E. coli* purine nucleotide phosphorylase (PDB 1A69) (Singleton *et al.*, 1999). Both proteins' Cα backbones superimpose with 1.9 Å RMSD over 119 out of 220 Pcp residues. The high structural homology may be considered as evidence that these three enzymes evolved from a common ancestor and could be classified in one super-family of enzymes.

1.2.4. Eukaryotic pyroglutamyl peptidases

Eukaryotic enzymes displaying N-terminal pyroglutamyl removal activity have been divided into two types on a mechanistic basis (Szewczuk and Kwiatkowska, 1970). In mammalian tissues Pcp exist in three distinct enzymatic forms: PcpI (EC 3.4.19.3), PcpII (EC 3.4.19.6) and serum thyroliberinase (EC 3.4.19.6) (Barrett *et al.*, 1998; Cummins and O'Connor, 1998). To date the enzyme activity or *pcp* genes have been identified in a range of protozoa, fungi, plant and animal organisms (Rawlings *et al.*, 2010). Contrary to archaeal and bacterial homologues, as yet there is no information on the PcpI nor PcpII structure from any eukaryotic source.

1.2.4.1. Pyroglutamyl peptidase type I

A eukaryotic PcpI functions intracellularly as a soluble, cytosolic cysteine peptidase and is classified, as its prokaryotic counterparts, as a member of C15 family (Rawlings *et al.*, 2010). So far it has been reported to occur in various mammalian tissues including human cerebral cortex, liver, kidney, pancreas, skeletal muscle and semen; rat, bovine and guinea pig brain (Cummins and O'Connor, 1998; Valdivia *et al.*, 2004). Immunohistochemical studies have helped to localize the enzyme also in the pituitary, hypothalamus, adenohypophysis and renal proximal tubules. PcpI activity is relatively high in vertebrate liver and kidney when compared to other tissues. There are also observed sex differences and age-related changes in the native serum pGlu-substrate hydrolyzing activity (Martinez *et al.*, 1999). Non-mammalian type I Pcps have been noted in avian, fish and amphibian tissues (Albert and Szewczuk, 1972; Tsuru *et al.*, 1982). In a number of plants the enzyme activity has been found in leaves, seeds, sprouts and roots (Szewczuk and Kwiatkowska, 1970). The amino acid sequence is known amongst others for Pcp homologues from rat (Abe *et al.*, 2003), bovine (Kilbane *et al.*, 2007), mouse and human (Dando *et al.*, 2003) sources and with the growing genome sequencing data now available this number will increase.

Mammalian enzymes have been identified to be monomers of relatively low molecular mass of about 24 kDa (Cummins and O'Connor, 1998; Dando *et al.*, 2003; Kilbane *et al.*, 2007). The first report of the cloning and sequencing of a vertebrate pyroglutamyl peptidase was published by Dando and co-workers and concerned the human (AJ278828) and mouse (AJ278829) PcpI homologues (Dando *et al.*, 2003). A biochemical study shows that eukaryotic PcpI enzymes resemble prokaryotic counterparts in terms of their broad pyroglutamyl substrate specificity and an absolute requirement for thiol-reducing reagents to maintain activity (1.2.3). Moreover, upon treatment with micromolar concentrations of thiol-blocking inhibitors, human PcpI loses its activity (Dando *et al.*, 2003). This implies that the free cysteine thiol group is important for the catalytic reaction. Interestingly, the influence of reducing agents has been shown to be tissue specific – inhibitory for brain and serum Pcps and stimulating for liver, spinal cord, kidney and adrenal activity (Prasad, 1987). Multiple amino acid sequence alignment of human, mouse, *B. amyloliquefaciens* and *T. litoralis* Pcp representatives shows complete conservation of the catalytical Glu-Cys-His triad between the species (figure 1.12).

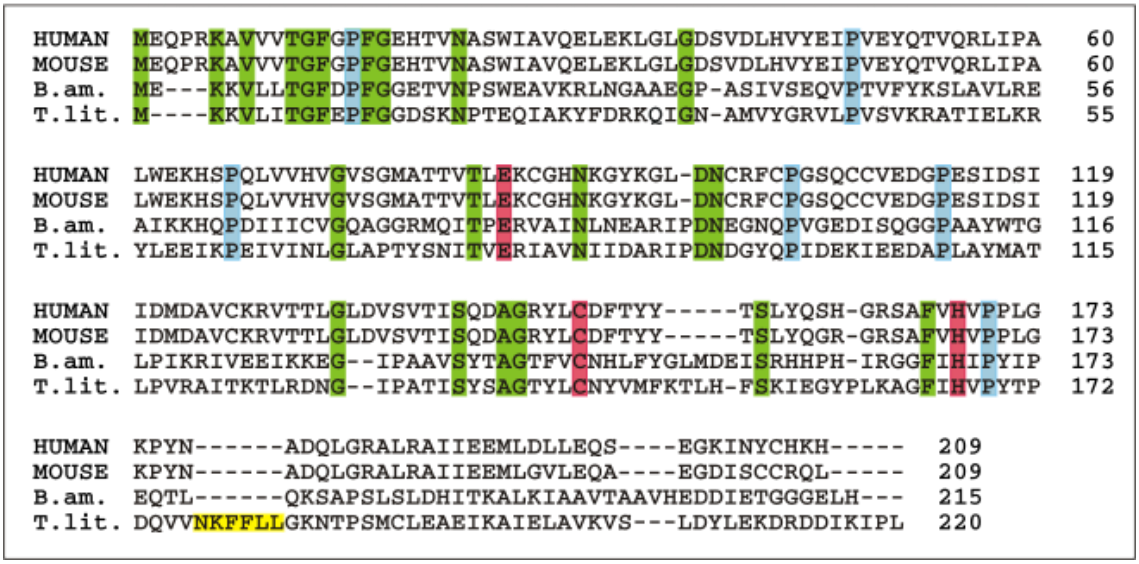

Figure 1.12. Alignment of human, mouse, *B. amyloliquefaciens* and *T. litoralis* Pcp amino acid sequences. The sequences were aligned using the ClustalX2 software (Larkin *et al.*, 2007). The conserved catalytic triad residues Glu85, Cys149 and His168 (human PcpI numbering (Dando *et al.*, 2003)) are marked in red. Other conserved residues are marked in green and conserved prolines, which tend to occur at the end of β-strands, are marked in blue. It is worth noting that *T. litoralis* Pcp contains hydrophobic insertion (marked in yellow) that participates in the formation of the tetrameric hydrophobic core (1.2.3) and does not appear in mammalian homologues.

The alignment shows greater sequence conservation between the species within the N-terminal region and relatively low similarity in the C-terminal part (figure 1.12). The interesting insertion in the *T. litoralis* Pcp sequence consisted mostly of hydrophobic residues 177-182 (marked in yellow in figure 1.12) and is lacking in the mammalian homologues. Moreover, Dando and co-workers performed a modelling of human PcpI using structures of *T. litoralis* (PDB 1A2Z) and *B. amyloliquefaciens* (PDB 1AUG) enzymes as templates (Dando *et al.*, 2003). The comparison of *T. litoralis* Pcp monomer and the human PcpI model is presented in figure 1.13. Despite the evolutionary distance between the species, there is a significant resemblance in the organization of secondary structural elements. It is worth noting that among the conserved residues there are six prolines which tend to occur at the β-strand end (figure 1.12). However, there is a striking difference in the *T. litoralis* Pcp structure that possesses the extended loop (marked with dashed line in figure 1.13). This region is involved in formation of the tetramer hydrophobic core (1.2.3) and may contribute to protein thermostability. The lack of such a loop in the model has been suggested as an explanation why human PcpI physiologically exists as a monomer (Dando *et al.*, 2003).

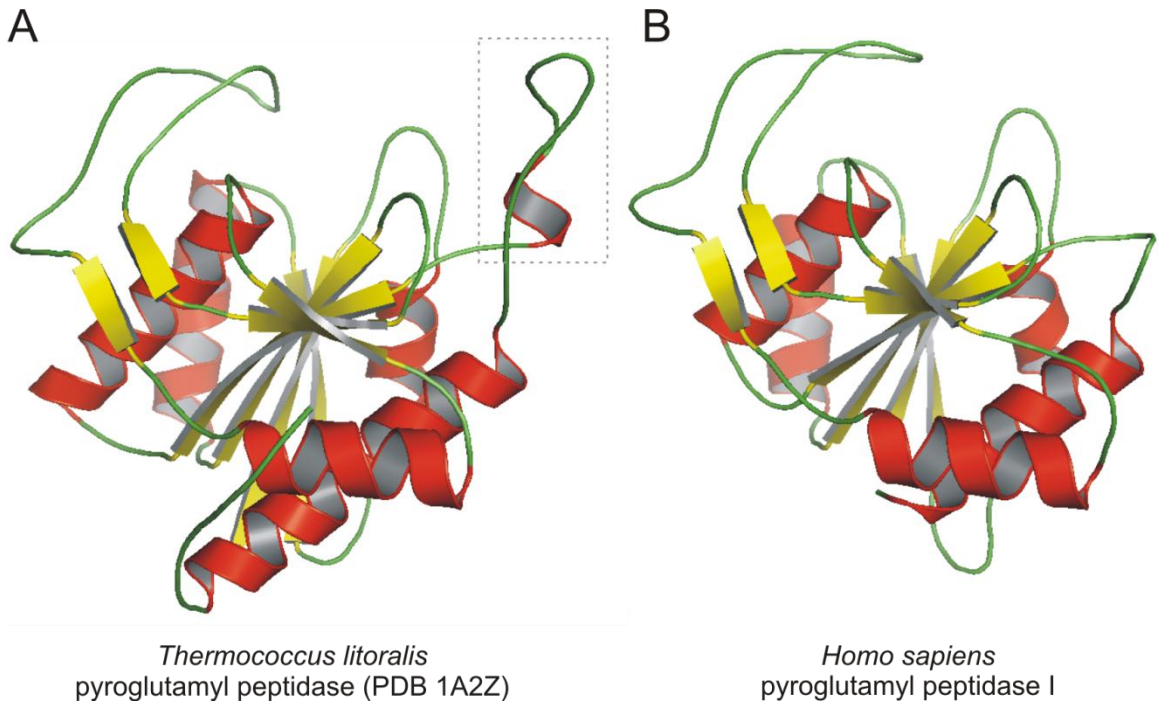

Figure 1.13. Comparison of *T. litoralis* Pcp monomer structure (A) with human PcpI model (B). Structural α-helices, β-strands and loops are shown in red, yellow and green, respectively. The distinctive extended loop in *T. litoralis* Pcp is marked with dashed line rectangle. Based on (Dando *et al.*, 2003).

Extended biochemical studies of human, mouse and bovine PcpI indicated that mammalian enzymes are relatively unstable *in vitro* (Dando *et al.*, 2003; Kilbane *et al.*, 2007; Mtawae *et al.*, 2008). Both wild-type and recombinant human PcpI have been found unstable in most of the water-miscible, hydrophilic solvents. Thermal stability analysis showed that enzyme activity rapidly declines above 45ºC and the half-life at 60ºC was estimated at 15 min. Moreover human PcpI remains active from pH 6.0 to 9.0 (with maximal activity at pH 7.0-8.5) displaying Michaelis-Menten kinetics with K_m value of 50 μM (Dando *et al.*, 2003). A range of biologically active peptides such as bombesin, neurotensin, LHRH or leukopyrokinin are successfully hydrolysed by mammalian PcpI. The only exception is eledoisin possessing a proline residue at the second position. This is consistent with substrate specificity of prokaryotic enzymes also unable to cleave the pGlu-Pro bond (1.2.3). Other studies analyzing the hydrolysis of dipeptides and tripeptides by bovine PcpI showed that the enzyme displays much higher affinity for the latter substrates (Cummins and O'Connor, 1996; Kilbane *et al.*, 2007). Similarly to prokaryotic homologues, mammalian type I Pcps also exhibit absolute requirement for thiol-reducing agents (e.g. β-mercaptoethanol, DTT or tris(2-carboxyethyl)phosphine (TCEP)) in activity assays. The reducing environment is essential for cysteine peptidases to prevent the reactive thiol group of the catalytic cysteine from oxidation. However, higher concentrations of these chemicals have inhibitory influence on the enzyme performance. PcpI activity is also diminished in a presence of reversible inhibitors such as 2-pyrrolidone and N-ethylmaleimide, sulfhydryl-blockers iodoacetate and iodoacetamide or transition metal ions including Ni^{2+}, Zn^{2+} and Cu^{2+}, (Dando *et al.*, 2003). Consequently, the latter inhibition has been seen to be partially recoverable by the addition of chelators such as ethylenediaminetetraacetic acid (EDTA) or by protein sample dialysis in order to remove the metal ions.

The ability of mammalian type I Pcps to process a variety of physiologically important molecules suggests its essential but as yet undefined role in peptide regulatory and degradation pathways. The possible functions of PcpI in a human body are further discussed in section 1.2.4.3.

1.2.4.2. Pyroglutamyl peptidase type II and serum thyroliberinase

Type II Pcp activity was first observed in synaptosomal membrane preparations of guinea pig brain (O'Connor and O'Cuinn, 1984). Since then it has been demonstrated in a variety of central nervous system tissues and appears to be preferably associated with postsynaptic membranes (Horsthemke *et al.*, 1984; Garat *et al.*, 1985; O'Leary and O'Connor, 1995). There are also PcpII activities detected in other body regions such as retina, lung or liver but none in heart, kidney and muscle (Vargas *et al.*, 1992). The enzyme is wider known as thyrotropin-releasing hormone-degrading ectoenzyme (TRHDE) as it displays very narrow substrate specificity restricted to TRH, TRH analogues and TRH-like peptides (1.2.2) (Wilk and Wilk, 1989; Gallagher *et al.*, 1997; Kelly *et al.*, 1997). The only notable exception was observed for rat and porcine brain enzyme to slowly hydrolyze pGlu-βNA, which is a substrate often used in PcpI assays (Bauer, 1994). The high degree of TRH specificity led to PcpII being considered as a neuropeptide-specific peptidase, which is an important element of the mammalian regulatory system of hypothalamic/pituitary/thyroid axis (Jeffcoate and Hutchinson, 1978; Wilk, 1986). There are reports regarding a stringent control of rat pituitary, adenohypophysial, but also liver PcpII and mRNA transcript levels by thyroid hormones and consequently the endocrine activity of TRH (Bauer, 1987, 1988; Suen and Wilk, 1989; Schomburg and Bauer, 1995).

PcpII activity has been identified both as membrane-anchored ectoenzyme, which the highest level is found in brain, and soluble serum enzyme originally referred as serum thyroliberinase (Taylor and Dixon, 1978; Bauer *et al.*, 1981; O'Connor and O'Cuinn, 1984). Concurrent analytical comparison of membrane-bound brain and liver type II Pcps with soluble serum thyroliberinase, confirmed that all of them are derived from the same gene and exhibit identical enzymatic features (Schmitmeier *et al.*, 2002). Moreover serum enzyme is generated *via* proteolytic processing of the particulate liver counterpart. An interesting discovery has been reported by the Chavez-Gutierrez group regarding production of truncated PcpII isoform (PPII*) in rat tissues (Chavez-Gutierrez *et al.*, 2005). PPII* mRNA species are derived from alternative transcript processing resulting in generation of a shorter and inactive enzyme version which lacks a part of the C-terminal domain. The formation of covalent PcpII-PcpII* heterodimers has been found to reduce peptidase performance and is considered to represent a mode of catalytic activity control.

The human enzyme consists of 1024 amino acids and the relatively sparse sequence differences between species are localized in a region C-terminal to the transmembrane domain (Schomburg *et al.*, 1999). PcpII, like many surface peptidases, functions as homodimer of a relatively large molecular mass of subunit of around 116 kDa (Bauer, 1994). A mutational study showed that the homodimerization occurs through the interchain disulfide bridge formed of two Cys68 residues of each subunit, located closely to the membrane-spanning domain (Papadopoulos *et al.*, 2000). This covalent linkage, however, seems not to be important for enzyme activity and trafficking to the cell surface.

PcpII is a glycosylated metalloenzyme with a zinc ion being essential for catalytic activity and has been classified in M1 family of peptidases (Czekay and Bauer, 1993; Rawlings *et al.*, 2010). The extracellular catalytic domain is well conserved among mammalian homologues and has been associated with the unusually narrow TRH hydrolysis specificity (Schomburg *et al.*, 1999). Isolation of cDNA encoding human PcpII and deduction of the amino acid sequence has enabled identification of 12 putative N-glycosylation sites as well as a characteristic consensus motif of the zinc-dependent metallopeptidases $HEXXHX_{18}E$ (Schomburg *et al.*, 1999). This motif coordinates the Zn^{2+} ion within the catalytic centre (Vallee and Auld, 1990). Additionally the extracellular domain contains eight cysteine residues that are believed to be necessary to maintain an active protein structure (Papadopoulos *et al.*, 2000). The study showed that PcpII can be inhibited by chelating agents such as 1,10-phenanthroline, 8-hydroxyquinoline and EDTA, but its activity is not affected by specific PcpI inhibitors (Cummins and O'Connor, 1998).

1.2.4.3. Physiological role of pyroglutamyl peptidase

The physiological role of PcpI, mainly due to its broad substrate specificity, still remains unclear. Since the enzyme activity is widely distributed and relatively high in tissues such as liver, kidney or skeletal muscles, it has been considered to play a significant role in peptide catabolism to free amino acids (Awade *et al.*, 1994; Cummins and O'Connor, 1998). This may also include the regulation of free cellular pGlu level and its consequent biological implications (1.2.2). Awade and co-workers also suggested that PcpI could play a detoxification role because high concentrations of

pGlu-containing peptides are cytotoxic and could abnormally acidify the cytoplasm (Awade *et al.*, 1994). A similar role has been suggested for prokaryotic Pcps in order to detoxify and assimilate nutrients from the external environment. PcpI could also participate in the absorption of peptides and proteins from the alimentary tract; this may be supported by the fact that the enzyme is found in the intestinal mucous membrane, duodenum and in small intestine (Albert and Szewczuk, 1972). A recent study showed that natural gluten peptides possess an N-terminal pGlu residue (Monsuur *et al.*, 2006). Moreover the *pcp* gene is located in close proximity to the genes associated with coeliac disease susceptibility. However, the involvement of the Pcp enzymatic activity in the disease aetiology and pathology has been excluded.

Analysis of PcpI levels in rat retina and hypothalamus exposed to environmental light and dark conditions resulted in observations that the peptidase levels fluctuate periodically that implicates a possible association with the daily biological clock (Sanchez *et al.*, 1996). Elevated PcpI activity has been observed in the spinal cord of patients suffering from motor neuron disease (Shaw *et al.*, 1996). The condition is characterised by the deposition of ubiquitinated proteins in degenerating spinal cord nerve cells that also implicates a potential role of the peptidase in associated protein degradation. Contrary to that, the level of Pcp activity is decreased in human breast cancer and dysregulated in N-methyl nitrosourea-induced breast cancer that may suggest possible contribution of the enzyme towards initiation and progression of the pathology (Carrera *et al.*, 2005).

PcpI ability to process a variety of physiologically important peptides suggests its potential but as yet undefined role in regulatory and degradation pathways in the central nervous system (CNS). The role of PcpI in the TRH degradation process has been studied. This showed that treatment of primary hypothalamic cell cultures with PcpI inhibitor, Z-Gly-Pro-CHN_2, results in elevated levels of TRH (Faivre-Bauman *et al.*, 1986). Later, however, it was suggested that PcpI involvement may be marginal as the enzyme inhibition by pGlu-diazomethylketone does not significantly affect the TRH concentration either *in vivo* or *in vitro* (Charli *et al.*, 1987). Moreover, immunoblot analysis confirmed the cytosolic localization of PcpI in pituitary gland cells, which are the target of TRH (Abe *et al.*, 2004). This finding suggests that the enzyme may not contribute to TRH hydrolysis since neuropeptides are thought not to access the cytosol. Interestingly, studies show that the K_m values for TRH hydrolysis are similar for both

mammalian PcpI and PcpII which indicates equivalent substrate affinity between both enzymes (Gallagher and O'Connor, 1998; Schomburg *et al.*, 1999; Abe *et al.*, 2004).

The cytosolic location of PcpI precludes its involvement in extracellular peptide catabolism. Cummins and co-workers have suggested therefore that PcpI may be a part of the intracellular degradation mechanism which counteracts an excessive production and secretion of neuropeptides (Cummins and O'Connor, 1998). This may happen in the case of suppression of neuropeptide-synthesising cells. The other proposal assumes that such peptides released from ageing or damaged vesicles may be returned back to the cell, supply amino acid pool and be re-incorporated into biosynthetic pathways (O'Cuinn *et al.*, 1990). Intracellular peptidases have been observed to undergo significant changes during brain development and, regarding this, PcpI has also been proposed to participate in maturation of the cerebellum and brain cortex (de Gandarias *et al.*, 1998). Lastly, a potential involvement of brain pyroglutamyl peptidase activity in the propensity of amyloid peptides is a particularly striking matter (He and Barrow, 1999). The formation of insoluble deposits consisting of pGlu-containing Aβs is a prominent feature in Alzheimer's pathology. Therefore the study of the linkage between the disease origin and physiological role of both PcpI and PcpII activities in brain seems to be particularly interesting for Alzheimer's therapy.

1.2.5. Application of pyroglutamyl peptidases

The presence of the N-terminal pGlu group is very problematic during the preparation of peptides for sequencing *via* Edman degradation procedure (Edman and Begg, 1967). Therefore, enzyme preparations, such as calf liver PcpI, are found commercially useful for peptide and protein unblocking to enable sequencing by this method (Leone *et al.*, 2011). Detection of Pcp activity is commercially applied in bacterial diagnostic, since the enzyme is not present in all of the strains (Mulczyk and Szewczuk, 1970). Analytical tests using chromogenic and fluorogenic pGlu substrates have been developed for differentiation of Enterobacteriacea, Staphylococci and other species (Mulczyk and Szewczuk, 1970, 1972; Facklam *et al.*, 1995).

Particularly archaeal Pcps seem to be an interesting enzymatic tool due to their enhanced thermostability as they could be utilized in reaction conditions that are unfavourable for mesophilic homologues. They could be employed in conventional chemical synthesis where pGlu is introduced to the peptides and proteins as a protecting group and then needs to be specifically removed. Thermostable enzymes are more resistant to organic solvents, which are used in such reactions. Contrary to that, *in vitro* instability of wild type mammalian PcpI counterparts is problem, which decreases their potential applicability in peptide processing (Mtawae *et al.*, 2008).

1.3. Aims of project

The aims of this project included:

- Stability and structural study on human PcpI
- Overexpression and structural study on human PcpII
- Comparative study on localisation and distribution of PcpI and PcpII in human AD and normal brain tissues
- Involvement of PcpI in processing of pGlu-modified Aβ peptides

Chapter 2 – General Materials and Methods

2.1. Reagent grade chemicals and equipment

All enzymes and reagents used in molecular biology were obtained from Promega Ltd, Fermentas or New England BioLabs. General reagents used for the preparation of buffers and solutions were obtained from Sigma Aldrich (UK) and Melford Laboratories Ltd (unless otherwise stated) and were of the best available quality. Double distilled (ddH_2O; Neptune, Purite Ltd) and autoclaved (Priorclave Compact 60, Priorclave Ltd) water was used for the preparation of the solutions for DNA and enzyme reactions. All purification columns employed in chromatography were obtained from Amersham Biosciences and were used and stored according to the manufacturer's instructions.

2.2. Growth media and antibiotics

2.2.1. Luria-Bertani broth (LB)

25 g of LB broth powder (Melford Laboratories Ltd) was dissolved in 1 L of ddH_2O (Purite Ltd) and sterilized in the autoclave for 20 min at 120ºC and 15 psi (Priorclave Compact 60, Prioclave)**.** An appropriate antibiotic (2.2.4) was added to the cooled media prior to use.

2.2.2. Selective agar plates

15 g of bacteriological agar (Agar No.1, Oxoid) was dissolved in 1 L of LB broth (2.2.1) and autoclaved for 20 min at 120ºC and 15 psi. An appropriate antibiotic (2.2.4) was added to the cooled liquid agar (~50ºC) and it was poured into Petri dishes (90 mm diameter) and left until solid. Plates with set agar were stored at 4ºC and warmed up to 37^{o}C prior to use.

2.2.3. SOC medium

Premade SOC medium was obtained from Invitrogen and was used in the final step of cell transformation with DNA substrate (2.7.1). The composition of the medium per 1 L was as follows:

2%	tryptone
0.5%	yeast extract
10 mM	NaCl
2.5 mM	KCl
10 mM	MgCl2•6H2O
20 mM	glucose

2.2.4. Antibiotics and other basic solutions

Solutions of the antibiotics, isopropyl-β-D-thiogalactopyranoside (IPTG) and 5-bromo-4-chloro-3-indolyl-β-D-galacto-pyranoside (X-gal) were prepared using autoclaved ddH_2O or reagent grade ethanol (Fisher Scientific UK Ltd) and sterilized by filtration using Minisart NML syringe filters (Sartorius UK). Next the solutions were aliquoted and stored at -20^{o}C. Stock concentrations of antibiotics, IPTG and X-gal are listed in table 2.1.

SOLUTION	STOCK CONCENTRATION	SOLVENT
Ampicillin	100 mg/ml	water
Carbenicillin	50 mg/ml	water
Chloramphenicol	35 mg/ml	ethanol
Gentamicin	20 mg/ml	water
Kanamycin	50 mg/ml	water
Tetracycline	12.5 mg/ml	70% ethanol
IPTG	1 M	water
X-gal	20 mg/ml	DMSO/DMF

Table 2.1. Concentrations of the stock solutions used in the growth media

2.3. Buffers and basic solutions

All buffers were filtered using a 0.22 μm nylon membrane filter (Whatman) and FilterSys™ FilterSystem glassware (Phenomenex). Buffer pH was adjusted at room temperature using Whatman PHA 2000 pH meter, which was calibrated immediately prior to use. Composition of buffers used in particular procedures and experiments are listed below.

2.3.1. Agarose gel electrophoresis

TAE Buffer (pH 8.0)

40 mM Tris acetate
5 mM sodium acetate
1 mM EDTA

2.3.2. SDS-polyacrylamide gel electrophoresis (SDS-PAGE)

Stacking gel	6.0%	
Acrylamide/Bis-acrylamide (30/0.8% w/v)	2.0 ml	
0.5 M Tris-HCl pH 6.8	2.5 ml	
10% (w/v) SDS water solution	1.0 ml	
10% (w/v) APS water solution	100 µl	
TEMED	10 µl	
ddH_2O	4.5 ml	
Separating gel	**12.5%**	**8.0%**
Acrylamide/Bis-acrylamide (30/0.8% w/v)	4.2 ml	2.7 ml
1.5 M Tris-HCl pH 8.8	2.5 ml	2.5 ml
10% (w/v) SDS water solution	1.0 ml	1.0 ml
10% (w/v) APS water solution	100 µl	100 µl
TEMED	10 µl	10 µl
ddH_2O	2.3 ml	3.8 ml

TEMED and APS were added to each gel solution to initiate polymerisation immediately before pouring between the glass plates.

Running buffer (pH 8.8)

5 mM Tris-HCl
0.38 M glycine
0.1% (w/v) SDS

Sample loading buffer

125 mM Tris-HCl pH 6.8
2% (w/v) SDS
20% (v/v) glycerol
0.001% (w/v) bromophenol blue
0.005% (v/v) β-Me

Coomassie Blue stain

0.05% (w/v) Coomassie Blue stain
50% (v/v) methanol
10% (v/v) acetic acid

2.3.3. Protein purification

2.3.3.1. Tris-HCl buffers (pH 7.5) – 6xHis-PcpI purification

Lysis buffer

50 mM Tris-HCl
8 mM β-Me
20 mM Imidazole
1 mM PMSF

Buffer A

50 mM Tris-HCl
8 mM β-Me

Buffer B

50 mM Tris-HCl
8 mM β-Me
1 M Imidazole

Buffer C

50 mM Tris-HCl
10 mM DTT
0.1 M NaCl
1 mM EDTA

2.3.3.2. K_2HPO_4/KH_2PO_4 buffers (pH 8.0)

Lysis buffer

50 mM K_2HPO_4/KH_2PO_4
5 mM β-Me
20 mM Imidazole
1 mM PMSF

Buffer A

50 mM K_2HPO_4/KH_2PO_4
5 mM β-Me

Buffer B

50 mM K_2HPO_4/KH_2PO_4
5 mM β-Me
1 M Imidazole

Buffer C

50 mM K_2HPO_4/KH_2PO_4
10 mM DTT
0.1 M NaCl
1 mM EDTA

2.3.3.3. Tris-HCl buffers (pH 7.5) – PcpI-6xHis purification

Lysis buffer	Buffer A	Buffer B	Buffer C
50 mM Tris-HCl	50 mM Tris-HCl	50 mM Tris-HCl	50 mM Tris-HCl
0.15 M NaCl	0.15 M NaCl	0.15 M NaCl	0.15 M NaCl
5 mM β-Me	5 mM β-Me	5 mM β-Me	10 mM DTT
20 mM Imidazole		0.5 M Imidazole	1 mM EDTA
1 mM PMSF			

2.3.3.4. Tris-HCl buffers (pH 7.5) – native PcpI purification

Lysis buffer	Buffer A	Buffer B
50 mM Tris-HCl	50 mM Tris-HCl	50 mM Tris-HCl
1.5 M $(NH_4)_2SO_4$	1.5 M $(NH_4)_2SO_4$	10 mM DTT
10 mM DTT	10 mM DTT	1 mM EDTA
1 mM EDTA	1 mM EDTA	
1 mM PMSF		

Buffer C	Buffer D
50 mM Tris-HCl	50 mM Tris-HCl
1.5 M NaCl	0.15 M NaCl
10 mM DTT	10 mM DTT
1 mM EDTA	1 mM EDTA

2.3.3.5. HEPPS buffers (pH 8.0)

Lysis buffer	Buffer A	Buffer B	Buffer C
50 mM HEPPS	50 mM HEPPS	50 mM HEPPS	50 mM HEPPS
0.1 M NaCl	0.1 M NaCl	0.1 M NaCl	0.1 M NaCl
5 mM β-Me	5 mM β-Me	5 mM β-Me	10 mM DTT
20 mM Imidazole		0.5 M Imidazole	1 mM EDTA
1 mM PMSF			

2.3.4. Activity assay

Buffer F (pH 8.0)

50 mM K_2HPO_4/KH_2PO_4
10 mM DTT
2 mM EDTA

2.3.5. In-Fusion™ cloning

TE buffer (pH 8.0)

10 mM Tris-HCl
1 mM EDTA

2.3.6. Phosphate buffered saline (PBS) buffers

PBS buffer (pH 7.4)		PBST buffer (pH 7.4)	
100 mM	Na_2HPO_4	100 mM	Na_2HPO_4
2 mM	KH_2PO_4	2 mM	KH_2PO_4
137 mM	NaCl	137 mM	NaCl
2.7 mM	KCl	2.7 mM	KCl
		0.05%	Tween

2.4. *Escherichia coli* strains

The following cloning and expression strains were used in the experimental work during this project.

2.4.1. DNA cloning strains

a) Nova Blue (Novagen)

genotype: *endA1 hsdR17(r_K^- m_K^+) supE44 thi-1 recA1 gyrA96 relA1 lac* F′[*proA*$^+$*B*$^+$ *lac*I^{q}ZΔ*M15*::Tn*10*] (Tet^R)

b) NEB 5-α (New England BioLabs)

genotype: *fhuA2*Δ*(argF-lac*I^{q}Z*)U169 phoA glnV44* Φ*80* Δ*(lac*Z*)M15 gyrA96 recA1 relA1 endA1 thi-1 hsdR17*

c) XL10-Gold® (Stratagene)

genotype: Tet^R Δ(*mcrA*)*183* Δ(*mcrCB-hsdSMR-mrr*)*173 endA1 supE44 thi-1 recA1 gyrA96 relA1 lac* Hte [F′*proAB lac*I^{q}ZΔ*M15* Tn*10* (Tet^R) Amy Cam^R]

d) OmniMAX™ 2 (Invitrogen)

genotype: F′[*pro*AB+ *lac*I^q *lac*ZΔM15 *Tn*10(Tet^R) Δ(*ccd*AB)] *mcr*A Δ(*mrr-hsd*RMS-*mcr*BC) φ80(*lac*Z) ΔM15 Δ(*lac*ZYA-*argF*) U169 *end*A1 *rec*A1 *sup*E44 *thi*-1 *gyr*A96 *rel*A1 *ton*A *pan*D

2.4.2. Protein expression strains

a) BL21-CodonPlus (DE3)-RIPL (Stratagene)

genotype: F$^-$ *omp*T *hsdS*(r_B^- m_B^-) *dcm*+ Tet^R *gal* λ(DE3) *endA* Hte [*argU proL* (Cam^R)] [*argU ileY leuW* Strep/Spec^R]

b) ArcticExpress™ (DE3)RIL (Stratagene)

genotype**:** F^- *omp*T *hsd*S(r_B^- m_B^-) *dcm*+ Tet^R *gal* λ(DE3) *endA* Hte [*cpn10 cpn60* $Gent^R$] [*argU ileY leuW* Str^R]

c) Rosetta™ 2(DE3) (Novagen)

genotype: F^- *omp*T *hsd*S_B(r_B^- m_B^-) *gal dcm* (DE3) pRARE2 (Cam^R)

d) Rosetta-gami™ 2(DE3) (Novagen)

genotype: Δ(*ara-leu*)*7697* Δ*lacX74* Δ*phoA Pvu*II *phoR araD139 ahpC galE galK rpsL* (DE3) F′[*lac*+ *lac*I^q *pro*] *gor522*::Tn*10 trxB* pRARE (Cam^R, Kan^R, Str^R, Tet^R)

e) BL21(DE3)pLysS (Promega)

genotype: F^- *omp*T *hsd*S_B (r_B^- m_B^-) *dcm gal* λ(DE3) pLysS (Cam^R)

2.5. Preparation of chemically competent cells

Chemically competent cells were prepared by treating with divalent cations using the method described by (Hanahan *et al.*, 1991). A single colony of a given *E. coli* strain was used to inoculate 10 ml of sterile LB broth (2.2.1). The culture was grown overnight at 30ºC on a shaking platform at 200 rpm (E25 Temperature-Controlled Excella™ Shaker, New Brunswick Scientific Co., Inc.). Fresh LB media (2.2.1) with appropriate antibiotic was inoculated with 1/100 v/v overnight culture. This was grown at 37ºC until an OD_{595} of 0.4 was reached. The optical density measurement was carried out in WPA Biowave CO8000 Cell Density Meter (Walden Precision Apparatus, UK). The cells were pelleted at 3000xg for 10 min at 4ºC (Harrier 18/80, Sanyo). Cells pellets were washed with 20 ml of ddH_2O to remove any contaminating antibiotics etc. and harvested again at 3000xg for 10 min at 4ºC. After that the cell pellet was gently re-suspended in 20 ml of cold 100 mM $MgCl_2$ (autoclaved stock) per 50 ml of initial culture volume and left on ice for 10 min. This was re-centrifuged at 3000xg for 10 min at 4ºC and the supernatant was discarded. The cell pellet was re-suspended in 5 ml of cold 100 mM $CaCl_2$ (autoclaved stock) per 100 ml of initial culture volume and left on ice for 2 h. Alternatively, the cells were incubated overnight which enhanced cell competency. The super competent cells were mixed with an equal volume of 40% glycerol and left on ice for 15 min. Next 50 µl cell aliquots were transferred into pre-chilled 1.5 ml tubes, immediately frozen in liquid nitrogen and stored at -80ºC. For

concurrent DNA transformations (2.7.1) fresh competent cell aliquot was taken directly prior to addition of glycerol.

2.6. Glycerol stocks

In order to preserve bacterial cultures for further applications, working glycerol stocks of given bacterial strains were prepared. 0.5 ml of 40% v/v glycerol stock (autoclaved) was placed in a sterile 1.5 ml tube and mixed with 0.5 ml of the required overnight *E. coli* culture. This was flash frozen in liquid nitrogen and stored at -80ºC. Cell glycerol stocks were then directly used to inoculate liquid LB media (2.2.1).

2.7. Techniques used during work with DNA samples

2.7.1. DNA transformation into competent cells

An appropriate amount of plasmid DNA was added to 50 µl aliquots of competent bacterial cells that were thawed on ice (2.5) (Hanahan, 1983). Competent cell samples were incubated on ice for 20 min followed by heat shock treatment at 42ºC for 45 s in a bench unstirred water bath (Grant Instruments Ltd) and then further incubated on ice for 2 min. 150 µl of pre-warmed LB or SOC media (2.2.1 and 2.2.4, respectively) was added to each aliquot and incubated at 37ºC for 1 h in a shaking incubator (E25 Temperature-Controlled Excella™ Shaker, New Brunswick Scientific Co., Inc.). Transformed cells were plated out onto Petri dishes containing agar with selective antibiotic (2.2.4). This was incubated overnight at 37ºC.

2.7.2. Plasmid preparation

Overnight *E. coli* cloning strain cultures harbouring the desired plasmid were harvested at 4ºC, 3000xg for 15 min in a cooling centrifuge (Harrier 18/80, Sanyo). The cell pellet was further subjected to plasmid extraction using the GeneJET™ Plasmid Miniprep kit (Fermentas) and GenElute^{TM} Plasmid Maxiprep (Sigma-Aldrich) kit according to the manufacturers' instructions.

2.7.3. DNA purification

Plasmid DNA obtained from mini- or maxipreparation (2.7.2) or a polymerase chain reaction (PCR) product, was purified and concentrated using the SureClean Plus kit (Bioline, UK) protocol in order to remove any contaminants such as buffer constituents, primers, non-specifics or enzymes. If the sample did not have to be quantitated, a pink synthetic polyacrylamide co-precipitant was used in order to facilitate visualization of cleaned-up nucleic acids. The SureClean Plus method is based on ethanol precipitation and is suitable if purified DNA is required for sequencing or cloning.

2.7.4. DNA quantitation

DNA concentration was determined on the basis of absorbance measurement at 260 nm using WPA UV-1101 Biotech Photometer (Walden Precision Apparatus, UK) or NanoDrop 8000 micro-volume UV-Vis spectrophotometer (Thermo Scientific). The protein contamination was estimated according to the absorbance ratio A_{260}/A_{280}. A280 was frequently used to measure protein concentration. A ratio of $A_{260}/A_{280} > 1.8$ indicates little protein contamination in a DNA sample (Sambrook *et al.*, 1989).

2.7.5. DNA digestion

Restriction enzyme cleavage of plasmid or PCR products was conducted to confirm the presence of the desired DNA fragments or to prepare DNA for subsequent cloning. The technique employs one or more restriction enzymes to selectively cut DNA strands into shorter fragments. Two different digestion methods were used – slow (2.7.5.1) and fast (2.7.5.2). Composition of the digestion reaction mixtures and protocol details are presented below. The results of the digestion were analyzed using DNA gel electrophoresis (2.7.8).

2.7.5.1. Double digestion reaction – slow method

A digestion reaction was carried out at 37ºC for 3 h. The suitable buffer was chosen according to directions of the 4-CORE® Buffer System (Promega) to maintain 100% activity for the used restriction enzymes. The reaction mixture composition is shown below.

x µl	0.5 µg/µl DNA (plasmid or PCR product)
1 µl	10 U first restriction enzyme
1 µl	10 U second restriction enzyme
2 µl	10x restriction enzyme buffer
0.2 µl	10 µg/µl BSA (bovine serum albumin)
to a final volume of 20 µl	ddH_2O

2.7.5.2. Double digestion reaction – fast method

The digestion reaction was carried out using the FastDigest® system (Fermentas) at 37ºC for 15 min. The reaction mixture composition is shown below.

x µl	0.5 µg/µl DNA (plasmid or PCR product)
1 µl	10 U first FastDigest® restriction enzyme
1 µl	10 U second FastDigest® restriction enzyme
2 µl	10x FastDigest® buffer
0.2 µl	10 µg/µl BSA
to a final volume of 20 µl	ddH_2O

2.7.6. DNA dephosphorylation

Linearized cloning vector (2.7.5) was dephosphorylated at the 5′ end with Antarctic Phosphatase (isolated from a recombinant *E. coli* source, New England BioLabs) in order to prevent its recircularization before ligation with insert DNA (2.7.7). The composition of the dephosphorylation reaction mixture is presented below.

x µl	1-5 µg/µl plasmid DNA
1 µl	5 U Antarctic Phosphatase
1 µl	10x Antarctic Phosphatase reaction buffer
to a final volume of 10 µl	ddH_2O

The reaction was carried out for 15 min at 37ºC and heat-inactivated for 5 min at 65ºC.

2.7.7. DNA ligation

Linearized (2.7.5) and dephosphorylated (2.7.6) plasmid DNA was joined with prepared insert DNA using the T4 DNA ligase (isolated from bacteriophage T4, Promega). The ratio of plasmid to insert DNA was varied if necessary. The composition of ligation reaction mixture is presented below.

1 µl	0.5-1 µg/µl plasmid DNA
x µl	insert DNA
1 µl	5 U T4 DNA ligase
1 µl	10x T4 DNA ligase reaction buffer
to a final volume of 10 µl	ddH_2O

The reaction was carried out for 1 h at 25°C or overnight at 4°C. The sample was heat-inactivated for 10 min at 65ºC and the reaction mixture used for transformation into competent cells (2.7.1).

2.7.8. DNA gel electrophoresis

2.7.8.1. Agarose gel preparation

The required amount of electrophoresis grade agarose (Melford labs, UK) was dissolved in TAE buffer (2.3.1) to make a 1% or 2% solution in case of an analytical or preparative procedure, respectively. The agarose suspension was heated in a microwave until completely melted. The agarose solution was cooled down and 1 µl of ethidium bromide was added to a final concentration of 0.1 µg/ml. This was poured into a horizontal electrophoresis casting plate with a fixed well-forming comb. The gel was left to solidify for about 30 min before using. Once set it was immersed into TAE buffer in the electrophoresis tank (Mini-Sub® CellGT, Bio-Rad UK).

2.7.8.2. Running and visualisation of gels

The DNA samples to be analyzed were mixed with 5x DNA loading buffer (Bioline, UK) and loaded into the agarose gel wells. To estimate the size of DNA, Hyperladder™ I and Hyperladder™ IV DNA markers (Bioline, UK) were applied, which allow for quantification of the fragments ranging from 200 bp to 10 kb and 100 bp – 1 kb, respectively (figure 2.1). The gel was run at 80-100V (PowerPac Basic power supply, Bio-Rad UK) for approx. 45 min or until dyes in the gel had reached the required distance. Next the gel was removed from the tank, visualized at 312 nm and documented using a Bio-Doc-H™ UV transilluminator (UVP).

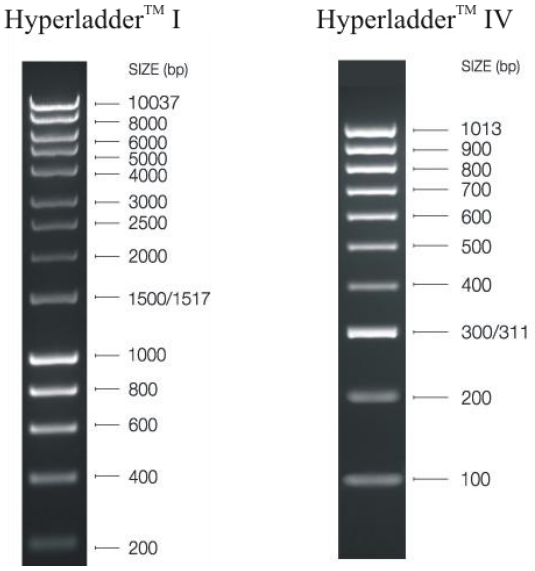

Figure 2.1. DNA markers Hyperladder™ I and Hyperladder™ IV (Bioline, UK) used for the estimation of DNA fragments size. Taken from www.bioline.com.

2.7.9. DNA gel extraction

Gel extraction was carried out as a method of selective DNA isolation. DNA samples were run using 2% agarose gel electrophoresis (2.7.8). The extraction was performed using the silica-membrane-based DNA purification method with the QIAquick Gel Extraction kit (Qiagen UK) following the manufacturer's instruction.

2.7.10. DNA sequencing

Standard sequencing of assayed DNA was conducted by Source BioScience UK Ltd using vector specific T7 or custom primers. All purified plasmid samples were supplied either as 100 ng/µl water solution or 1 µg air dried pellet.

2.8. Techniques used during work with protein samples

2.8.1. Protein extraction

The method of protein extraction from bacterial cells was chosen depending on the overexpression scale. The detergent-based method (2.8.1.1) was used for small volume culture growth (100 ml) designed for qualitative determination of protein overexpression. The sonication method (2.8.1.2) was applied for larger culture volumes of 1 L and above designed mainly for protein purification.

2.8.1.1. Detergent-based method

In order to extract the desired protein, pelleted bacterial cells were lysed with BugBuster® 10x Protein Extraction Reagent (Novagen), which was previously diluted in a suitable buffer of pH 8.0. The reagent is composed of Tris-buffer based mixture of non-ionic and zwitterionic detergents that enhance cell wall perforation with the avoidance of protein damage. A 25 U/µl Benzonase® Nuclease (Novagen) was added to the cell extract in order to reduce the viscosity. The whole procedure for the protein extraction was carried out according to the manufacturer's instructions.

2.8.1.2. Sonication

The bacterial cell pellets were carefully resuspended in 10 volumes (w/v) of cold lysis buffer (2.3.3) and incubated at room temperature for 30 min. Serine protease inhibitor phenylmethylsulfonyl fluoride (PMSF) and 2 µl of 25 U/µl Benzonase® Nuclease (Novagen) were added to the lysis buffer immediately before the resuspension of the pellet. A beaker containing the bacterial cell suspension was placed on ice and kept there during the ultrasound treatment procedure. Sonication was carried out using a bench mounted ultrasonic disintegrator (MSE Soniprep 150, Sanyo). A titanium probe was immersed in the suspension and the manifold sonication was conducted at a frequency of 10 kHz and in ten 10 s blasts. This technique allows for a rapid cell disruption and protein liberation by the application of the high frequency sonic energy. A disadvantage of the sonication technique is a possibility of protein damage due to its oxidation by the free radicals, singlet oxygen species and hydrogen peroxide, which may be concomitantly synthesized in the foam bubbles. Therefore, the procedure was carried out with high attention to avoid foaming of the protein suspension. In the next step the extract was centrifuged at 4ºC, 12000xg and for 20 min (GS-15R Centrifuge, Beckman). The supernatant was decanted for further protein purification.

2.8.2. SDS-Polyacrylamide Gel Electrophoresis (SDS-PAGE)

Protein samples were analysed using SDS-PAGE in denaturating conditions (Laemmli, 1970). The purpose of this technique is to separate proteins according to their electrophoretic mobility and molecular weight.

2.8.2.1. Acrylamide gel preparation

Two glass plates, combs and a casting frame were fixed into the casting stand (Mini-PROTEAN Tetra system, Bio-Rad UK). The separating gel (2.3.2) was poured into the casting chamber to about 2 cm below the top of the shorter plate. The desired density of separating gel was obtained by varying the concentration of the crosslinking acrylamide/bisacrylamide solution. Next, 1 ml of ddH_2O was added on top of the gel

to prevent drying and it was left to solidify. Once the gel had polymerized, water was removed and a 4% stacking gel (2.3.2) was poured on top of the separating gel and left to set for 1 h.

2.8.2.2. Protein samples preparation

All protein samples to be analyzed were mixed with sample loading buffer (2.3.2) with a 2:1 ratio and then heat-treated at 95ºC for 10 min in a bench Dri-Block® heater (DB-2A, Techne) to ensure denaturation of the proteins. The samples were spun down for 2 min at room temperature at the maximum speed in a bench microcentrifuge (MiniSpin®, Eppendorf, UK).

2.8.2.3. Molecular weight standards

Identification of desired protein and assessment of its molecular mass was facilitated with Precision Plus Protein™ (Bio-Rad UK) and BenchMark™ His-Tagged (Invitrogen) molecular weight markers presented in figure 2.2.

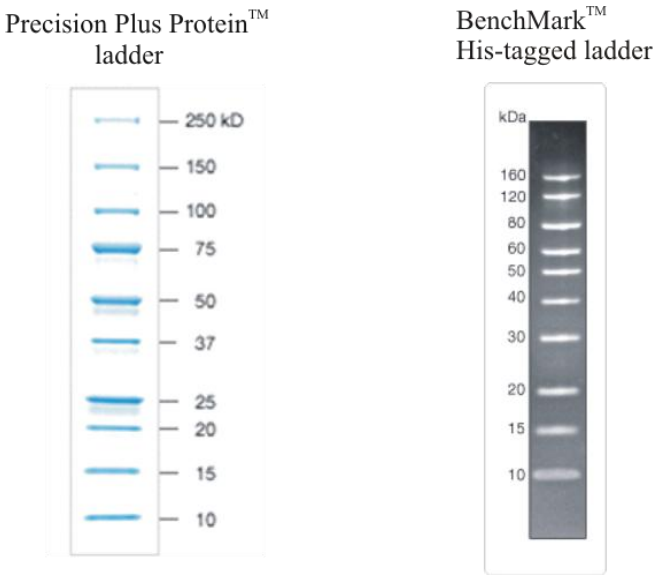

Figure 2.2. Precision Plus Protein™ (Bio-Rad) and BenchMark™ His-Tagged (Invitrogen) protein molecular weight standards allowing quantification of protein sizes ranging from 10 kDa to 250 kDa and form 10 kDa to 160 kDa, respectively. The figures were taken from www3.bio-rad.com and www.invitrogen.com.

2.8.2.4. Running and visualisation of gels

The gel casting frame was fixed in the electrode assembly and inserted into the vertical electrophoresis apparatus (Bio-Rad UK)**.** The internal reservoir was filled with running buffer (2.3.2). Gel wells were precisely cleaned of acrylamide remnants with the running buffer. Next, prepared protein samples (2.8.2.2) along with molecular weight marker were slowly loaded into the wells in predetermined order using a 100 µl Hamilton syringe (Hamilton, USA). Then the outer compartments of the casting frame were filled up with running buffer. The electrophoresis was run at 30 mA (PowerPac 300 power supply, Bio-Rad UK) until the dye front reached the bottom of the gel (approx. 1 h). When finished the apparatus was disassembled and the gel was submerged in Coomassie Blue stain (2.3.2) and heated in a microwave oven for 3 min. The stain was replaced with ddH_2O and the gel de-staining was continued in a microwave for 20 min. The gel was visualized on a bench white light transilluminator and documented in Perfection V30 scanner (Epson).

2.8.3. Determination of protein concentration

2.8.3.1. Measurement of A_{280}

The concentration of purified protein was determined using the standard measurement of absorbance at 280 nm (Warburg and Christian, 1942) in WPA UV-1101 spectrophotometer (Walden Precision Apparatus, UK). The protein extinction coefficient was determined with the ProtParam tool using the ExPASy proteomics server (Expert Protein Analysis System, www.expasy.org, (Gasteiger *et al.*, 2003)) on the basis of amino acid sequence.

2.8.3.2. The Bradford assay

The protein concentration at all stages of purification was determined using the Bradford assay (Bradford, 1976). In this method Coomassie Brilliant Blue G-250 dye binds selectively to arginine and aromatic residues, which has a consequence in a shift of absorbance maximum from 470 nm to 595 nm. Protein samples were mixed with ready-to-use Bio-Rad Protein Assay (Bio-Rad UK) solution according to the manufacturer's instructions. A linear range of BSA solutions from 0.1 to 2.0 mg/ml were used to produce a standard curve. The absorbance at 595 nm was measured using a WPA UV-1101 spectrophotometer (Walden Precision Apparatus, UK).

2.8.4. Fluorometric enzyme activity assay

The 6xHis-PcpI activity was assayed on the basis of the modified protocol by Browne and O'Cuinn and utilized L-pyroglutamyl-7-amido-4-methylcoumarin (L-pGlu-AMC) as the enzyme substrate (figure 2.3) (Browne and O'Cuinn, 1983). For the assay each 25 µl protein sample was placed in a separate well of 96-well fluorometer microplate and this was done in triplicate. Next, each protein sample was mixed with 100 µl of 250 µM pGlu-AMC in buffer F (2.3.4) and incubated at 37ºC for 30 min. The reaction was terminated by the addition of 100 µl of 1.5 M acetic acid. The negative control was prepared by the addition of acetic acid to the protein sample prior to mixing with pGlu-AMC. Detection of liberated product (7-amino-4-methylcoumarin, AMC, figure 2.3) was analysed in Infinite® 200 microplate reader (TECAN) with excitation at 370 nm and emission read at 440 nm. The readings were visualised using associated i-control™ software (TECAN). A standard curve was prepared using the fluorometric readings from a range of AMC solutions with concentrations between 0 to 400 µM and is presented in appendix V.

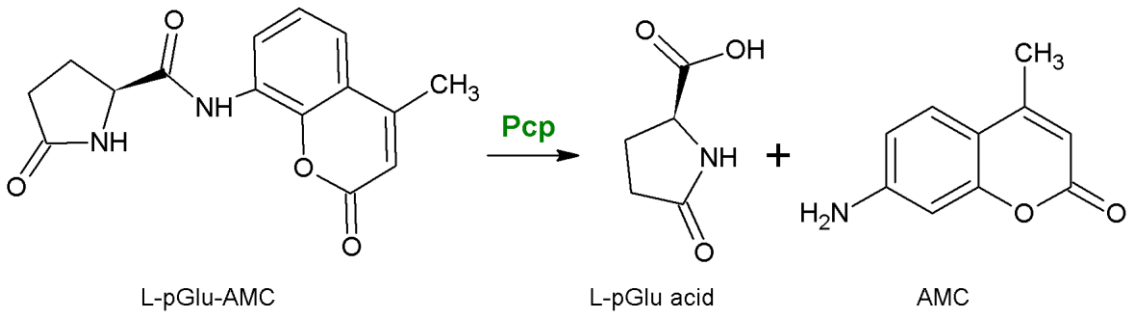

Figure 2.3. The reaction of the enzymatic hydrolysis of L-pyroglutamyl-7-amido-4-methylcoumarin (L-pGlu-AMC) by Pcp liberating free L-pGlu acid and 7-amino-4-methylcoumarin (AMC).

2.8.5. Dynamic Light Scattering

The polydispersity and aggregation state of the protein in a solution was evaluated using the dynamic light scattering (DLS) technique (Proteau *et al.*, 2010). The principle of DLS uses the properties of scattered light to measure the rate of diffusion of protein particles. This is further processed to establish a size distribution for the sample. The molecular weight of a particle is determined from its Stokes radius or a hydrodynamic radius (MW-R) which depends on the conformation, size and density. This technique shows to be particularly useful in identification of trace amounts of an aggregated protein (0.1% estimated % mass).

The purified protein sample (~1.0 mg/ml) was centrifuged at 13,400xg at 4ºC and then the supernatant was gently pipetted into a UV quartz cuvette and left to incubate for 10 min. The measurements were conducted at room temperature in DynaPro™ DLS instrument (Wyatt Technology) and ddH_2O was used to set solvent parameters. Collected data were analysed and viewed using Dynamics 6.7.3 software (Wyatt Technology).

2.8.6. Western blotting

The gel obtained in the SDS-PAGE was transferred to a nitrocellulose membrane using iBlotter (Invitrogen) at 100V for 1 h according to the manufacturer's instructions. Next, the membrane was blocked for 30 min in a PBST buffer (2.3.6) containing 5% milk powder. This was replaced with a 1:500 solution of a mouse anti-His_6 Mab primary antibody (R&D systems) and incubated for 2 h at room temperature. The membrane was washed with PBST buffer (3x 10 min) and subsequently incubated in a 1:5000 solution of a goat anti-mouse-horseradish peroxidase-coupled secondary antibody (Pierce) for 1 h at room temperature. Next, the membrane was washed with PBST buffer (3x 10 min). In order to visualise the protein, the membrane was covered with 2 ml of ECL-Plus™ reagent (GE Health care), incubated for 5 min and then analysed and documented using a Xograph imaging apparatus (Xograph Healthcare).

Chapter 3 – Studies on human pyroglutamyl peptidase I

3.1 Human PcpI

Human pyroglutamyl peptidase type I is placed in the C15 peptidase family of the MEROPS classification (Rawlings *et al.*, 2010). The enzyme functions as a cysteine ω-exopeptidase, which specifically removes the N-terminal pyroglutamyl group from peptide and protein substrates. It also exhibits a strict requirement for thiol-reducing agents in order to maintain its catalytic activity (2.1.3). In vertebrates, the highest level of PcpI was found in liver and kidney, but it can be also localised in many other tissues such as skeletal muscle, cerebral cortex, pituitary or renal proximal tubules (Cummins and O'Connor, 1998). Studies show that the native mammalian enzymes appear to exist as soluble monomeric proteins with a low protein sequence similarity (below 30%) to their dimeric or tetrameric prokaryotic counterparts. The first X-ray crystal structure of a Pcp enzyme was reported for *T. litoralis* (Singleton *et al*., 1999) followed by *B. amyloliquefaciens* (Odagaki *et al.*, 1999), *P. furiosus* (Tanaka *et al*., 2001) and *P. horikoshii* (Sokabe *et al*., 2002). However, as yet there is no structural information on any eukaryotic PcpI despite the fact that its activity has been demonstrated from a broad range of plant and animal sources (Cummins and O'Connor, 1998). No peptidase gene sequence has yet been identified in any of the yeast or fungal genomes. Mammalian representatives which were purified and characterised so far include human, murine and bovine type I Pcps (Dando *et al.*, 2003; Kilbane *et al.*, 2007). Multiple reports indicate that mammalian enzymes have comparable biochemical features to other type I Pcps, but are relatively unstable *in vitro* (Dando *et al.*, 2003; Kilbane *et al.*, 2007; Mtawae *et al.*, 2008).

This chapter presents experimental work on the native and recombinant human PcpI enzymes regarding their overexpression, purification and crystallisation trials. Site-directed mutagenesis, chemical modification of the protein and screening for optimal buffer conditions were additionally conducted towards the improvement of human PcpI stability *in vitro*.

3.2. Preparation of human PcpI

The amino acid sequences of the native and recombinant human PcpI forms were used to determine the protein parameters using the bioinformatical tools available on the ExPASy server (www.expasy.org, (Gasteiger *et al.*, 2003)). Experimental pI was estimated using isoelectric focusing by S. Connelly (Connelly, 2006). The peptidase with N-terminal hexahistidine affinity tag, C-terminal tag and native protein are named as 6xHis-PcpI, PcpI-6xHis and PcpI, respectively. The amino acid sequence and parameters are presented in table 3.1. Although all known mammalian sequences contain a putative NAS glycosylation site (table 3.1), to date studies have not considered that the active form of the enzyme is glycosylated (Cummins and O'Connor, 1998).

PcpI protein sequence:

MGSS**HHHHHH**SSGLVPRGSH (N-terminal His-tag)
MEQPRKAVVVTGFGPFGEHTVNASWIAVQELEKLGLGDSVDLHVYEIPVE
YQTVQRLIPALWEKHSPQLVVHVGVSGMATTVTLEKCGHNKGYKGLDNC
RFCPGSQCCVEDGPESIDSIIDMDAVCKRVTTLGLDVSVTISQDAGRYLCDF
TYYTSLYQSHGRSAFVHVPPLGKPYNADQLGRALRAIIEEMLDLLEQSEGK
INYCHKH

(C-terminal His-tag) KLAAALQ**HHHHHH**

	6xHis-PcpI	native PcpI	PcpI-6xHis
Length (aa)	229 aa	209 aa	222 aa
Molecular weight (Da)	25301.7 Da	23138.3 Da	24657.0 Da
Experimental pI	6.30	5.55	not determined
Theoretical pI	6.12	5.54	6.08
Extinction coefficient	24410	24410	24410

Table 3.1. Amino acid sequence and biophysical parameters of human native and His-tagged PcpI. The native protein sequence is shown in black font and both N-terminal and C-terminal His-tag sequences are shown in blue. The potential N-glycosylation motif NAS is highlighted in orange. The parameters were computed using bioinformatic tools in the ExPASy server (www. expasy.org, (Gasteiger *et al.*, 2003)) and the experimental pI was established by S. Connelly within his PhD project (Connelly, 2006).

3.2.1. Materials and methods

The cDNA encoding human PcpI was obtained *via* PCR amplification from a human pituitary gland cDNA library and was previously supplied by Cambridge Bioscience Ltd (UK). The re-cloning into a pET-28a(+) (appendix I) expression vector and initial work on recombinant human PcpI had been conducted by S. Connelly as a part of his PhD project (Connelly, 2006). The *E. coli* BL21(DE3)pLysS (2.4.2) carrying the recombinant vector pET-28a(+)/*pcpI* had been stored as glycerol stocks at -80ºC and were used in further work. The pET-28(+) vectors enable the production of the proteins with either an N-terminal or a C-terminal hexahistidine tag, which facilitates their selective purification using nickel affinity chromatography.

Both recombinant and native PcpI were overexpressed in selected *E. coli* cells. Initial purification procedure of 6xHis-PcpI was based on the protocol applied in the PhD project by S. Connelly (Connelly, 2006).

3.2.1.1. Preparation of pET-28a(+)/*pcpI* recombinant plasmid

3.2.1.1.1. Minipreparation of pET-28a(+)/pcpI recombinant plasmid

For the plasmid minipreparation procedure 10 ml of fresh LB media containing 50 μg/ml kanamycin and 30 μg/ml chloramphenicol was inoculated with a glycerol stock of the *E. coli* BL21(DE3)pLysS cells (2.4.2) harbouring the recombinant pET-28a/*pcpI*. This was incubated overnight at 37ºC in a shaking incubator. Next the pET-28a(+)/*pcpI* was extracted according to the protocol of GeneJET™ Plasmid Miniprep kit (Fermentas) (2.7.2). The result of the minipreparation was determined by a double digestion with *Nde*I and *Not*I restriction enzymes (2.7.5.1) followed by agarose gel electrophoresis (2.7.8). The recombinant plasmid sample was further purified (2.7.3), quantified (2.7.4) and sequenced using standard T7 primers (2.7.10).

3.2.1.1.2. Maxipreparation of pET-28a(+)/pcpI recombinant plasmid

The *E. coli* NovaBlue (Novagen) competent cells (2.4.1) were transformed with prepared pET-28a(+)/*pcpI* (2.7.1) in order to obtain a higher quantity of the DNA. The cells were plated on the Petri dishes containing agar (2.2.2) with 50 μg/ml kanamycin and incubated overnight at 37ºC**.** A single colony was used to inoculate 10 ml of LB media containing 50 μg/ml kanamycin and this was grown overnight at 37ºC in a shaking incubator. Next day 1 ml of the *E. coli* culture was transferred to 100 ml of LB media containing 50 μg/ml kanamycin and was grown at 37ºC until the OD_{595} reached 2.0. The pET-28a(+)/*pcpI* extraction was carried out using the GenElute^{TM} Plasmid Maxiprep kit (Sigma-Aldrich) (2.7.2). The result of the maxipreparation was determined by a double digestion with *Nde*I and *Not*I restriction enzymes (2.7.5.1) followed by 1% agarose gel electrophoresis (2.7.8). The recombinant plasmid sample was further purified (2.7.3) and quantified (2.7.4).

3.2.1.2. Overexpression of 6xHis-PcpI

3.2.1.2.1. Preparation of chemically competent cells

Preliminary overexpression of 6xHis-PcpI was performed in the *E. coli* BL21-CodonPlus®(DE3)-RIPL strain (2.4.2) obtained from Stratagene. The strain cells are engineered to produce extra copies of *argU, ileW, leuY* and *proL* tRNAs that recognize rare arginine, isoleucine, leucine and proline codons. This has been designed in order to overcome rare *E. coli* codon bias problems and therefore enable an efficient high-level expression of proteins from heterologous organisms compared to conventional BL21 strains. Comparison of codon usage in *Escherichia coli* and *Homo sapiens* is presented in table 3.2. A lack of suitable codons causes depletion of the internal host tRNA pools. This can result in delayed translation leading to codon substitutions and misincorporations that affect the functional properties of the protein.

ORGANISM	AGG arginine	AGA arginine	CUA leucine	AUA isoleucine	CCC proline
Escherichia coli	1.2	2.1	3.9	4.4	5.5
Homo sapiens	11.4	11.5	6.5	6.9	20.0

Table 3.2. Comparison of codon frequencies in *Escherichia coli* and *Homo sapiens*. The frequency is described as the number of codons per thousand of total. A higher number indicates more significant bias between human and *E. coli* tRNA pools. Based on data taken from www.stratagene.com.

The *E. coli* BL21-CodonPlus®(DE3)-RIPL cells were made competent according to the general chemical procedure described in section 2.5. Competent cell aliquots were directly used for the transformation procedure (2.7.1) or stored as glycerol stocks at -80ºC (2.6).

3.2.1.2.2. Screening for optimal overexpression conditions

The *E. coli* BL21-CodonPlus®(DE3)-RIPL competent cells (3.2.1.2.1) were transformed with the pET-28a(+)/*pcpI* plasmid (3.2.1.1) following the protocol described in section 2.7.1. The cells were plated on Petri dishes containing 50 μg/ml kanamycin and 35 μg/ml chloramphenicol and incubated overnight at 37ºC. Next a single colony was used to inoculate 10 ml of LB media supplemented with 50 μg/ml kanamycin and 35 μg/ml chloramphenicol and this was grown overnight at 37ºC in a shaking incubator. Next day 8 flasks containing 100 ml of LB media with the above antibiotics were inoculated each with 1 ml of the overnight culture and grown in a shaking incubator at 37ºC. The induction of the protein overexpression was initiated by the addition of IPTG (2.2.4) to a final concentration of 1 mM. At this point cultures were continued to grow at 25ºC (4 flasks with cultures induced at an OD_{595} of 0.6, 0.8, 1.0 and 1.2, respectively) and 37ºC (4 flasks with cultures induced at an OD_{595} of 0.6, 0.8, 1.0 and 1.2, respectively). Samples for the protein overexpression analysis were collected from each flask prior to induction with IPTG as well as after 4 h, 6 h and overnight incubation. Protein isolation was carried out according to the detergent-based

procedure (2.8.1.1) and the results of the protein expression were analysed using the SDS-PAGE technique with a 12.5% separating gel (2.8.2).

3.2.1.3. Purification of 6xHis-PcpI

3.2.1.3.1. Production of 6xHis-PcpI

The optimal conditions for 6xHis-PcpI production in BL21-CodonPlus®(DE3)-RIPL cells were established on the basis of protein overexpression screening in small scale culture growth (3.2.1.2.2). The *E. coli* BL21-CodonPlus®(DE3)-RIPL carrying pET-28a(+)/*pcpI* were grown overnight at 37ºC in 10 ml LB media containing 50 μg/ml kanamycin and 35 μg/ml chloramphenicol in a shaking incubator. Next day this was used as a starting inoculation culture for six flasks containing 1 L of LB with the above antibiotics and was further grown at 37ºC in a shaking incubator until an OD_{595} of 0.6 had been reached. At this point the expression of the 6xHis-PcpI was induced by the addition of IPTG to a final concentration of 1 mM. The incubation was continued for a further 6 h at 25ºC and after that the cells were harvested by centrifugation at 6000xg for 20 min. The cell pellet was stored at -20ºC.

3.2.1.3.2. Protein extraction

For protein purification purpose the cell paste (3.2.1.3.1) was resuspended in 10 volumes of Tris-HCl lysis buffer (2.3.3.1). The cell lysate was subjected to a protein extraction procedure using the sonication technique (2.8.1.2). The result of 6xHis-PcpI overexpression was analysed by the SDS-PAGE technique using a 12.5% separating gel (2.8.2).

3.2.1.3.3. Nickel affinity chromatography

Immobilized metal-ion affinity chromatography (IMAC) is one of the most efficient and popular methods of protein purification. His-tagged protein molecules are retained on the resin through the specific coordinative bond between histidines and immobilized ions such as nickel, cobalt or copper. Then bound material can be eluted by the application of competitive molecules (e.g. imidazole) or a change in pH.

The XK 26/20 column packed with the Ni^{+} Sepharose^{TM} resin (Amersham Biosciences) was pre-equilibrated with three column volumes of Tris-HCl buffer A (2.3.3.1). Then the crude supernatant obtained after protein isolation (3.2.1.3.2) was loaded onto the column using an injection superloop (GE Healthcare). This was washed with three column volumes of buffer A (2.3.3.1) to remove unbound proteins. Next three column volumes of buffer B (2.3.3.1) were introduced over a gradient of 0-100% to elute remaining, bound proteins. Both buffers A and B contained β-mercaptoethanol, as 6xHis-PcpI was reported to exhibit a strong requirement for thiol-reducing agents in order to maintain its activity (2.1.3). An elution buffer B also contains imidazole, which acts as a binding competitor for nickel ions. During purification 5 ml elution fractions were collected over the entire elution volume and the whole procedure was carried out at a flow rate of 3 ml/min. On the basis of the elution profile appropriate fractions were analysed for protein presence and purity by the SDS-PAGE technique using a 12.5% separating gel (2.8.2). Protein samples were stored at 4ºC.

3.2.1.3.4. Gel filtration chromatography

All fractions which contained 6xHis-PcpI collected after nickel column purification (3.2.1.3.3) were pooled together. The protein solution was concentrated by the gradual addition of ammonium sulfate to the saturation of 80%. The mixture was stirred gently for 2 h or more at 4ºC and then the precipitated protein was pelleted by centrifugation at 13500xg for 30 min. Next the pellet was resuspended in Tris-HCl buffer C (2.3.3.1). This was applied onto a Superdex^{TM} 200 Hi-load 16/60 gel filtration column (Amersham Biosciences) which was pre-equilibrated with buffer C. The protein sample was eluted with 120 ml (one column volume) of buffer C at a flow rate of

0.5-1.0 ml/min. Over the entire filtration process 1.5 ml fractions were collected and later analysed for protein purity using the SDS-PAGE technique using a 12.5% separating gel (2.8.2). The concentration of the purified protein sample was determined *via* absorbance measurement at 280 nm as described in section 2.8.3.1. The extinction coefficient for 6xHis-PcpI was calculated as 24410 M^{-1} cm^{-1} (ProtParam, www.expasy.org). Protein samples were stored at 4ºC. The calibration curve for the HiLoad™ 16/60 Superdex™ 200 column is shown in appendix IV.

3.2.1.3.5. Protein activity

The activity of 6xHis-PcpI was assayed after each purification step using the fluorometric method described in section 2.8.4.

3.2.1.3.6. Modifications to the purification procedure of 6xHis-PcpI

Significant instability of 6xHis-PcpI in Tris-HCl based purification buffers was a serious difficulty as the protein could not be used in subsequent experiments such as crystallisation studies. Preliminary attempts to overcome this problem were focused on minor alterations in the content of purification buffers and observation how they influence the protein's behaviour. List of applied modifications is presented in table 3.3.

MODIFICATION		PURPOSE
Buffer additives	0.15 M NaCl	maintains ionic strength of buffer, improves protein solubility (Dominy *et al.*, 2002)
	50 mM L-Arg	reduces hydrophobic interactions, improves protein solubility and stability (Guilloteau *et al.*, 1996; Golovanov *et al.*, 2004)
	50 mM L-Glu	
	0.5% Triton X-100	improves protein solubility (Choi *et al.*, 2005)
	5% glycerol	improves protein stability (Vagenende *et al.*, 2009)
K_2HPO_4/KH_2PO_4 based buffers pH 8.0 **(**2.3.3.2)		alternative to Tris-HCl buffer, reported to be used in purification of human and bovine PcpI (Kilbane *et al.*, 2007; Mtawae *et al.*, 2008)

Table 3.3. List of additives and modifications used in the buffers for the 6xHis-PcpI purification in order to improve protein stability.

3.2.1.4. Cloning of PcpI cDNA for production of PcpI-6xHis and native PcpI

The incorporation of a polyhistidine affinity tag has become one of the most commonly used methods to facilitate efficient protein purification. Its advantage lies mainly in relatively small length, which is believed to have no or little effect on a protein's structure or activity compared to a more bulky appendage, such as GST (glutathione S-transferase), CBP (calmodulin-binding protein) or MBP (maltose-binding protein). It has applications in experiments requiring high yields of at least partially purified material that can be carried out at a low cost. The Ni-NTA (nickel-nitrilotriacetic acid) resins used for purification of His-tagged proteins are amongst the least expensive ones along with MBP or GST columns (Lichty *et al.*, 2005). However, studies show that the potential influence of the His-tag and its localisation on the macromolecule folding and purification yield cannot be excluded (Woestenenk *et al.*, 2004; Eschenfeldt *et al.*, 2010; Spadiut *et al.*, 2010). Sometimes, if experimental work with the protein becomes problematic due to its instability or insolubility, it is advisable to remove or shift the tag from one terminus to the other. The high instability of 6xHis-PcpI in solution could be a result of the enhanced flexibility of

its N-terminus extended by the extra 20 amino acid residues which contribute additional 8% to the total molecular mass. Homology modelling of human PcpI (figure 1.13) showed that its amino terminus is organised in one of the internal β-strands of the central β-sheet. The attachment of the His-tag could possibly disturb this arrangement and in fact may lead to structural disorder and in result trigger excessive aggregation and precipitation. Contrary to that the protein's C-terminus is organised in α-helix with the terminal residues exposed to the surface. Therefore it was decided to overexpress both the untagged protein (native PcpI) and the protein with C-terminal His-tag (PcpI-6xHis) in order to evaluate if these modifications could contribute to stabilisation of PcpI *in vitro* and facilitate its concentration and crystallisation.

3.2.1.4.1. PCR amplification of PcpI cDNA

PCR amplification of the cDNA encoding PcpI was conducted in the way to receive inserts for the production of the native and C-terminally His-tagged PcpI variants. Gene primers for the reactions were supplied by Eurofins MWG Operon and are listed in table 3.4.

Primer	Sequence	Restriction enzyme	GC content	T_m
native PcpI**F** (forward)	CAGCCATATGGAGCAG CCGAGGAAGGCG	*Nde*I	64.3%	72.4ºC
native PcpI**R** (reverse)	CTCGAATTCTCAGTGTTT GTGGCAATAGTTGATTTTG	*Eco*RI	37.8%	67.2ºC
PcpI-6xHis**F** (forward)	CAAACCATGGAGCAGCCGA G	*Nco*I	60%	61.4ºC
PcpI-6xHis**R** (reverse)	AGCGCAAGCTTGTG TTTGTGGCAATA	*Hin*dIII	46.2%	63.2ºC

Table 3.4. List of PCR primers used for amplification of the PcpI cDNA.

The composition of the amplification reaction mixture is presented below.

1 µl 50 ng/µl pET-28a/*pcpI*

1 µl 10 µM forward primer

1 µl 10 µM reverse primer

12.5 µl 2x GoTaq® Hot Start Green Master Mix*

9.5 µl ddH_2O

* GoTaq® Hot Start Green Master Mix (Promega) is a ready-to-use solution containing optimal concentrations of GoTaq® Hot Start Polymerase, 400 µM dNTPs, 4 mM $MgCl_2$ and 2x GoTaq® reaction buffer (pH 8.5). The GoTaq® polymerase activity is temporary blocked at temperatures below 70°C by being bound to a proprietary antibody and it can be restored by the heating for 2 min during the initial denaturation step at 94–95°C. The mix also contains blue and yellow dyes that allow monitoring of DNA run during electrophoresis.

PCR amplification was performed in a Mastercycler® thermal cycler (Eppendorf). A range of tubes containing reaction mixture was prepared and each one of them was subjected to a different annealing temperature within a set gradient. The individual steps of PCR are described in table 3.5.

Step	Temperature	Time	
Initial denaturation	96ºC	3 min	
Denaturation	96ºC	1 min	30x
Annealing	temperature gradient 55ºC – 68ºC	1 min	
Extension	72ºC	1 min	
Final extension	72ºC	7 min	
Cooling	4ºC	-----	

Table 3.5. PCR cycling steps during the reaction of amplification of the PcpI cDNA.

The result of the PCR amplification was checked by 2% agarose gel electrophoresis as described in section 2.7.8.

3.2.1.4.2. Ligation of PcpI insert with pET-28b(+) and pET-22b(+)

The PCR products obtained during the amplification of cDNA encoding human PcpI (3.2.1.4.1) were purified using the gel extraction method described in section 2.7.9. Next both inserts as well as the pET-28b(+) and pET-22b(+) plasmids were cut with suitable restriction enzymes (2.7.5.2):

- digestion with *Nde*I and *Eco*RI for the native PcpI cDNA and pET-22b(+)
- digestion with *Nco*I and *Hin*dIII for the PcpI-6xHis cDNA and pET-28b(+)

The linearized pET-28b(+) and pET-22b(+) plasmids were subsequently dephosphorylated at the 5′ end (2.7.6) and after that subjected to the ligation reaction with the *pcpI* inserts (2.7.7). Next the ligation reaction mixtures were used for transformation into *E. coli* NovaBlue competent cells (2.7.1). The transformants treated with the pET-22b(+) or pET-28b(+) mixtures were incubated overnight at 37ºC, on the agar plates (2.2.2) containing 100 μg/ml ampicillin or 50 μg/ml kanamycin, respectively.

3.2.1.4.3. Preparation of pET-28b(+)/pcpI and pET-22b(+)/pcpI recombinant plasmids

A few single *E. coli* NovaBlue colonies, obtained from the transformation with the pET-22b(+) or pET-28b(+) ligation reaction mixtures (3.2.1.4.2), were picked and used for the inoculation of 10 ml of LB media (2.2.1) containing 100 μg/ml ampicillin or 50 μg/ml kanamycin, respectively. This was grown overnight at 37ºC in a shaking incubator. Next the cultures were subjected to DNA extraction according to the protocol of GeneJET™ Plasmid Miniprep kit (Fermentas) (2.7.2). The result of the minipreparation was determined by a double digestion with *Nde*I and *Eco*RI for the pET-22b(+)/*pcpI* or with *Nco*I and *Hin*dIII for the pET-28b(+)/*pcpI* (2.7.5.2). This was followed by the agarose gel electrophoresis (2.7.8). The sample containing recombinant plasmids with inserts were further purified (2.7.3), quantified (2.7.4) and sequenced using standard T7 primers (2.7.10).

3.2.1.5. Overexpression of the PcpI-6xHis

The protocol of the overexpression of PcpI-6xHis was based on the optimal conditions previously obtained for 6xHis-PcpI (3.2.1.3.1). The *E. coli* BL21-CodonPlus®(DE3)-RIPL competent cells (3.2.1.2.1) were transformed with the pET-28b(+)/*pcpI* plasmid (3.2.1.4.3) following the protocol described in section 2.7.1. The cells were plated on Petri dishes containing agar with 50 μg/ml kanamycin and 35 μg/ml chloramphenicol. This was incubated overnight at 37ºC**.** Next a single colony was used to inoculate 10 ml of LB media supplemented with 50 μg/ml kanamycin and 35 μg/ml chloramphenicol and this was grown overnight at 37ºC in a shaking incubator. Next day a flask containing 100 ml of LB media with the above antibiotics was inoculated with 1 ml of the overnight culture and grown in a shaking incubator at 37ºC. The induction of the protein overexpression was initiated by the addition of IPTG (2.2.4) to a final concentration of 1 mM once the culture has reached the OD_{595} of 0.6. The incubation was continued for a further 6 h at 25ºC. Protein isolation was carried out according to the detergent-based procedure (2.8.1.1) and the results of the protein expression were analysed using the SDS-PAGE technique using a 12.5% separating gel (2.8.2).

3.2.1.6. Overexpression of the native PcpI

The protocol for the overexpression of the native PcpI was based on the optimal conditions previously obtained for 6xHis-PcpI (3.2.1.3.1). The *E. coli* BL21-CodonPlus®(DE3)-RIPL competent cells (3.2.1.2.1) were transformed with the pET-22b(+)/*pcpI* plasmid (3.2.1.4.3) following the protocol described in section 2.7.1. The cells treated with pET-22b(+)/*pcpI* were plated on Petri dishes containing agar with 100 μg/ml ampicillin and 35 μg/ml chloramphenicol. This was incubated overnight at 37ºC. Next a single colony was used to inoculate 10 ml of LB media supplemented with 100 μg/ml ampicillin and 35 μg/ml chloramphenicol and this was grown overnight at 37ºC in a shaking incubator. The next day a flask containing 100 ml of LB media with the above antibiotics was inoculated with 1 ml of the overnight culture and grown in a shaking incubator at 37ºC. The induction of the protein overexpression was initiated by the addition of IPTG (2.2.4) to a final concentration of 1 mM once the culture has

reached the OD_{595} of 0.6. The incubation was continued for further 6 h at 25ºC. Protein isolation was carried out according to the detergent-based procedure (2.8.1.1) and the results of the protein expression were analysed by the SDS-PAGE technique using a 12.5% separating gel (2.8.2).

3.2.1.7. Purification of the PcpI-6xHis

The protein production and purification steps for the PcpI-6xHis were exactly the same as for 6xHis-PcpI and consisted of nickel affinity chromatography (3.2.1.3.3) and gel filtration chromatography (3.2.1.3.4). In this case however, lysis and purification buffers were enriched with 0.15 M NaCl as it was observed to improve protein solubility. The content of the buffers is presented in section 2.3.3.3. Collected fractions were analysed for protein purity by the SDS-PAGE technique using a 12.5% separating gel (2.8.2). The concentration of purified protein was determined by the absorbance measurement at 280 nm as described in section 2.8.3.1. Extinction coefficient for PcpI-6xHis was calculated as 24410 $M^{-1}cm^{-1}$ (ProtParam, www.expasy.org). The activity of PcpI-6xHis was assayed after each purification step using the fluorometric method described in section 2.8.4. Protein samples were stored at 4ºC.

3.2.1.8. Purification of the native PcpI

3.2.1.8.*1. Production and extraction of the native PcpI*

The *E. coli* BL21-CodonPlus®(DE3)-RIPL carrying pET-22b(+)/*pcpI* were grown overnight at 37ºC in 10 ml LB media containing 50 μg/ml ampicillin and 35 μg/ml chloramphenicol in a shaking incubator. Next day this was used as a starting inoculation culture for six flasks containing 1 L of LB with the above antibiotics and was further grown at 25ºC in a shaking incubator until OD_{595} of 0.6 had been reached. At this point the expression of PcpI was induced by the addition of IPTG to a final concentration of 1 mM. The incubation was continued for 6 h at 25ºC and after that the cells were harvested by centrifugation at 6000xg for 20 min. The cell pellet was stored at -20ºC. The extraction of the native PcpI was conducted exactly the same way as for 6xHis-PcpI (3.2.1.3.2).

3.2.1.8.*2. Phenyl Sepharose chromatography*

The application of hydrophobic chromatography for purification is very useful when dealing with non-tagged proteins. The protein to be purified is brought into a high ionic strength (high salt content) buffer, which facilitates binding between the hydrophobic protein surface and the column matrix. The bound proteins can be gradually eluted using a reverse gradient with a buffer of low ionic strength (e.g. lower salt concentration).

The XK 26/20 column packed with Phenyl Sepharose^{TM} (Amersham Biosciences) was pre-equilibrated with three column volumes of Tris-HCl buffer A (2.3.3.4). Then the crude supernatant obtained after protein isolation (3.2.1.8.1) was loaded onto the column using an injection superloop (GE Healthcare). The column was washed with three column volumes of buffer A (2.3.3.4) to remove unbound material. Next three column volumes of buffer B (2.3.3.4) were introduced over a gradient of 100-0% to elute remaining, bound proteins. During purification 5 ml elution fractions were collected over the entire elution volume and whole procedure was carried out at a flow rate of 3 ml/min. On the basis of the elution profile appropriate fractions were analysed for the presence of protein and purity by the SDS-PAGE technique using a 12.5% separating gel (2.8.2). Protein samples were stored at 4ºC.

3.2.1.8.*3. Ion-exchange chromatography*

At a pH different from isoelectric point (pI) given proteins become differentially charged and this feature is used during ion-exchange chromatography. The purified material in low ionic strength buffer can be retained on the column matrix through the electrostatic interactions between charged surface residues and the oppositely charged matrix in the column. Next the bound proteins can be gradually eluted through a gradient with a buffer of an increased ionic strength (e.g. high salt concentration).

The XK 26/20 column packed with the FFS-Sepharose^{TM} (cation exchange column, Amersham Biosciences) was pre-equilibrated with three column volumes of Tris-HCl buffer B (2.3.3.4). Then the pooled fractions containing PcpI, obtained after Phenyl Sepharose^{TM} chromatography (3.2.1.8.2) were loaded onto the column using an

injection superloop (GE Healthcare). The column was washed with three column volumes of buffer B (2.3.3.4) to remove unbound material. Next three column volumes of buffer C (2.3.3.4) were introduced over a gradient of 0-100% to elute remaining, retained proteins. During purification 5 ml elution fractions were collected over the entire elution volume and the whole procedure was carried out at a flow rate of 3 ml/min. On the basis of elution profile appropriate fractions were analysed for the presence of protein and purity by the SDS-PAGE technique using a 12.5% separating gel (2.8.2). Protein samples were stored at 4ºC.

3.2.1.8.*4. Gel filtration chromatography*

All fractions which contained native PcpI collected after cation exchange purification (3.2.1.8.3) were pooled together. The protein solution was concentrated by the gradual addition of ammonium sulfate to 80% saturation. The mixture was stirred gently for 2 h or more at 4ºC and then the precipitated protein was pelleted by centrifugation at 13500xg for 30 min. Next the pellet was resuspended in Tris-HCl buffer D (2.3.3.4). This was applied onto Superdex^{TM} 200 Hi-load 16/60 gel filtration column (Amersham Biosciences) which was pre-equilibrated with buffer D. The protein sample was eluted with 120 ml (one column volume) of buffer D at a flow rate of 0.5-1.0 ml/min. Over the entire filtration process 1.5 ml fractions were collected and later analysed for protein purity by the SDS-PAGE technique using a 12.5% separating gel (2.8.2). The concentration of purified protein sample was determined by the absorbance measurement at 280 nm as described in section 2.8.3.1. The extinction coefficient for the native PcpI was calculated as 24410 $M^{-1}cm^{-1}$ (ProtParam, www.expasy.org). Protein samples were stored at 4ºC.

3.2.1.8.*5. Protein activity*

The activity of the native PcpI was assayed after each purification step using the fluorometric method described in section 2.8.4.

3.2.1.9. DLS analysis of the native PcpI and PcpI-6xHis

The polydispersity and aggregation state of both the native PcpI and PcpI-6xHis was assayed directly after gel filtration step using the DLS method as described in section 2.8.5. Both samples were centrifuged and kept on ice before the measurement.

3.2.1.10. NDSB additives

Non-detergent sulfobetaines (NDSBs) are zwitterionic compounds containing a charged sulfobetaine hydrophilic group and a short hydrophobic group (figure 3.1). An important advantage of NDSBs is the fact that they do not possess large hydrophobic structures which make them difficult to form micelles and hence they are not classified as detergents. They were also shown to have no or little effect on enzymatic activity. Multiple reports confirm that the addition of NDSBs can significantly increase protein solubility, prevent aggregation and aid in refolding of proteins found in inclusion bodies or chemically and thermally denatured proteins (Vuillard *et al.*, 1995; Expert-Bezancon *et al.*, 2003; Xiang *et al.*, 2008; D'Amico and Feller, 2009). They are also very popular as the additives to assist in protein crystallisation and facilitate purification of integral membrane proteins (Willis *et al.*, 2005). However, the molecular mechanisms of their protecting action against aggregation remains poorly understood. It has been thought that the short hydrophobic chains can interact with the protein's surface regions. This may prevent undesired hydrophobic interactions and therefore aggregation, and also would explain the difference in efficiency of individual NDSBs. On the other hand over a wide pH range this group of compounds can be differentially charged and alternatively create ionic interactions with protein surface residues. Such a phenomenon could help to abolish the non-specific ionic or dipole protein-protein interactions (Vuillard *et al.*, 1995).

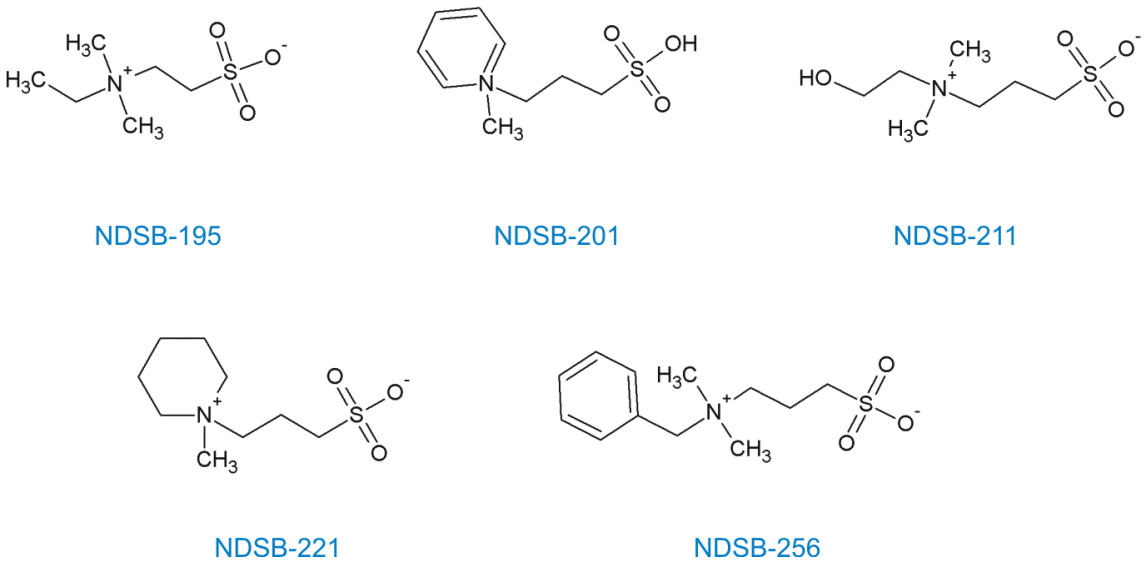

Figure 3.1. The range of NDSBs employed to improve solubility and stability of PcpI. The number by each individual compound name relates to its molecular weight.

Since there are no strict guidelines pointing to which one of the NDSBs is more efficient than the others, in order to observe their influence on the PcpI stability during the concentration process, each one of the compounds was individually tested by the addition to the purified sample of the native PcpI or PcpI-6xHis. Final concentrations of sulfobetaines NDSB-195, NDSB-201, NDSB-211, NDSB-221 or NDSB-256 in the protein solution were 0.5 M or 1.0 M. This was incubated at 4ºC for 30 min and the sample was then concentrated using a Vivaspin20 centrifugal concentrator with a 30 kDa molecular weight cut-off (Sartorius Stedim Biotech S.A.). The intention of this process was to obtain a protein concentration suitable for the initial crystallisation trials (at least 10 mg/ml).

3.2.2. Results and discussion

3.2.2.1. Preparation of pET-28a(+)/*pcpI* recombinant plasmid

The *E. coli* BL21(DE3)pLysS culture cells after overnight growth were harvested by centrifugation and subjected to pET-28a(+)/*pcpI* plasmid isolation as described in section 3.2.1.1.1. Subsequent restriction enzyme digestion (2.7.5.1) and 1% agarose gel electrophoresis (2.7.8) confirmed successful plasmid extraction and a presence of the PcpI cDNA insert. The band corresponding to the insert can be observed at approx. 630 bp as seen on the agarose gel electropherogram (figure 3.2).

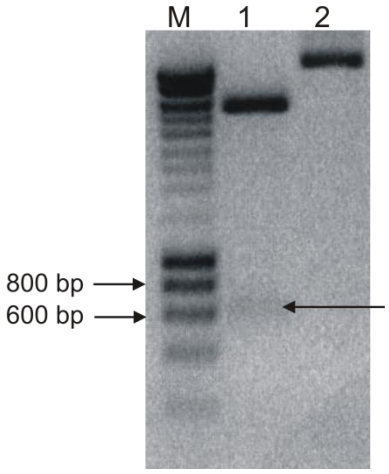

Figure 3.2. The result of agarose gel electrophoresis of pET-28a(+)/*pcpI* restriction digestion products. Individual lanes represent marker Hyperladder I (M), uncut plasmid (1) and cut plasmid (2). The insert band can be observed at approx. 630 bp.

The concentration and purity of the prepared pET-28a(+)/*pcpI* sample was determined by absorbance measurement at 260 nm as described in section 2.7.4. Plasmid DNA was sent for sequencing using the standard T7 primers (2.7.10), which confirmed the presence of the *pcpI* insert and its correct nucleotide sequence (appendix III).

Next the pET-28a/*pcpI* sample obtained from the minipreparation (3.2.1.1.1) was used for a transformation of *E. coli* NovaBlue competent cells (3.12). The culture cells after overnight growth were harvested by centrifugation and subjected to pET-28a/*pcpI* plasmid isolation as described in section 3.2.1.1.2. The plasmid DNA was cut in a double restriction digest reaction (2.7.5.1). Next the analysis by 1% agarose gel electrophoresis (2.7.8) confirmed the presence of the 630 bp of pET-28a/*pcpI* insert cDNA. The purified and quantified plasmid sample was subsequently used for the protein overexpression study.

3.2.2.2. Overexpression study of 6xHis-PcpI

Recombinant human 6xHis-PcpI was produced in BL21-CodonPlus(DE3)-RIPL, which improves the expression of rare *E. coli* codons as described in section 3.2.1.2.1. Screening for the optimal expression conditions (3.2.1.2.2) was conducted using different OD_{595} values of the growth culture before the protein synthesis was induced with IPTG, postinductory incubation temperature and the time of culture growth. The results of 6xHis-PcpI expression were determined by the SDS-PAGE technique using a 12.5% separating gel (2.8.2). Both soluble and insoluble fractions were analysed and the resulting gel pictures are presented in figures 3.3, 3.4, 3.5 and 3.6 for the induction at OD_{595} of 0.6, 0.8, 1.0 and 1.2, respectively. A calculated molecular weight of human 6xHis-PcpI is 25.3 kDa (3.1).

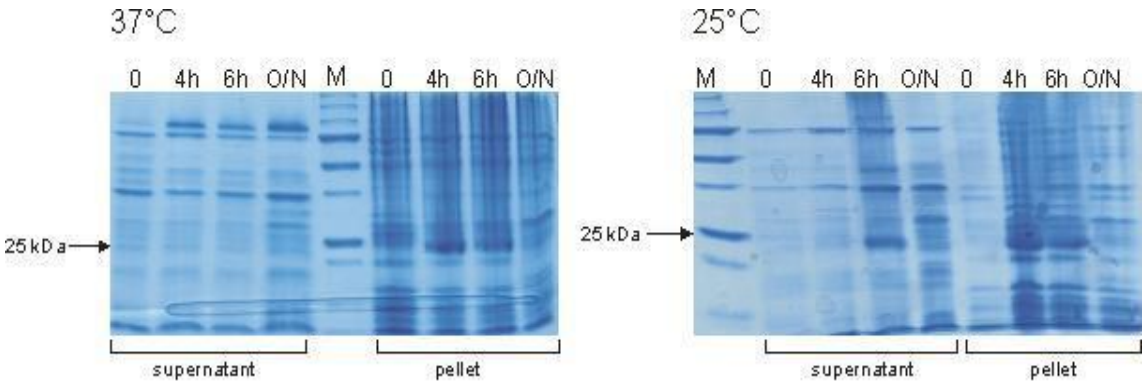

Figure 3.3. The result of SDS-PAGE analysis of 6xHis-PcpI expression induced at OD_{595} 0.6 in BL21-CodonPlus®(DE3)-RIPL cells. The supernatant and pellet fractions come from the samples collected prior to induction (0) and after 4 h, 6 h and overnight (O/N) incubation.

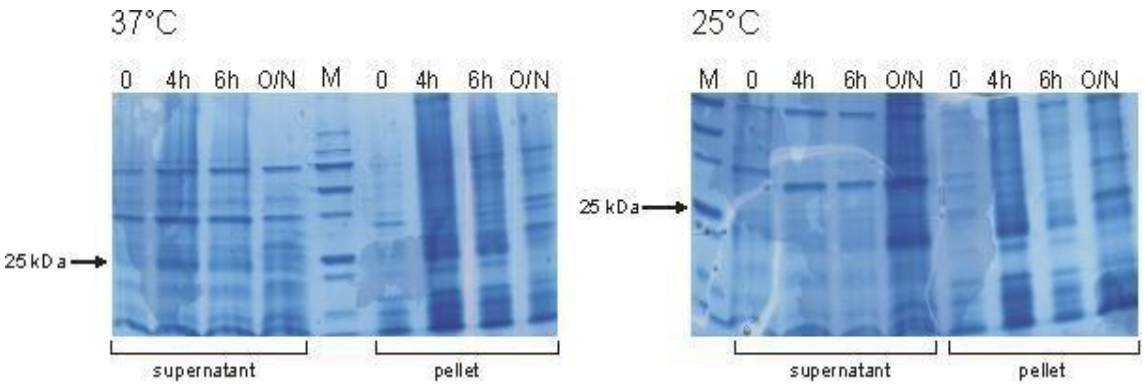

Figure 3.4. The result of SDS-PAGE analysis of 6xHis-PcpI expression induced at OD_{595} 0.8 in BL21-CodonPlus®(DE3)-RIPL cells. The supernatant and pellet fractions come from the samples collected prior to induction (0) and after 4 h, 6 h and overnight (O/N) incubation.

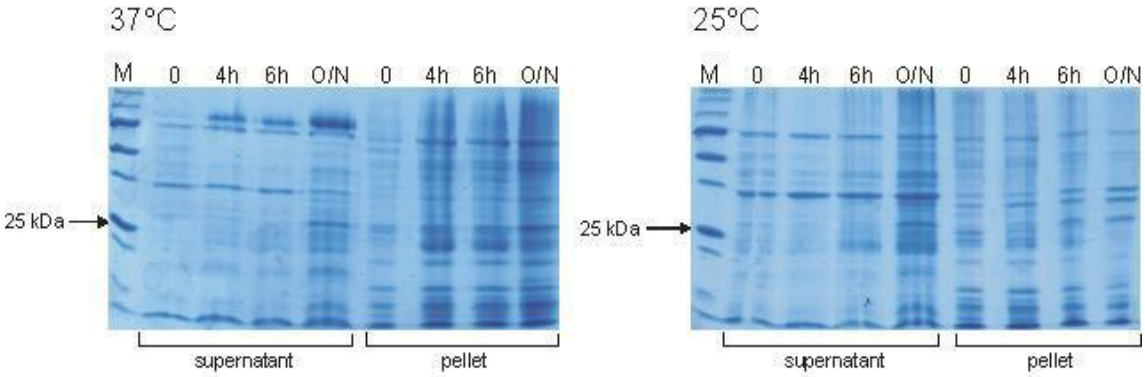

Figure 3.5. The result of SDS-PAGE analysis of 6xHis-PcpI expression induced at OD_{595} 1.0 in BL21-CodonPlus®(DE3)-RIPL cells. The supernatant and pellet fractions come from the samples collected prior to induction (0) and after 4 h, 6 h and overnight (O/N) incubation.

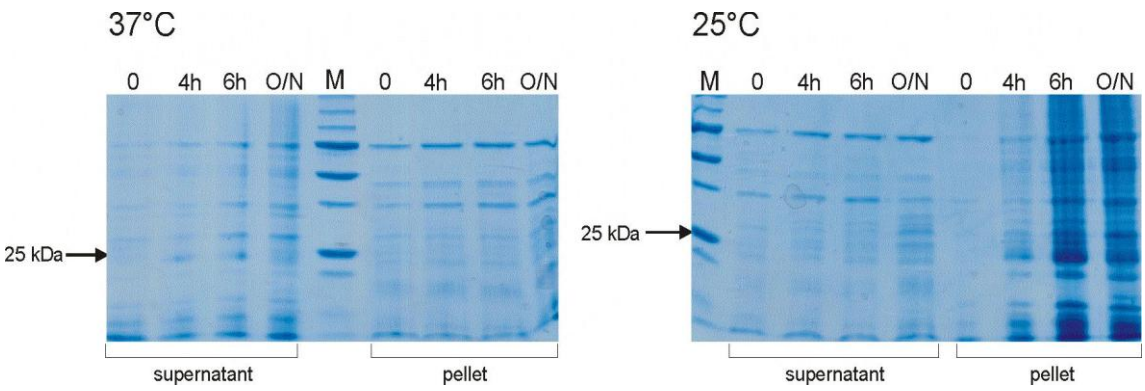

Figure 3.6. The result of SDS-PAGE analysis of 6xHis-PcpI expression induced at OD_{595} 1.2 in BL21-CodonPlus®(DE3)-RIPL cells. The supernatant and pellet fractions come from the samples collected prior to induction (0) and after 4 h, 6 h and overnight (O/N) incubation.

The overexpression of 6xHis-PcpI in BL21-CodonPlus®(DE3)-RIPL was particularly enhanced when IPTG was added at an OD_{595} of 0.6 or 0.8. In the gel representing the result of the protein expression induced at the OD_{595} of 0.6, a strong band of approx. 25 kDa can be observed. When induced at higher OD_{595} 1.0 and 1.2, protein synthesis seems to be weaker or the protein was found in the pellet fractions of cell lysate. Lower temperature **(**25°C) also positively influences 6xHis-PcpI overexpression as it slows down the cellular metabolism and may promote more stable protein-folding conformations (Battistoni *et al.*, 1992; Vasina and Baneyx, 1997)**.** However, the major drawback of such cultivation at lower temperatures is a slower rate of bacterial biomass production, so the higher yield of the desired protein can be obtained after longer period of incubation. It was decided to conduct future 6xHis-PcpI with an addition of IPTG inducer at OD_{595} of 0.6 and incubation at 25°C for 6 h.

3.2.2.3. Purification of 6xHis-PcpI

3.2.2.3.1. Production and extraction of 6xHis-PcpI

The production and extraction of 6xHis-PcpI from BL21-CodonPlus®(DE3)-RIPL was conducted as described in sections 3.2.1.3.1 and 3.2.1.3.2. After harvesting 2.5 g of bacterial cell paste was obtained from 1 L of culture. A result of 6xHis-PcpI overexpression was confirmed by the SDS-PAGE technique using a 12.5% acrylamide gel, which is presented in figure 3.7.

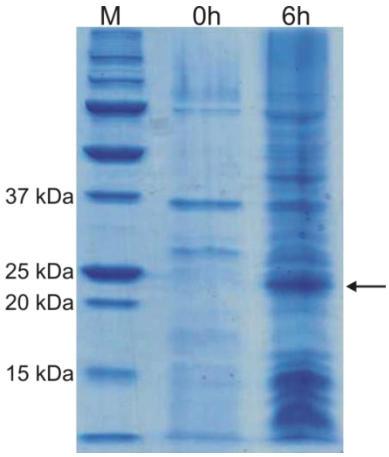

Figure 3.7. The result of SDS-PAGE confirming the overexpression of recombinant 6xHis-PcpI (approx. 25 kDa). Individual lanes represent sample 6 h after induction (6h), before induction (0h) and a protein molecular weight marker (M).

The successful production of the protein in a soluble form enabled further purification procedure using nickel affinity chromatography and gel filtration techniques.

3.2.2.3.2. Nickel affinity chromatography

The supernatant obtained after 6xHis-PcpI extraction procedure was applied to Ni^{+} Sepharose column and subjected to protein purification as described in section 3.2.1.3.3. The elution profile presented in figure 3.8 allowed for determination of

fractions containing 6xHis-PcpI, which were further analysed using SDS-PAGE to assess the purity of the eluted protein. A result of this analysis is presented in figure 3.9.

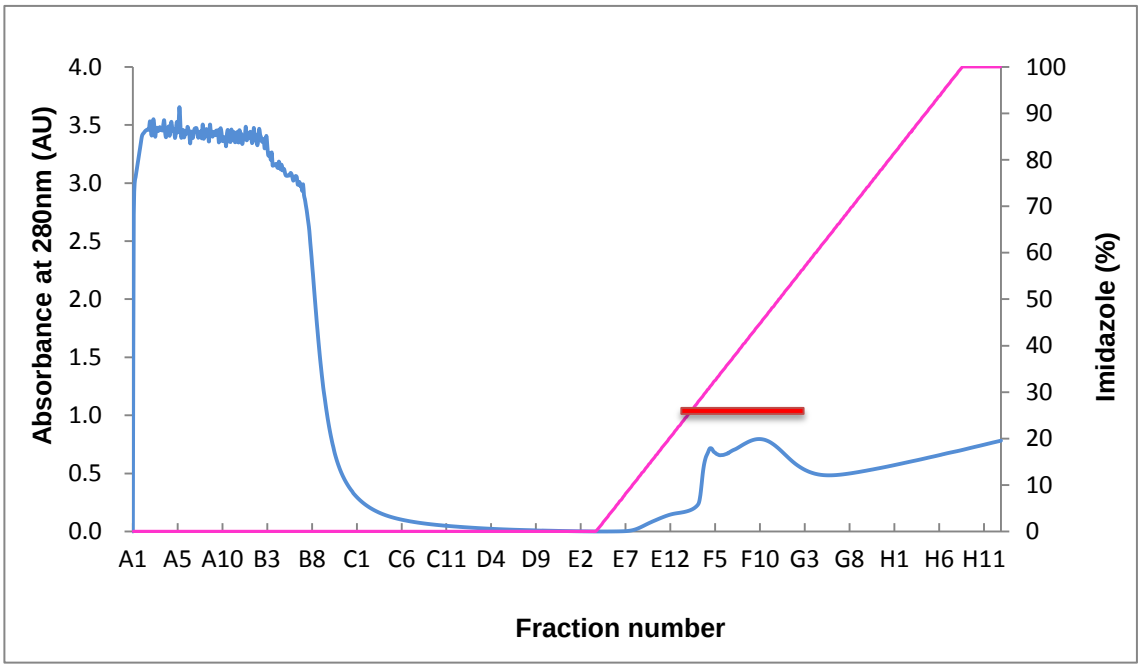

Figure 3.8. The nickel affinity protein elution profile of the human recombinant 6xHis-PcpI. The fractions containing the protein are marked by the red bar. The A_{280} trace is coloured in blue and the imidazole gradient is coloured in pink.

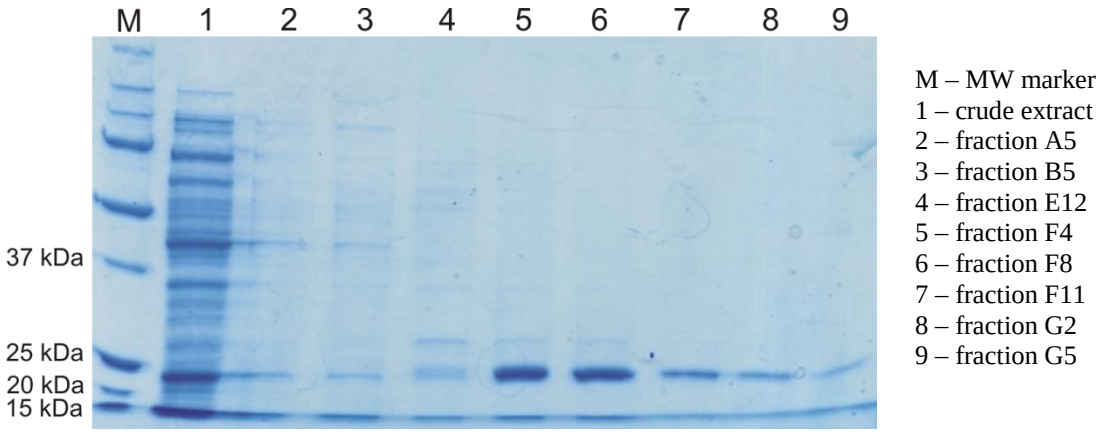

Figure 3.9. The result of the SDS-PAGE analysis of the human recombinant 6xHis-PcpI purified through nickel affinity chromatography.

As 6xHis-PcpI was not completely purified, fractions with the protein were mixed and subjected to subsequent purification steps (3.2.2.3.3).

3.2.2.3.3. Gel filtration chromatography

A high purity and homogeneity of 6xHis-PcpI was required for the purpose of crystallisation trials. In order to achieve this and remove any potential protein aggregates, the 6xHis-PcpI fractions from Ni^{+} Sepharose^{TM} column purification were pooled together. The protein sample was further subjected to the precipitation by 80% ammonium sulfate as described in section 3.2.1.3.4. A subsequent purification step was conducted using gel filtration column (3.2.1.3.4). The resulting elution profile and SDS-PAGE analysis are presented in figures 3.10 and 3.11, respectively.

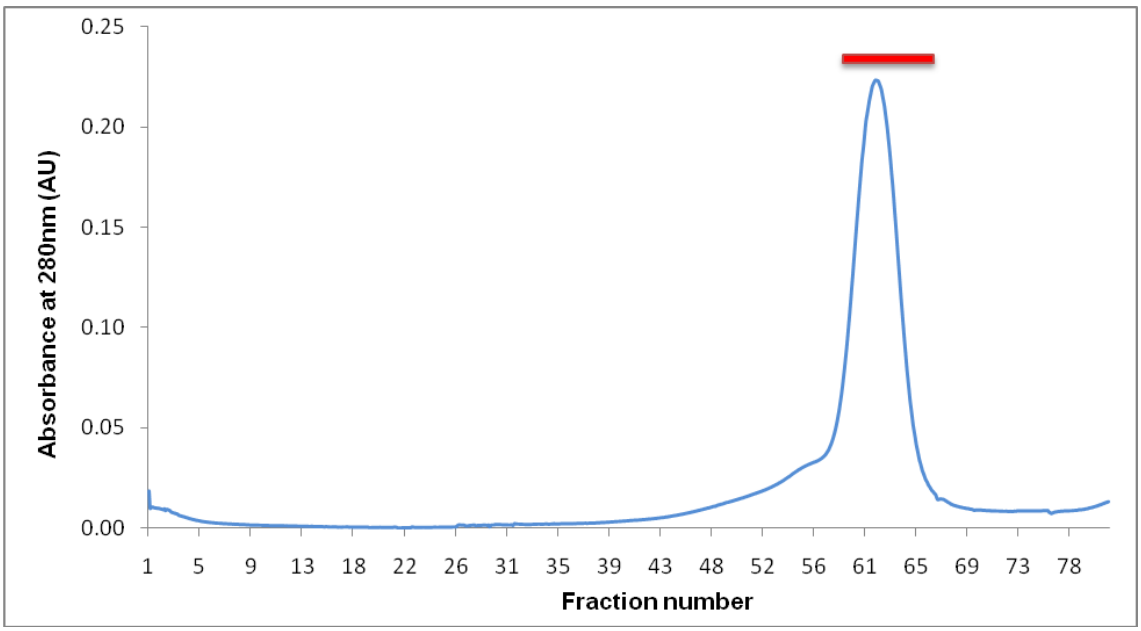

Figure 3.10. The gel filtration protein elution profile of the human recombinant 6xHis-PcpI. The fractions containing the protein are marked by the red bar. The A_{280} trace is coloured in blue.

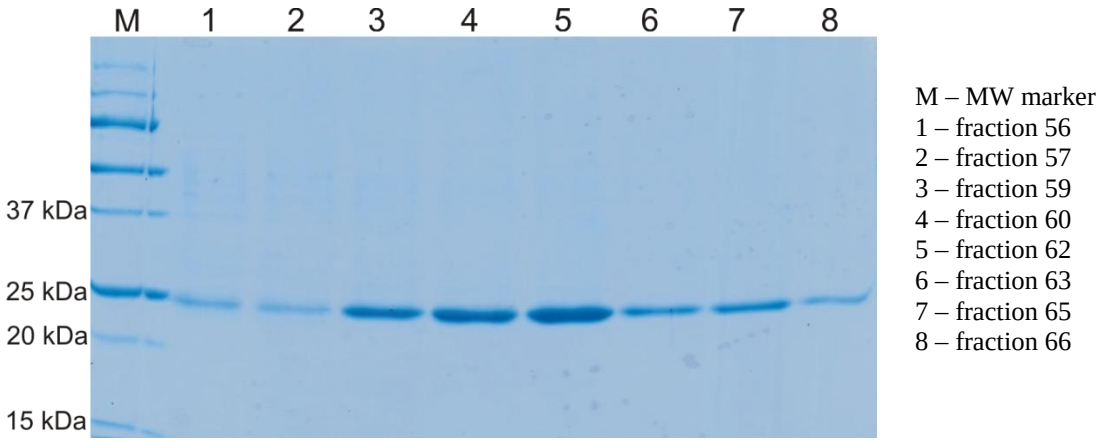

Figure 3.11. The result of SDS-PAGE analysis of the human recombinant 6xHis-PcpI purified by gel filtration chromatography.

The purification of human 6xHis-PcpI from BL21-CodonPlus®(DE3)-RIPL cell lysate was successful. As it can be seen in figure 3.11, eluted gel filtration fractions contained highly purified 6xHis-PcpI with a lack of any contaminating material. The concentration and activity after each purification step was determined using the Bradford assay and the fluorometric enzyme activity assay described in sections 2.8.3.2 and 2.8.4, respectively. The purification result is presented in the table 3.6.

Fraction	Total Protein (mg)	Total Activity (U)	Specific Activity (U/mg)	Purification Fold	% Yield
Crude Extract	783.0	284.5	0.36	1.0	100
Ni Sepharose	66.7	159.3	2.39	6.6	56
Superdex™ 200	29.5	97.7	3.31	9.1	34

Table 3.6. The purification table for human recombinant 6xHis-PcpI. All values are presented for purification from 1 L of BL21-CodonPlus®(DE3)-RIPL cell culture.

Although the purification of human recombinant 6xHis-PcpI gives a satisfying yield (34%) and purity, the protein was observed to be unstable *in vitro*. Attempts to overcome this issue were conducted and are described in section 3.2.2.3.4.

3.2.2.3.4. Modifications to purification procedure of 6xHis-PcpI

The 6xHis-PcpI was attempted to be concentrated up to minimum of 10 mg/ml necessary for the crystallisation study. This was performed at 4ºC using a Vivaspin20 centrifugal concentrator with a 30 kDa molecular weight cut-off with regenerating polyethersulfone membrane (Sartorius Stedim Biotech S.A.). Unfortunately, it was noticed that 6xHis-PcpI was extremely unstable and easily precipitated out of the solution and it could not be concentrated beyond ~0.13 mg/ml. This problem was attempted to be overcome by the application of various buffer additives known for their stabilising properties as described in section 3.2.1.3.6. None of the buffer additives, however, significantly helped to improve 6xHis-PcpI stability and the protein still appeared to precipitate out of solution. Moreover, the application of K_2HPO_4/KH_2PO_4 based buffers or the addition of Triton X-100 and glycerol resulted in the purification yield being much lower than in original buffer system. Minor improvement was observed when 0.15 M NaCl was included. Particularly, the yield from the gel filtration purification step was increased and the protein was able to be concentrated up to around 1.0 mg/ml. This has led to a decision to include 0.15 M NaCl in purification buffers for PcpI-6xHis (3.2.1.7).

The unsuccessful attempts to overcome 6xHis-PcpI instability and obtain a concentrated sample to conduct crystallisation studies it was decided to generate C-terminally His-tagged PcpI (PcpI-6xHis) and native PcpI (3.2.1.4).

3.2.2.4. Cloning of PcpI cDNA for production of PcpI-6xHis and native PcpI

3.2.2.4.1. PCR amplification of PcpI cDNA

The amplification of cDNA encoding PcpI (3.2.1.4.1) was successful and was confirmed by the 2% agarose gel electrophoresis. The positive result of the reaction was obtained over the whole range of the applied annealing temperature gradient. The bands corresponding to the inserts of the native PcpI and PcpI-6xHis can be observed at approx. 630 bp as seen on figures 3.12 and 3.13, respectively.

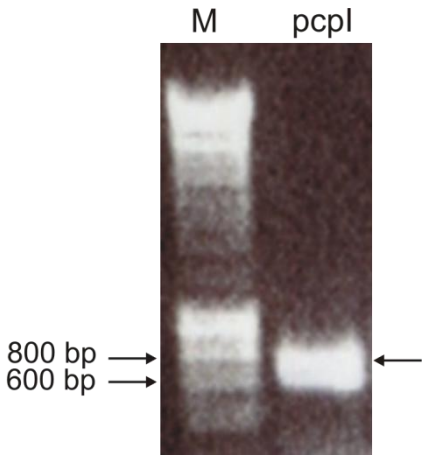

Figure 3.12. The result of the amplification of cDNA encoding human PcpI (627 bp). The insert was flanked with *Nde*I and *Eco*RI restriction sites to clone it into pET-22b(+) expression vector. M – marker Hyperladder I.

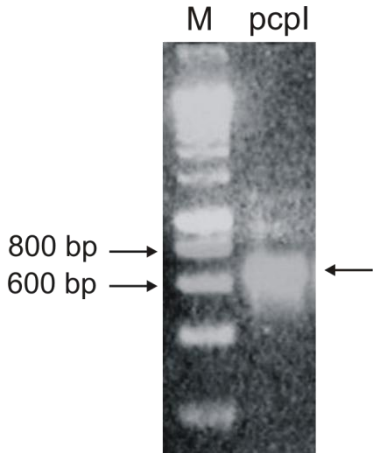

Figure 3.13. The result of the amplification of cDNA encoding human PcpI (627 bp). The insert was flanked with *Nco*I and *Hin*dIII restriction sites to clone into pET-28b(+) expression vector. M – marker Hyperladder I.

3.2.2.4.2. Ligation of PcpI insert with pET-28b(+) and pET-22b(+)and preparation of recombinant plasmids

Both ligation reactions of PcpI inserts with pET-28b(+) and pET-22b(+) (3.2.1.4.2) were successful and was confirmed by the presence of colonies carrying recombinant plasmids. Both recombinant plasmids were isolated as described in section 3.2.1.4.3. The presence of the desired inserts was shown using a double digestion reaction with suitable restriction enzymes and subsequent 1% agarose gel

electrophoresis. The results for the pET-28b(+)/*pcpI* and pET-22b(+)/*pcpI* are presented in figures 3.14 and 3.15, respectively.

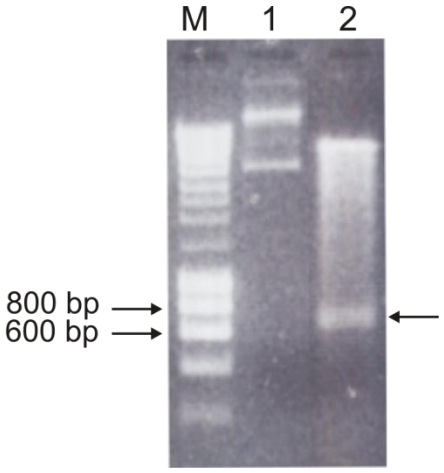

Figure 3.14. The result of agarose gel electrophoresis of pET-28b(+)/*pcpI* restriction digestion products. Individual lanes represent marker Hyperladder I (M), uncut plasmid (1) and cut plasmid (2). Insert band can be observed at approx. 630 bp.

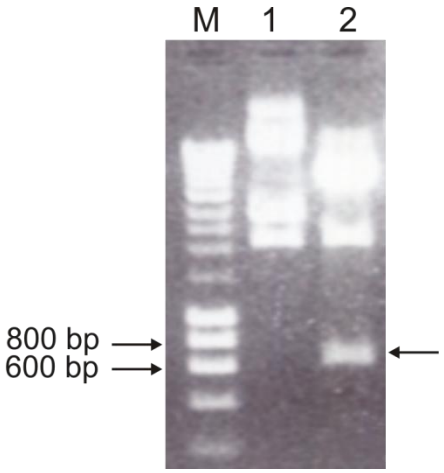

Figure 3.15. The result of agarose gel electrophoresis of pET-22b(+)/*pcpI* restriction digestion products. Individual lanes represent marker Hyperladder I (M), uncut plasmid (1) and cut plasmid (2). Insert band can be observed at approx. 630 bp.

The correct sequence of both inserts was confirmed by DNA sequencing (2.7.10, appendix III). The pET-28b(+)/*pcpI* and pET-22b(+)/*pcpI* were further used for the overexpression of PcpI-6xHis and native PcpI, respectively (3.2.2.5).

3.2.2.5. Overexpression of PcpI-6xHis and native PcpI

The overexpression of PcpI-6xHis and native PcpI in the BL21-CodonPlus®(DE3)-RIPL strain was successful and yielded soluble proteins fractions. This was confirmed by SDS-PAGE gels presented in figures 3.16 and 3.17, respectively.

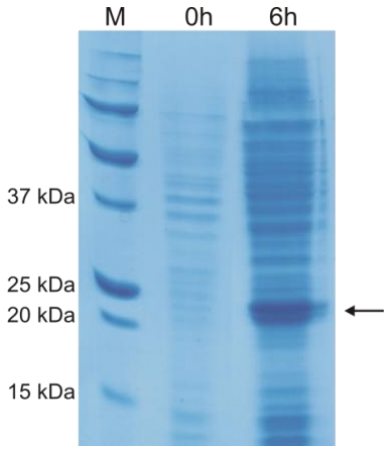

Figure 3.16. The result of SDS-PAGE confirming the overexpression of PcpI-6xHis (approx. 24 kDa). Individual lanes represent sample 6 h after induction (6h), before induction (0h) and a protein molecular weight marker (M).

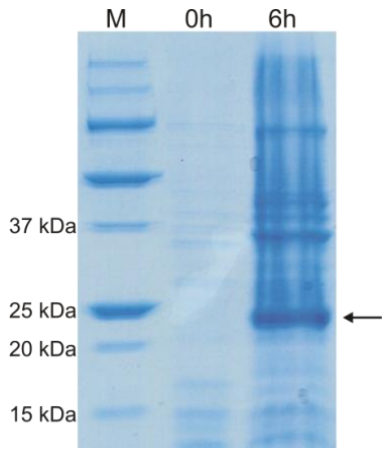

Figure 3.17. The result of SDS-PAGE confirming the overexpression of native PcpI (approx. 23 kDa). Individual lanes represent sample 6 h after induction (6h), before induction (0h) and a protein molecular weight marker (M).

Both PcpI-6xHis and native PcpI were present in soluble fractions which facilitated further protein purification steps (3.2.2.6 and 3.2.2.7, respectively).

3.2.2.6. Purification of PcpI-6xHis

3.2.2.6.1. Nickel affinity chromatography

The production and extraction of PcpI-6xHis from BL21-CodonPlus®(DE3)-RIPL was conducted as described in sections 3.2.1.3.1 and 3.2.1.3.2. Around 2.5 g of bacterial cell paste was obtained from 1 L of culture after harvesting. This was used for protein extraction and the supernatant, obtained during the procedure, was applied to Ni^{+} Sepharose column and subjected to protein purification as described in section 3.2.1.7. The elution profile presented in figure 3.18 allowed for determination of fractions containing PcpI-6xHis, which were further analysed using SDS-PAGE to assess the purity of the eluted protein. A result of this analysis is presented in figure 3.19.

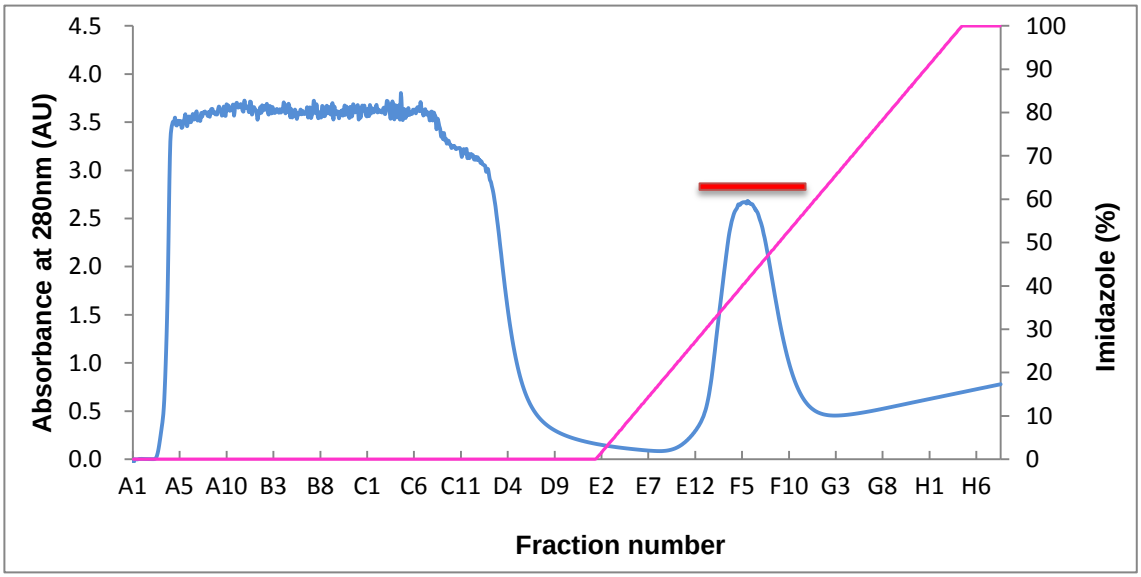

Figure 3.18. The nickel affinity protein elution profile of the human recombinant PcpI-6xHis. The fractions containing the protein are marked by the red bar. The A_{280} trace is coloured in blue and imidazole gradient is coloured in pink.

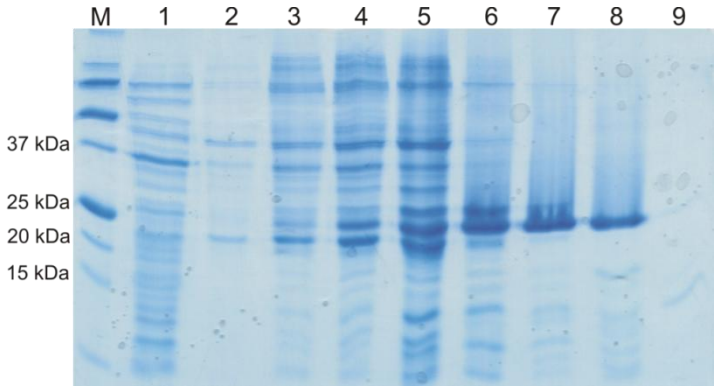

Figure 3.19. The result of SDS-PAGE analysis of the human recombinant PcpI-6xHis purified through nickel affinity chromatography.

As PcpI-6xHis was not totally purified, all fractions with the protein were mixed and subjected to subsequent gel filtration step (3.2.2.6.2).

3.2.2.6.2. Gel filtration chromatography

The purpose of PcpI-6xHis purification is to produce a protein sample of high purity and homogeneity in order to conduct crystallisation trials. All fractions obtained after Ni^{+} Sepharose^{TM} column purification which contained the protein were pooled together and further subjected to precipitation by 80% ammonium sulfate. Next the protein precipitate was resuspended in purification buffer and applied to a gel filtration column. The resulting elution profile and SDS-PAGE analysis are presented in figures 3.20 and 3.21, respectively.

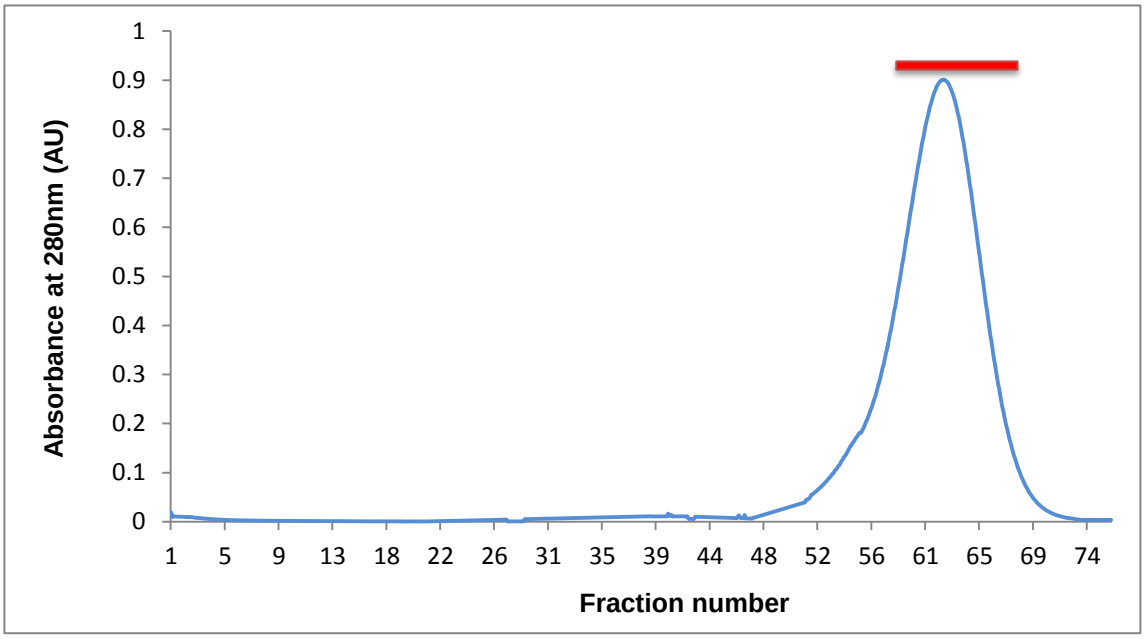

Figure 3.20. The gel filtration protein elution profile of the human recombinant PcpI-6xHis. The fractions containing the protein are marked by the red bar. The A_{280} trace is coloured in blue.

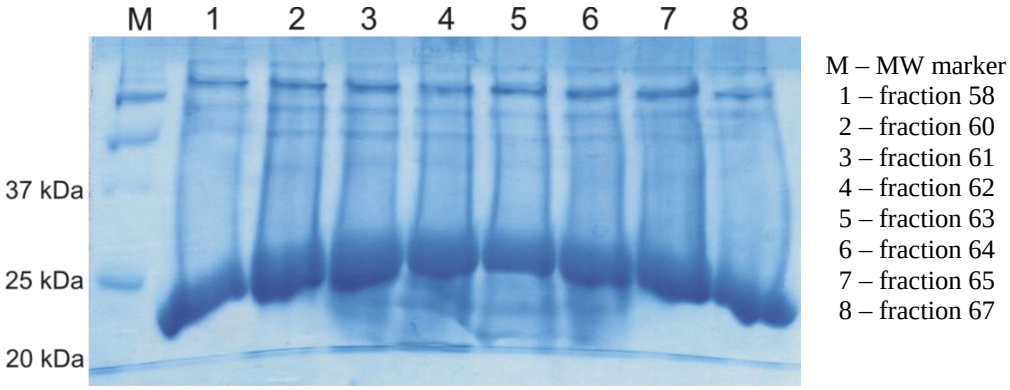

Figure 3.21. The result of SDS-PAGE analysis of the human recombinant PcpI-6xHis purified by gel filtration chromatography.

The purification of human recombinant PcpI-6xHis from BL21-CodonPlus®(DE3)-RIPL cell lysate was successful. The protein concentration and activity after each purification step was determined using the Bradford assay and the fluorometric enzyme activity assay described in sections 2.8.3.2 and 2.8.4, respectively. The purification result is presented in the table 3.7.

Fraction	Total Protein (mg)	Total Activity (U)	Specific Activity (U/mg)	Purification Fold	% Yield
Crude Extract	838.0	301.7	0.36	1.0	100
Ni^+ Sepharose	199.6	247.0	1.24	3.4	82
Superdex^{TM} 200	42.3	186.1	4.40	12.2	62

Table 3.7. The purification table for human recombinant PcpI-6xHis. All values are presented for purification from 1 L of BL21-CodonPlus®(DE3)-RIPL cell culture.

The purification of PcpI with the C-terminal His-tag was shown to be more effective (62% recovery) when compared to its 6xHis-PcpI yield (34%, section 3.2.2.3.3). The reason of this improvement may probably be explained by the fact that the shift of the tag to protein's C-terminus could offer better accessibility of the histidine residues when binding to Ni^+ Sepharose. Additionally, there may be a difference in the folding process between both recombinant PcpI forms where C-terminal tag localisation is definitely favourable. The advantage of such a shift can be seen in around two-fold better purification recovery of PcpI-6xHis over 6xHis-PcpI as well as in observable increase of the *in vitro* stability of the former form (3.2.2.6.3).

3.2.2.6.3. Stability of PcpI-6xHis

A centrifuged sample of PcpI-6xHis directly after the gel filtration step was analysed for homogeneity using the DLS technique as described in section 2.8.5. The result of the analysis was presented in figure 3.22.

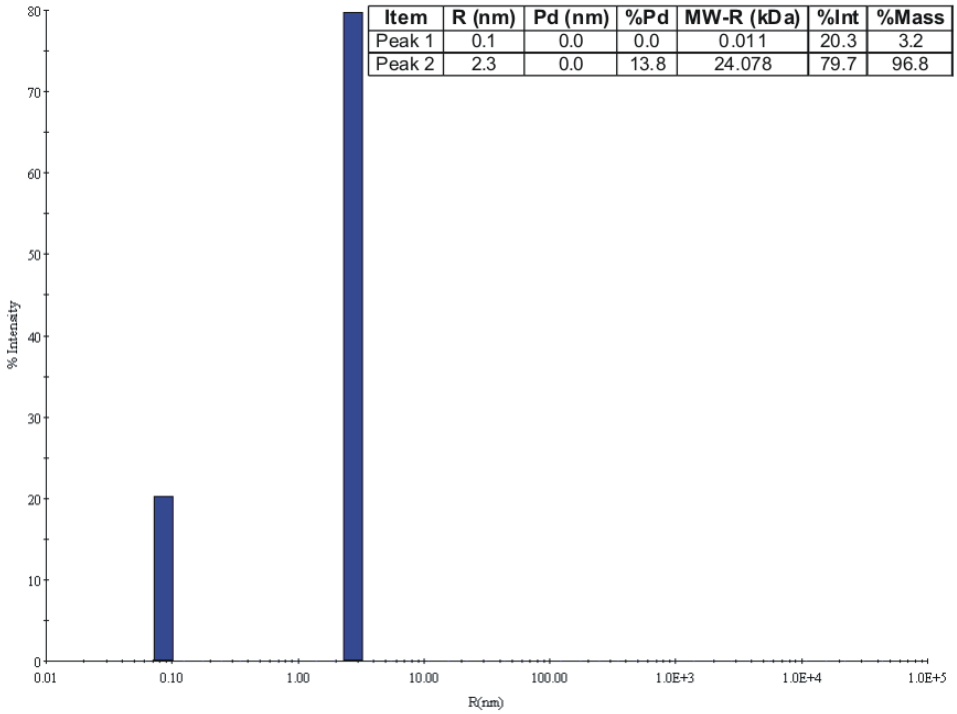

Figure 3.22. Result of DLS analysis of PcpI-6xHis. Peak no. 2 corresponds to the protein with estimated mass MW-R for 24.1 kDa. Polydispersity index was 13.8% indicating mostly homogenous state of the protein.

The DLS experiment indicates that the analysed PcpI-6xHis sample contains a single species with a polydispersity index calculated for 13.8% (below 15% threshold). Lack of undesired aggregates is significant improvement supporting the fact that modification of PcpI would increase its stability. It is worth noting that although DLS analysis suggests that PcpI is stable in given conditions this cannot be an indication of the general protein stability particularly during a prolonged period and as a concentrated protein sample. This result however confirms the purity and homogeneity of the sample required for protein crystallisation.

It was reported in section 3.2.2.3.4 that, despite multiple attempts, PcpI with the N-terminal His-tag could not be concentrated beyond 1.0 mg/ml. For the case of PcpI-6xHis this was increased to ~2.5 mg/ml when concentrated solely in gel filtration buffer and reached the desired 5.5 mg/ml when the sample was enriched with NDSB additives (3.2.1.10). Above this point the protein was seen to heavily precipitate out of solution. All of the available sulfobetaines NDSB-195, NDSB-201, NDSB-211, NDSB-221 or NDSB-256 were tested in order to identify their influence on the protein behaviour. None of the compounds could be distinguished as the one having the best stabilising propensity towards PcpI-6xHis, however the NDSB-195 (figure 3.1) was shown to be the most advantageous in this matter. This betaine contains the shortest bridge (C_2) between N^+ and SO_3^- which may offer some positive protein protecting features over the other tested chemicals that could adopt a cyclic conformation in solution. Some reports favour NDSB-195 as having the best solubilising properties and being the most stable at high pH (Vuillard *et al.*, 1995).

PcpI-6xHis concentrated up to ~5.5 mg/ml with NDSB-195 was subjected to preliminary crystallisation experiments using the vapour diffusion technique (3.4.2.4.1).

3.2.2.7. Purification of native PcpI

3.2.2.7.1. Phenyl sepharose chromatography

The production and extraction of native PcpI from BL21-CodonPlus®(DE3)-RIPL was conducted as described in section 3.2.1.8.1. The harvesting of 1 L of bacterial culture yielded around 2.0 g of cell paste. Next this was used for protein extraction and the supernatant, obtained during the procedure, was applied to a Phenyl Sepharose™ column and subjected to protein purification as described in section 3.2.1.8.2. The elution profile presented in figure 3.23 allowed the determination of fractions containing native PcpI, which were further analysed using SDS-PAGE to assess the purity of the eluted protein. The result of this analysis is presented in figure 3.24.

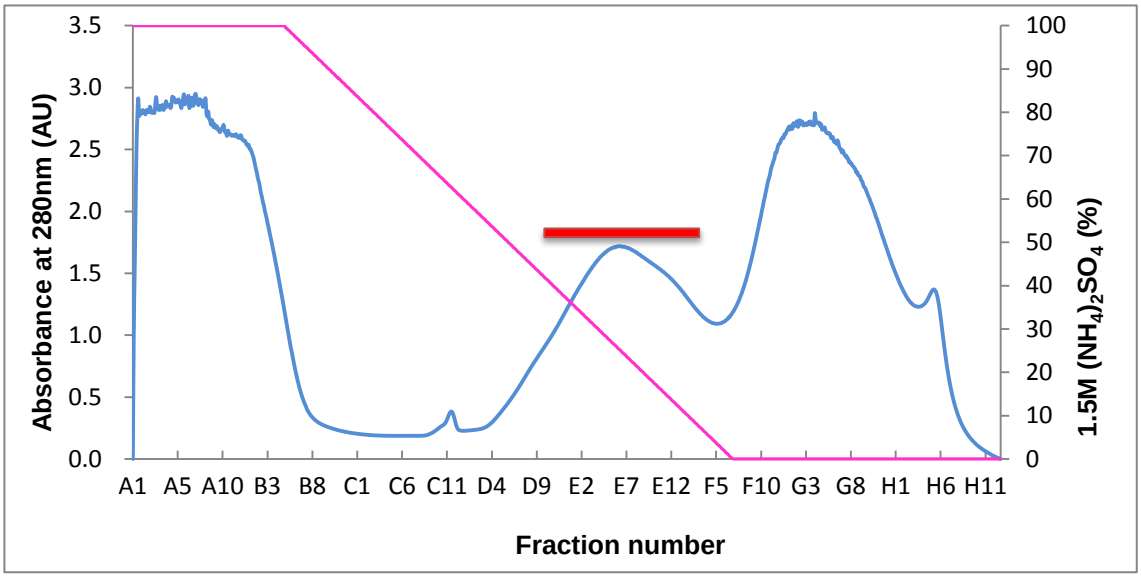

Figure 3.23. The Phenyl Sepharose™ protein elution profile of the human native PcpI. The fractions containing the protein are marked by the red bar. The A_{280} trace is coloured in blue and the 1.5 M $(NH_4)_2SO_4$ gradient is coloured in pink.

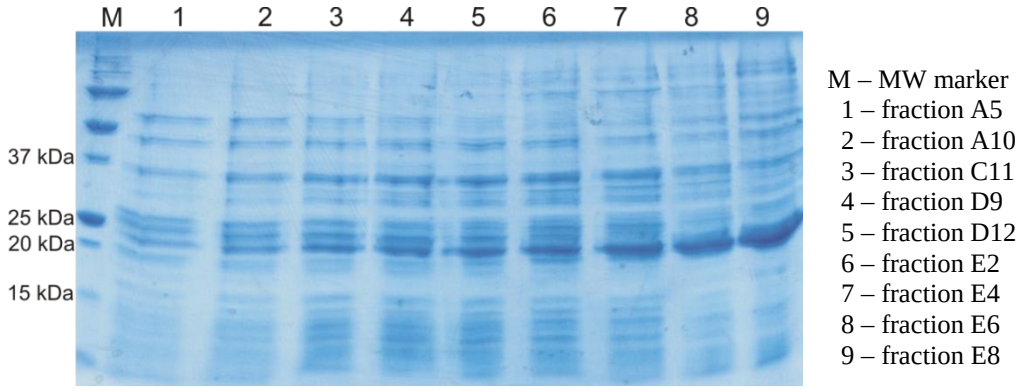

Figure 3.24. The result of SDS-PAGE analysis of the human native PcpI purified by Phenyl Sepharose™ chromatography.

As the Phenyl Sepharose™ column only partially purified native PcpI, all fractions containing the protein were mixed and subjected to a further ion-exchange chromatography step (3.2.2.7.2).

3.2.2.7.2. Ion-exchange chromatography

Preparation of the native PcpI sample to be purified using FFS-Sepharose™ cation exchange column was conducted as described in section 3.2.1.8.3. The elution profile presented in figure 3.25 allowed for determination of fractions containing native PcpI**,** which were further analysed using SDS-PAGE to assess the purity of the eluted protein. A result of this analysis is presented in figure 3.26.

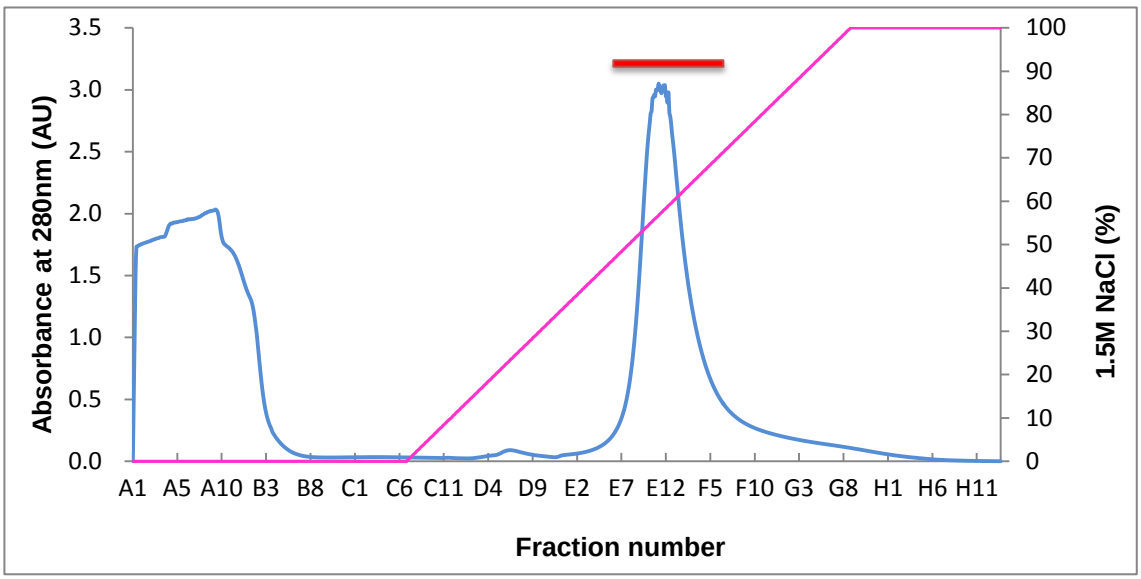

Figure 3.25. The FFS-Sepharose™ cation exchange protein elution profile of the human native PcpI. The fractions containing the protein are marked by the red bar. The A_{280} trace is coloured in blue and the 1.5 M NaCl gradient is coloured in pink.

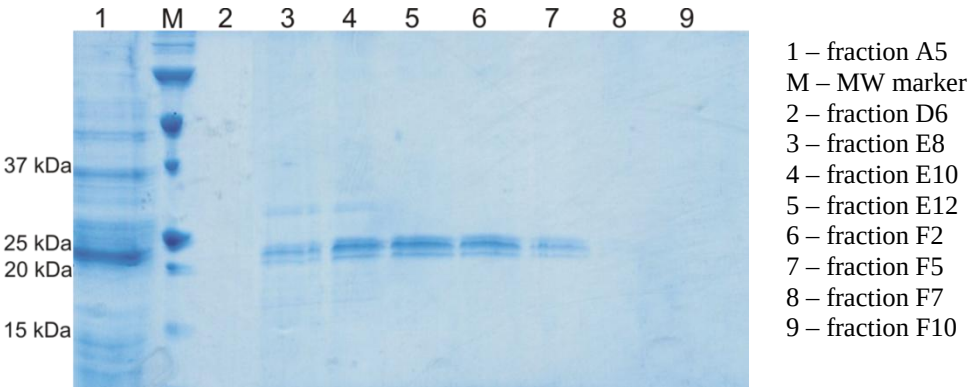

Figure 3.26. The result of SDS-PAGE analysis of the human native PcpI purified through FFS-Sepharose™ cation exchange chromatography.

FFS-Sepharose^{TM} column purification yielded a highly purified native PcpI sample as can be seen from the SDS-PAGE analysis (figure 3.26)**.** In order to improve the degree of the purity all fractions containing the protein were mixed and subjected to a further gel filtration step (3.2.2.7.3).

3.2.2.7.3. Gel filtration chromatography

Purification of native PcpI, as in the case of PcpI-6xHis, is aimed to produce a protein sample of high purity and homogeneity required for crystallisation experiments. All fractions obtained after FFS-Sepharose^{TM} column purification which contained native PcpI were pooled together and further subjected to the precipitation by 80% ammonium sulfate. Next the protein precipitate was resuspended in purification buffer and applied to a gel filtration column. The resulting elution profile and the SDS-PAGE analysis are presented in figures 3.27 and 3.28, respectively.

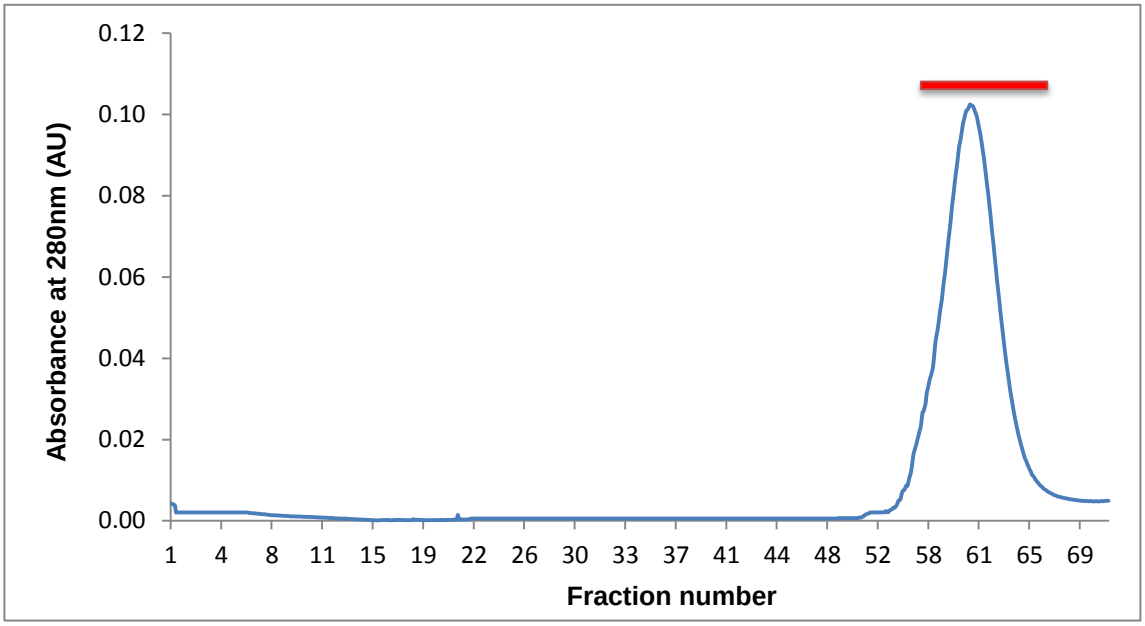

Figure 3.27. The gel filtration protein elution profile of the human native PcpI. The fractions containing the protein are marked by the red bar. The A_{280} trace is coloured in blue.

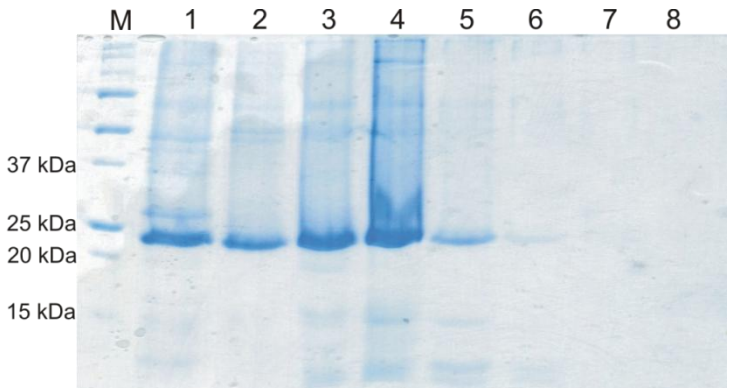

Figure 3.28. The result of SDS-PAGE analysis of the human native PcpI purified by gel filtration chromatography.

The purification of human native PcpI from BL21-CodonPlus®(DE3)-RIPL cell lysate was successful. The protein concentration and activity after each purification step was determined using the Bradford assay and the fluorometric enzyme activity assay described in sections 2.8.3.2 and 2.8.4, respectively. The purification result is presented in the table 3.8.

Fraction	Total Protein (mg)	Total Activity (U)	Specific Activity (U/mg)	Purification Fold	% Yield
Crude Extract	874.0	218.1	0.25	1.0	100
Phenyl Sepharose™	236.2	168.0	0.71	2.9	77
FFS-Sepharose™	39.7	101.9	2.57	10.3	47
Superdex™ 200	15.3	52.4	3.42	13.7	24

Table 3.8. The purification table for human native PcpI. All values are presented for purification from 1 L of BL21-CodonPlus®(DE3)-RIPL cell culture.

The purification of untagged native PcpI showed it to be less effective (24% recovery) when compared to 6xHis-PcpI or PcpI-6xHis yield (34%, section 3.2.2.3.3 and 62%, section 3.2.2.6.2, respectively). This can be understood since the presence of any type of affinity tag attached to the protein aims to increase selectivity during its

separation from the rest of cellular material. The purification fold is noticeably low for the Phenyl Sepharose™ step which may be explained by the fact that hydrophobic interactions are very unspecific (hence relatively high total protein mass, table 3.8) so typical elution peaks are very broad. Subsequently the FFS-Sepharose™ cation exchange step yielded a good level of purification which was improved in gel filtration. The resulting 24% yield is low however native PcpI at this stage was reasonably stable (3.2.2.7.4) and its total amount was sufficient to concentrate it and prepare initial crystallisation screening dishes.

3.2.2.7.4. Stability of PcpI-6xHis

A centrifuged sample of native PcpI directly after gel filtration step was analysed for homogeneity using DLS technique as described in section 2.8.5. The result of the analysis was presented in figure 3.29.

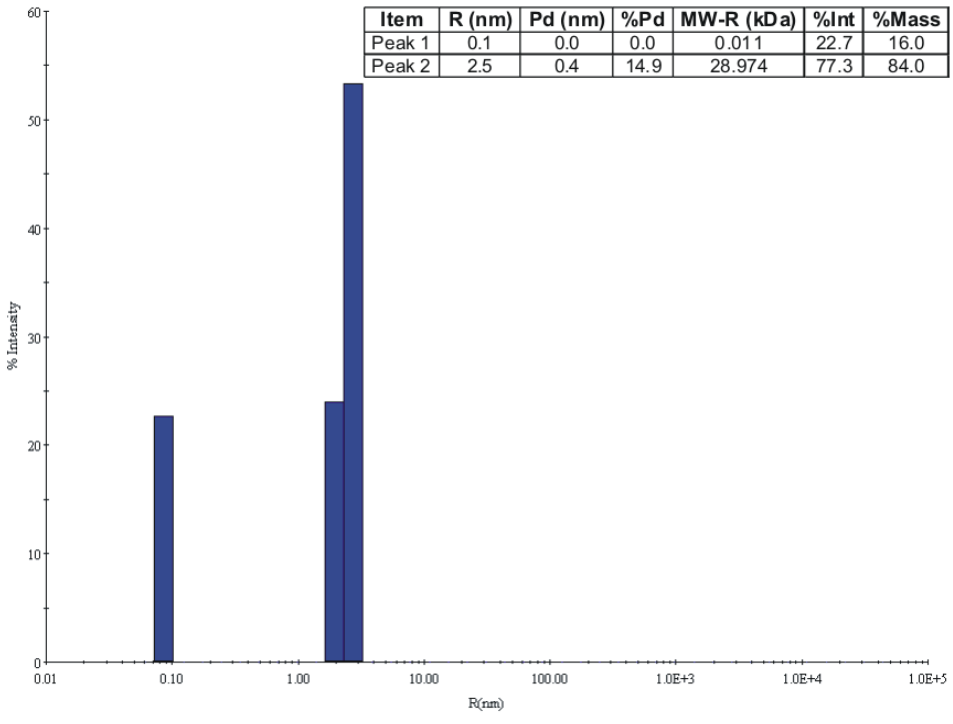

Figure 3.29. Result of DLS analysis of native PcpI. Peak no. 2 corresponds to the protein with estimated mass MW-R for 29 kDa. Polydispersity index was 14.9% indicating mostly homogenous state of the protein.

The DLS experiment indicates that the analysed native PcpI sample contains a single species with an acceptable polydispersity index calculated for 14.9%. Returned molecular weight of the species is nearly 29 kDa (figure 3.29) and is a bit higher than the real one 23.1 kDa. This can be explained by the fact that a particle size is estimated on the basis of hydrodynamic (Stokes) radius and depends on both mass and conformation. It is possible that untagged PcpI may be less stable than PcpI-6xHis and undergoes slow denaturation or an aggregation process. This may explain a slightly higher polydispersity index comparing to PcpI-6xHis (13.8% vs. 14.9%, respectively). However, this data generally suggests the stability of native PcpI in solution and, at least in tested conditions, lack of undesired aggregates. The result also confirms the purity and the homogeneity of the protein sample which was subsequently subjected to concentration and crystallisation experiments (3.5.3.1).

The attempts to concentrate native PcpI were not successful and resulted in a maximum of 1.0 mg/ml sample above which a heavy precipitation was observed. Therefore, as in case of PcpI-6xHis, native PcpI samples were separately enriched with a range of NDSB compounds as described in section 3.2.1.10. In this case the protein solubility was slightly improved, however it could not be concentrated beyond ~2.8 mg/ml even in a presence of NDSB-195. Despite persisting problem with protein stability it was decided to prepare the 2.8 mg/ml native PcpI sample (with NDSB-195) and subject it to initial crystallisation trials using vapour diffusion technique (3.4.2.4.1).

The instability of PcpI created a serious problem which, until solved, prevents the use of the protein in crystallographic structural studies. An initial study on the untagged and C-terminally His-tagged PcpI brought slight improvement to this question and enabled at least preliminary crystallisation experiments to be carried out. Therefore it was decided to conduct a further study regarding PcpI stability involving site-directed mutagenesis, thermofluor shift assay and chemical modification of surface residues (3.3)

3.3. Stability studies on human PcpI

Stability and solubility of proteins are strongly correlated with their ability and usefulness for the production of high-quality crystals, therefore any improvement of these properties directly influences rates of crystallisation. Therefore, it is understood that this question is considered as a one of the most significant in protein science and became extensively studied over years. Multiple methods that aim to interfere with protein behaviour *in vitro* have been reported and include screening for optimal expression, purification and storage conditions, application of additives and stability enhancers, protein engineering or chemical modifications (Richards, 1997; van den Burg and Eijsink, 2002; Pace *et al.*, 2004; Littlechild *et al.*, 2007). The problems with PcpI instability in solution that were approached in this project, were previously often observed during experimental work (Doolittle and Armentrout, 1968; Szewczuk and Kwiatkowska, 1970; Connelly, 2006; Mtawae *et al.*, 2008). Interestingly, Pcp representatives from extremophilic sources such as *T. litoralis*, *P. furiosus* and *P. horikoshii* are recognised as those exhibiting thermostable properties (2.1.3). The reason of such a difference lies in the fact that prokaryotic peptidases acquire tetrameric structural conformations and some of them possess hydrophobic insertions or make disulfide bonds and ionic interactions, which probably elevate this unusual stability. There are reports on stabilising effect of thiol-reducing agents or, to some degree, EDTA on type I Pcps, so these compounds were included in purification buffers. This, however, seems to be insufficient method to overcome the problem of excessive precipitation of the protein out of the solution, particularly during sample concentration prior to crystallisation trials. Therefore it was necessary to attempt other available tools that could help in this matter and these include screening for optimal buffer conditions (thermofluor-based thermal shift assay), site-directed mutagenesis of cysteine residues or their modification with 5,5′-dithiobis-(2-nitrobenzoic acid) (DTNB) as well as methylation of surface lysine residues.

3.3.1. Fluorescence-based thermal stability assay

In most applications that take longer period of time, protein stability is a decisive factor, which influences the effectiveness and the results of a given experiment. The environment, which helps to maintain stable protein, is also favourable to decrease its tendency to aggregate and prevent its denaturation during analytical and biophysical experiments or storage. Analysis of the influence of generic ingredients like buffers, salts and detergents as well as protein-ligand interactions as potential protein-stabilisers is of high value, particularly in cases of increased protein lability.

The fluorescence-based thermal stability (thermofluor shift) assay was developed by Pantoliano and co-workers and was originally used for rapid identification of ligands for target proteins as a strategy for drug discovery (Pantoliano *et al.*, 2001). The method allows for a high-throughput screen of optimal buffer conditions and additives that can promote protein stabilisation against thermal denaturation (Ericsson *et al.*, 2006; Niesen *et al.*, 2007). It is particularly useful when designing conditions for crystallisation of proteins for structural studies. The principle of this method is based on the observation that folded and unfolded proteins can be easily distinguished by the interaction with a specific fluorescent dye (fluoroprobe). The fluorescence is quenched in aqueous solution, but the emission can be readily detected when the dye binds to the protein hydrophobic interior which becomes exposed during thermally-induced unfolding. Progressive changes in fluorescence intensity as a function of temperature follow a typical sigmoidal melting curve with a sharp transition between a folded and unfolded state. Transition midpoint (T_m, melting temperature) of the unfolding varies depending on the buffer/ligand conditions creating the protein environment and therefore can define their influence on its stability when compared to control parameters (e.g. T_m in water or in the absence of ligand or buffer). An important advantage of this method is its universality as no advanced knowledge on the tested protein is required in order to perform the screening for optimal stabilising conditions.

The thermofluor shift assay of human PcpI was performed using SYPRO® Orange dye (Sigma), which is considered to be the most favoured for its properties for this method due to its high signal-to-noise ratio (Niesen *et al.*, 2007).

3.3.1.1. Materials and methods

3.3.1.1.1. Sample preparation

Purified PcpI sample was concentrated up to 1.0 mg/ml and mixed with other compounds prior to the assay. The mix for 22 reactions consisted of:

115.5 µl PcpI (0.5-1.0 mg/ml)
0.578 µl 5000x SYPRO® Orange
46.2 µl 2x NaCl (double protein concentration)
45.6 µl ddH_2O

Next 9 µl of the mix was combined with 1 µl of a given buffer solution (table 3.9) in 100 µl strip tubes (Qiagen), placed in a Rotor-Gene 6000 real-time PCR cycler (Corbett Life Sciences).

No.	Buffer solutions	pH
1.	ddH_2O (Control)	
2.	100 mM Glycine	10
3.	100 mM L-Arginine	9.5
4.	100 mM Bicine	9.0
5.	100 mM CHES	8.5
6.	100 mM di-Sodium Tetraborate	8.5
7.	100 mM HEPPS	8.0
8.	100 mM Tris-HCl	8.0
9.	100 mM Imidazole	8.0
10.	100 mM Ammonium Sulfate	7.5
11.	100 mM HEPES	7.5
12.	100 mM MOPS	7.2
13.	100 mM PIPES	7.0
14.	100 mM Sodium osate	7.0
15.	100 mM Bis-Tris Propane	6.7
16.	100 mM MES	6.5
17.	100 mM Zinc Acetate	6.5
18.	100 mM Sodium Citrate	5.6
19.	100 mM Sodium Acetate	4.6
20.	50 mM Tris-HCl, 0.15 M NaCl, 5 mM β-Me (buffer A+ β-Me)	7.5
21.	50 mM Tris-HCl, 0.15 M NaCl (buffer A)	7.5

Table 3.9. List of the buffer solutions tested for PcpI stability in the thermofluor shift assay.

Moreover the screening was repeated with the same selection of buffers and with addition of the reversible PcpI inhibitors – 2-pyrrolidone or L-pGlu acid. Each of the inhibitors was added to the protein sample with 5-fold molar excess and incubated for 1 h at 4ºC prior to preparation of the master mix.

3.3.1.1.2. Thermofluor shift assay

The assay was performed in the Rotor-Gene 6000 real-time PCR cycler (Corbett Life Sciences). All samples with screening conditions were prepared in triplicate and heated from 25ºC to 90ºC at a rate of 0.2ºC/min. Fluorescence intensity measurements were taken simultaneously and collected by a software package associated with the cycler. The excitation and emission wavelengths were 490 nm and 575 nm, respectively.

3.3.1.1.3. Analysis of thermofluor shift data

In order to calculate the temperature midpoint values T_m the fluorescence intensity data were fitted using Xlfit^{TM} curve-fitting software (ID Business Solutions Ltd). T_m which is an inflection point of the transition curve was calculated for each sample after fitting to a Boltzmann model using the equation shown in figure 3.30.

$$I = A + \frac{B - A}{1 + e^{(\mathrm{Tm}-\mathrm{T})/\mathrm{C}}}$$

Figure 3.30. Boltzmann equation: **I** stands for a fluorescence intensity at the temperature **T**; **A** and **B** are minimum and maximum fluorescence intensities, respectively; **C** is a slope of the transition curve; $\mathbf{T_m}$ is the temperature midpoint for the unfolding transition.

Individual PcpI T_m values for all tested buffers were compared with the reference value T_0 which was the protein in ddH_2O (control). The change in unfolding temperatures – $\Delta T_m = T_m - T_0$ – was calculated for each sample. Positive ΔT_m indicates that given conditions prompt stabilising structural changes towards a more ordered and less flexible conformation, whereas negative ΔT_m can be considered as a sign of protein disordered state and misfolding.

3.3.1.1.4. Optimisation for HEPPS buffer

The results of the experiment showed that the highest ΔT_m was obtained for the PcpI sample containing HEPPS buffer at pH 8.0. Therefore it was decided to carry out the optimisation of the thermofluor shift screening with a set of HEPPS buffers where the pH was varied: 7.3, 7.5, 7.7, 7.9, 8.1, 8.3, 8.5 and 8.7. Sample preparation and the assay performance were conducted as described in sections 3.3.1.1.1 and 3.3.1.1.2, respectively.

3.3.1.2. Results and discussion

3.3.1.2.1. Thermofluor shift assay

Fluorescence intensity data obtained for all PcpI samples containing individual buffer components (3.3.1.1.1) were plotted against assayed temperature values and are presented in figure 3.31. For all tested conditions the fluorescence intensity function acquires a bell-shape-like profile reaching a maximum peak and then gradually decreases. This is often observed and may be a result of a probable precipitation or aggregation of the denatured protein and fluoroprobe complex (Niesen *et al.*, 2007). Therefore the data beyond the maximum were excluded from fitting to the Boltzmann model (3.3.1.1.3).

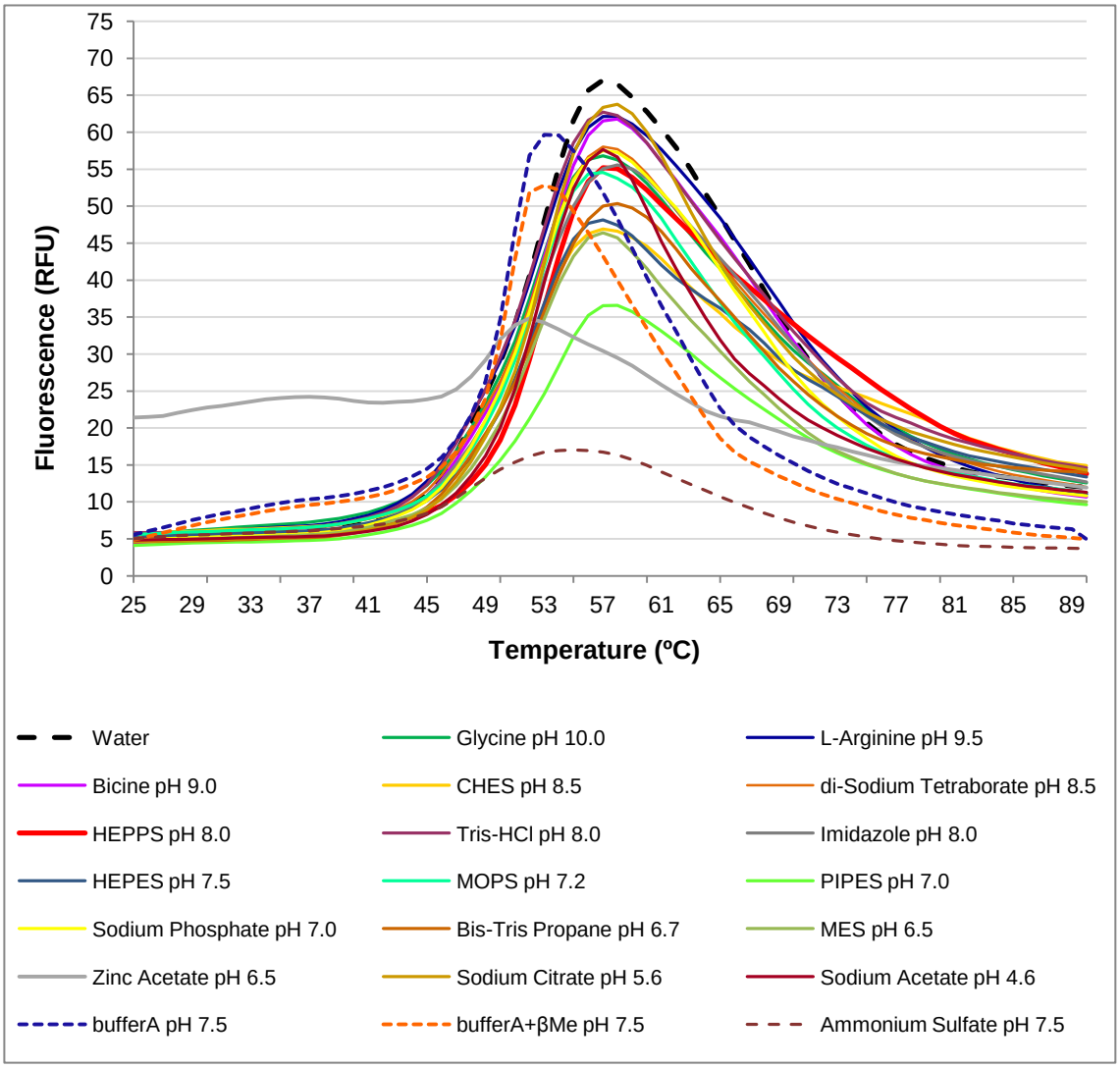

Figure 3.31. Thermofluor shift assay results for the set of given buffers reflecting state of the protein in each condition. The data after the maximum peak were excluded from fitting as these relate to precipitated protein-dye complex and do not fit to the Boltzmann model.

The PcpI stability screening was conducted solely with a selection of buffers as well as with the buffers individually combined with reversible inhibitors – 2-pyrrolidone or L-pGlu acid. The protein T_m values were calculated for each condition using Xlfit^{TM} curve-fitting software (3.3.1.1.3) and compared with reference T_0. Comparison of the obtained changes in the unfolding temperature (ΔT_m) for each screen is presented in figure 3.32.

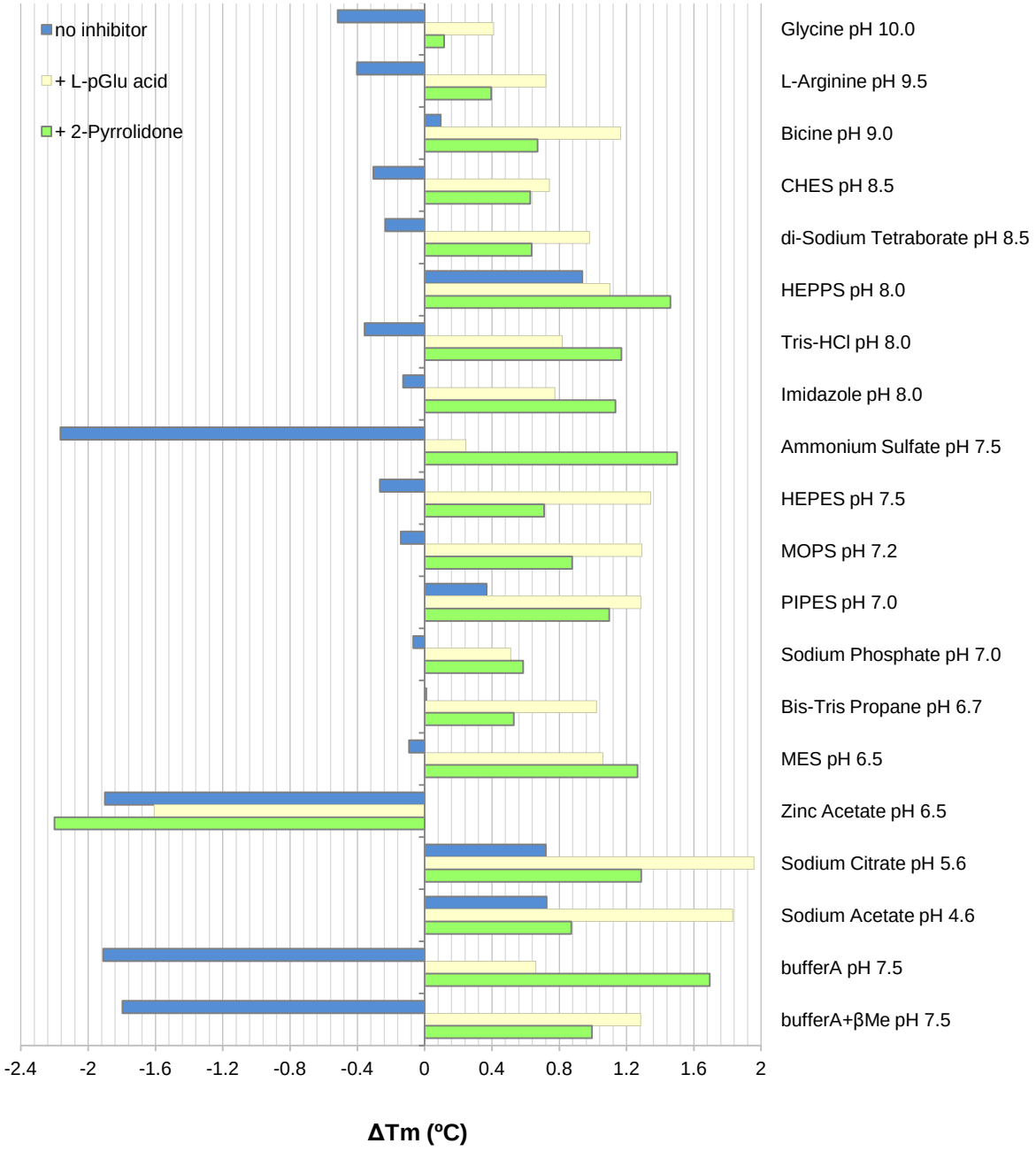

Figure 3.32. Comparison of the changes in ΔT_m of PcpI in given buffer conditions (blue bars) as well as in presence of reversible inhibitors 2-pyrrolidone (green bars) or L-pGlu acid (yellow bars). Negative ΔT_m indicate destabilising protein environment, whereas positive values indicate that buffer conditions prompt stabilising structural changes of the protein.

The condition screening, which consisted of 20 different buffers showed varied results in terms of their influence on PcpI stability (figure 3.32). Representative buffers, which prompted the most significant positive shift of melting temperature ($+\Delta T_m$) were HEPPS (pH 8.0), PIPES (pH 7.0), sodium citrate (pH 5.6) and sodium acetate (pH 4.6). Both HEPPS and PIPES belong to a specific group of tertiary and secondary aminoalkanesulfonic acids also known as Good buffer series (Good *et al.*, 1966). They are widely used as biological buffers because of the sufficient coverage of the physiological pH range and above, as well as their similarity to amino acids in ability to function in multiple ionization states e.g. zwitterionic form. Moreover, their stabilising effect may be a result of binding to a protein that has been confirmed by the fact that many structures in the PDB contain ordered MES or HEPES (Newman, 2004). This finding supports their usefulness in crystallisation experiments.

The stabilising influence of sodium citrate and sodium acetate has already been observed for the case of a number of proteins (Ericsson *et al.*, 2006). However due to acidic pH of these buffers, close to the PcpI pI (theoretical value 6.08) and that they create potential problems in some other applications (e.g. nickel affinity purification), they were not considered to be used further in this study.

Surprisingly the most destabilising effect (negative ΔT_m) on PcpI was observed for Tris-based buffers used so far in the purification – buffer A (-1.9ºC) and buffer A+β-Me (-1.8ºC) (2.3.3.3). Similar but even stronger influence on PcpI disorder was seen for ammonium sulfate (-2.2ºC) used for the protein precipitation and concentration prior to the gel filtration step (3.2.1.7 and 3.2.1.8.4). Negative ΔT_m value (although lower than the parameter of buffer A) was also obtained for Tris-HCl (-0.36ºC). Differences between both conditions lies in pH (Tris-HCl pH 8.0 vs. buffer A pH 7.5) and the presence of 0.15 M NaCl in buffer A. NaCl increases the ionic strength of the solution and its inclusion in the purification buffers was due to the observation of its positive effect on 6xHis-PcpI solubility (3.2.2.3.4). It may be concluded that the stabilising effect of Tris-HCl may be a function of pH where a more alkaline environment has a better influence on PcpI. It is worth noting that Tris-HCl has a relatively narrow buffering capacity in the 7.5-9.2 range and its pH is strongly temperature-dependent. Therefore the buffer at pH 7.5, being at the edge of the buffering range can easily lose its properties with insignificant temperature shifts, which may result in the protein being exposed to unfavourable conditions. Moreover, the presence of any reducing agents, such as β-Me, in unstable buffer may addtionally decrease pH of the solution leading it

towards the pI of PcpI and result in a reduction of its solubility. These findings have helped to understand why PcpI was extremely unstable and easily precipitated out of solution during sample concentration and could not be kept for more than a few days at both 4ºC or room temperature. It is worth noting that the other buffer from the Tris group – Bis-Tris propane pH 6.7 – surprisingly had a minimal positive effect on PcpI conformational order. The reason for this may be explained by the fact that Bis-Tris has a wider buffering capacity from pH 6 to 9.5 and its zwitterionic structure precludes dramatic pH and ionic strength changes of the solution (Stellwagen *et al.*, 2008).

Despite the negative thermal shift values for most of the tested buffers in all the cases, with exception of zinc acetate, addition of either of the inhibitors dramatically increased protein stability (figure 3.32). This can be observed even for the most destabilising buffer A and ammonium sulfate. Such a change is not suprising since binding of inhibitor or any other ligand prompts protein towards a less flexible and more ordered conformation. Both inhibitors due to their highly stabilising properties were included in crystallisation experiments (3.4.2.4.3).

The best positive ΔT_m result obtained for HEPPS buffer led to the decision to use this for further optimisation screening but with varied pH values as described in section 3.3.1.1.4.

3.3.1.2.2. Optimisation for HEPPS buffer

Investigation for the optimal pH value of HEPPS was performed on the group of buffers as described in section 3.3.1.1.4. Comparison of the changes obtained in the unfolding temperature (ΔT_m) for each pH is presented in figure 3.33.

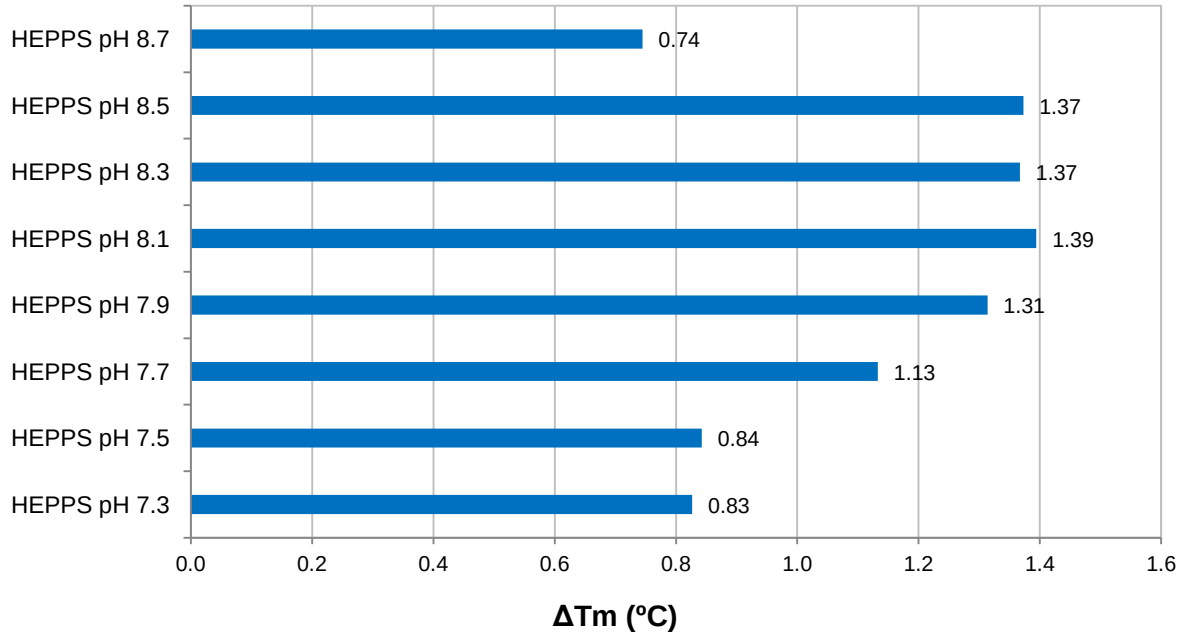

Figure 3.33. Comparison of the changes in ΔT_m of PcpI in a set of HEPPS buffers with varied pH.

Results of the optimisation show that all of the tested buffers have a stabilising effect on PcpI. The best ΔT_m value was obtained in the presence of HEPPS at pH 8.1. The shift in transition temperature is very similar for conditions of pH from 7.9 to 8.5 and starts decreasing beyond this range. This indicates that PcpI stability is pH-sensitive and, based on this finding, application of HEPPS buffer at pH 8.0 in the purification system seems to be the best solution.

3.3.1.2.3. Application of HEPPS-based buffers

Results obtained from the thermofluor shift assay led to a decision to replace the purification buffer system of PcpI from Tris-based to HEPPS-based, the content of which is shown in section 2.3.3.5. All Tris-HCl solutions (including buffer A) displayed a negative effect on the structural confirmation of human PcpI contrary to the stabilising action of HEPPS (figure 3.32). The characteristic properties of HEPPS, as a zwitterionic member of Good's buffer family, are limited effect on biochemical reactions and interaction with mineral cations, high solubility and stability, very low sensitivity to temperature, concentration or ionic strength of the solution and non-toxicity (Good *et*

al., 1966). The disadvantage of Tris (primary amine) is its ionic character and therefore its potential ability to interact with the other compounds in the solution. This may seriously affect the buffer properties and have implications on protein behaviour and assessment of experimental results. An exemplary phenomenon was reported from studies on haemoglobin function, where Tris-HCl buffer interaction with chloride anions impeded accurate measurements (Weber, 1992). The replacement of Tris-HCl with zwitterionic HEPES (belonging to Good's buffer series) prevented an occurrence of such binding and dramatically improved the protein stability.

The protocol for the purification of PcpI-6xHis and native PcpI remained the same as in 3.2.1.3 and 3.2.1.8, respectively, only with the omission of the ammonium sulfate precipitation step. Instead, concentration of the protein sample prior to gel filtration was performed in a Vivaspin20 centrifugal concentrator with a 30 kDa molecular weight cut-off (Sartorius Stedim Biotech S.A.). The replacement of Tris-based to HEPPS-based buffer system resulted in significant improvement of PcpI stability in solution. The purification yield was not much higher than previously obtained for PcpI-6xHis (3.2.2.6.2, table 3.7) and was around 65-70% (results not shown). However, the protein sample was extremely stable during storage at 4ºC and in concentration steps prior to gel filtration and before the crystallisation experiments. Both native PcpI and PcpI-6xHis could be surprisingly easily concentrated even up to 70 mg/ml. This indicates that the problem with the PcpI instability in solution was overcome and both protein forms were further subjected to crystallisation experiments described in section 3.4.

3.3.2. Study on human PcpI cysteine mutants

Analysis of the human PcpI sequence indicated a relatively high number of cysteine residues (figure 3.34). The peptidase has one cysteine as a part of catalytic triad (Cys149, 1.2.4.1) and seven remaining ones, which seems to be unusual for the human enzyme when compared to known Pcps from other sources. Only one non-catalytic cysteine can be found in homologues from *B. amyloliquefaciens*, *P. furiosus* or *T. litoralis* (1.2.3). Moreover, in the latter two tetrameric proteins, this cysteine participates in a formation of the inter-subunit disulfide bridge (1.2.3). Interestingly, in human PcpI four cysteine residues (Cys99, Cys102, Cys107 and Cys108) are found within a disordered, loop region as can be seen in figure 3.34. This cluster could potentially work as a regulatory subdomain for the cysteine-based control of PcpI activity. Changes in the configuration of the cluster may undoubtedly trigger protein conformational changes and, depending on conditions, have influence on its stability. Cysteine residues are often referred as redox switches of enzymes (Spadaro *et al.*, 2010). The nucleophilic thiol group in the residue is known to be very reactive and can be easily oxidised forming disulfide bonds or a range of oxidised derivatives such as sulfenic, sulfinic, and sulfonic acids, often having important impact on the protein function. This thiol-dependent control of redox state has a wider effect on diverse biological processes, such as protein folding, response to stress or signal transduction. Exemplary reversible oxidation of mitochondrial protein thiols is considered to have protective function against oxidative damage as a part of a biological defence system (Costa *et al.*, 2003). Moreover, any abnormal perturbations in the intracellular redox homeostasis, including oxidative stress, can lead to cellular dysfunction and subsequent pathological conditions.

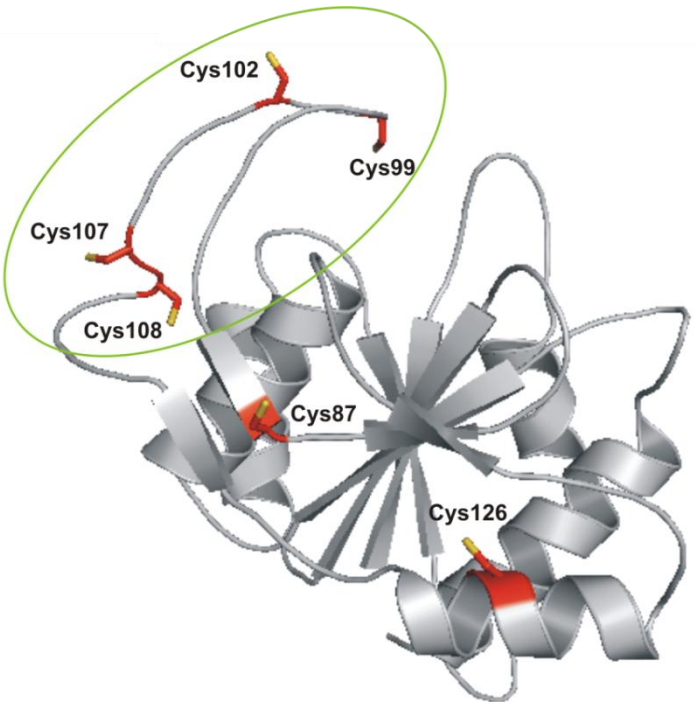

Figure 3.34. Cartoon representation of the model of human PcpI with marked positions of cysteine residues (in red stick mode). The model was created using the homology modelling applications in the MOE™ software (Chemical Computing Group Inc.). The structure of the *B. amyloliquefaciens* Pcp (1AUG) was used as a template and the output was evaluated using a Ramachandran plot presented in appendix VI. Missing from the model are the first 7 N-terminal residues (MEQPRKA) and 10 C-terminal residues (EGKINYCHKH), owing it to lack of homology between the query sequence and the template. Therefore Cys206 cannot be marked as it is outside of sequence validated for the generation of the model. The cysteine-rich loop, containing Cys99, Cys102, Cys107 and Cys108 tandem, is encircled in green. All of the non-catalytical cysteine residues were mutated to alanine residues.

A surprisingly high number of cysteine residues in human PcpI sequence implicates their potential influence on the activity and structural stability. All of the non-catalytic cysteines shown in figure 3.34 (along with the C-terminal C206 residue) may probably be surface exposed and therefore can easily participate in a range of intermolecular interactions (such as disulfide bridging) and be a target for chemical modifications. In order to assess their significance for the protein performance it was decided to conduct a study on the range of single and multiple PcpI cysteine mutants.

3.3.2.1. Materials and methods

3.3.2.1.1. Site-directed mutagenesis of cysteine residues

The pET-28b(+)/*pcpI* plasmid construct (3.2.1.4.3) was used as a PCR template to conduct a series of mutations switching cysteine residues with alanine residues in the human PcpI. This was performed using QuikChange® Lightning Site-Directed Mutagenesis kit (Stratagene) according to manufacturer's instruction. The basic protocol employs high fidelity *Pfu*Ultra HF DNA polymerase, which extends oligonucleotide primers containing the desired mutation and in result producing mutated plasmid construct. The product sample is treated with the *Dpn*I endonuclease, which is specific for methylated and hemi-methylated substrates. This helps to digest the parental DNA template and separate the mutated constructs, which are unmethylated.

The composition of the site-directed mutagenesis reaction mixture is presented below.

50 ng/µl pET-28b(+)/*pcpI*	1 µl
forward primer	~125 ng/µl
reverse primer	~125 ng/µl
10x reaction buffer*	5 µl
dNTP mix*	1 µl
QuikSolution^{TM} reagent*	1.5 µl
*Pfu*Ultra HF DNA polymerase*	1 µl
ddH_2O	to a final volume of 50 µl

*composition is proprietary, provided with the QuikChange® Lightning kit (Stratagene)

All primers used for cysteine to alanine mutations were supplied by Eurofins MWG Operon and are listed in tables 3.10 (single mutations) and 3.11 (multiple mutations).

Primer	Sequence	GC content	T_m
C87A (forward)	GTCACACTGGAGAAAGCCGGACAC AACAAGG	54.8%	70.8ºC
C87A (reverse)	CCTTGTTGTGTCCGGCTTTCTCCAG TGTGAC	54.8%	70.8ºC
C99A (forward)	GGGCTGGACAACGCCCGCTTTTGCC	68.0%	71.2ºC
C99A (reverse)	GGCAAAAGCGGGCGTTGTCCAGCCC	68.0%	71.2ºC
C102A (forward)	CAACTGCCGCTTTGCCCCCGGCTCC	72.0%	72.8ºC
C102A (reverse)	GGAGCCGGGGGCAAAGCGGCAGTTG	72.0%	72.8ºC
C107A (forward)	CGGCTCCCAGGCCTGCGTGGAGGAC	76.0%	74.5ºC
C107A (reverse)	GTCCTCCACGCAGGCCTGGGAGCCG	76.0%	74.5ºC
C108A (forward)	CGGCTCCCAGTGCGCCGTGGAGGAC	76.0%	74.5ºC
C108A (reverse)	GTCCTCCACGGCGCACTGGGAGCCG	76.0%	74.5ºC
C126A (forward)	CATGGATGCTGTGGCCAAGCGAGTCACC	60.7%	71.0ºC
C126A (reverse)	GGTGACTCGCTTGGCCACAGCATCCATG	60.7%	71.0ºC
C206A (forward)	CAGAGGGCAAAATCAACTATGCCCAC AAACACTGA	45.7%	69.5ºC
C206A (reverse)	TCAGTGTTTGTGGGCATAGTTGATTTTG CCCTCTG	45.7%	69.5ºC

Table 3.10. List of the primers used for site-directed mutagenesis to produce the PcpI derivatives with single cysteine mutations.

Primer	Sequence	GC content	T_m
C99/102A (forward)	GACAACGCCCGCTTTGCCCCCGGCTC	73.1%	74.3ºC
C99/102A (reverse)	GAGCCGGGGGGCAAAGCGGGCGTTGTC	73.1%	74.3ºC
C107/108A (forward)	GCTCCCAGGCCGCCGTGGAGGACGG	80.0%	75º.0C
C107/108A (reverse)	CCGTCCTCCACGGCGGCCTGGGAGC	80.0%	75.0ºC
C99/102/107/108A	sequential mutagenesis using C99/102A and C107/108A primers		
C87/99/102/107/108/126/206A (CtA)	sequential mutagenesis using C87A, C99/102A, C107/108A, C126A and C206A primers		

Table 3.11. List of the primers used for site-directed mutagenesis to produce PcpI derivatives with multiple cysteine mutations. Multiple mutants C99/102/107/108A and C87/99/102/107/108/126/206A (CtA) were produced *via* multi-step mutagenesis using suitable primers.

The reactions were carried out in the Piko® thermal cycler (Finnzymes) and the cycling parameters are outlined in table 3.12.

Step	Temperature	Time	
Initial denaturation	95ºC	2 min	
Denaturation	95ºC	20 s	18x
Annealing	60ºC	10 s	
Extension	68ºC	2,5 min	
Final extension	68ºC	5 min	
Cooling	4ºC	-----	

Table 3.12. Thermal cycling parameters for the site-directed mutagenesis.

Next, 2 μl of the *Dpn*I restriction enzyme solution was added directly to each amplification reaction, which was briefly spun down and further incubated at 37°C for 5 min in order to digest the parental, non-mutated DNA template. All reactions were subjected to a plasmid transformation into XL10-Gold® ultracompetent cells (2.4.1) according to a protocol described in section 2.7.1.

3.3.2.1.2. Preparation of recombinant plasmid constructs

Random single *E. coli* XL10-Gold® colonies, obtained from the transformation with the site-directed mutagenesis reaction mixtures (3.3.2.1.1), were picked and used for the inoculation of 10 ml of LB media (2.2.1) containing 50 μg/ml kanamycin. This was grown overnight at 37ºC in a shaking incubator. Next the cultures were subjected to DNA extraction according to the protocol of GeneJET™ Plasmid Miniprep kit (Fermentas) (2.7.2). The result of the minipreparation was analysed by 1% agarose gel electrophoresis (2.7.8). The obtained mutated plasmid constructs were further purified (2.7.3), quantified (2.7.4) and the results of the mutagenesis experiments were checked by DNA sequencing using standard T7 primers (2.7.10).

3.3.2.1.3. Overexpression of PcpI cysteine mutants

The protocol of the overexpression of 11 cysteine mutants: C87A, C99A, C102A, C107A, C108A, C126A, C206A, C99/102A, C107/108A, C99/102/107/108A and CtA (all non-catalytic cysteines mutated to alanines), was based on the one established for the synthesis of PcpI-6xHis (3.2.1.5). The BL21-CodonPlus®(DE3)-RIPL (3.2.1.2.1) were transformed with the cysteine-mutated pET-28b(+)/*pcpI* plasmid constructs following the protocol described in section 2.7.1. The cells were plated on Petri dishes containing agar with 50 μg/ml kanamycin and 35 μg/ml chloramphenicol. This was incubated overnight at 37ºC. Next a single colony from each transformation was used to inoculate 10 ml of LB media supplemented with 50 μg/ml kanamycin and 35 μg/ml chloramphenicol and this was grown overnight at 37ºC in a shaking incubator. Next day a flask containing 100 ml of LB media with the above antibiotics was inoculated with 1 ml of the overnight culture and grown in a shaking incubator at 37ºC. The induction of the protein overexpression was initiated by the addition of IPTG (2.2.4) to a final

concentration of 1 mM once the culture had reached an OD_{595} of 0.6. The incubation was continued for a further 6 h at 25ºC. Protein isolation was carried out according to the detergent-based procedure (2.8.1.1) and the results of the protein expression were analysed by the SDS-PAGE technique using a 12.5% separating gel (2.8.2).

3.3.2.1.4. Purification and crystallisation trials of PcpI cysteine mutants

All 11 PcpI cysteine mutants were designed to contain a C-terminal His-tag in order to facilitate their purification using nickel affinity chromatography (3.2, 3.3.2.1.1). The production and purification steps followed the protocol set for the non-mutated PcpI-6xHis using the nickel affinity column (3.2.1.3.3) and the gel filtration column (3.2.1.3.4). The thermofluor shift assay performed on PcpI-6xHis showed that application of HEPPS buffer can provide the best stabilising environment for the protein. Therefore the HEPPS-based buffer system was used for the purification and storage of all PcpI cysteine mutants and composition of which is presented in section 2.3.3.5. Fractions collected during the purification procedure were analysed for protein purity by the SDS-PAGE technique using a 12.5% separating gel (2.8.2). The concentration of the purified protein samples was determined by absorbance measurement at 280 nm (2.8.3.1, extinction coefficient 24410 $M^{-1}cm^{-1}$ (ProtParam, www.expasy.org))**.** The activity of the mutated variants was assayed using the fluorometric method described in section 2.8.4. Protein samples were stored at 4ºC.

All cysteine-mutated PcpI-6xHis isoforms were tested for enzymatic activity using the fluorimetric activity assay utilising L-pGlu-AMC as the substrate as described in section 2.8.4.

Purified samples of PcpI cysteine mutants were concentrated in Vivaspin20 centrifugal concentrators (Sartorius Stedim Biotech S.A.) and further subjected to crystallisation trials using the microbatch technique as described in section 3.4.3.2.

3.3.2.2. Results and discussion

3.3.2.2.1. Mutated pET-28b(+)/pcpI derivatives

Site-directed mutagenesis of the pET-28b(+)/*pcpI* (3.3.2.1.1) resulted in obtaining mutated plasmid variants as designed for the 11 PcpI-6xHis cysteine mutants: C87A, C99A, C102A, C107A, C108A, C126A, C206A, C99/102A, C107/108A, C99/102/107/108A and CtA. All pET-28b(+)/*pcpI* derivatives were prepared as described in 3.3.2.1.2 and analysed by DNA sequencing (2.7.10). The results confirmed the correct mutation had taken place for all of the selected cysteine residues, which had been replaced by alanines (appendix VII).

3.3.2.2.2. Overexpression of PcpI cysteine mutants

The PcpI-6xHis cysteine mutants: C87A, C99A, C102A, C107A, C108A, C126A, C206A, C99/102A, C107/108A, C99/102/107/108A and CtA were successfully produced in BL21-CodonPlus(DE3)-RIPL cells, facilitating the production of the rare *E. coli* codons as described in section 3.2.1.2.1. All mutant enzymes were overexpressed from the mutated derivatives of pET-28b(+)/*pcpI*, in order to incorporate the C-terminal His-tag. The results were analysed by the SDS-PAGE technique using a 12.5% separating gel and the results for the PcpI-6xHis C107A, C107/108A and CtA are shown in figure 3.35.

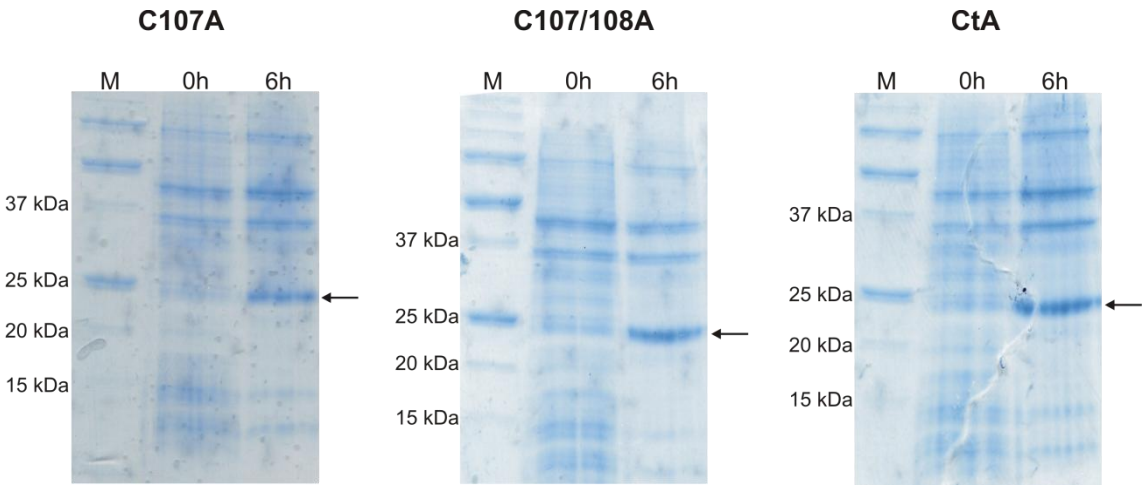

Figure 3.35. The result of the SDS-PAGE analysis confirming the overexpression of the mutated forms of PcpI-6xHis: C107A, C107/108A and CtA. Individual lanes represent a sample 6 h after induction (6h), before induction (0h) and a protein molecular weight marker (M).

All mutated enzymes were overexpressed successsfully in a soluble form and were further subjected to protein purification (3.3.2.2.3).

3.3.2.2.3. Purification of PcpI cysteine mutants

The purification of the PcpI cysteine mutants was performed following the protocol established for PcpI-6xHis as described in section 3.2.1.7. On average 2.5 g of cell paste was obtained per 1 L of bacterial culture. This was used for protein extraction and the supernatant, obtained during the procedure, was applied to a Ni^{+} Sepharose column and subjected to protein purification as described in section 3.2.1.7. The representative elution profile for C107/108A, shown in figure 3.36, allowed for determination of fractions containing the PcpI-6xHis cysteine mutant, which were further analysed using the SDS-PAGE to assess the purity of the eluted protein. A result of this analysis is presented in figure 3.37.

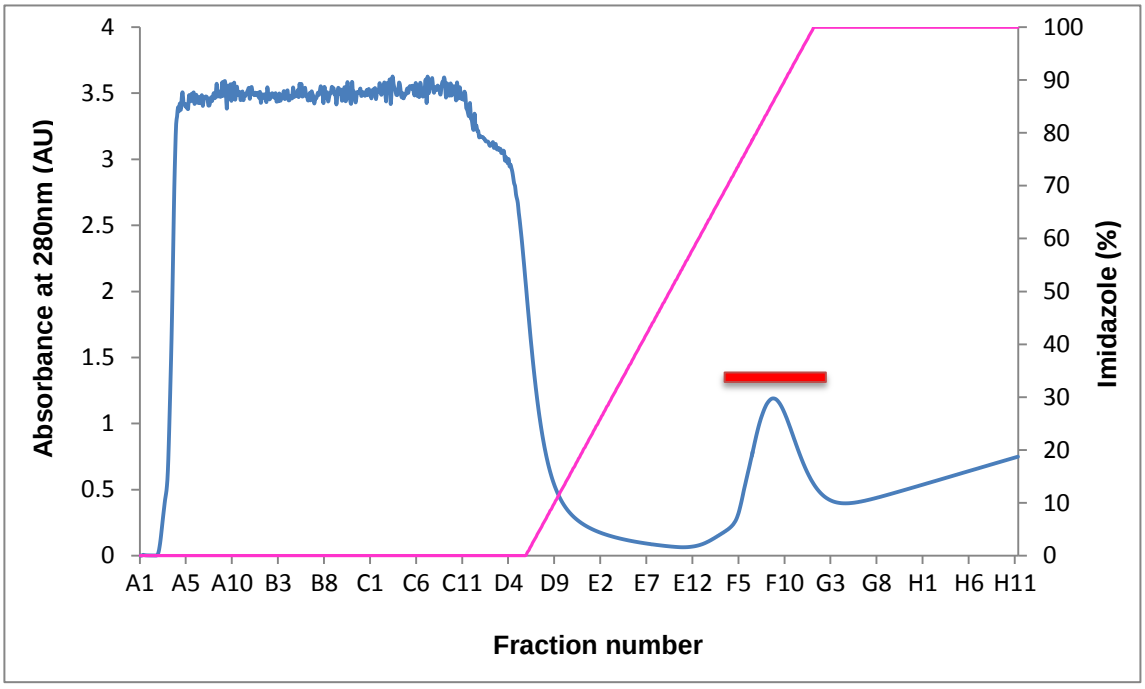

Figure 3.36. The nickel affinity protein elution profile of the C107/108A PcpI-6xHis mutant. The fractions containing the protein are marked by the red bar. The A_{280} trace is coloured in blue and the imidazole gradient is coloured in pink.

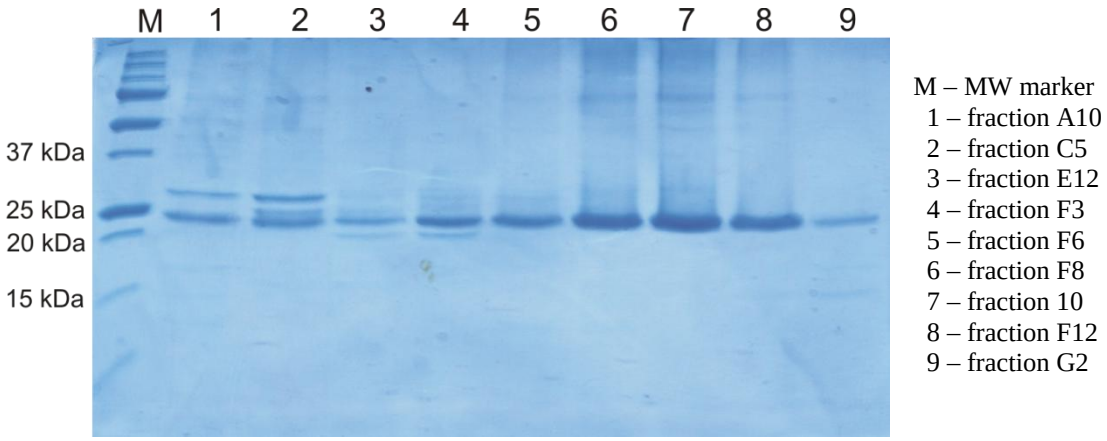

Figure 3.37. The result of the SDS-PAGE analysis of the C107/108A PcpI-6xHis mutant purified by nickel affinity chromatography.

All cysteine-mutated PcpI-6xHis variants were observed to have a similar elution profile from the nickel affinity purification step and were found in fractions eluted with the same concentration of imidazole.

The mutated isoforms were intended to be used in crystallisation trials, therefore their samples were required to be of the high purity and homogeneity. In order to achieve this and remove any undesired contaminants, the fractions collected from Ni^{+} Sepharose™ column purification, which contained the desired protein were pooled together, concentrated using Vivaspin20 centrifugal concentrators and run through the gel filtration column (3.2.1.3.4). The resulting representative elution profile and the SDS-PAGE analysis for C107/108A mutant are presented in figures 3.38 and 3.39, respectively.

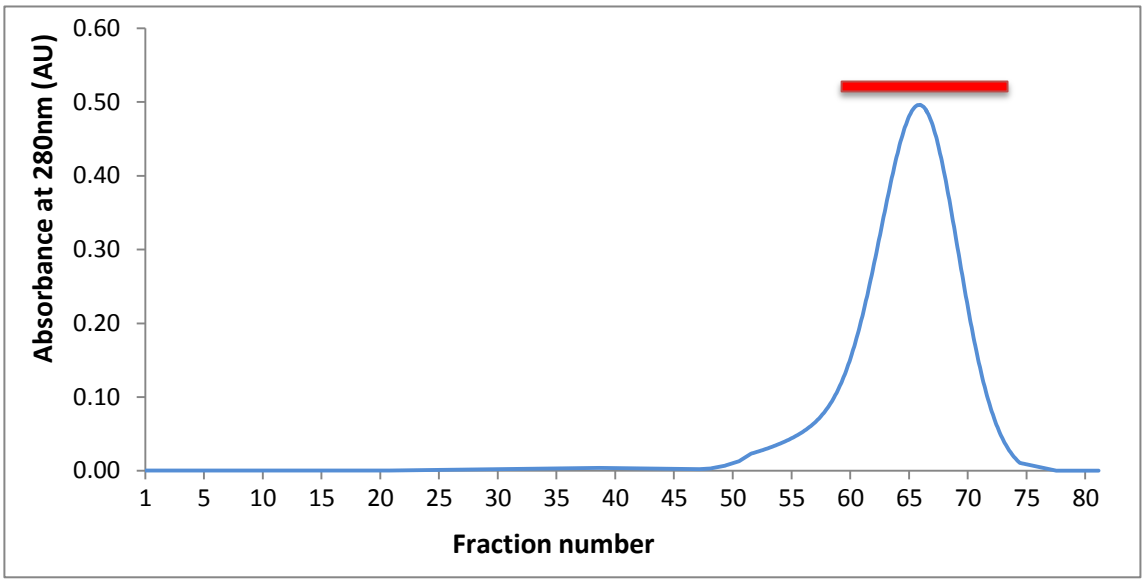

Figure 3.38. The gel filtration protein elution profile of the C107/108A PcpI-6xHis mutant. The fractions containing the protein are marked by the red bar. The A_{280} trace is coloured in blue.

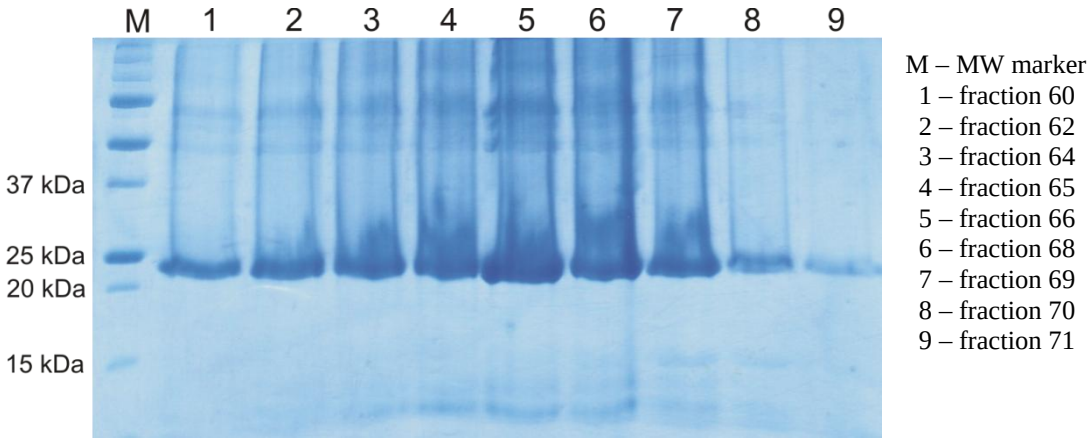

Figure 3.39. The result of the SDS-PAGE analysis of the C107/108A PcpI-6xHis mutant purified by gel filtration chromatography.

The cysteine-mutated isoforms were generally found to be eluted in the fractions typical for proteins of around 25 kDa (appendix IV) and the position of the peak was the same as previously observed for all non-mutated PcpI forms (3.2.2.3.3, 3.2.2.6.2 and 3.2.2.7.3). The only surprising phenomenon was observed for the C107A mutant (figure 3.40), which eluted in the fractions typical for a protein with a mass between 43 and 75 kDa (appendix IV).

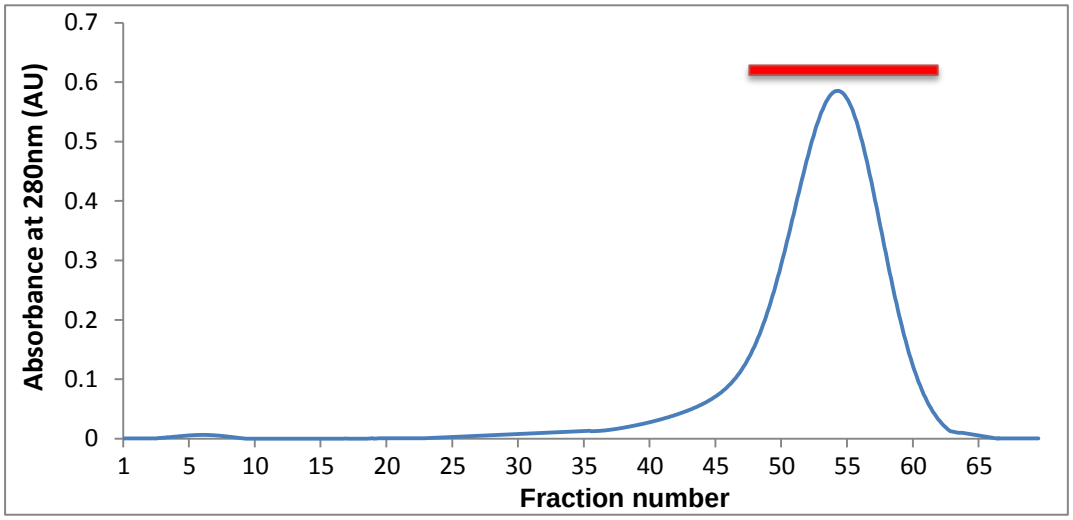

Figure 3.40. The gel filtration protein elution profile of the C107A PcpI-6xHis mutant. The fractions containing the protein are marked by the red bar. The A_{280} trace is coloured in blue.

Analysis of the eluted fractions by the SDS-PAGE technique revealed that the presence of a protein of around 45 kDa which may suggest that C107A exists in a dimeric form (figure 3.41).

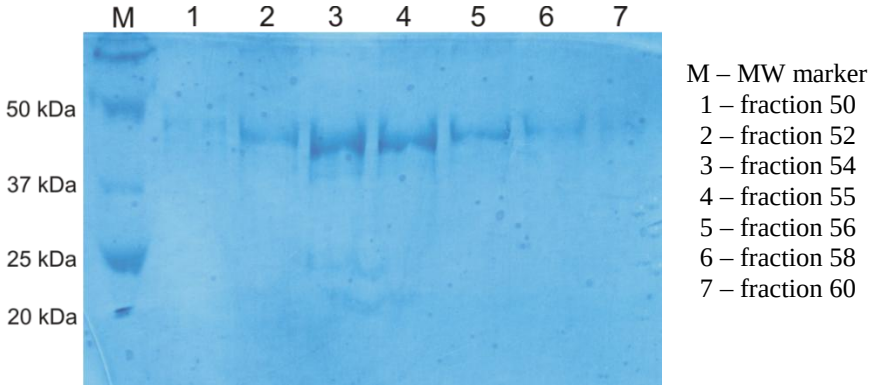

Figure 3.41. The result of the SDS-PAGE analysis of the C107A PcpI-6xHis mutant purified by gel filtration chromatography.

Additionally, the results of the fluorimetric activity assay (2.8.4) showed that all of the mutated proteins were enzymatically active, with an exemption of C107A. These results for C107 PcpI mutant may implicate an important role of this residue in the human PcpI. The adjacent C107 and C108 residues are believed to be located within a flexible, cysteine-rich loop (figure 3.34) and may possibly undergo an oxidation to cystine creating a strained 8-membered intramolecular ring. The disulfide bridge between neighbouring cysteines (vicinal disulfide) is a rare structural element resulting in the formation of a tight turn of the polypeptide backbone. Studies on small model peptides showed that the side chains of the ring-forming cysteines exist in the equilibrium of the *cis-trans* conformation (Kim *et al.*, 1999). Such a formed peptide units show frequent deviation from planarity with a torsion angle ranging from 159 to –131º (Carugo *et al.*, 2003). The polypeptide segments containing a vicinal cystine bridge are found to be significantly bent with the two side chains protruding on the same (cis) side of the backbone. On the contrary, in reduced state cysteine side chains are located on the opposite (trans) positions and the lack of backbone constraints makes it more extended and flexible.

Vicinal disulfides have been reported and characterised in a range of enzymes, receptors and toxins (reviewed in (Carugo *et al.*, 2003). The biological function of this interaction is not fully understood and it is considered to have both roles in the regulation of redox homeostasis (e.g. participation in electron exchange) as well as in the control of the structural conformation of the protein backbone. Formation and decomposition of the vicinal disulfide has been observed to have an impact on the protein performance and structural conformation. Such a regulatory effect is thought to occur in the nicotinic receptor which is unable to bind ACh when its intramolecular Cys-Cys bridge is unformed (Czajkowski and Karlin, 1995). Similarly, the reduction of the cystine ring found within an active site of the methanol dehydrogenase from *Methylophilus* sp. has been seen to cause its rapid inactivation (Blake *et al.*, 1994). The vicinal disulfide is also thought to play an important role in binding and cation reduction in mercuric ion reductase, which activity has been seen to be abolished as a result of the oxidation of the adjacent active site C558 and C559 residues (Engst and Miller, 1999). Interestingly, the disulfide ring is more resistant to reduction than the disulfide bond between two cysteines separated by another amino acid (CXC motif) (Zhang and Snyder, 1989).

In some cases the oxidation of adjacent cysteine residues may destabilise structural conformation of a given protein. For example, the reduction of a vicinal disulfide bond seems to be necessary to maintain structural stability of a Janus-faced atracotoxin despite the complete loss of its neurotoxic activity (Wang *et al.*, 2000). Similarly, the alternative formation of two possible cystine rings inactivates human ribonuclease inhibitor (Kim *et al.*, 1999).

An interesting role of this kind of interaction between adjacent cysteine residues was proposed in the report by Cemazar and co-workers after the observation of the non-native vicinal disulfide bridge in the transient intermediates of the Amaranthus α-amylase inhibitor during its oxidative folding (Cemazar *et al.*, 2003). Molecular modelling analysis led to the suggestion that the cystine ring is created within a flexible loop region and it may impose structural constraints on the folding intermediates. This formation of the transient vicinal disulfides is believed to govern the protein folding process by creating a compact fold and facilitating the reshuffling to native disulfide bridges by the positioning of the cysteine residues in close proximity.

The presence of the adjacent C107 and C108 residues and their localisation within a flexible cysteine-rich loop can be seen in the human PcpI structure model (figure 3.34), and may have a significant impact on the protein behaviour and stability. Potential formation of the C107-C108 ring could provide conformational constraints on the polypeptide backbone necessary for proper folding, structure stability and activity as it was observed in the aforementioned studies. Therefore observed existence of C107A in a dimeric form (and a lack of higher oligomers) may be explained by the possible intermolecular disulfide bridge between unbound C108 residues. Since the C107A mutant was seen to be inactive one may suggest that the C107-C108 tandem may serve as an artificial redox switch, which regulates enzymatic activity. Such an observation, however, has not been made for the C108A mutant, which retained all of the properties of the native PcpI and was enzymatically active. This finding implies that in the native protein C108 may be more reactive than C107 residue or its side chain is better exposed to participate in the dimerization. The study on the thimet oligopeptidase showed that the dimer formation by intermolecular disulfide bond could inactivate the protein due to blocking of the opening of the substrate channel (Sigman *et al.*, 2003). Other explanation suggests the induction of structural changes preventing substrate binding or hindering conformational changes required for enzymatic activity (Ray *et al.*, 2002).

It is difficult to determine at this point if a formation of dimer is forced due to the C107A mutation and a probable interaction between C108 residues or it can appear naturally as a control of the protein behaviour. Studies showed that eukaryotic type I Pcps exist in a soluble monomeric form (1.2.4.1). On the contrary, Pcps from bacterial and archaeal sources are known to function as dimers or tetramers and in the cases of ***P.*** *furiosus* and *T. litoralis* representatives, formation of the inter-subunit disulfide bridge is thought to have a stabilising effect on the protein (1.2.3). Although the cysteine residue involved in this disulfide Cys190 (*T. litoralis* numbering) does not have an equivalent cysteine residue in the human PcpI sequence, one may suggest that an unusually high and odd number of cysteines in the latter one potentially gives an opportunity for the formation of similar dimer or oligomer.

Finally, it is worth noting that four cysteines in the flexible loop in the human PcpI could be involved in the coordination of a metal ion. The presence of such a cluster is typical for metal binding domains, where the metal ion plays an important structural function (Berg, 1990). However, previous reports on the incubation of human PcpI with EDTA resulted in no change in activity, which could indicate an absence of any metal ion of structural or activity-related importance (Dando *et al.*, 2003). Nonetheless, one of the approaches, as a part of the PcpI stabilisation study, was the addition of 50 μM $ZnCl_2$ to the *E. coli* culture prior to induction with IPTG (3.2.1.5). This is a common procedure for the expression of proteins containing zinc-binding motifs (Niedziela-Majka *et al.*, 1998). The presence of the structural zinc has been shown to stabilise protein domains (Guy *et al.*, 2003), however in this case it was not observed to improve PcpI stability.

All studied cysteine mutated variants PcpI-6xHis were purified, concentrated and used in a microbatch crystallisation procedure 3.4.2.4.2. The trial was performed using a variety of the commercially available screens (3.4.2.3). The results of these experiments were discussed in section 3.4.3.2.

3.3.3. Modification of the surface residues

Chemical modifications of protein residues in order to improve crystallisability are relatively less often used approaches. Frequently problems with obtaining good quality crystals are related to the difficult properties of the protein molecule arising from disorder fragments of the polypeptide chain such as extended surface loops. In other cases flexible, solvent-exposed amino acid side chains can also be problematic in crystallisation experiments. To overcome this, these residues can be suitably mutated or chemically modified. The important advantages of chemical modification are the elimination of repeated procedures beginning with re-cloning and finishing with purification, avoidance of the possibility of protein misfolding and, finally, manipulation of only surface residues (Walter *et al.*, 2006). Currently, the best known and used methods include modification of cysteine residues with DTNB, iodoacetate or N-ethylmaleimide as well as reductive methylation of the exposed amino groups resulting in conversion of primary amines to tertiary amines (Ellman, 1959; Rayment, 1997).

3.3.3.1. Materials and methods

3.3.3.1.1. Modification of surface cysteines with DTNB

Exposed thiol groups in the protein can be modified with DTNB also known as Ellman's reagent (Ellman, 1959). The method is based on the reaction of protein thiols with DTNB, which results in the production of the intermolecular disulfide bond and a release of the 2-nitro-5-thiobenzoate (NTB^-) (figure 3.42). In aqueous solution at neutral or alkaline pH NTB^- is subsequently ionized to the NTB^{2-} anion which produces a yellow color. This reaction is stoichiometric, therefore spectrophotometrical quantification of the NTB^{2-} helps to determine the amount of thiol groups that were modified by the DTNB.

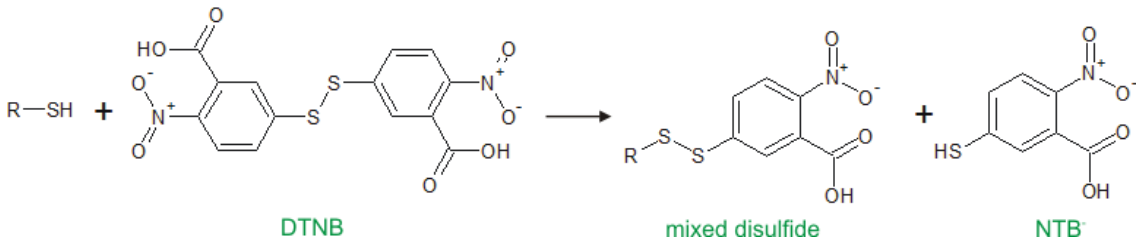

Figure 3.42. Reaction of a thiol group with DTNB.

The modification of PcpI cysteine residues was conducted according to the protocol described by Mi and co-workers (Mi *et al.*, 2008). DTNB powder was dissolved in dilution buffer (20 mM Tris-HCl pH 8.0 and 200 mM NaCl) to 2.0 mM and this was added to the purified PcpI-6xHis solution at a 5-fold molar excess. This was further incubated on ice for 30 min in order to complete the reaction. Next the mixture was purified by gel filtration chromatography as described in section 3.2.1.7 to remove excess DTNB and the reaction products. The pre-equilibration of the column and elution were performed using dilution buffer. Purified and modified PcpI-6xHis was concentrated in Vivaspin20 centrifugal concentrators (Sartorius Stedim Biotech S.A.) and further subjected to crystallisation trials using the microbatch technique as described in section 3.4.3.2.

3.3.3.1.2. Methylation of the surface lysines

Some of the amino acid residues found on the surface of the proteins, such as lysine or glutamic acid possess long and flexible side chains, which are often thought to hinder the process of crystallisation. Methylation of the side chain amines of the surface lysines has been shown to promote the process of formation of a crystal lattice presumably by immobilization of this mobile region.

The protocol of the methylation was taken from the report by Rayment and co-workers (Rayment, 1997). A purified sample of PcpI-6xHis (3.2.1.7) in HEPPS buffer C (2.3.3.5) was enriched with NaCl in order to obtain final volume of 250 mM. The sample was brought to a concentration of 0.5 mg/ml and after that it was mixed with 20 µl of the freshly prepared 1 M dimethylamine-borane complex (ABC; Fluka) and 40 µl of 1 M formaldehyde (from 37% stock) per 1 ml of the protein solution. This was gently mixed and incubated for 2 h at 4ºC. After that the next portion of 20 µl of ABC and 40 µl of 1 M formaldehyde was added per 1 ml of the original protein

sample, and this was continued to incubate for another 2 h at 4ºC. Next 10 µl of the ABC was added to the mixture and left for overnight incubation at 4ºC. After incubation any potential protein aggregates and contaminants were removed by centrifugation of the treated PcpI-6xHis sample. The protein was further purified using the gel filtration method. Pre-equilibration of the column and protein elution were performed using Tris-HCl buffer (20 mM Tris-HCl pH 7.5, 200 mM NaCl, 1 mM DTT). Appropriate fractions containing PcpI-6xHis were pooled together and subjected to buffer exchange (HEPPS buffer C, 2.3.3.5) using Vivaspin20 centrifugal concentrators (Sartorius Stedim Biotech S.A.). Then the protein sample was concentrated to the required concentration and subjected to crystallisation experiments using microbatch technique as described in section 3.4.3.2.

3.3.3.2. Results and discussion

The human PcpI-6xHis was subjected to the modification of exposed cysteine residues with DTNB (3.3.3.1.1) and lysine methylation (3.3.3.1.2). Significant aggregation of the protein was observed during the lysine methylation procedure, formation of which was concluded from the gel filtration elution profile (figure 3.43). This is however often observed as the reaction with ABC can cause significant protein precipitation (up to 50%) (Walter *et al.*, 2006). Although the aggregation was not seen on the SDS-PAGE gel (not shown), only the fractions collected during monomer elution were used for further applications.

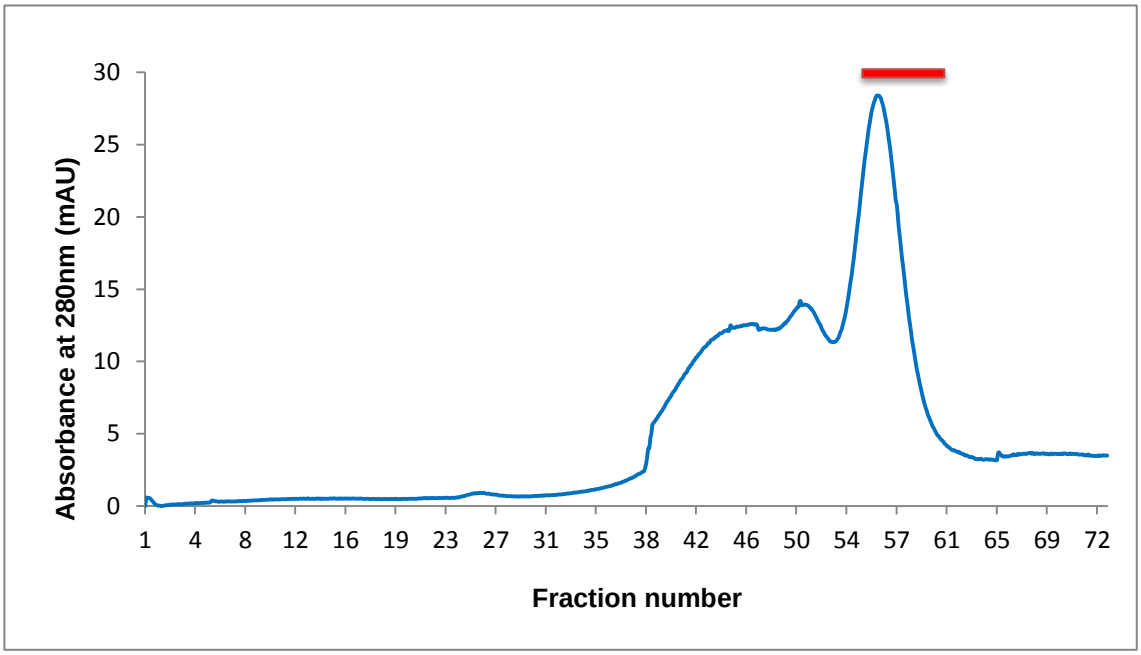

Figure 3.43. The gel filtration protein elution profile of the lysine-methylated PcpI-6xHis. The fractions containing the protein are marked by the red bar. Probable protein aggregates were eluted in a broad peak in the fractions 38-55. The A_{280} trace is coloured in blue.

Modified protein sample was concentrated up to 10 mg/ml and used in a microbatch crystallisation procedure 3.4.2.4.2. The trial was performed using a variety of the commercially available screens (3.4.2.3). The results of these experiments were discussed in section 3.4.3.2.

3.4. Crystallisation study on human PcpI

3.4.1. Introduction to protein crystallisation

X-ray crystallography and Nuclear Magnetic Resonance (NMR) spectroscopy are currently the most effective and popular methods to resolve three-dimensional protein structure. The goal of protein crystallisation is to produce well-ordered crystals suitable for X-ray diffraction that would result in good quality analytical data. The development of this technique has significantly accelerated since the first generation of earthworm hemoglobin crystals by Hünefeld in 1840 and the pioneering studies on the X-ray crystal structure of myoglobin in 1950. Nowadays it is widely used in a range of life science areas. Crystallisation itself is considered to be inherently difficult mainly due to the frequent problems with finding optimal and sometimes unique conditions to enhance protein crystal nucleation and growth. Moreover, the fragile nature of protein crystals and the fact that they disintegrate easily due change in temperature, pH, ionic strength or by dehydration often requires time-consuming optimisation of those parameters. The successful production of diffracting crystals is governed by a number of environmental factors such as protein purity (at least 97% pure) and concentration, pH, temperature, and precipitants. The values of all these parameters are usually unique for different proteins so their estimation can be facilitated by a high-throughput screening for optimal conditions or investigated through more time-consuming "trial and error" process.

The process of crystallisation can be differentiated into two stages: nucleation and crystal growth. First the purified and concentrated protein must undergo slow reduction of solubility to reach supersaturation. Very often this would result in the formation of an amorphous protein precipitate. However, in appropriate conditions, protein molecules can create non-covalent interactions, adopt proper geometrical orientation and align in an ordered crystalline aggregate. The aggregated state also must be more energetically favourable than the soluble one in order to allow for the crystal growth. Both crystal nucleation and growth can occur within the protein supersaturation region of the phase diagram (figure 3.44).

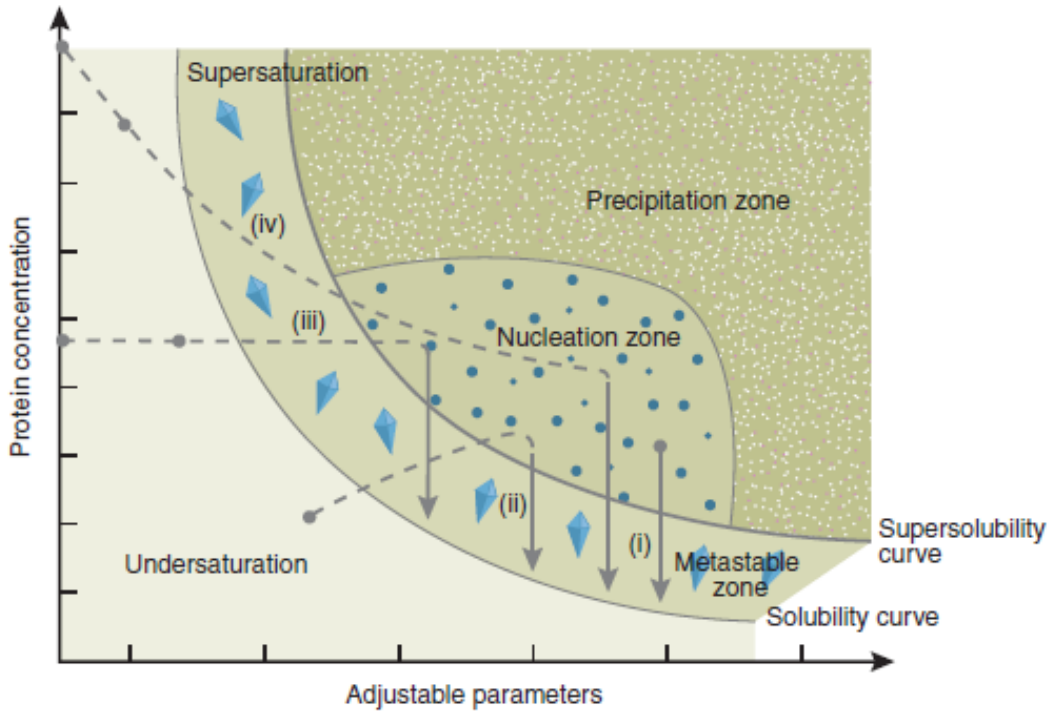

Figure 3.44. A schematic phase diagram of protein crystallisation. The different routes to reach the solubility curve are represented for four most popular methods of crystallisation: (i) microbatch, (ii) vapour diffusion, (iii) dialysis and (iv) free-interface diffusion (FID). Adjustable parameters refer to the concentration of precipitant or additive, pH and temperature. Taken from (Chayen and Saridakis, 2008).

The phase diagram (figure 3.44) indicates the relation between the protein concentration and the range of parameters that create the environment of crystallisation. The initial protein-precipitant solution first needs to reach the nucleation zone (labile zone), where the generation of the nuclei commences, and further progress to the metastable zone and solubility curve in order to produce crystals. The diagram presents different methods of crystallisation and the routes which given solutions follow to reach the destination point. It is worth noting that both dialysis and free-interface diffusion require much more concentrated protein solution than the remaining two methods and the process can start at two alternative points. In both cases the undersaturated solution may contain protein only or protein with a relatively low precipitant concentration. Many difficulties regarding the crystallisation process can be approached by the manoeuvres within the phase diagram. For example the transition from an

undersaturated to a supersaturated solution can be achieved by the proper combination of protein and precipitating agent or other influencing parameters. Another problem may be addressed when the system is maintained for too long within a nucleation zone. This usually results in rapid formation of a great number of nuclei and excessive production of small crystals. In order to overcome this, the system must be adjusted in the way so it could approach the nucleation zone slowly enough to allow the developing nuclei sufficient time to grow.

The two most popular techniques – vapour diffusion and microbatch crystallisation, were used in the study of human PcpI.

The principle of the vapour diffusion relies on process leading to equilibration between a droplet of purified protein mixed with precipitant solution and a larger reservoir containing the same precipitant solution but in higher concentrations. Over the course of time in a closed system water evaporates from the droplet, leading to the increase of precipitant concentration which can provide optimal conditions for crystallisation (Chayen, 1998). The technique can be performed in two variants known as the hanging drop and sitting drop methods, which differ in the shape and vertical orientation of the droplet in the setup. This may potentially have a small influence on the equilibration process.

Crystallisation under oil, widely known as microbatch crystallisation is particularly useful for high-throughput, automated screening for optimal conditions. The technique combines a small drop of a concentrated protein sample with the precipitant solution and this is further incubated under a small layer of the paraffin oil and silicon oil mixture (Chayen, 1997; D'Arcy *et al.*, 2003). Application of the oil allows for a slow diffusion of water from the droplet and a concentration of the sample and the reagents.

Human native PcpI, C-terminally His-tagged PcpI, cysteine mutants and PcpI with surface-modified residues were purified to homogeneity, concentrated and subjected to crystallisation trials using vapour diffusion and microbatch techniques.

3.4.2. Materials and methods

3.4.2.1. Protein sample preparation

The purified protein samples were quantified using absorbance measurement at 280 nm (2.8.3.1) and concentrated in a suitable purification gel filtration buffer (2.3.3). Protein concentration was conducted at 4ºC using a Vivaspin20 centrifugal concentrator with a 30 kDa molecular weight cut-off and regenerating polyethersulfone membrane (Sartorius Stedim Biotech S.A.). Immediately prior to crystallisation experiments the protein sample was centrifuged at 13,400xg for 5 min at 4ºC to pellet any possible aggregates.

3.4.2.2. Vapour diffusion technique

Crystallisation experiments employing the vapour diffusion technique (sitting and hanging drop methods) were conducted in 24 well ComboPlate™ plates (Greiner Bio-One) with CrystalClene^{TM} cover slides (Molecular Dimensions Ltd). Additionally, in the sitting drop method trial Micro-Bridge® inserts were employed (PSR1000, Crystal Microsystems). Typically, 0.5 or 1.0 ml of precipitant solution (reservoir) was pipetted into a well. A 1 µl (or more) of concentrated protein solution was mixed with reservoir solution in a desired ratio on a cover slide (hanging drop method) or microbridge (sitting drop method). The cover slides were sealed to the upper edge of the plate using Dow Corning high vacuum grease (Molecular Dimensions Ltd). Plates were then incubated at 4ºC or 18ºC and examined for crystal growth under a light microscope.

3.4.2.3. Microbatch screening technique

Crystallisation experiments employing the microbatch screening technique were conducted in Hampton 96 well plates using an Oryx6 crystallisation robot according to the manufacturer's instructions (Douglas Instruments Ltd).

Commercial screening kits of precipitation solutions used in this method included:

- Crystallization Basic Kit for Proteins 82009 (Sigma)
- Crystallization Extension Kit for Proteins 70437 (Sigma)
- JCSG-plus™ (Molecular Dimensions Ltd)
- PACT-premier™ (Molecular Dimensions Ltd)
- Structure Screen 1 and Structure Screen 2 (Molecular Dimensions Ltd)
- pHClear and pHClear II (Qiagen)

The Oryx6 robot was set up to dispense equal volumes (0.5-1.0 µl) of the concentrated protein solution and precipitation solution in the bottom of each well. This was immediately covered with 1:1 (v/v) mixture of paraffin oil and silicon oil to prevent excessive evaporation of the well content. Plates were then incubated at 18ºC and controlled for crystal growth under a light microscope.

3.4.2.4. Crystallisation experiments

3.4.2.4.1. Vapour diffusion crystallisation trials

Preliminary purifications of PcpI-6xHis and native PcpI in Tris-HCl based buffer system (2.3.3.3 and 2.3.3.4, respectively) resulted in the observation that both enzyme forms are extremely unstable and began precipitating out of solution during sample preparation procedure (3.4.2.1), when concentrated in the presence of NDSB-195 (3.2.2.6.3 and 3.2.2.7.4) above ~5.5 mg/ml and ~2.8 mg/ml, respectively. Various attempts were made in order to overcome the instability problem as described in section 3.4. Concentrating to at least 10 mg/ml is necessary to obtain a supersaturated protein solution facilitating its progress into the metastable zone (figure 3.39). Nonetheless, despite a relatively low protein concentration it was decided to perform a preliminary condition screening employing the vapour diffusion technique (3.4.2.2). Prior to the experiment a PcpI-6xHis and native PcpI samples were also assessed for homogeneity using DLS (3.2.2.6.3 and 3.2.2.7.4) in order to evaluate a possible aggregation state. A range of ammonium sulfate solutions (5-100% with 5% increments) were used in the reservoir as a precipitating reagent. In the case of both native PcpI and PcpI-6xHis, samples were mixed with reservoir solution in varied ratios such as 9:1, 8:2, 7:3 and 5:5

(protein:reservoir) to make up to 10 µl of a final droplet volume. The principle of the vapour diffusion crystallisation technique is a change of the droplet composition as it aims to reach equilibrium with the reservoir solution. This, in consequence, leads to the increase of protein concentration and its eventual supersaturation. The trials were performed using both sitting and hanging drop methods for native and recombinant PcpI-6xHis. Two sets of crystallisation plates were prepared, which were incubated both at 4ºC and 18ºC.

3.4.2.4.2. Microbatch crystallisation trials

The samples of the native PcpI, PcpI-6xHis, 11 cysteine mutants of PcpI-6xHis (3.3.2) as well as DTNB-modified and lysine-methylated PcpI-6xHis variants were purified in HEPPS based gel filtration buffer (2.3.3.5) and concentrated to a minimum of 10 mg/ml (3.4.2.1). Biochemical modification of the protein has often proved to improve crystallisation or enhance crystal quality (Rayment *et al.*, 1993; Oubridge *et al.*, 1995). Individual mutations of cysteines to alanines in this case reduce surface charge quantity and alter its distribution that may be important for generation of protein crystals. A search for crystallisation conditions was conducted using the microbatch screening technique and commercial kits as described in section 3.4.2.3. All plates were incubated at 18ºC.

3.4.2.4.3. Co-crystallisation trials

The presence of an inhibitor, co-factor or substrate transition state analogue in the active site often makes the protein less flexible and hence may facilitate its crystallisation (Hassell *et al.*, 2007). The choice of the inhibitor for PcpI was based on the results of thermofluor assay (3.3.1), which showed that the addition of the 2-pyrrolidone or L-pGlu acid increases the T_m of the protein by around 1.5ºC or 1.1ºC (for HEPPS buffer). 2-pyrrolidone is a reversible inhibitor being a pyroglutamate analogue and has been previously used to stabilise PcpI during purification and storage (Armentrout and Doolittle, 1969; Mudge and Fellows, 1973). Quantified native PcpI and PcpI-6xHis were enriched with a 5-fold molar excess of either 2-pyrrolidone or L-pGlu acid, incubated for 1 h at 4ºC and then subjected to the

standard sample preparation (3.4.2.1). Both protein samples were concentrated to around 15 mg/ml in HEPPS gel filtration buffer (2.3.3.4) and the crystallisation experiments were conducted using the microbatch technique as described in section 3.4.2.3. All plates were incubated at 18ºC.

3.4.2.4.4. Optimisation of crystallisation conditions

The optimisation of crystallisation conditions for PcpI-6xHis+2-pyrrolidone and native PcpI+2-pyrrolidone was conducted using the microbatch screening technique (3.4.2.3). The inhibitor was added in a 5-fold molar excess in relation to PcpI-6xHis and native PcpI prior to sample preparation as described in 3.4.2.4.3. A range of optimisation conditions was designed using XSTEP Optimization software provided with Oryx 6 crystallisation robot (Douglas Instruments Ltd). Varied condition parameters including pH, precipitant concentration and protein concentration were combined and are presented in table 3.13. All crystal plates were incubated at 18°C.

Varied parameter	Range	Increment
PcpI-6xHis/native PcpI concentration	5 – 25 mg/ml	5 mg/ml
pH	4.5 – 7.5	0.5
PEG 3350 concentration	7.5% – 25%	2.5%

Table 3.13. Parameters for the crystallisation conditions used during the optimisation procedure.

3.4.2.4.5. Crystal microseeding

The vapour diffusion technique (hanging drop) was employed to conduct the crystal streak microseeding procedure. The principle of this method is to use the pre-formed protein crystal nuclei in new crystallisation solutions in order to determine the optimal conditions for crystal growth. A droplet with PcpI-6xHis+2-pyrrolidone crystals and mother liquor was transferred to a small plastic tube containing 10 µl of the condition solution that they were produced in. Next the crystals were crushed using a needle, pipetting and vortexed to generate microcrystalline powder. Then individual

1:100 and 1:1000 dilutions of the microseed stock were prepared in a precipitant solution. A clean cat whisker was dipped into the diluted solution and ran through the pre-equilibrated drop consisting of the equal volumes of concentrated protein and chosen precipitant condition. The parameters of conditions used during microseeding are presented in table 3.14. All plates were treated as described in section 3.4.2.2 and incubated at 18ºC.

Varied parameter	Range	Increment
PcpI-6xHis/native PcpI concentration	10 – 50 mg/ml	5 mg/ml
pH	5.1 – 5.9	0.2
PEG 3350 concentration	10% – 20%	2%

Table 3.14. Parameters for the crystallisation conditions used during the microseeding procedure.

3.4.2.4.6. Preparation of crystals and X-ray data collection

The crystals of PcpI-6xHis+2-pyrrolidone were prepared for X-ray data collection by two methods depending on their quality and quantity. A small nylon loop was used to pick up a crystal which was immediately immersed in prepared cryo-protectant solution and then plunged in liquid nitrogen. Alternatively a crystal was flash frozen in liquid nitrogen directly from the droplet. X-ray diffraction of the crystals was analysed at Diamond Light Source synchrotron on I03 beamline using the Pilatus 6M detector.

3.4.3. Results and discussion

3.4.3.1. Vapour diffusion crystallisation trials

Concentrated protein samples of the native PcpI (approx. 2.8 mg/ml) and PcpI-6xHis (approx. 5.5 mg/ml) were subjected to crystallization trials using vapour diffusion technique as described in section 3.4.2.4.1. Prior to this, samples of both proteins were assessed using DLS measurement which returned a small polydispersity value and showed their homogeneity (3.2.2.6.3 and 3.2.2.7.4). Analysed proteins came directly from the gel filtration purification step in Tris-HCl buffer (2.3.3.3 and 2.3.3.4). A range of ammonium sulfate solutions (5-100% with 5% increments) were used in the reservoir. The use of simple single salt solutions was aimed to identify a protein precipitation point in initial crystallisation trials. This, if successful, could be further used as a starting point for optimization screening. Unfortunately, for both PcpI variants immediate precipitation was observed in a droplet upon mixing with a higher concentration of ammonium sulfate solutions (35% and above). The precipitation turned brown within a few days which indicates that this precipitant is unfavoured in crystallization conditions and causes protein denaturation. A few reports and experience using human PcpI showed the enzyme to be extremely unstable at room temperature after extended period of time. However, concurrent incubation at 4ºC, which should help to stabilize the protein and slow the equilibration process between a drop and a well, did not significantly improve precipitation. The observations were consistent for both hanging and sitting drop method. Moreover, both native PcpI and PcpI-6xHis were also noticed to progressively precipitate in conditions of lower ammonium sulfate concentration. This can be explained by the increase of precipitant concentration in a droplet with time which aims to reach equilibrium with reservoir solution. The other possibility is negative influence of ammonium sulfate on the stability of both proteins. This was later confirmed by the thermofluor shift assay (3.3.1) which showed that ammonium sulfate (pH 7.5) decreases T_m by 2.17ºC in case of PcpI-6xHis. It was decided therefore to search firstly the conditions that would stabilize the enzyme in solution and help to obtain a higher protein concentration to carry on further crystallisation trials.

3.4.3.2. Microbatch crystallisation trials

The thermofluor shift assay resulted in identification of HEPPS buffer as the most stabilizing for PcpI-6xHis of all tested conditions (3.3.1). The subsequent application of this buffer system (2.3.3.4) for purification of the native PcpI, PcpI-6xHis and cysteine mutants of PcpI-6xHis helped to stabilise the proteins particularly during the concentration step. Concentrated protein samples of the native PcpI (~12 mg/ml), PcpI-6xHis (~15 mg/ml), all cysteine mutants (concentrated to 10-15 mg/ml) and PcpI-6xHis derivatives subjected to lysine methylation and cysteine DTNB-modification (~10 mg/ml), were subjected to crystallization trials using the microbatch technique as described in section 3.4.2.4.2. The screening yielded very few results and in most of the cases immediate protein precipitation was observed upon mixing with the condition solution. Despite a number of wells staying clear for an initial few days no protein crystals were observed even after longer period of incubation. Additional difficulty was found in some cases with an early appearance of salt and polyethylene glycol (PEG) crystals. This was problematic in the analysis of the experimental results and is undesirable if in a given condition the protein requires longer time for crystal growth. Despite a broad screening for crystallisation conditions for all PcpI forms it brought no positive results. Therefore it was decided to additionally enhance the protein stability using its inhibitors.

3.4.3.3. Co-crystallisation trials

Concentrated samples of the native PcpI (~12 mg/ml) and PcpI-6xHis (~15 mg/ml), both mixed with a 5-fold molar excess of either 2-pyrrolidone or L-pGlu acid, were subjected to crystallisation experiment using the microbatch technique as described in section 3.4.2.4.3. This time the level of protein precipitation was much slower comparing to trials without inhibitors. Numerous wells stayed clear for a few days indicating improved protein stabilisation, where previously fast precipitation had occurred. After 2 weeks many of the wells contained small crystalline particles, which were soft by crushing with a fine needle that is an indication of protein crystals. Most of these were too small however to test them. Only small plate crystals found for PcpI-6xHis+2-pyrrolidone mixture in a condition of 0.1 M Bis-Tris pH 5.5 and

15% PEG3350 were confirmed as protein using X-ray diffraction screening (3.4.2.4.6). A cryo-protectant solution consisted of 0.1 M Bis-Tris pH 5.5, 15% PEG 3350 and 30% PEG400 was used. The crystals and resultant diffraction pattern are presented in figures 3.45 and 3.46, respectively.

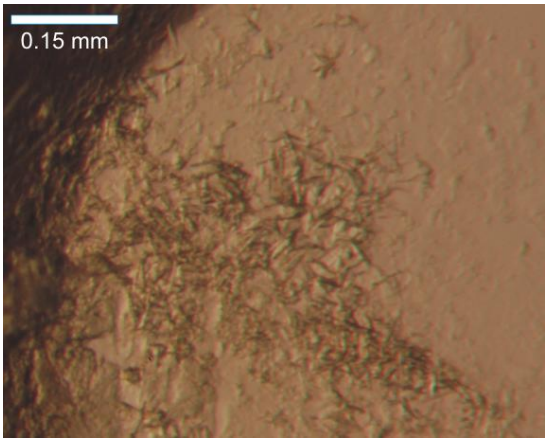

Figure 3.45. Crystals of human recombinant PcpI-6xHis+2-pyrrolidone obtained from incubation with 0.1 M Bis-Tris pH 5.5 and 15% w/v PEG3350.

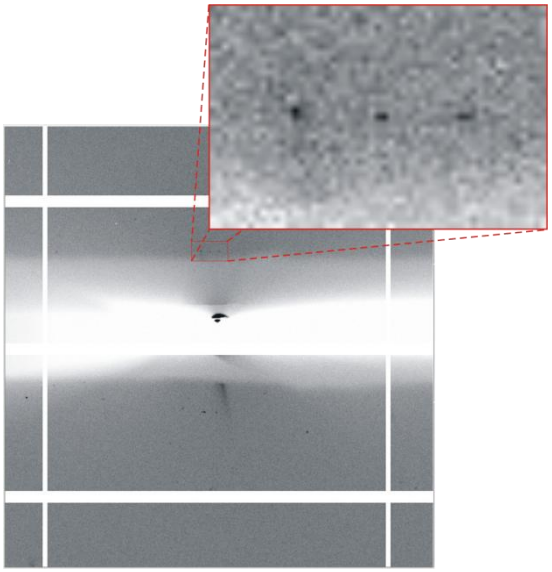

Figure 3.46. An X-ray diffraction pattern of a PcpI-6xHis+2-pyrrolidone crystal. The fragment with a regular reflection arrangement is zoomed in and the spots are found at the resolution of 28 Å.

The crystals were not of a good quality; too small and diffracting to around 28 Å. This however helped to establish a starting crystallisation condition for a further optimisation process.

3.4.3.4. Optimisation of crystallisation conditions

The precipitant solution 0.1 M Bis-Tris pH 5.5 and 15% PEG 3350, which PcpI-6xHis crystals were found at, was used as a starting point for optimisation of the crystallisation conditions. Although the crystals were only found for PcpI-6xHis mixed with 2-pyrrolidone, it was decided to conduct the experiment also for native PcpI+2-pyrrolidone. The optimisation procedure was performed as described in section 3.4.2.4.4. Unfortunately, the designed conditions did not yield any good quality crystals although they were frequently checked over a 2 months period. In wells where higher protein concentrations were used (~15-25 mg/ml) immediate precipitation was observed. Many wells returned small crystalline particles for PcpI-6xHis+2-pyrrolidone, similar to those obtained in co-crystallisation trials (3.4.3.2) however they did not follow any pattern in relation to pH or precipitant concentration. There was no such crystallisation observed in the plates with the native PcpI indicating that it is less stable than its C-terminally His-tagged form.

3.4.3.5. Crystal microseeding

The microseeding procedure was conducted using PcpI-6xHis crystals resulted from co-crystallisation trials in 0.1 M Bis-Tris pH 5.5 and 15% PEG 3350 (3.4.3.3). This condition was used as a basis for a design of new reservoir solutions as described in section 3.4.2.4.5. Unfortunately, the conditions used also did not yield any good quality crystals. The plates were frequently checked over a 2 months period, however within this time most of the protein precipitated in droplets. Similarly to microbatch optimisation (3.4.3.4), wells where higher protein concentrations were used (up to 50 mg/ml) immediate precipitation was observed.

Crystallisation experiments on human PcpI did not yield good quality crystals that could provide data for structural study of the protein. However, they helped to establish conditions suitable for nucleation. These parameters were further used for a design of optimisation and microseeding conditions. Unfortunately, neither of those promoted crystal growth so far. Human PcpI is known to be very unstable protein and may be sensitive for even minor changes in the content of precipitating solutions. This could in turn affect crystallisation ability and therefore it is necessary to continue optimisation screening over a narrow range of condition parameters with minor increments.

Chapter 4 – Studies on human pyroglutamyl peptidase II

4.1. Human PcpII

Human pyroglutamyl peptidase type II, better known as thyrotropin-releasing hormone-degrading enzyme (TRH-DE), is a member of the M1 family of Zn-dependent metallopeptidases in the MEROPS classification (Rawlings *et al.*, 2010). The enzyme catalytic activity is highly specific towards a degradation of TRH and TRH-like neurohormones, important for physiological regulation of the multiple functions within the central nervous system. Analysis of PcpII distribution in primary murine cultures showed that it can be exclusively found on the surface of neurons (but not on glial cells), which facilitates its regulating function in quenching of the neurotropic TRH signal (Bauer *et al.*, 1990; Cruz *et al.*, 1991). Initial reports regarding Pcp did not differentiate the type I (3.1) and type II form of the peptidase until the study by the O'Connor group, which proposed the existence of two pGlu-removing activities displaying distinct biochemical properties (O'Connor and O'Cuinn, 1984). One of them was the inhibition of PcpII activity by chelating agents such as 1,10-phenanthroline, 8-hydroxyquinoline and EDTA, but its activity is not affected by specific PcpI inhibitors (Cummins and O'Connor, 1998).

PcpII is a large glycoprotein of liver origin and can be found in the body as a brain and liver enzyme (both membrane-bound) or as a soluble serum enzyme, which is thought to be generated by an alternative post-translational proteolytic cleavage (Schmitmeier *et al.*, 2002). The different homologues have 12 potential N-glycosylation sites and differ only in their glycostructures. The brain enzyme possesses an oligomannose moiety, whereas the two remaining ones contain, typical for serum, terminal α(2-6)-sialic acid units linked to galactose (Schmitmeier *et al.*, 2002). All PcpII variants, like many surface peptidases, function as homodimers of a relatively large molecular mass of 230 kDa (brain enzyme) or 250 kDa (liver and serum enzymes). The amino acid sequence of the extracellular catalytic domain is well conserved among mammalian homologues and contains a characteristic exopeptidase (G/A)(A/G)MEN motif and a catalytic consensus $HEXXHX_{18}E$ motif, which coordinates the Zn^{2+} ion within the active centre of the zinc-dependent metallopeptidases (Vallee and Auld, 1990; Schomburg *et al.*, 1999). Additionally the extracellular domain contains eight

cysteine residues that are believed to be necessary to maintain an active protein structure and are involved in homodimerization (Cys68, human protein numbering) (Papadopoulos *et al.*, 2000). To date there is no published structural data on any PcpII protein.

This chapter presents experimental work on the human PcpII enzyme including a screening for the optimal overexpression conditions in bacterial, baculovirus/insect and mammalian systems. Apart from the protein expression study, preliminary homology modelling of the protein three-dimensional structure was conducted, in the absence of any crystallographic structural information on any type II Pcp representative. This could provide some idea about the protein conformation and would help to investigate how the substrate binds in the active site.

4.2. Preparation of human PcpII

4.2.1. Materials and methods

4.2.1.1. Prediction of structural domains and conserved regions

Due to the fact that PcpII is a large membrane-anchored ectoenzyme preliminary amino acid sequence analysis was performed in order to identify potential domain boundaries and functionally important regions of the protein. The query sequence was submitted to the GlobPlot protein disorder, domain and globularity prediction server (Linding *et al.*, 2003) and searched against the Pfam protein database (pfam.sanger.ac.uk). The results returned by Globplot (not shown) predicted the existence of 3 putative PcpII domains separated by short low-complexity fragments: an N-terminal domain (transmembrane, 1-61), a middle domain (catalytic, 130-793) and a C-terminal domain (801-1024). The search against the Pfam collection resulted in the identification of the region (141-530) conserved in protein members of the M1 family of peptidases (Rawlings and Barrett, 1995). Initial overexpression experiments of the full protein in the bacterial cells may be problematic. Therefore on the basis of the presented domain predictions it was decided to perform an expression study of chosen PcpII fragments: PcpII/L141-M541, PcpII/S62-G793 and PcpII/L141-H1024 (figure 4.1). All

of the truncated PcpII fragments cover the catalytic domain region with the consensus $HEXXHX_{18}E$ motif. The longest PcpII/S62-H1024 and PcpII/L141-H1024 variants consist of the catalytic and C-terminal domains. The expression of such a long fragment (901 aa) may be more difficult than the synthesis of the complete catalytic domain. However, the structural study on some metallopeptidases, such as aminopeptidase A, neprilysin or perfringolysin O, resulted in the observation that the presence of the C-terminal domain or its specific residues may be essential for the correct folding and function of whole protein (Shimada *et al.*, 1999; Navarrete Santos *et al.*, 2002; Rozenfeld *et al.*, 2004).

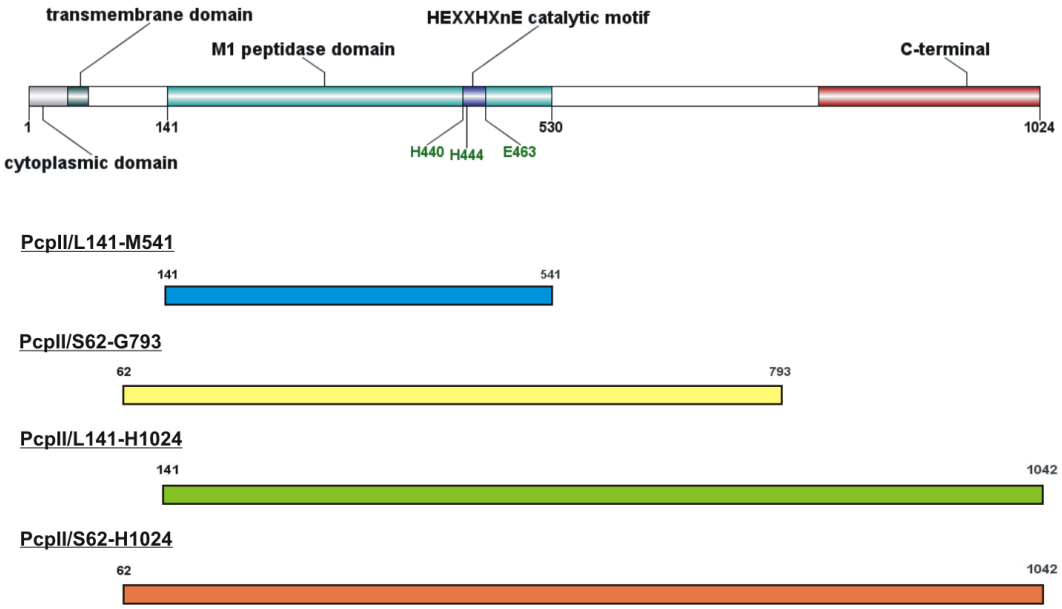

Figure 4.1. Schematic representation of the full-length PcpII (PcpIIFL) and truncated PcpII fragments: PcpII/L141-M541 (blue), PcpII/S62-G793 (yellow), PcpII/L141-H1024 (green) and PcpII/S62-H1024 (orange). The position of the individual domains, the consensus $HEXXHX_{18}E$ motif and the catalytic triad residues are marked in the diagram representing the full-length protein.

The amino acid sequences of the native and truncated isoforms of human PcpII were used to determine the protein parameters using the bioinformatic tools available on the ExPASy server (www.expasy.org, (Gasteiger *et al.*, 2003)). The expression studies were conducted for a range of the protein variants such as full-length PcpII (referred further as PcpIIFL), PcpII/L141-M541, PcpII/S62-G793, PcpII/L141-H1024 and PcpII/S62-H1024. The amino acid sequence of PcPIIFL with predicted domain boundaries and potential N-glycosylation sites as well as parameters for the relevant

PcpII isoforms are presented in table 4.1. The nucleotide and amino acid sequences of the individual proteins are found in appendices VIII-XI.

PcpII protein sequence:

MGEDDAALRAGSRGLSDPWADSVGVRPRTTERHIAVHKRL (1-40 cytoplasmic)
VLAFAVSLVALLAVTMLAVLL (41-61 transmembrane)
SLRFDECGASATPGADGGPSGFPERGGNGSLPGSARRNHHAGGDSWQPEAGGVASPGTT
SAQPPSEEEREPWEPWTQLRLSGHLKPLHYNLMLTAFMENFTFSGEVNVEIACRNATRY
VVLHASRVAVEKVQLAEDRAFGAVPVAGFFLYPQTQVLVVVLNRTLDAQRNYNLKIIYN
ALIENELLGFFRSSYVLHGERRFLGVTQFSPTHARKAFPCFDEPIYKATFKISIKHQAT
YLSLSNMPVETSVFEEDGWVTDHFSQTPLMSTYYLAWAICNFTYRETTTKSGVVVRLYA
RPDAIRRGSGDYALHITKRLIEFYEDYFKVPYSLPKLDLLAVPKHPYAAMENWGLSIFV
EQRILLDPSVSSISYLLDVTMVIVHEICHQWFGDLVTPVWWEDVWLKEGFAHYFEFVGT
DYLYPGWNMEKQRFLTDVLHEVMLLDGLASSHPVSQEVLQATDIDRVFDWIAYKKGAAL
IRMLANFMGHSVFQRGLQDYLTIHKYGNAARNDLWNTLSEALKRNGKYVNIQEVMDQWT
LQMGYPVITILGNTTAENRIIITQQHFIYDISAKTKALKLQNNSYLWQIPLTIVVGNRS
HVSSEAIIWVSNKSEHHRITYLDKGSWLLGNINQTGYFRVNYDLRNWRLLIDQLIRNHE
VLSVSNRAGLIDDAFSLARAGYLPQNIPLEIIRYLSEEKDFLPWHAASRALYPLDKLLD
RMENYNIFNEYILKQVATTYIKLGWPKNNFNGSLVQASYQHEELRREVIMLACSFGNKH
CHQQASTLISDWISSNRNRIPLNVRDIVYCTGVSLLDEDVWEFIWMKFHSTTAVSEKKI
LLEALTCSDDRNLLNRLLNLSLNSEVVLDQDAIDVIIHVARNPHGRDLAWKFFRDKWKI
LNTRYGEALFMNSKLISGVTEFLNTEGELKELKNFMKNYDGVAAASFSRAVETVEANVR
WKMLYQDELFQWLGKALRH

	PcpIIFL	PcpII/ L141-M541	PcpII/ S62-G793	PcpII/ L141-H1024	PcpII/ S62-H1024
cDNA length (bp)	3072	1203	2196	2652	2889
Protein length (aa)	1024	401	732	884	963
Molecular weight (Da)	116999.6	46285.3	83702.3	102399.4	109657.0
Theoretical pI	6.50	6.07	6.32	6.78	6.41
Extinction coefficient (M^{-1} cm^{-1})	217080	82530	159880	195080	211580

Table 4.1. Amino acid sequence and biophysical parameters of human PcpII and its truncated isoforms. The amino acid sequence of the protein is presented with marked predicted cytoplasmic (blue), transmembrane (yellow) and extracellular domains. Disordered fragments, which separate structural domains, are highlighted in grey. Potential N-glycosylation sites are marked in red font and the consensus catalytic $HEXXHX_{18}E$ motif is highlighted in green. The parameters were computed using the bioinformatic tools in the ExPASy server (www. expasy.org, (Gasteiger *et al.*, 2003)).

4.2.1.2. Cloning and expression of PcpII in bacterial cells

The expression screening in the bacterial system was conducted for three protein variants: PcpII/L141-M541, PcpII/S62-G793 and PcpII/L141-H1024. The cloning experiment employed pET-28a(+) vector (appendix I) in order to incorporate an N-terminal His-tag in all proteins. Additionally, PCR amplification of PcpII/L141-M541 insert was designed to enable the expression of the protein with the pelB leader sequence utilizing the pET-22b(+) vector (appendix II). The pelB is an N-terminal, 22 aa signal sequence of the pectate lyase B from *Erwinia carotovora* (Lei *et al.*, 1987). The fusion of this leader with a protein of interest enables its secretion to the bacterial periplasmic space, where it is subsequently cleaved off by a signal peptidase.

The cDNA encoding human PcpII was supplied as the pCMV-SPORT6/*trhde* construct from Open Biosystems Ltd. The clone was provided as *E. coli* DH5α in LB broth with 8% glycerol and 100 μg/ml ampicillin.

4.2.1.2.1. Preparation of the pCMV-SPORT6/trhde plasmid

In order to obtain a higher amount of the pCMV-SPORT6/*trhde* construct, the *E. coli* DH5α strain glycerol stock was used to inoculate 10 ml of LB media (2.2.1) containing 100 μg/ml ampicillin. This was grown overnight at 37ºC in a shaking incubator. Next the culture was subjected to DNA extraction according to the protocol of the GeneJET™ Plasmid Miniprep kit (Fermentas) (2.7.2). The result of the minipreparation was determined by a double digestion with *Not*I and *Eco*RV restriction enzymes (2.7.5.2). This was followed by 1% agarose gel electrophoresis (2.7.8). The samples containing the recombinant plasmids with inserts were further purified (2.7.3), quantified (2.7.4) and sequenced using the T7 (forward) and M13 (reverse) primers (2.7.10). Next pCMV-SPORT6/*trhde* was used as a template for the PCR amplification of the desired PcpII fragments.

4.2.1.2.2. PCR amplification of cDNA of PcpII fragments

PCR amplification of the cDNA fragments encoding PcpII/L141-M541, PcpII/S62-G793 and PcpII/L141-H1024 was conducted to obtain the inserts suitable for cloning into pET-28a(+) and the production of N-terminally His-tagged proteins. Additional amplification was conducted for PcpII/L141-M541 cDNA (PCR product referred as *pcpII/L141-M541-pelB*) to allow its cloning into pET-22b(+) in order to obtain a protein with N-terminal pelB leader sequence. Gene primers for the reactions were supplied by Eurofins MWG Operon and are listed in table 4.2.

Primer	Sequence	Restriction enzyme	GC content	T_m
L141-M541**F** (forward)	CAGCCATATGCTGTCGGGCCACCTGAAG	*Nde*I	60.7%	71.0ºC
L141-M541**R** (reverse)	CTCGAATTCTCACATAAAATTAGCCAGCATTCTT	*Eco*RI	35.3%	64.7ºC
S62-G793**F** (forward)	AGCCATATGAGCCTGCGCTTC	*Nde*I	57.1%	61.8ºC
S62-G793**R** (reverse)	CTCGAATTCTTACCCAAGCTTG	*Eco*RI	45.5%	58.4ºC
L141-H1024**F** (forward)	CAGCGCTAGCCTGTCGGGCCACCTGAAG	*Nhe*I	67.9%	73.9ºC
L141-H1024**R** (reverse)	TCTGCGGCCGCTTAGTGTCTTAGAGCTTTTCCTAAC	*Not*I	37.9%	62.4ºC
L141-M541pelB**F** (forward)	GATGGCCATGGCACTGTCGG	*Nco*I	65.5%	72.7ºC
L141-M541pelB**R** (reverse)	CTCGAATTCTCACATAAAATTAGCCAGCATTCTT	*Eco*RI	35.3%	64.7ºC

Table 4.2. List of PCR primers used for amplification of the PcpII cDNA fragments. L141-M541pelB**F** and L141-M541pelB**R** (identical with L141-M541R) were used for production of the insert enabling incorporation into the pET-22b(+) expression vector.

The composition of the amplification reaction mixture is presented below.

1 µl 50 ng/µl pCMV-SPORT6/*trhde*
1 µl 10 µM forward primer
1 µl 10 µM reverse primer
12.5 µl 2x GoTaq® Hot Start Green Master Mix*
9.5 µl ddH_2O

* The specification and properties of the GoTaq® Hot Start Green Master Mix (Promega) were outlined in section 3.2.1.4.1.

PCR amplification was performed in a Mastercycler® thermal cycler (Eppendorf). A range of tubes containing reaction mixture were prepared and each one of these was subjected to a different annealing temperature within a set gradient. The individual steps of PCR are described in table 4.3.

Step	Temperature	Time	
Initial denaturation	96ºC	3 min	
Denaturation	96ºC	1 min	30x
Annealing	temperature gradient 55ºC – 68ºC	1 min	
Extension	72ºC	1 min/1kb	
Final extension	72ºC	7 min	
Cooling	4ºC	-----	

Table 4.3. Thermal cycling steps during the reaction of amplification of the PcpII cDNA fragments.

The result of the PCR amplification was checked by 2% agarose gel electrophoresis as described in section 2.7.8.

4.2.1.2.3. Ligation of PcpII cDNA fragments with pET-28a(+) and pET-22b(+)

The PCR products obtained during the amplification of cDNA encoding human PcpII (4.2.1.2.2) were purified using the gel extraction method described in section 2.7.9. Next all inserts as well as the pET-28a(+) and pET-22b(+) plasmids were digested with suitable restriction enzymes (2.7.5.2):

- digestion with *Nde*I and *Eco*RI of the *pcpII/L141-M541*, *pcpII/S62-G793* inserts and pET-28a(+)
- digestion with *Nhe*I and *Not*I of the *pcpII/L141-H1024* insert and pET-28a(+)
- digestion with *Nco*I and *Eco*RI of the *pcpII/L141-M541-pelB* insert and pET-22b(+)

The linearized pET-28a(+) and pET-22b(+) plasmids were subsequently dephosphorylated at the 5′ end (2.7.6) and after that subjected to the ligation reaction with each of the *pcpII* insert variants (2.7.7). Next the ligation reaction mixtures were used for transformation into *E. coli* NEB 5-α competent cells (2.7.1). The transformants treated with the pET-28a(+) or pET-22b(+) mixtures were incubated overnight at 37ºC, on the agar plates (2.2.2) containing 50 μg/ml kanamycin or 100 μg/ml ampicillin, respectively.

4.2.1.2.4. Preparation of pET-28a(+)/pcpII and pET-22b(+)/pcpII recombinant plasmids

A few single *E. coli* NEB 5-α colonies, obtained from the transformation with the pET-28a(+) or pET-22b(+) ligation reaction mixtures (4.2.1.2.3), were picked and used for the inoculation of 10 ml of LB media (2.2.1) containing 50 μg/ml kanamycin or 100 μg/ml ampicillin, respectively. This was grown overnight at 37ºC in a shaking incubator. Next the cultures were subjected to DNA extraction according to the protocol of the GeneJET™ Plasmid Miniprep kit (Fermentas) (2.7.2). The result was determined by a double digestion of the plasmid preparations (2.7.5.2):

- digestion with *Nde*I and *Eco*RI of the pET-28a(+)/*pcpII/L141-M541* and pET-28a(+)/*pcpII/S62-G793*
- digestion with *Nhe*I and *Not*I of the pET-28a(+)/*pcpII/L141-H1024*

- digestion with *Nco*I and *Eco*RI of the pET-22b(+)/*pcpII/L141-M541-pelB*

This was followed by the agarose gel electrophoresis (2.7.8). The sample containing recombinant plasmids with inserts were further purified (2.7.3), quantified (2.7.4) and sequenced using standard T7 primers (2.7.10).

4.2.1.2.5. Protein overexpression in E. coli strains

Preliminary overexpression trials of PcpII/L141-M541, PcpII/S62-G793 and PcpII/L141-H1024 variants were performed in a range of commercially available *E. coli* strains designed to facilitate protein production. The tested strains included (2.4.2):

- BL21-CodonPlus®(DE3)-RIPL (alleviates rare *E. coli* codon bias, 3.2.1.2.1)
- ArcticExpress™ (DE3)RIL (alleviates rare *E. coli* codon bias and produces chaperonins facilitating protein expression at lower temperatures)
- Rosetta™ 2(DE3) (alleviates rare *E. coli* codon bias)
- Rosetta-gami™ 2(DE3) (alleviates rare *E. coli* codon bias and enhances disulfide bond formation)
- BL21(DE3)pLysS (enable expression of a protein toxic to the host cell)

All of the *E. coli* cells intended for the overexpression of PcpII fragments were made competent according to general chemical procedure described in section 2.5. Aliquots of the competent cells were directly used for the transformation procedure (2.7.1) or stored as glycerol stocks at -80ºC (2.6).

4.2.1.2.6. Screening for optimal overexpression conditions

The *E. coli* competent cells of each protein expression strain (4.2.1.2.5) were individually transformed with previously prepared recombinant constructs**:** pET-28a(+)/*pcpII/L141-M541*, pET-28a(+)/*pcpII/S62-G793*, pET-28a(+)/*pcpII/L141-H1024* and pET-22b(+)/*pcpII/L141-M541-pelB* (4.2.1.2.4). The transformation was conducted following the protocol described in section 2.7.1. All transformants were plated on Petri dishes containing 50 μg/ml kanamycin (pET-28a(+)) or 100 μg/ml ampicillin (pET-22b(+)) and 35 μg/ml chloramphenicol and incubated overnight

at 37ºC. Next day a random colony from each was used to inoculate 10 ml of LB media supplemented with selected antibiotics as above. This was grown overnight at 37ºC in a shaking incubator. Next day 5 flasks (per each tested strain) containing 100 ml of LB media with the above antibiotics were inoculated each with 1 ml of the overnight culture and grown in a shaking incubator at 37ºC. The induction of the protein overexpression was initiated by the addition of IPTG (2.2.3) to the final concentration of 1 mM. At this point cultures were continued to grow at 25ºC (5 flasks with cultures induced at an OD_{595} of 0.4, 0.6, 0.8, 1.0 and 1.2, respectively) and 37ºC (5 flasks with cultures induced at an OD_{595} of 0.4, 0.6, 0.8, 1.0 and 1.2, respectively). The exception from this rule was made for the ArcticExpress™ (DE3)RIL strain which after addition of IPTG was incubated at 12ºC. Samples for the protein overexpression analysis were collected from each flask prior to induction with IPTG and then every 5 h over a 30 h period. In the case of the ArcticExpress™ (DE3)RIL the culture sample was collected prior to induction with IPTG and after 24 h incubation. Protein isolation was carried out according to the detergent-based procedure (2.8.1.1) and the results of the protein expression were analysed using the SDS-PAGE technique with an 8% separating gel (2.8.2).

4.2.1.3. Cloning and expression of PcpII in insect and mammalian cells

The use of bacterial cells for heterologous expression of large, multi-domain mammalian or viral proteins often can be difficult or impossible. The production of proteins in the *E. coli* system is rapid and uncomplicated but it does not provide many of the post-translational modifications occurring in eukaryotic cells. This can often result in a misfolded protein, which is targeted to inclusion bodies or the yield of the production can be insufficient for subsequent applications. Therefore it is advisable to consider an expression screening in a more advanced host type such as mammalian or insect cells. Eukaryotic cell-based protein production generally requires more time and labour; however the popularization of these methods has significantly increased over the last decade and nowadays they are routinely used for basic research and large-scale commercial applications.

A key factor for the popularity of the insect cell system is its effectiveness in high-yield production of post-translationally modified eukaryotic proteins in a relatively

short period of time. This can be achieved by employing the specifically designed baculovirus vector expression system (BEVS) which is widely used to express foreign proteins (Mirzaei *et al.*, 2008; Shrestha *et al.*, 2008). Baculoviruses are a family of large, rod-shaped viruses infecting the insect population (Summers and Anderson, 1972). The most common expression system is based on *Autographa californica* nuclear polyhedrosis virus (AcNPV), where heterologous genes are introduced into a region of the genome that is not essential for viral replication and is under the control of the strong polyhedrin promoter, which drives expression in the last stages of the virus cycle (Kochan *et al.*, 1993). Such a construct is further transfected and propagated in cultured insect cells and insect larvae. The most popular host lines used for transfection are derived from *Spodoptera frugiperda* (*Sf*9 or *Sf*21) or *Trichoplusia ni* (High Five) species (Vadakkadathmeethal *et al.*, 2005). A prominent advantage of the baculovirus-mediated expression is the relatively large size of the viral genome, which enables the introduction of larger cDNA fragments and therefore expression of larger or multi-domain proteins. Moreover, if needed, a production of multi-protein complexes can be achieved by a simultaneous transfection with multiple constructs or by introduction of two or more expression cassettes in a single baculovirus (Berger *et al.*, 2004).

Mammalian cell lines represent an alternative for insect cell-based protein expression. They are most often used for secreted and membrane proteins or in cases where the most authentic post-translational modifications are essential for protein function. Several cell lines are commonly used as hosts for gene transfection and expression, such as COS (CV-1 cells of simian origin), CHO (chinese hamster ovary cells), HeLa (immortal human cells) and HEK (human embryonic kidney cells). A HEK293 is one of the most extensively used for the expression of a variety of recombinant proteins and was obtained by the exposure of HEK cell cultures to sheared DNA fragments of human adenovirus type 5 (Ad5) (Graham *et al.*, 1977; Thomas and Smart, 2005). The cells are transfected with a plasmid vector carrying a cDNA insert under control of different constitutive (e.g. CMV or SV40) or inducible promoters which force the expression of the desired gene products. An important variant of this cell line is the HEK 293T containing the SV40 large T-antigen, which facilitates episomal amplification of plasmids with the SV40 origin of replication. This in result increases a number of plasmid copies to persist in the transfected cells and the level of the desired protein expression (Van Craenenbroeck *et al.*, 2000).

This part of the experimental work involving cloning and expression of PcpII in eukaryotic cell systems was entirely conducted in the Oxford Protein Production Facility (OPPF, Research Complex at Harwell).

4.2.1.3.1. Expression vector constructs

A series of versatile pOPIN-based vectors was used to screen expression conditions for human PcpII (table 4.4). The pOPIN constructs were developed in OPPF on the basis of the parent pTriEx2 vector (Novagen) as described by Berrow and co-workers, and enable rapid high-throughput screening for protein expression in *E. coli*, mammalian and baculovirus-infected insect cells (Berrow *et al.*, 2007). The detailed characteristics and maps of the pOPIN series are available from Addgene plasmid repository (www.addgene.org) and their preparation procedure was described in the report by Berrow and co-workers (Berrow *et al.*, 2007). This set of vectors facilitates ligation-independent incorporation of a desired cDNA insert within the commercial In-Fusion™ PCR cloning system (Clontech), which allows for the precise engineering of His-tagged protein constructs. The principle of this method relies on the generation of the 15 bp 5′ and 3′ extensions in the PCR product, which can be subsequently fused to the homologous ends of a linearized vector. The joining is catalysed by the In-Fusion™ proof-reading exonuclease, which digests the double-stranded extensions and generates single-stranded DNA overhangs enabling the annealing between a vector and insert. The assembled construct further undergoes final repair within the *E. coli* host cell. The method was shown to be suitable for the cloning of large PCR fragments (3-11kb) over a wide range of DNA concentration (Marsischky and LaBaer, 2004; Berrow *et al.*, 2009).

All pOPIN-based vectors developed in the OPPF contain the *lacZ* insert encoding β-galactosidase that makes them suitable for the blue-white colony screening technique (Berrow *et al.*, 2007). The linearization of each vector with two restriction enzymes results in releasing of the *lacZ* cassette and incorporation of the desired insert DNA (Maas, 1999). In case this process is not successful, an intact gene expresses the active β-galactosidase, which cleaves colourless X-gal giving a bright blue insoluble product. The characteristic blue colour of colonies therefore is an indication of the presence of

non-recombinant vector, whereas a white colony is a sign of the successful ligation with the insert of interest.

Vector	Fusion Tag	Tag Sequence
pOPINE	C-terminal His-tag	-KHHHHHH
pOPINF	N-terminal His-tag	MAHHHHHHSSGLEVLFQGP-
pOPING	cleavable secretion leader	MGILPSPGMPALLSLVSLLSV LLMGCVAETG-
	C-terminal His-tag	-KHHHHHH
pOPINH	cleavable secretion leader, N-terminal His-tag	MGILPSPGMPALLSLVSLLSV LLMGCVAETMAHHHHHHSS GLEVLFQGP-
pOPINI	N-terminal His-tag	MAHHHHHHSSG-
pOPINTTG	cleavable secretion leader	MGILPSPGMPALLSLVSLLSV LLMGCVAETG-
	C-terminal His-tag	-KHHHHHH
pOPINTTGNeo-3C-GFP-His	cleavable secretion leader, N-terminal His-tag	MGILPSPGMPALLSLVSLLSV LLMGCVAETMAHHHHHHSS GLEVLFQGP-
	C-terminal GFP (green fluorescent protein)	-----
pOPINTTGNeo-3C-Halo7-His	cleavable secretion leader, N-terminal His-tag	MGILPSPGMPALLSLVSLLSV LLMGCVAETMAHHHHHHSS GLEVLFQGP-
	C-terminal HaloTag	-----
pOPINTTGNeo-3C-CD4-His	cleavable secretion leader, N-terminal His-tag	MGILPSPGMPALLSLVSLLSV LLMGCVAETMAHHHHHHSS GLEVLFQGP-
	C-terminal CD4 tag	-----
pOPINE-3C-GFP-His	cleavable secretion leader, N-terminal His-tag	MGILPSPGMPALLSLVSLLSV LLMGCVAETMAHHHHHHSS GLEVLFQGP-
	C-terminal GFP (green fluorescent protein)	-----
pOPINE-3C-Halo7-His	N-terminal His-tag	MAHHHHHHSSGLEVLFQGP-
	C-terminal HaloTag	-----

Table 4.4. The series of the pOPIN vectors used in the human PcpII expression study. Individual vectors differ with the type and position of a fusion tag, which is later incorporated in the recombinant protein. The N-terminal His-tags, with the exception of that from pOPINI, are cleavable from the protein with human rhinovirus 3C protease and all of the C-terminal His-tags are removable by carboxypeptidase A (Berrow *et al.*, 2007).

4.2.1.3.2. PCR amplification of PcpII fragments

On the basis of previous structural predictions of PcpII domain boundaries, PCR amplification was designed to obtain cDNA fragments encoding PcpIIFL as well as for its N-terminally truncated variants PcpII/S62-H1024 (no transmembrane domain) and PcpII/L141-H1024 (structured region). List of PCR inserts generated for cloning in appropriate pOPIN-based vectors is presented in table 4.5. Forward and reverse primer extensions, which were designed to facilitate the In-Fusion™ cloning, are listed in appendix XII.

The composition of the master mix (44 µl/reaction) for a single PCR reaction mixture:

2 µl 100 ng/µl pCMV-SPORT6/*trhde*
25 µl 2x KOD Hot Start Buffer*
10 µl 2 mM dNTP mix
1 µl 2.5 U/ µl KOD Xtreme™ Hot Start DNA Polymerase*
6 µl ddH_2O

* The KOD Xtreme™ Hot Start PCR system (Novagen) is optimized for the amplification of GC-rich (up to 90%) and long templates. The high fidelity KOD Xtreme™ DNA polymerase produces blunt-ended DNA products and is combined with two monoclonal antibodies, which permit hot start thermocycling.

PCR amplification was conducted in a 96-well plate. The master mix solution was dispensed into each well (44 µl/reaction) using a multi-channel pipette followed by the addition of 3 µl of each forward and reverse primer (10 µM). The plate was sealed with an adhesive film and placed in the Veriti® 96-Well Thermal Cycler (Applied Biosystems). The thermal cycling procedure was run according to the parameters listed in table 4.6.

VECTOR	PCR INSERT	OPPF NUMBER
pOPINE	PcpII/S62-H1024	8979
pOPINE	PcpII/L141-H1024	8981
pOPINF	PcpII	7468
pOPINF	PcpII/S62-H1024	8983
pOPINF	PcpII/L141-H1024	9076
pOPING	PcpII/S62-H1024	7465
pOPING	PcpII/L141-H1024	7211
pOPINH	PcpII/S62-H1024	7467
pOPINH	PcpII/L141-H1024	7210
pOPINI	PcpII	7469
pOPINTTG	PcpII/S62-H1024	7466
pOPINTTG	PcpII/L141-H1024	7212
pOPINTTGNeo-3C-GFP-His	PcpII/S62-H1024	8984
pOPINTTGNeo-3C-Halo7-His	PcpII/S62-H1024	8708
pOPINTTGNeo-3C-CD4-His	PcpII/S62-H1024	8709
pOPINE-3C-GFP-His	PcpII/S62-H1024	8980G
pOPINE-3C-GFP-His	PcpII/L141-H1024	8982G
pOPINE-3C-Halo7-His	PcpII/S62-H1024	8980
pOPINE-3C-Halo7-His	PcpII/L141-H1024	8982

Table 4.5. List of PCR inserts generated for cloning in the pOPIN-based vectors. Each construct is referred to by its individual number in the OPPF target database.

Step	Temperature	Time
Initial denaturation	94ºC	2 min
Denaturation	98ºC	10 s
Annealing	60ºC	30 s
Extension	68ºC	2 min 30 s
Final extension	68ºC	2 min
Cooling	4ºC	-----

30x

Table 4.6. The thermal cycling steps used during the reaction of amplification of the PcpII cDNA fragments.

Next 2 µl of the *Dpn*I restriction enzyme solution was added directly to each amplification reaction, which was briefly centrifuged and further incubated at 37°C for 1 h in order to digest the parental, non-methylated DNA template. The result of the PCR reaction was checked by 1% agarose gel electrophoresis as described in section 2.7.8. The less hazardous SYBR® Safe gel stain (Invitrogen) was used in place of ethidium bromide, which enables DNA visualisation using a blue or UV light illuminator.

4.2.1.3.3. In-Fusion™ cloning of PCR products

The pOPIN-based expression vectors produced in OPPF were digested with the appropriate restriction enzymes and subsequently subjected to DNA electrophoresis (2.7.8), gel extraction (2.7.9) and purification (2.7.3) procedures (Berrow *et al.*, 2007). Linearized vectors were stored at -20°C in 10 mM Tris-HCl buffer (pH 8.0) as 10 µg aliquots, which were ready to use for In-Fusion™ reactions in a 96-well plate (100 ng/well).

The PCR products obtained during the amplification of cDNA encoding human PcpII (4.2.1.3.2) were purified using a silica-membrane-based DNA purification method with a NucleoSpinR Extract II kit (Invitrogen) according to the manufacturer's instructions. The purified cDNA inserts of the PcpIIFL, PcpII/S62-H1024 and PcpII/L141-H1024 were combined with the appropriate, linearized pOPIN-based vectors (table 4.5) using the In-Fusion™ PCR cloning system (Clontech). The cloning

kit was supplied in In-Fusion™ Dry-Down mix format containing lyophilized ready-to-use reaction components including proprietary In-Fusion™ exonuclease. For each reaction, the lyophilized reaction pellet was resuspended in a microtube with 10 µl of mixed solution containing 1 µl (100 ng) of the linearized pOPIN-based vector, 100 ng of a purified PCR insert and the required amount of ddH_2O (to total up to 10 µl volume). This was briefly mixed and transferred to a PCR 96-well plate, which was sealed with an adhesive film. The reaction was carried out for 30 min at 42ºC in a Veriti® 96-Well Thermal Cycler (Applied Biosystems). Next the plate was placed on ice and each reaction was diluted with 40 µl of TE buffer (2.3.5). All of the reaction mixtures were subjected to a transformation into *E. coli* OmniMAX™2 T1-phage resistant competent cells (Invitrogen) (2.7.1). 10 µl of cell suspension was plated on 6-well Corning® Costar® cell culture plates (Sigma-Aldrich) containing LB agar with 50 µg/ml carbenicillin, 20 µg/ml X-gal and 1 mM IPTG and incubated overnight at 37ºC**.**

4.2.1.3.4. Preparation of recombinant pOPIN/pcpII plasmid constructs

The identification of colonies carrying recombinant pOPIN-based plasmids with an appropriate *pcpII* insert (pOPIN/*pcpII*) was enabled by the application of blue-white colony screening (4.2.1.3.1). Random white colonies (2 per each pOPIN/*pcpII* construct) were picked to inoculate 1.5 ml of LB with 50 µg/ml carbenicillin in a 96 deep-well block. The block was sealed with gas-permeable adhesive film and incubated overnight at 37°C in a shaking incubator. Next the cultures were pelleted by centrifugation at 5000xg for 15 min at 4°C (Avanti® HP-26 XP with AllSpin JS-5.3 rotor, Beckman). Cell pellets were subjected to automated, 96-well format plasmid preparation using a QIAgen BioRobot 8000, Wizard SV96 kit (Promega) and a QiaVAC96 manifold (Qiagen) according to the manufacturer's instructions.

4.2.1.3.5. Verification of recombinant pOPIN/pcpII plasmid constructs

All prepared pOPIN/*pcpII* constructs (4.2.1.3.4) were verified using the PCR-based method as described in section 4.2.1.3.2., except that the gene-specific forward primer was replaced by a standard T7 forward primer (5′-TAATACGACTCACTATAGGG-3′), which is present in all pOPIN-based vectors.

The following composition of the master mix (22 µl/reaction) was prepared for a single PCR reaction:

2.5 µl 2x KOD Hot Start Buffer
2.5 µl 2 mM dNTP mix
1 µl 25 mM $MgCl_2$
1.5 µl 10 µM T7 forward primer
0.5 µl 2.5 U/µl KOD Xtreme™ Hot Start DNA Polymerase
14 µl ddH_2O

PCR amplification was conducted in a 96-well plate. The master mix solution was dispensed into each well (22 µl/reaction) using a multi-channel pipette followed by the addition of 1.5 µl of reverse primer (10 µM) and 1.5 µl of the appropriate pOPIN/*pcpII* construct sample. The plate was sealed with an adhesive film and placed in the Veriti® 96-Well Thermal Cycler (Applied Biosystems). The thermal cycling procedure was run according to parameters listed in table 4.7.

Step	Temperature	Time	
Initial denaturation	94ºC	2 min	
Denaturation	94ºC	30 s	30x
Annealing	60ºC	30 s	
Extension	68ºC	2 min 30 s	
Final extension	68ºC	4 min	
Cooling	4ºC	-----	

Table 4.7. Thermal cycling steps during the PCR-based verification of pOPIN/*pcpII* constructs.

The result of the PCR was analysed by 1% agarose gel electrophoresis as described in section 2.7.8 with SYBR® Safe gel stain (Invitrogen) used for DNA visualisation of the pOPIN/*pcpII* constructs which were subjected for DNA sequencing (2.7.10). The purified plasmid samples were subsequently used for transfection into either insect *Sf*9 cells or mammalian HEK 293T cells.

4.2.1.3.6. Construction of baculoviruses and expression in insect cell lines

The production of recombinant baculoviruses and insect cell expression screening for a range of pOPIN/*pcpII* preparations, which included 7210, 7211, 7212, 7465, 7466, 7467, 7468, 7469 constructs (OPPF reference number, table 4.4) was conducted solely by Dr J.E. Nettleship (OPPF). The cell lines that were tested as expression hosts included *Sf*9 and VE-*Sf*9 (vankyrin enhanced *Sf*9), which were co-transfected with each pOPIN/*pcpII* plasmid preparation and linearized *A. californica* bacmid. The procedures of the baculovirus construction and transfection are presented in detail in reports published by the OPPF group (Berrow *et al.*, 2007; Nettleship *et al.*, 2010).

4.2.1.3.7. Preparation and transfection of HEK 293T cells

The expression screening for all pOPIN/*pcpII* constructs in HEK 293T cells was conducted according to a protocol by Nettleship and co-workers (Nettleship *et al.*, 2009). HEK 293T cells were maintained in DMEM ((Dulbecco's modified Eagle's medium, (Dulbecco and Freeman, 1959)) supplemented with 10% foetal calf serum (FCS, Sigma), non-essential amino acids (1:100) and L-glutamine (1:100) (Invitrogen), and incubated in a 5% CO_2/95% air environment. All work involving cell manipulation and preparation of transfection reactions was carried out under a Class 2 laminar flow cabinet.

Before transfection the HEK 293T cells were seeded in 24-well plates at a density sufficient to give 75–80% confluency after 24 h growth (around 1.5-2x10^5 cells/ml). For each well to be used, a 60 µl of serum-free DMEM, supplemented with non-essential amino acids (1:100) and L-glutamine (1:100), was mixed with a 2 µl of 1.33 mg/ml GeneJuice™ transfection reagent (Novagen). Next ~1 µg of each pOPIN/*pcpII* construct

(table 4.5) was added to the above mix, stirred thoroughly and incubated for 10 min at room temperature. Meanwhile, the media from the HEK 293T cell layer in the 24-well plate was carefully aspirated and immediately replaced with 1 ml of DMEM with 2% FCS, non-essential amino acids (1:100) and L-glutamine (1:100). Then the DNA/GeneJuice^{TM} cocktail was added to the cells and these were incubated for 3 days at 37°C in a 5% CO_2/95% air environment.

4.2.1.3.8. Verification of protein expression

The analysis of the PcpIIFL, PcpII/S62-H1024 and PcpII/L141-H1024 expression in HEK 293T cells involved separated screening for secreted and intracellular products. In order to analyse the secretion of proteins into the media, the culture supernatant 3 days post transfection was transferred into a 24 deep-well block and harvested for 10 min at 17000xg at 4ºC (Avanti® HP-26 XP with AllSpin JS-5.3 rotor, Beckman) . The adherent cells, which remained after aspiration of the supernatant, were subjected for analysis of intracellular expression of the desired proteins. The plate with cells was frozen at -80°C for at least 30 min. Next it was defrosted and the cells were washed with 100 µl of PBS buffer (2.3.6). A 10 µl aliquot of the supernatant from either the secretory or intracellular expression preparation was mixed with 10 µl of sample loading buffer (2.3.2) and heated at 95°C for 3 min. The expression yield was analysed by SDS-PAGE (2.8.2) using pre-cast Novex® 4-12% gel in NuPAGE® MOPS running buffer (Invitrogen). In the next step the His-tagged proteins were detected by Western blotting as described in section 2.8.6.

4.2.2. Results and discussion

4.2.2.1. Cloning and expression of PcpII in bacterial cells

4.2.2.1.1. Preparation of pCMV-SPORT6/trhde plasmid

The *E. coli* DH5α culture cells after overnight growth were harvested by centrifugation and subjected to pCMV-SPORT6/*trhde* plasmid isolation as described in section 4.2.1.2.1. Subsequent restriction enzyme digestion (2.7.5.1) and 1% agarose gel electrophoresis (2.7.8) confirmed successful plasmid extraction and a presence of the PcpII cDNA insert. The band corresponding to the insert can be observed at approx. 3000 bp as seen on the agarose gel electropherogram (figure 4.2).

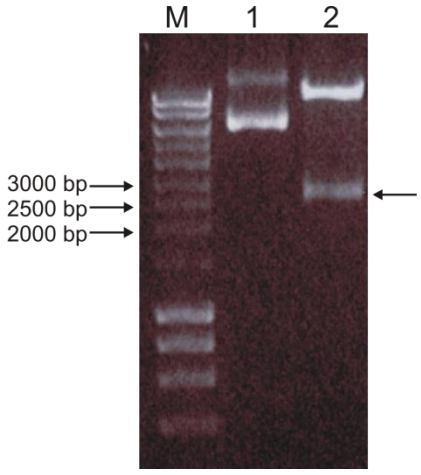

Figure 4.2. The result of agarose gel electrophoresis of pCMV-SPORT6/trhde restriction digestion products. Individual lanes represent marker Hyperladder I (M), uncut plasmid (1) and cut plasmid (2). Insert band can be observed at approx. 3000 bp.

The concentration and purity of the prepared pCMV-SPORT6/*trhde* sample was determined by the absorbance measurement at 260 nm as described in section 2.7.4. Plasmid DNA was sent for sequencing using T7 (forward) and M13 (reverse) primer (2.7.10), which confirmed the presence of the PcpII cDNA insert and its correct nucleotide sequence (appendix VIII). Next the purified and quantified plasmid sample was subsequently used for the PCR amplification of cDNA encoding the desired PcpII fragments.

4.2.2.1.2. PCR amplification of cDNA of PcpII fragments

The amplification of cDNA encoding the PcpII fragments (4.2.1.2.2) appeared to be very difficult, probably because of the relatively long fragments to be amplified and the possibility of the formation of secondary DNA structures. However, after a few attempts the desired PCR products were obtained, which were confirmed by 2% agarose gel electrophoresis. The positive result of the reaction was seen over the whole range of the applied annealing temperature gradient. The bands corresponding to the inserts of the PcpII/L141-M541, PcpII/S62-G793 and PcpII/L141-H1024 can be observed at approx. 1200 bp, 2200 bp and 2500 bp, respectively (figure 4.3). The result of PCR amplification for PcpII/L141-M541 cDNA to clone into pET-22b(+) is presented in figure 4.4.

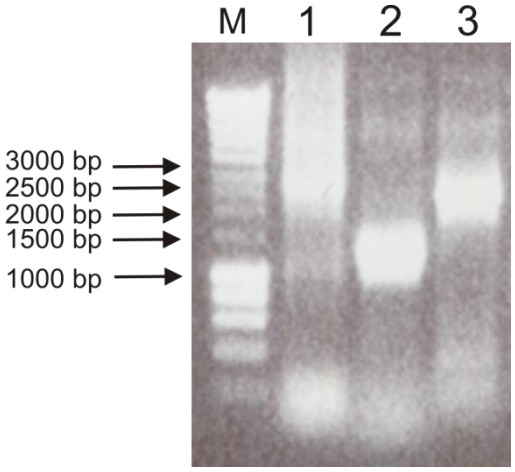

Figure 4.3. The result of the amplification of cDNA encoding (1) PcpII/L141-H1024 (~2500 bp), (2) PcpII/L141-M541 (~1200 bp) and (3) PcpII/S62-G793 (~2200 bp) and M – marker Hyperladder I.

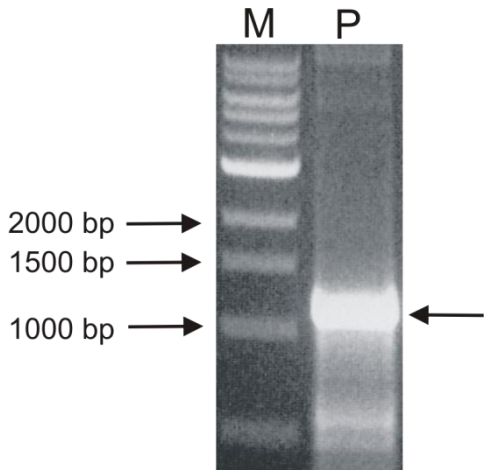

Figure 4.4. The result of the amplification of cDNA encoding PcpII/L141-M541 (~1200 bp) designed to be cloned into pET-22b(+). M – marker Hyperladder I.

4.2.2.1.3. Preparation of pET-28a(+)/pcpII and pET-22b(+)/pcpII recombinant plasmids

The ligation reactions of all PcpII inserts with pET-28a(+) or pET-22b(+) vectors (4.2.1.2.3) were successful and confirmed by the obtaining of colonies carrying the recombinant plasmids. The pET-28a(+)/*pcpII/L141-M541*, pET-28a(+)/*pcpII/S62-G793*, pET-28a(+)/*pcpII/L141-H1024* and pET-22b(+)/*pcpII/L141-M541-pelB* constructs were isolated and the presence of the desired inserts was shown using a double digestion reaction with suitable restriction enzymes and subsequent 1% agarose gel electrophoresis as described in section 4.2.1.2.4. The correct sequence of all inserts was confirmed by DNA sequencing (2.7.10, appendices IX, X an XI). All constructs were further used in an attempt to overexpress given PcpII fragments in a range of *E. coli* expression strains (4.2.1.2.5).

4.2.2.1.4. Overexpression trials of PcpII fragments

Screening for the optimal expression conditions was conducted using a variety of *E. coli* strains (4.2.1.2.5) at different growth temperatures and the process was monitored over a prolonged period of time. The results of the overexpression were determined using the SDS-PAGE technique with an 8% separating gel (2.8.2). Unfortunately none of the PcpII truncated variants was found to be expressed

in the soluble or insoluble fractions. Individual expression strains, which were used for the screening, are specifically designed to overcome potential problems associated with the synthesis of the human protein in the *E.coli*-based system, such as rare codon bias, insufficient disulfide formation, structural misfolding or protein toxicity for the host cell (4.2.1.2.5). PcpII is a large, multi-domain glycoprotein, therefore it seems to be understood that its production (even in a truncated version) as a correctly folded protein may be hindered by the inability of the *E. coli* cell-based expression system to provide the essential post-translational modifications. The unsuccessful result of these experiments led to the decision to attempt alternative protein production possibilities in more advanced eukaryotic systems, such as these utilizing insect or mammalian host cells, which could provide better conditions for PcpII expression (4.2.1.3).

4.2.2.2. Cloning and expression of PcpII in insect and mammalian cells

4.2.2.2.1. PCR amplification of PcpII fragments

The amplification of cDNA encoding all desired PcpII fragments (4.2.1.3.2) was successful and was confirmed by the 1% agarose gel electrophoresis. The bands corresponding to the representative inserts of the PcpIIFL, PcpII/S62-H1024 and PcpII/L141-H1024 can be observed at approx. 3000 bp, 2900 bp and 2700 bp, respectively (figure 4.5).

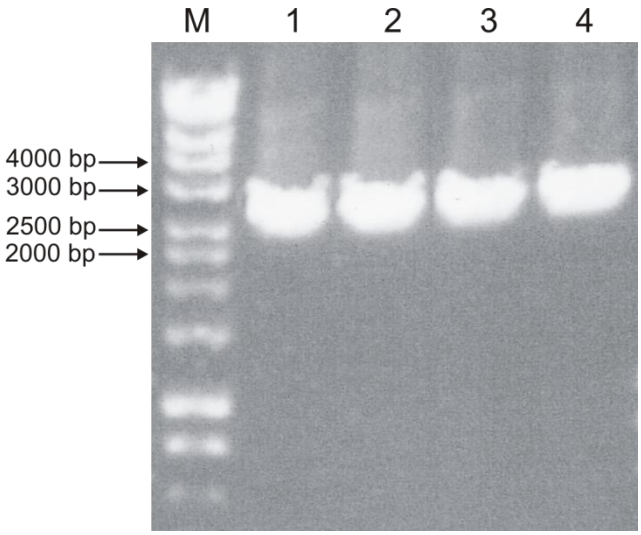

Figure 4.5. The result of the amplification of the representative PCR products. Each fragment was amplified using a different set of forward and reverse primers in order to facilitate cloning into the appropriate pOPIN-based vector (table 4.4). The individual lanes represent PCR inserts designed for different cloning constructs: 1 – PcpII/L141-H1024 (~2700 bp, OPPF No: 8981); 2,3 – PcpII/S62-H1024 (~2900 bp, OPPF No: 8979 and 8980, respectively) and 4 – PcpIIFL (~3000 bp, OPPF No: 7468); M – marker HyperladderI.

4.2.2.2.2. Preparation of recombinant pOPIN/pcpII plasmid constructs

Successfully amplified cDNA fragments encoding PcpIIFL, PcpII/S62-H1024 and PcpII/L141-H1024 proteins (4.2.2.2.1) were subjected to In-Fusion™ cloning as described in section 4.2.1.3.3. Each PCR product contained an additional 5′ and 3′ flanking sequence to enable the annealing with the homologous fragment of the target pOPIN-based vector (table 4.5). A range of created pOPIN/*pcpII* constructs underwent a successful PCR-based verification, which showed that all of them carried the desired insert. This was additionally confirmed by DNA sequencing. All recombinant constructs were further tested for protein expression in insect and mammalian cell lines.

4.2.2.2.3. Expression in insect cell lines

The screening utilizing the baculovirus-mediated expression vector system in *Sf*9 and VE-*Sf*9 was conducted for three PcpII variants: PcpIIFL, PcpII/S62-H1024 and PcpII/L141-H1024 from the range of pOPIN-based constructs listed in table 4.8.

CONSTRUCT	OPPF NUMBER
pOPINH/*pcpII/L141-H1024*	7210
pOPING/*pcpII/L141-H1024*	7211
pOPINTTG/*pcpII/L141-H1024*	7212
pOPING/*pcpII/S62-H1024*	7465
pOPINTTG/*pcpII/S62-H1024*	7466
pOPINH/*pcpII/S62-H1024*	7467
pOPINF/*pcpII*	7468
pOPINI/*pcpII*	7469

Table 4.8. List of recombinant constructs used for the screening expression conditions in the baculovirus-mediated insect cell system.

The total protein samples were evaluated by Western blotting technique employing an anti-His primary antibody (2.8.6). However, the result showed no detectable secreted, soluble or cell-associated expression for any of the above PcpII variants neither in the *Sf*9 nor VE-*Sf*9 tested host cell line. The VE-*Sf*9 is a genetically engineered version of the *Sf*9, which produces vankyrin displaying a positive influence on the cell longevity and the level of recombinant protein expression (Fath-Goodin *et al.*, 2006).

There may be diverse reasons behind the lack of expression of neither of PcpII forms in baculovirus/insect cell system; however it is worth noting that only a selected range of the prepared pOPIN-based constructs was screened using this method. All of the tested constructs were designed to produce recombinant proteins with the N-terminal signal sequence facilitating secretion into the growth media. The exemption are 7468 (pOPINF/*pcpII*) and 7469 (pOPINH/*pcpII*) variants, which allow for the expression of the full-length PcpII with its native signal sequence. It is difficult to predict a result of the utilisation of an alternative vector or expression system. Many

proteins have been observed to be expressed and secreted at a comparable level in both insect and mammalian systems (Dr J.E. Nettleship, personal communication). Nonetheless, it would be advisable in this case to attempt PcpII expression, particularly of its truncated variants, using not tested pOPINH/*pcpII* variants as well as evaluate their effectiveness when in mammalian cell lines. Most of the created pOPIN-based vectors (table 4.5) do not incorporate the secretion leader and allow for synthesis of His-tagged protein remaining in the intracellular fraction. This may appear to be more suitable for finding the optimal conditions for the protein production. Another explanation of the problem may be the fact that human PcpII functions as a glycoprotein and the full-length form is thought to possesses 12 potential N-glycosylation sites (table 4.1) (Schmitmeier *et al.*, 2002). There are reports indicating that insect cells lack several of the enzymes essential for synthesis of mammalian-type N-glycans (Yun *et al.*, 2005; Harrison and Jarvis, 2006). Therefore it is possible that PcpII may not be properly N-glycosylated during post-translational processing, which may in turn affect its structural folding and stability or compromise its activity. Such a limitation of the insect cell system can be potentially considered as one of the reasons behind the unsuccessful PcpII expression.

4.2.2.2.4. Expression in HEK 293T cells

The expression screening in HEK 293T cell line was conducted for a total of 19 different pOPIN-based constructs carrying cDNA inserts encoding PcpIIFL, PcpII/S62-H1024 and PcpII/L141-H1024 which are listed in table 4.9.

CONSTRUCT	OPPF NUMBER
pOPINE/*pcpII/S62-H1024*	8979
pOPINE/*pcpII/L141-H1024*	8981
pOPINF/*pcpII*	7468
pOPINF/*pcpII/S62-H1024*	8983
pOPINF/*pcpII/L141-H1024*	9076
pOPING/*pcpII/S62-H1024*	7465
pOPING/*pcpII/L141-H1024*	7211
pOPINH/*pcpII/S62-H1024*	7467
pOPINH/*pcpII/L141-H1024*	7210
pOPINI/*pcpII*	7469
pOPINTTG/*pcpII/S62-H1024*	7466
pOPINTTG/*pcpII/L141-H1024*	7212
pOPINTTGNeo-3C-GFP-His/*pcpII/S62-H1024*	8984
pOPINTTGNeo-3C-Halo7-His/*pcpII/S62-H1024*	8708
pOPINTTGNeo-3C-CD4-His/*pcpII/S62-H1024*	8709
pOPINE-3C-GFP-His/*pcpII/S62-H1024*	8980G
pOPINE-3C-GFP-His/*pcpII/L141-H1024*	8982G
pOPINE-3C-Halo7-His/*pcpII/S62-H1024*	8980
pOPINE-3C-Halo7-His/*pcpII/L141-H1024*	8982

Table 4.9. List of the recombinant constructs used for the screening of expression conditions in the mammalian cell system.

The results of the expression from screened constructs (table 4.8) in both secreted and intracellular fractions were verified using the SDS-PAGE and Western blotting as described in section 4.2.1.3.8 and are presented in figure 4.6.

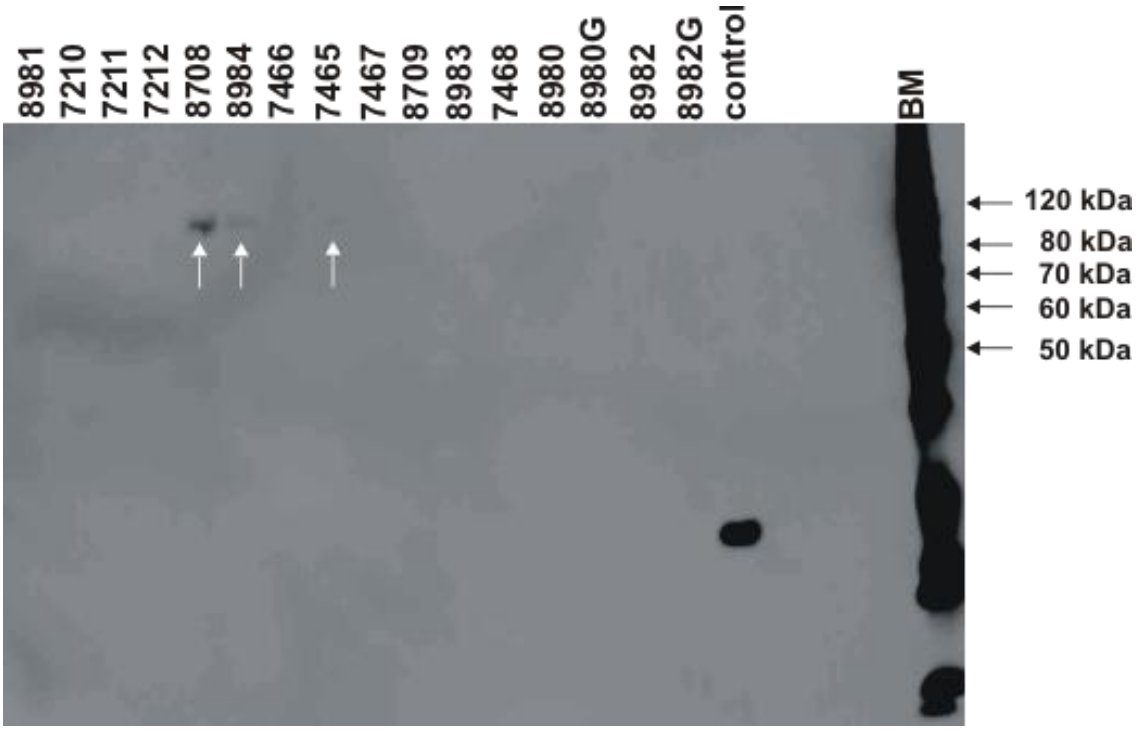

Figure 4.6. The result of the expression screening of PcpII proteins in HEK 293T cells from a range of the pOPIN-based vectors. The SDS-PAGE and Western blotting analysis of the supernatant fractions with secreted proteins is shown and indicates the presence of secreted, His-tagged proteins expressed from constructs 8708, 8984 and 7465. All of these constructs were designed to produce PcpII/S62-H1024 protein (approx. 109 kDa), which is a truncated version of PcpII without the transmembrane domain. The lanes are labelled with corresponding OPPF identifiers (table 4.8), control (positive) – control His-tagged protein and BM – BenchMark™ His-tagged protein standard (2.8.2.3, Invitrogen).

Western blotting analysis of the supernatant fraction confirmed the presence of the His-tagged protein corresponding to the given constructs:

8708 – pOPINTTGNeo-3C-Halo7-His/*pcpII/S62-H1024*

8984 – pOPINTTGNeo-3C-GFP-His/*pcpII/S62-H1024*

7465 – pOPING/*pcpII/S62-H1024*

The staining related to 8984 and 7465 products is very faint and may be a sign of very low expression level. All of the above recombinant vectors were designed to allow synthesis of PcpII/S62-H1024 protein with a leader signal sequence and either an N-terminal (8708 and 8984) or C-terminal (7465) His-tag. Moreover, 8708 and 8984

allow for production of protein coupled with HaloTag or GFP, respectively. The former tag is a product of commercial technology, which was reported to facilitate effective purification even at low protein levels and, along with GFP, is widely used for verification of expression yield using fluorescent imaging, respectively (Ebe, 2007; Los and Wood, 2007). There was no detectable expression for any of the PcpII variants in the intracellular fraction. It must be noted that PcpII/S62-H1024 is a truncated version of PcpIIFL without its N-terminal part containing the transmembrane domain. It may be concluded that in this case the removal of the partially hydrophobic N-terminus could prevent global protein misfolding and thus promote protein stability and secretion. Such a deletion was reported to greatly improve secretion level of the N-terminally truncated human Fas ligand, which is a transmembrane glycoprotein, or increase surface expression of Parkin-associated endothelin-like receptor (Muraki, 2008; Dunham *et al.*, 2009). The successful production of PcpII/S62-H1024 from the pOPINTTGNeo-3C-Halo7-His/*pcpII/S62-H1024*, pOPING/*pcpII/S62-H1024* and pOPINTTGNeo-3C-GFP-His/*pcpII/S62-H1024* constructs in HEK 293T cells, although at a very low level, helped to establish preliminary conditions for the protein expression. This system however requires further optimisation in order to obtain higher amounts of active protein to conduct a structural study on human PcpII.

4.3. Homology modelling of human PcpII

Information on the three-dimensional structure of a protein is often essential to understand its function and interaction with other molecules as well as a prerequisite for rational drug design or site-directed mutagenesis. Many proteins fail to crystallize or cannot be produced in sufficient amounts to conduct a structural study using X-ray crystallography or NMR spectroscopy. In such cases homology model-building using bioinformatic tools and a solved protein structure of greater than 30% sequence identity as a model is an alternative and reliable method to obtain structural information (Krieger *et al.*, 2003). Although this approach may not be as accurate as obtaining experimental data, it has proved to be useful to provide a preliminary structure of the growing number of the proteins identified in genomic sequencing.

Human PcpII belongs to the M1 family of Zn-dependent aminopeptidases (Rawlings *et al.*, 2010). Although this group of enzymes plays an important role in a variety of the cellular and cell signalling pathways, their structural characteristics, related to the exopeptidase performance, remains poorly explored. Only 7 out of 55 M1 metallopeptidases have solved protein structures including leukotriene A4 hydrolase (Rudberg *et al.*, 2004), alanyl aminopeptidase (Kochan *et al.*, 2011), endoplasmic reticulum aminopeptidase 1 (ERAP1) (Ito *et al.*, 2006) or tricorn interacting factor F3 (Rudberg *et al.*, 2004; Kyrieleis *et al.*, 2005; Ito *et al.*, 2006; Kochan *et al.*, 2011)All of them were observed to share a common three-domain protein (apart from the unique four-domain structure of tricorn interacting factor F3) architecture of a saddle-like N-terminal domain and thermolysin-like catalytic domain. The latter feature placed the M1 family in clan MA (Rawlings *et al.*, 2010). PcpII seems to be a specific enzyme, as it exclusively releases the N-terminal pGlu group from TRH peptide, therefore it is the only ω-peptidase within the M1 family. Moreover, PcpII and aminopeptidase N are both anchored in a cell membrane with an N-terminal cytoplasmic/transmembrane domain, and the bulk of the protein being localised in the extracellular space (Chavez-Gutierrez *et al.*, 2006). Ectoenzymes are also recognized as surface antigens, where for example aminopeptidase N functions as the myeloid leukaemia marker CD13 (Razak and Newland, 1992).

The protein sequence of human PcpII was used for homology modelling procedure in order to generate a three-dimensional model and perform docking simulations of TRH into the enzyme's active site.

4.3.1. Materials and methods

4.3.1.1. Search for a homologous PDB structure

The PcpII amino acid sequence was subjected to BLAST (Basic Local Alignment Search Tool, blast.ncbi.nlm.nih.gov) online homology search engine utilizing the blastp algorithm (BLOSUM62 matrix, gap penalties: existence 11 and extension 1) in order to find similar proteins with solved PDB structure. Predictions of structural domains and search for conserved regions were conducted using online servers for the purpose of the protein expression study as described in section 4.2.1.1.

4.3.1.2. Modelling of the PcpII catalytic domain

The three-dimensional model building was conducted using MOE^{TM} molecular modelling tool (Chemical Computing Group). The PcpII query sequence (appendix VIII) was aligned with the human endoplasmic reticulum aminopeptidase 1 (ERAP1) sequence and subsequently it was modelled on this template. The preliminary backbone generation resulted in 100 intermediate models, which were evaluated using the in-built residue packing quality function. The best-scored intermediate model was subjected to energy minimization using the Amber99 force field within 9 Å radius from the central Zn atom and until a 0.01 RMS gradient. The zinc ion was manually added to the model using coordinates from the ERAP1 template. The backbone beyond 9 Å radius was fixed. In order to understand the structural basis of TRH recognition by the enzyme, the docking simulation in the PcpII active site was conducted. The hormone structure was created using the MOE^{TM} molecular builder application and the Monte Carlo docking simulation method was applied yielding 150 intermediate models. Next, the energy of the best ranked PcpII-TRH complex was minimized using the MMFF94X force field and evaluated with the Affinity dG scoring algorithm, whereas hydrogen-bonding energy was refined using the LigX application. The quality of the PcpII homology model was assessed with Ramachandran plot generated in MOE^{TM} and the RAMPAGE server (Lovell *et al.*, 2003).

4.3.2. Results and discussion

4.3.2.1. Search for a homologous PDB structure

The BLAST search of the PcpII amino acid sequence against the PDB database returned the group of enzymes belonging to the M1 family of metallopeptidases. The structures with the top scoring are presented in table 4.10.

PROTEIN	PDB ID	REFERENCE
human ERAP1 (soluble domain)	2XDT	(Kochan *et al.*, 2011)
Thermoplasma acidophilum Tricorn protease-interacting factor F3	3Q7J	(Kyrieleis *et al.*, 2005)
Colwellia psychrerythraea Cold-active aminopeptidase	3CIA	(Bauvois *et al.*, 2008)
human Leukotriene A4 hydrolase (LTA4H)	3CHO	(Kirkland *et al.*, 2008)
Escherichia coli Aminopeptidase N	2HPO	(Addlagatta *et al.*, 2006)
Plasmodium falciparum M1 neutral aminopeptidase	3EBG	(McGowan *et al.*, 2009)

Table 4.10. List of the PDB structures of the proteins displaying the highest homology to human PcpII returned during the BLAST search against PDB database.

The sequential alignment of the above proteins and human PcpII was conducted to study the conservation level within this M1 family representatives. Surprisingly, none of the aligned sequences covered the N-terminal domain of PcpII, therefore it was decided to conduct the modelling of the most conserved central catalytic region (L141-M541). The alignment of the sequences of human ERAP1 soluble domain with PcpII/L141-M541 revealed their 98% coverage as well as 40% identity and 56% similarity. Therefore ERAP1 structure (2XDT) was used as a template to generate three-dimensional model of the catalytic domain of PcpII.

4.3.2.2. PcpII catalytic domain model

Three-dimensional model of the PcpII catalytic domain was constructed using a structure of the soluble domain of human ERAP1 (2XDT) as a template for homology modelling. The ERAP1, similarly to human PcpII, belongs to the gluzincin family of zinc-dependent metalloproteases sharing the consensus $HEXXHX_{18}E$ motif (Kochan *et al.*, 2011). It acts as a multi-functional enzyme participating in maturation of a variety of antigenic peptides from N-terminally extended peptide precursors necessary for presentation by the class I major histocompatibility complex (MHC). Contrary to PcpII, this peptidase exhibits wider substrate specificity dictated, surprisingly by strong preferences to positively charged internal residues rather than to peptide N- or C-termini, due to large active site cavity, which carries a strong negative electrostatic potential (Evnouchidou *et al.*, 2008).

The L141-M541 residues used for this procedure, were shown to be conserved in protein members of M1 family of peptidases as was revealed in a result of the search against the Pfam collection (Rawlings and Barrett, 1995). It is worth noting that the BLAST search of the sole N-terminal cytoplasmic/transmembrane domain did not return any homologous proteins or protein fragments that may suggest that this part is unique for human PcpII. The overlay of the model and template Cα backbones is presented in figure 4.7 with a RMSD of 1.33 Å. The catalytic domain is composed of an α-helical region and a β-sheet region, which forms a narrow but solvent accessible active site containing a zinc atom. In the model, active site triad of His440, His444 and Glu463 (PcpII numbering) superimpose relatively well with the corresponding residues in the template as was shown in figure 4.8. Within a consensus $HEXXHX_{18}E$ motif most of the residues were highly conserved between the query and subject sequence and only 5 residues showed lack of similarity. A Ramachandran plot for the model was generated at 2 Å (appendix XIII) with a calculation of 84.5% of residues being in favoured and 14.0% in allowed regions. This would suggest relatively good quality of the homology model of PcpII catalytic domain.

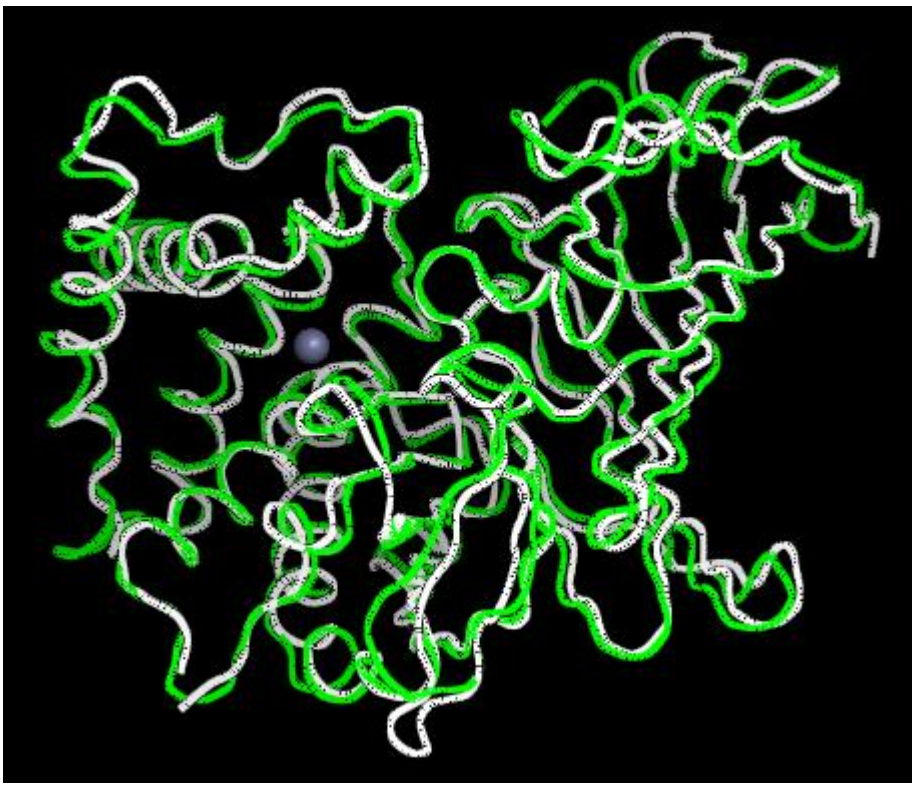

Figure 4.7. A superposition of the Cα backbones of ERAP1 template (white) and PcpII model (green). The catalytic zinc atom is shown as a grey sphere. The organization of the catalytic domain relies on the two α-helical (left) and β-sheet (right) regions, which form the active site of the enzyme.

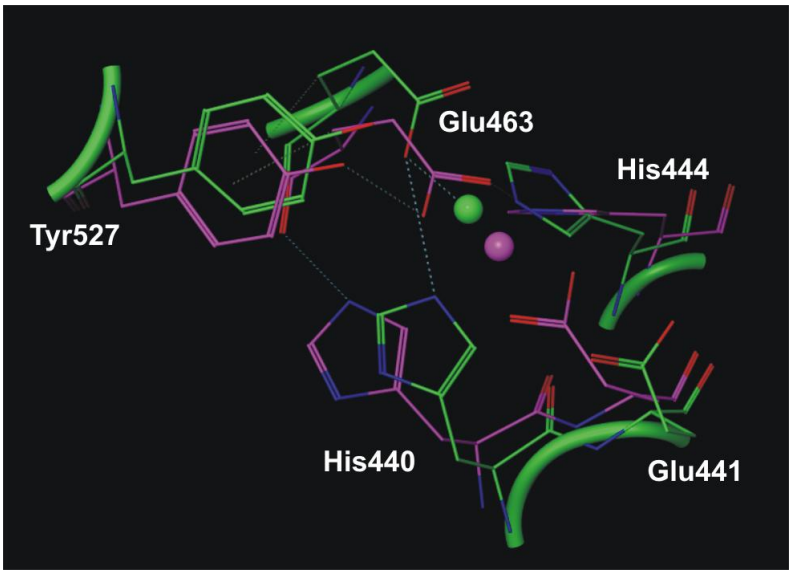

Figure 4.8. A superposition of the active site residues of ERAP1 (purple) and PcpII model (green). The residues superimposed at RMSD 1.33 Å and are labelled according to the human PcpII numbering and two spheres in the centre represent the catalytic zinc atoms.

4.3.2.3. Docking of TRH in PcpII active site

The TRH docking simulations were performed with generation of 150 potential arrangements in the active site. The analysis of the obtained variants of the peptide positioning, which were also supported by the knowledge about the catalytically important residues gained from previous study on human PcpII, helped to identify the most probable substrate binding mode (Papadopoulos *et al.*, 2001; Chavez-Gutierrez *et al.*, 2006). The two-dimensional depiction of the docked TRH conformation in the active site moiety was generated in MOE™ and is shown in figure 4.9. This helped to identify some of the surrounding, potentially important residues in a corresponding 3D representation (figure 4.10).

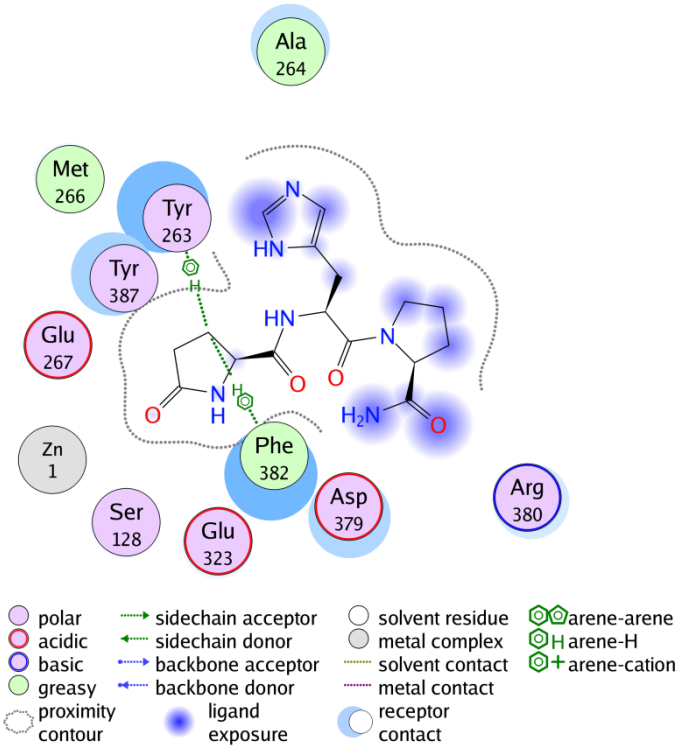

Figure 4.9. The two-dimensional depiction of the docked TRH conformation within the human PcpII active site. The residues that were found in close proximity to the peptide are presented (numbering was shifted according to their position in PcpII/L141-M541 sequence). It is worth noting that carbonyl group of the N-terminal pGlu interacts with the catalytic Zn atom, where the distance was calculated for 2.5 Å. Two aromatic residues, Tyr263 (Tyr403 in full-length PcpII) and Phe382 (Phe522) are shown to be involved in hydrogen bonding with the pGlu moiety and possibly may orientate it to facilitate the interaction with catalytic Zn and active site triad.

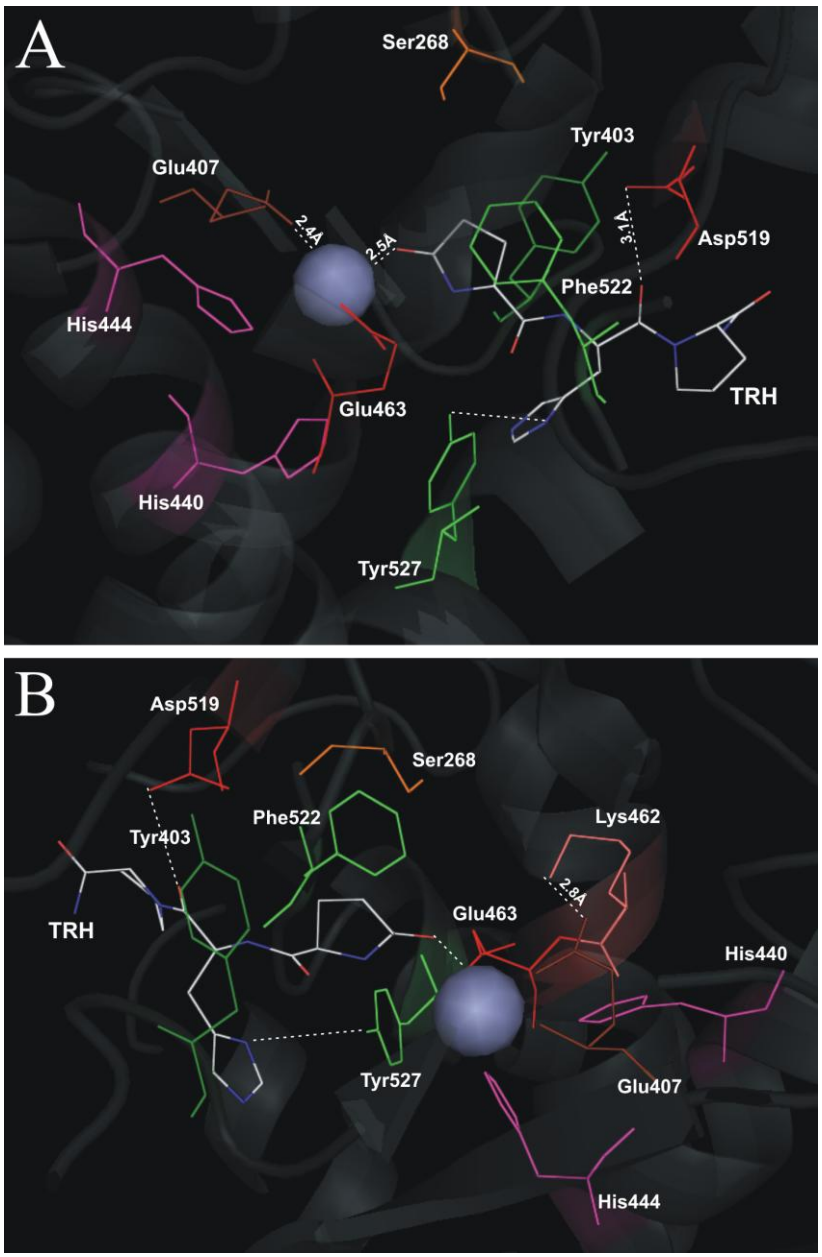

Figure 4.10. Two views of the TRH peptide docked into the active site of the human PcpII model. The TRH structure is presented in white with red oxygen and blue nitrogen atoms, whereas the zinc ion is shown as a grey sphere. Important amino acid residues lining the active site are displayed and coloured (numbering as in full-length PcpII sequence). The pyrrolidone ring of TRH and the benzene rings of Tyr403 and Phe 522 are organised in stacked parallel fashion (A) and Lys462 creates a salt bridge with Glu407 of 2.8 Å (B).

The active site moiety of the PcpII catalytic domain model was seen to be created by three α-helices and two loops, which carry the residues of the $HEXXHX_{18}E$ motif participating in zinc-binding, such as His440, Glu441, His444, Glu463 or Tyr527 residue known to be involved in a stabilisation of the substrate. The interesting parallel organisation of the Tyr403 and Phe 522 aliphatic side chains with the N-terminal pyrrolidone ring stacked in between is probably necessary for the proper orientation of the pGlu. The distance of pGlu from both residues was calculated to be are around 4.5 Å and it can form strong hydrogen bonds as shown in figure 4.9. The pyrrolidone carbonyl group interacts with catalytic zinc atom at 2.5 Å distance and can create a hydrogen bond with the hydroxyl group of Ser268 that was suggested in previous rat PcpII modelling study (Chavez-Gutierrez *et al.*, 2006). This serine residue is also thought to be involved in the recognition of the pGlu of TRH. Similar hydrogen bonding occurs between a TRH histidine and Tyr527 as well as TRH proline and Asp519 (figure 4.10). Both of these interactions probably have a substrate stabilising function and are necessary for proper orientation of the rest of TRH in relation to the catalytic triad of PcpII. In the modelled PcpII active site the carboxylate group of Glu407 forms a strong salt bridge interaction with the amine group of Lys462 at a 2.8 Å distance. A similar observation was made for the homology model of the rat PcpII, which was generated using LTA4H as a template, however at around 3.1 Å distance (Chavez-Gutierrez *et al.*, 2006).

The position of the human PcpII active site was seen to be buried but allowing an accessible channel suitable to accommodate a TRH molecule (figure 4.11).

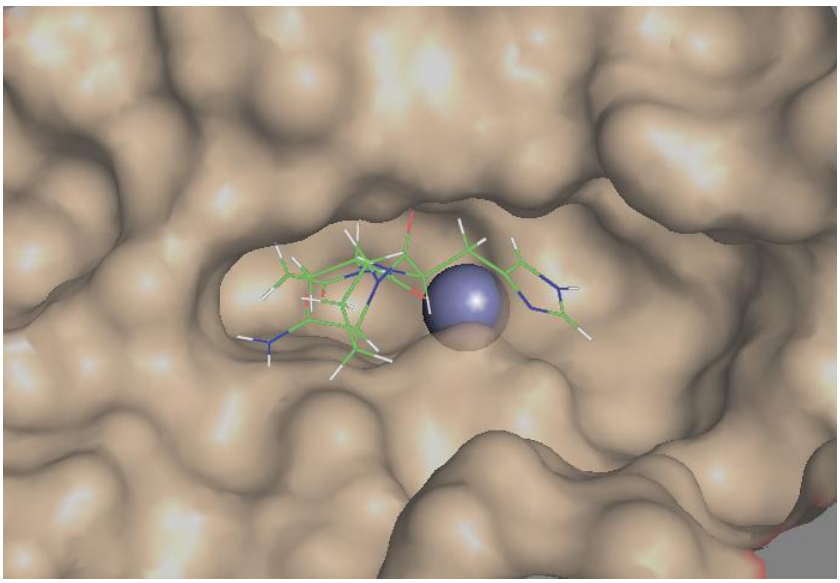

Figure 4.11. The surface presentation of the PcpII active site pocket with the accommodated TRH molecule. The TRH is shown in a stick mode and the zinc ion as grey sphere.

The generation of the human PcpII catalytic domain model has enabled a closer insight into the structure of this protein domain. Additional docking studies have helped to identify catalytically important residues and suggest the interaction involved in substrate binding and recognition. Structural information gained from the homology model could prove useful in design of further experimental work on PcpII including site-directed mutagenesis and identification of potential enzyme inhibitors. This may also have further implications for the comparative study of the functional and physiological properties of the other enzymes from the M1 metallopeptidase family.

Chapter 5 – Study on the role of pyroglutamyl peptidases in Alzheimer's disease pathology

5.1. Pyroglutamyl modifications in AD pathology

The association of the pGlu-modified Aβ peptides with AD aetiology has been intensively studied since the observation of their abundant deposition in amyloid plaques found in the diseased brain tissues (He and Barrow, 1999; Larner, 1999). A proteolytic truncation and modification of APP precursor yielding various Aβ derivatives commonly occurs under physiological conditions and was described in detail in section 1.1.3. The pGlu cap is known to play a protective role against the degradation by most of the proteases in the body. The enzymes, QC and Pcp, are directly involved in the processing of the N-terminal pGlu residue in peptides and proteins (1.1.3). The former enzyme is able to convert N-terminal glutamic acid or a glutamine residue to pGlu, which can be later exclusively removed by the latter peptidase, which is often an introduction to proteolytic catabolism of a given substrate. An excessive formation of a range of pGlu-modified Aβs, namely AβpGlu(3-40/42) and AβpGlu(11-40/42), may therefore imply possible imbalance between QC and Pcp activities as one of the reasons associated with the development of AD. There are, however, only a few reports published so far which could support this implication. The involvement of QC was already confirmed to be of importance, after a series of observations of a significantly suppressed AβpGlu(3-40/42) formation in transgenic mouse and rat models, which were treated with the inhibitors of the enzyme (Cynis *et al.*, 2006; Schilling *et al.*, 2008a; Schilling *et al.*, 2008b). Moreover, the analysis of the QC distribution in transgenic mice hippocampus indicated that the enzyme contributes to the formation of both focal and diffuse (soluble) pGlu-Aβ derivatives (Hartlage-Rubsamen *et al.*, 2011). These findings have come into focus as a new potential therapeutic option for AD treatment. On the contrary to QC, the role of the Pcp enzymes remains to be investigated and, as yet, there are no published studies regarding the relationship between the activity of these peptidases and the accumulation of pGlu-Aβ peptides in the diseased tissues. This chapter presents experimental work on the human PcpI and PcpII enzymes and their potential involvement in Alzheimer's pathology.

This includes immunohistochemical staining of the AD and control brain tissues as well as qualitative assessment of the processing of pGlu-Aβ peptides by the human PcpI.

5.2. Immunostaining of AD brain tissue sections

5.2.1. Introduction to immunohistochemistry

The beginning of immunohistochemistry (IHC) is linked with the first report on the fluorescent-based detection of the specific cellular components in analysed tissue material (Coons *et al.*, 1941). Over the last decades IHC has become a routine research and diagnostic tool, which bridges immunological, histological and chemical disciplines. The principle of this technique is the identification of target antigen using specific antibody, which is suitably labelled with a reporter molecule to facilitate its visualisation. This further helps to determine the distribution and localization of the desired components in the cellular or tissue context and to compare it with a control material. Nowadays, IHC methods are widely applied in detection of the physiological disease markers or in drug development to investigate drug effectiveness on the target disorder.

The development of immunohistochemical methods generally aims to improve sensitivity and specificity of the detection of target antigens. In order to meet these requirements, different aspects of the IHC are constantly being improved and mainly consider the methods of sample preparation, antigen retrieval or production of specific antibodies and their effective labelling.

Antibodies are the Y-shaped immunoglobulin (Ig) proteins consisting of two identical light chains and two identical heavy chains. The heavy chains are different and can be divided into a few subtypes, which determine the class of the antibodies (Polak and Van Noorden, 2003). The arm of the molecule, which contains variable and constant fragments belonging to both chains, is known as Fab (fragment antigen-binding) region and participates in binding to an appropriate antigen (protein, peptides, nucleic acids, carbohydrates etc.). There has been a successful trend to employ the Fab fragment only for IHC experiments, however the remaining portion of Ig, known as Fc (fragment constant), is required for interaction with other (secondary) antibodies,

which is a principle of the multistep staining procedure. The Fc was also found to stabilise the overall binding of the molecule to solid substrates such as tissue material (Ramos-Vara, 2005). The antibody is designed to specifically recognise and bind to the unique site of the antigen called epitope, which is usually 5-21 aa long (Roitt and Delves, 2001). The production of a desired antibody is based on the immunization of animals triggered by the introduction of a specific antigen. There are two types of commercially available antibodies, monoclonal and polyclonal. Monoclonal antibodies are obtained by fusing the immortal myeloma cells with lymphocytes raised against desired antigen. The lymphocytes are isolated from a single animal source (mostly mice) which had been earlier immunised with that antigen. The fusion results in creation of hybrydoma (hybrid myeloma) cells that produce desired immunoglobulin. Monoclonal antibodies display much higher specificity when compared to those of polyclonal origin, which are produced in multiple species such as rabbit, goat, horse and chicken (Roitt and Delves, 2001). Polyclonal antibodies have the advantage for the potential recognition of different isoforms of a given epitope, but at the same time they may bind to unspecific molecules, which could generate undesired background staining. Therefore the choice between both variants depends on the purpose of their application and desired specificity of the interaction with the target antigen.

The proper interaction between the antibody and the antigen absolutely requires the latter one to maintain its tertiary structure. However, normal cell morphology, tissue architecture and the conformation of target epitopes can be compromised by an improper fixation of the sample material to be analysed. Fixation of tissues is necessary in order to preserve the cellular components and prevent them from disintegration prior to subsequent procedures (Ramos-Vara, 2005). The most common fixative is formaldehyde, mainly due to its reliability and low cost, and despite of its potential influence on the conformation of proteins or interaction with nucleic acids, which may significantly affect their antigenic properties. Sometimes the compromised antigenicity can be restored through a range of antigen retrieval methods, e.g. proteolytic digestion, heat or chemical treatment (Ramos-Vara, 2005). Nonetheless, this aspect of IHC is considered as one of the most challenging and it requires a precise optimisation of the fixation conditions for every individual specimen. In order to maintain a rigid structure of the fixed material and to enable its long-term storage, it is embedded in a support medium such as paraffin wax. Alternatively, if given tissue is too sensitive for

de-waxing reagents, it can be covered with cryo-embedding media and then flash-frozen in liquid nitrogen.

The interaction of an antigen with antibody can be detected using a conjugated fluorochrome, enzyme reaction, radioactive element or colloidal gold and documented using light and electron microscopy or autoradiography techniques (Polak and Van Noorden, 2003). The detection system can be direct, which means that the primary antibody is labelled and the reaction can be relatively quick. An alternative method is indirect, more time-consuming and is generally suitable for more sensitive detection. It is a two-step procedure, where the target epitope is bound by a primary native antibody (first layer) being itself an antigen for a secondary antibody (second layer), which is conjugated with a desired reporter agent. The most commonly employed detection systems are based on enzyme activities, such as peroxidase, alkaline phosphatase or glucose oxidase, which catalyse the formation of a coloured or fluorescent product visible under a light microscope or UV light (Davey and Busch, 1970). Alternatively, the antibody can be tagged with a fluorochrome, such as fluorescein or rhodamine, and its localisation can be detected by UV light (Haaijman *et al.*, 1986). The choice of the best detection method to use is related to the expression and availability of the target antigen and the desired amplification of the signal.

The obtaining of the satisfactory results using IHC method sometimes may be difficult and can be achieved by the optimal combination of a variety of factors such as the preparation and treatment of tissue sample to be analysed, selection of antibodies and the detection system.

This part of the experimental work involving immunostaining of human PcpI and PcpII in the AD and control brain cortex tissue sections was entirely conducted in the Peninsula Medical School (PMS, Exeter).

5.2.2. Materials and methods

5.2.2.1. AD brain tissue sections

The frozen tissue sections of the post mortem superior temporal gyrus of the temporal cortex were acquired from the London Brain Bank for Neurodegenerative Diseases, the Newcastle Brain Tissue Resource and the Manchester Brain Bank. The control samples came from 10 different subjects (5 male and 5 female) with the age range of 54 to 95 years and *post mortem* delay range of 17 to 50 h. The specification of the sporadic and familial AD tissue samples is presented in table 5.1.

The tissue samples had been cryogenically frozen in liquid nitrogen, cut into 10 µm sections and mounted (two sections per slide) onto SuperFrost Ultra Plus® adhesive slides (VWR). The sections were kept at -80ºC until use.

Autopsy Number	Age	Sex	PMD (h)	PATHOLOGICAL DIAGNOSIS
Sporadic AD				
A108/09	84	F	24	AD BNE Braak stage IV (Limbic stage AD) with focal amyloid angiopathy
A087/09	82	M	20	AD Braak stage VI BNE 5
A062/09	94	M	40	AD Braak/HP-tau stage V with mild amyloid angiopathy
A061/09	103	F	12	AD modified Braak stage V with mild focal amyloid angiopathy
A052/09	84	M	33	AD modified Braak stage V with early amyloid angiopathy
A050/09	81	F	21	AD BNE modified Braak stage VI with focal amyloid angiopathy & localised limbic pathology
A031/09	80	M	15	AD Braak stage VI
A034/08	74	M	51	AD Braak stage VI with mild amyloid angiopathy
A332/07	87	F	48	AD Braak stage VI with moderate amyloid angiopathy
A331/07	80	F	13	AD Braak stage V with mild amyloid angiopathy
Familial AD				
A211/95	61	M	15	FAD APP(Val717Gly)
A238/96	69	F	10	FAD APP(Val717Ile)
A051/97	62	F	23	FAD APP(Val717Ile)
A029/98	42	M	6	FAD PSEN1(delta 4)
A188/98	72	F	3	FAD APP(Val717Ile)
A148/99	65	F	22	FAD PSEN1(Glu280Gly)
N79/95	41	F	63	FAD PSEN1(Thr113-114ins)
N46/93	64	M	24	FAD PSEN1(Ala246Glu)
N5/93	46	M	24	FAD PSEN1(Thr113-114ins)
M 04/13	63	M	11	FAD APP(Gly692Ala)
M 99/06	57	F	48	FAD PSEN1(Met139Val)

Table 5.1. List of AD tissue samples used for immunostaining. PMD column contains *post mortem* delay time of sample collection, BNE – BrainNet Europe, HP-tau – hyperphosphorylated tau, APP – amyloid precursor protein, PSEN1 – presenilin1.

5.2.2.2. Staining of PcpI and PcpII

The immunohistochemical staining of human PcpI and PcpII was performed according to a modified method by (Gutowski *et al.*, 1999). The procedure was carried out using Vectastain Elite ABC kits (Vector Laboratories) with an anti-rabbit secondary antibody for PcpI and an anti-goat secondary antibody for PcpII staining. For the experiment, one slide with two sections was used from each control and AD specimen.

All samples were thawed at room temperature, fixed in acetone for 10 min at 4°C and next they were washed 2x 5 min in freshly prepared PBS buffer (2.3.6). Appropriate blocking serum (Elite ABC kits) was diluted 1:40 in PBS and 75 µl was placed on each section. This was incubated for 30 min at room temperature. The primary antibody solution for PcpI (polyclonal rabbit Anti-PGPEP1 (Sigma-Aldrich)) was prepared at the dilution of 1:40 and 1:100 in PBS. Concurrently, the primary antibody solution for PcpII (polyclonal goat TRH-DE (K-15 (Santa Cruz Biotechnology)) was prepared at the dilution of 1:50, 1:100 and 1:200 in PBS. In sections destined for a negative control (A149/01, table 5.1), the treatment with primary antibodies was replaced by the addition of PBS. Next, 75 µl of each primary antibody dilution was applied to the appropriate sections and incubated for 45 min at room temperature. All slides were subsequently washed with PBS (3x 5 min) and then treated with 75 µl of the appropriate biotinylated secondary antibody (Elite ABC kits), which was previously diluted 1:200 in PBS. This was further incubated for 30 min at room temperature and then washed again with PBS (3x 5 min). The A (avidin) and B (biotinylated peroxidase) solutions (Elite ABC kits) were 1:100 diluted and mixed in PBS, and then 75 µl of the mixture was applied to each section, which was followed by 45 min incubation at room temperature and 3x 5 min PBS wash. The slides were placed under a fume hood in a solution of PBS containing 0.05% (w/v) 3,3′-diaminobenzidine tetrahydrochloride (DAB), 0.04% (w/v) $NiCl_2$ and 0.04% (v/v) H_2O_2 and kept for 5 min to develop a black staining. Such colouration is a result of the activity of peroxidase, which in the presence of H_2O_2 catalyses the oxidation of the DAB substrate to an intense brown precipitated product, which by addition of $NiCl_2$ changes the colour to black or blue black (Hsu and Soban, 1982). The sections were washed in running water and gradually dehydrated by the multi-step immersing in industrial methylated spirit and xylene. Next, all slides were mounted using DPX (dibutyl phthalate xylene, Sigma-Aldrich) and left overnight to dry. The results of the staining were visualised under Olympus BX60 light microscope and documented using mounted digital camera (Nikon).

5.2.2.3. Co-staining of PcpI and PcpII with Aβs or neurofilaments

The double staining of the control and AD sections from each case was performed in two stages. First all sections were subjected to the staining with primary antibodies of PcpI or PcpII at the dilutions of 1:100 or 1:50, respectively. Negative control slides (A149/01, table 5.1) were consequently prepared by replacement of the primary antibody solutions with PBS. The immunostaining procedure was the same as described in section 5.2.2.2, with exception of the final step, where $NiCl_2$ was omitted in the staining solution to enable a development of the brown colouration. The second staining was conducted as described in 5.2.2.2 with the primary antibodies for neurofilaments (polyclonal rabbit anti-neurofilament 200 (Sigma-Aldrich)) or Aβ (polyclonal rabbit anti-Aβ(22-35)) being separately applied at the dilutions of 1:150 both. This was conducted in such a way that one section from each slide pretreated with either anti-PcpI or anti-PcpII antibody was subjected to anti-Aβ staining and the other one to anti-neurofilament staining. The Vectastain Elite ABC kit (Vector Laboratories) with anti-rabbit secondary antibody was utilised in conjugation with the above primary antibodies. In this step the colour development was performed using the Vector® VIP Peroxidase Substrate kit (Vector Laboratories) according to the manufacturer's instructions. The peroxidase reaction produces an intense, pink/purple precipitate. The slides were washed under running water, dehydrated and mounted as in 5.2.2.2. The results of the staining were visualised under an Olympus BX60 light microscope and documented using a mounted digital camera (Nikon).

5.2.3. Results and discussion

5.2.3.1. Comparison of PcpI and PcpII level in control and diseased sections

The comparison of the individual sections treated with a range of diluted solutions of primary antibodies (5.2.2.2), indicated that the optimal detection was achieved for dilutions 1:40 for PcpI and 1:50 for PcpII immunostaining. Negative control sections of the A149/01 specimen (normal adult brain), which were treated solely with the appropriate secondary antibodies, showed very pale, negligible background staining (figure 5.1). This may indicate rather high specificity of the applied primary anti-PcpI and anti-PcpII antibodies.

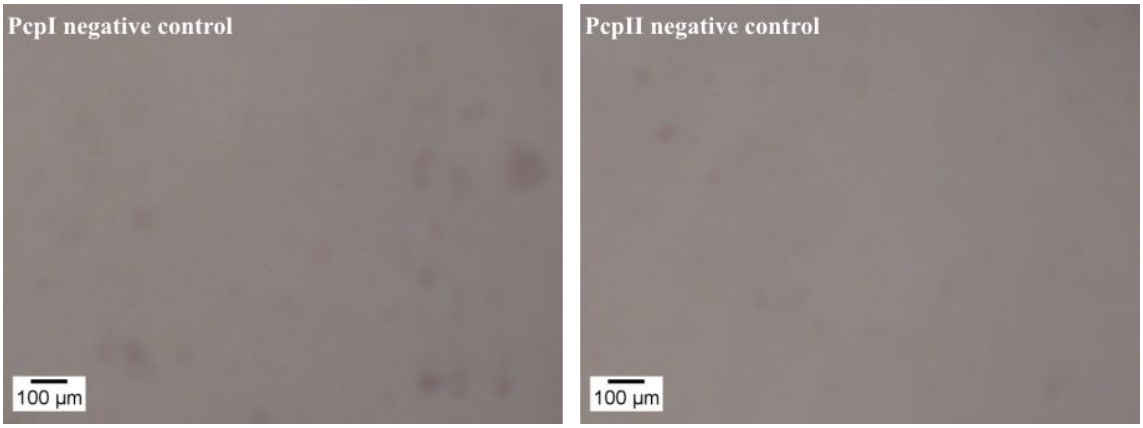

Figure 5.1. Negative control sections for PcpI (left) and PcpII (right) immunostaining.

The immunostaining results for all AD cases obtained for both PcpI and PcpII, were compared with the corresponding control normal adult brain sections. Representative results for the control A149/01 (normal adult brain) and sporadic AD A332/07 (Braak stage VI with moderate amyloid angiopathy) samples are presented in figures 5.2 (PcpI) and 5.3 (PcpII).

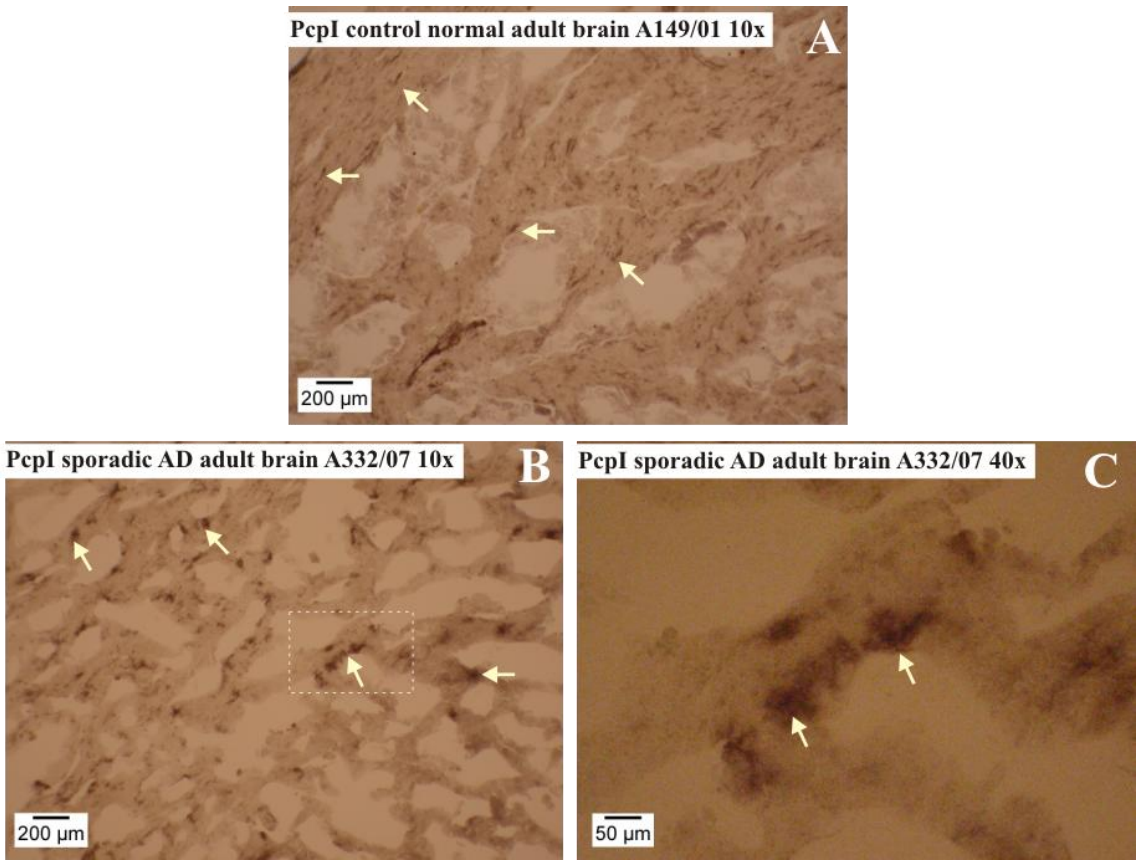

Figure 5.2. Comparison of the immunostaining results of PcpI in control (A) and sporadic AD (B and C) cortical tissue sections. Magnification of each picture is shown in its heading. Black colouration, marked with white arrows, indicates localisation of PcpI and white rectangle in picture B demonstrates a magnified area, which was shown in picture C.

The detection of PcpI antigen can be observed in both the control and AD tissue section (figure 5.2). In the diseased sample the staining is much stronger and focused that indicates an increased level of the protein when compared to normal brain. There is a noticeable difference between a texture of control and diseased sections, with the latter one being significantly disintegrated. This was seen in all of the tested samples and may be explained by the profound tissue loss and general brain shrinkage commonly observed in AD (1.1.2.1). For the case of normal brain sections the natural tissue loss may have also occurred due to the age of the patient (95 years, male) or this may be due to potential damage made during sample preparation. At this stage it may be difficult to associate the up-regulated PcpI synthesis with any particular cell activity. However, the amorphous shape of the colouration (figure 5.2, picture C) and a relatively

high number of the diffused clusters in the AD tissue may suggest that the peptidase can be overexpressed in activated microglial cells. Microglia are resident phagocytic cells acting in all tissues of the CNS, which provide early defence against a variety of the infectious agents (Graeber and Streit, 1990). They account for around 5% of the total cerebral cortex cell population and play a variety of physiological roles (Lawson *et al.*, 1990). In the normal state microglial secretory proteases participate in processes such as the regulation of neuronal growth, neuronal function and regenerative stages of the CNS (Kohsaka *et al.*, 1996). Upon injury, inflammatory activation of microglia induces production and secretion of a number of proteolytic enzymes involved in the degradation of extracellular matrix, damaged neuronal cells, toxic deposits, etc. Chronically activated microglial cells are common in progressive neurodegenerative disorders including AD and are known to be involved in amyloid uptake from the immediate environment and its proteolytic clearance (Rogers *et al.*, 2002). Moreover, the microglia activation in Alzheimer's pathology is associated with an increased level of numerous proteases such as neprilysin, insulin-degrading enzyme, cathepsin B or matrix metalloproteinases MMP-1 and MMP-3 (Wood, 2003; De Strooper, 2010).

There are few reports determining a potential influence of PcpI in AD pathogenesis and development. One of the studies, regarding this matter, resulted in the observation that the oral administration of rivastigmine up-regulates basal and potassium ion-stimulated Pcp activity by 18% in the frontal cortex of transgenic mice (Ramirez-Exposito *et al.*, 2001). This drug is an acetylcholinesterase inhibitor widely used for AD treatment, but a relationship between both enzymes remains unclear. In turn comparative analysis of the alanyl, arginyl, pyroglutamyl and leucyl peptidase activity in the cerebral cortex of the AD and normal brain did not confirm their association with the characteristic changes of the pathology (Mantle *et al.*, 1989). However, the observation of a prominent elevation of PcpI synthesis in AD tissue (figure 5.2) and the fact that N-terminal pGlu-modified molecules cannot be degraded by any other enzyme, may imply that the peptidase indeed is necessary for the clearance of the biological material affected by the neurodegeneration. This question is particularly interesting since the substantial group of Aβ species found in AD is represented by AβpGlu(3-40/42) and AβpGlu(11-40/42) peptides (1.1.3.3), therefore their uptake and degradation by microglia would require Pcp activity. An expression level of the enzyme could be determined by the co-staining of PcpI and microglia antigens and a subsequent comparative analysis of control and diseased tissues.

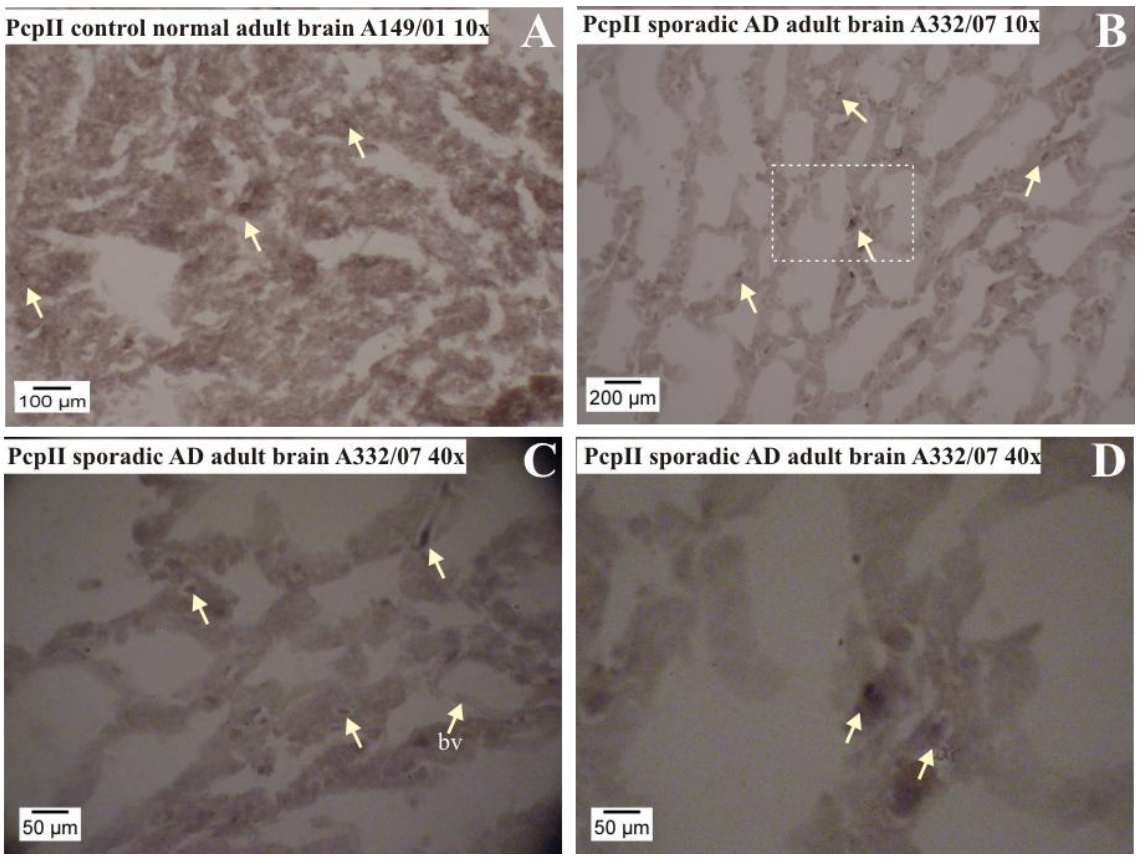

Figure 5.3. Comparison of the immunostaining results of PcpII in control (A) and sporadic AD (B, C and D) cortical tissue sections. Magnification of each picture is shown in its heading. Black colouration, marked with white arrows, indicates localisation of PcpII, bv stands for blood vessel and white rectangle in picture B demonstrates magnified area, which was shown in picture D.

Immunostaining of PcpII (figure 5.3) showed slightly higher level of the protein in AD sections than in control, but the accurate comparative analysis is hindered by the background staining in the latter one. The increase in PcpII amount seems to be lower to than that observed for PcpI. Both control and diseased sections came from the same samples as those used for PcpI staining, hence there is similar tissue disintegration. The localisation of PcpII is also focused and may reflect the position of neuronal cell bodies (visible in horizontal and cross section in picture C) as presented sections demonstrate the area of the grey matter. The report by Cruz and co-workers showed that PcpII is predominantly localized in neuronal cells, which is consistent with its role in TRH-mediated synaptic transmission (Cruz *et al.*, 1991). Moreover, the same study

confirmed that glial cell cultures display PcpI but not PcpII activity. There are no reports regarding PcpII status in AD, apart from the study indicating the *trhde* gene, encoding PcpII, as being one of a number of genes up-regulated in human neuroblastoma cultured cells exposed to a toxic Aβ(1-42)-Aluminium complex (Gatta *et al.*, 2011). The direct physiological consequences of this up-regulation for AD pathogenesis remain unclear, however the authors pointed to the fact that key protein activities affected by the above complex are linked either to regulation of neuronal apoptosis or to maintenance of the structural and functional integrity of synapses. Due to the fact that neurons undergo progressive deterioration during AD development, it would be advisable to conduct co-staining of PcpII and hyperphosphorylated tau or the antigens associated with neuroapoptosis. The comparative analysis with a normal tissue could, for example, help to determine if PcpII synthesis becomes up-regulated in normal or compromised neuronal cells.

5.2.3.2. Immunostaining of PcpI and PcpII with Aβs or neurofilaments

The double-staining experiment was conducted in order to investigate the localisation and distribution of both PcpI and PcpII in relation to potential amyloid deposits, which are the key hallmarks of AD. The results showing co-staining of human PcpI and Aβ or neurofilaments are presented in figure 5.4. Consequently, the results showing co-staining of human PcpII and Aβ or neurofilaments are presented in figure 5.5. The representative sections of the A136/01 specimen of a normal adult brain with amyloid angiopathy (age 89, female) were used as the control. The staining of the A238/96 specimen from the familial AD case with APP Val717Ile mutation was shown as an exemplary result.

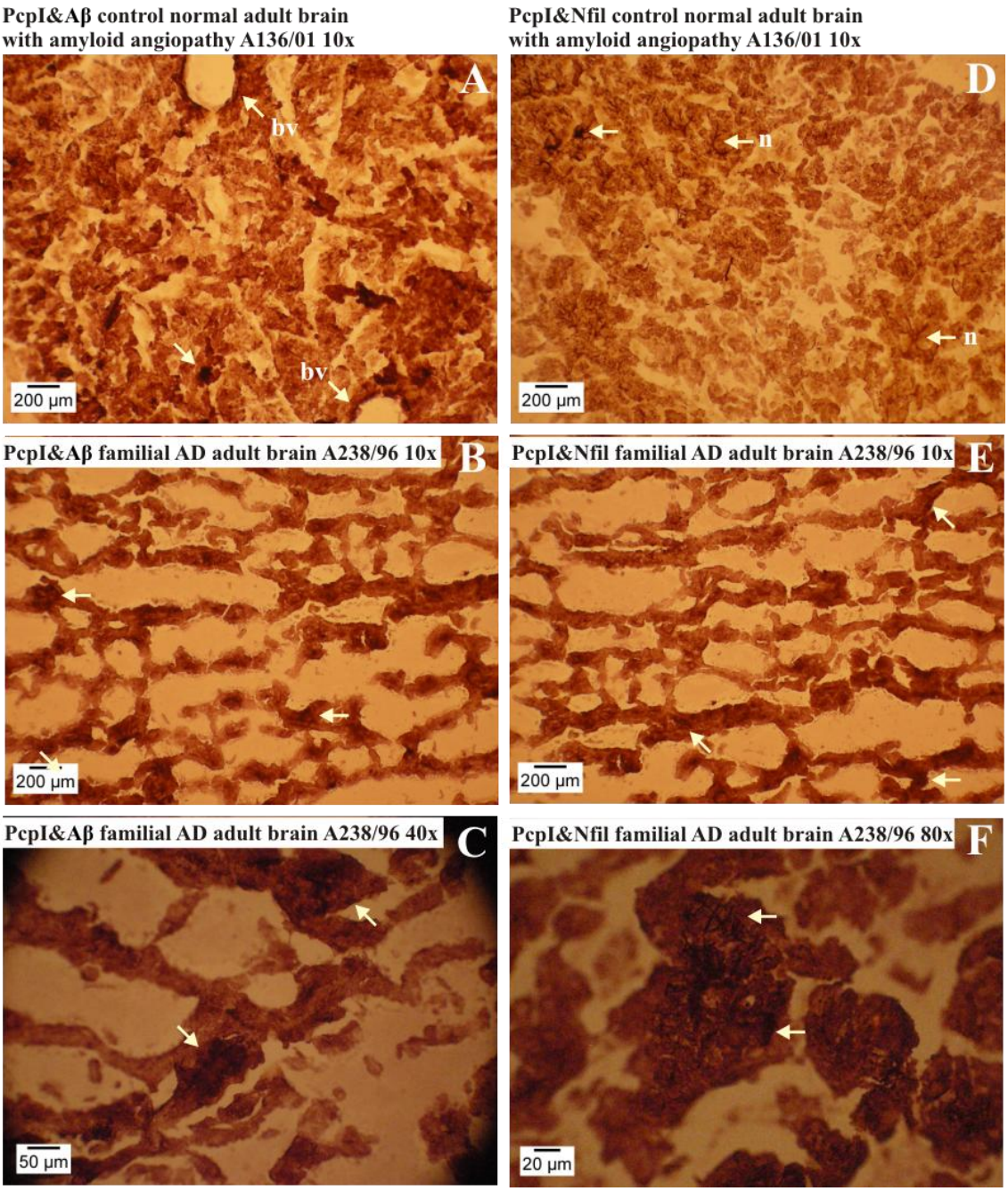

Figure 5.4. Double-immunostaining results of PcpI with Aβs (A – control, B and C – familial AD) and PcpI with neurofilaments (Nfil) (D – control, E and F – familial AD) in the cortical tissue sections. Magnification of each picture is shown in its heading. Dark brown or black colouration indicates localisation of PcpI and purple staining indicates localisation of Aβs or neurofilaments, respectively. White arrows point to the areas of the intense stainings, suggesting potential co-localisation of PcpI with either Aβs or neurofilaments, whereas arrows marked as bv or n point to blood vessel or neurites, respectively.

The results presented for both PcpI and PcpII IHC experiments were difficult to analyse due to a strong background colouration obtained from second staining step using Vector® VIP Peroxidase Substrate kit (Vector Laboratories) (5.2.2.3). Nonetheless, it was possible to detect areas of more intense colour related to PcpI (dark brown/black) and Aβ (purple, figure 5.4 A,B,C) or neurofilaments (purple, figure 5.4 D,E,F).

The staining of the control section with anti-PcpI and anti-Aβ antibodies revealed a presence of the cross-sections of two blood vessels (figure 5.4/A) with visible vascular amyloid deposits. This finding agrees with the characteristics of the sample, which was taken from a normal brain with amyloid angiopathy. Black stains around the vessels may also indicate a strong accumulation of PcpI, which seems to be interesting as the studies show that AβpGlu(3-40) accounts for around 11% of total vascular amyloid (Kuo *et al.*, 1997; Harigaya *et al.*, 2000). This may suggest a potential up-regulation of the peptidase in order to counteract the deposition of these highly hydrophobic species. The staining also revealed significant tissue shrinkage in AD sections and a presence of clusters detecting PcpI and Aβ (figure 5.4 B,C) or PcpI and neurofilament (figure 5.4 E,F) antigens. As it was mentioned above (5.2.3.1), PcpI could be possibly localised in microglia, since this type of cell becomes activated during neurodegenerative diseases mainly through increased synthesis of the proteolytic enzymes. Numerous studies showed that reactive microglia can be embedded in the core of senile plaques and that amyloid deposition may precede the activation of these cells (reviewed in (Lee and Landreth, 2010). Senile plaques are lesions preferentially found in grey matter and are key hallmarks associated with dementia by Alzheimer (Alzheimer, 1907). They are primarily composed of an Aβ core, associated molecules, dystrophic neuronal processes and reactive microglia (Dickson, 1997). The co-localisation of PcpI with both Aβs and neurofilaments may indicate their presence within senile plaques as it can be seen in pictures C and F, respectively. The elevated levels and deposition of pGlu-modified Aβs in AD may suggest an imbalance between production and catabolism of the peptides, which could be a result of inactivation or decreased production of the pGlu-removing activity. Surprisingly, the results obtained for immunostaining of PcpI showed that this level is increased when compared to the level in control tissues. Up-regulation of PcpI in diseased brain may indicate its essential participation in microglia-mediated clearance of neurodegenerative damage. Moreover, the ability of the enzyme to degrade AβpGlu(3-40/42) or AβpGlu(11-40/42)

peptides (1.1.3.3) is worth investigating as it could verify its effectiveness as a tool in AD treatment strategy.

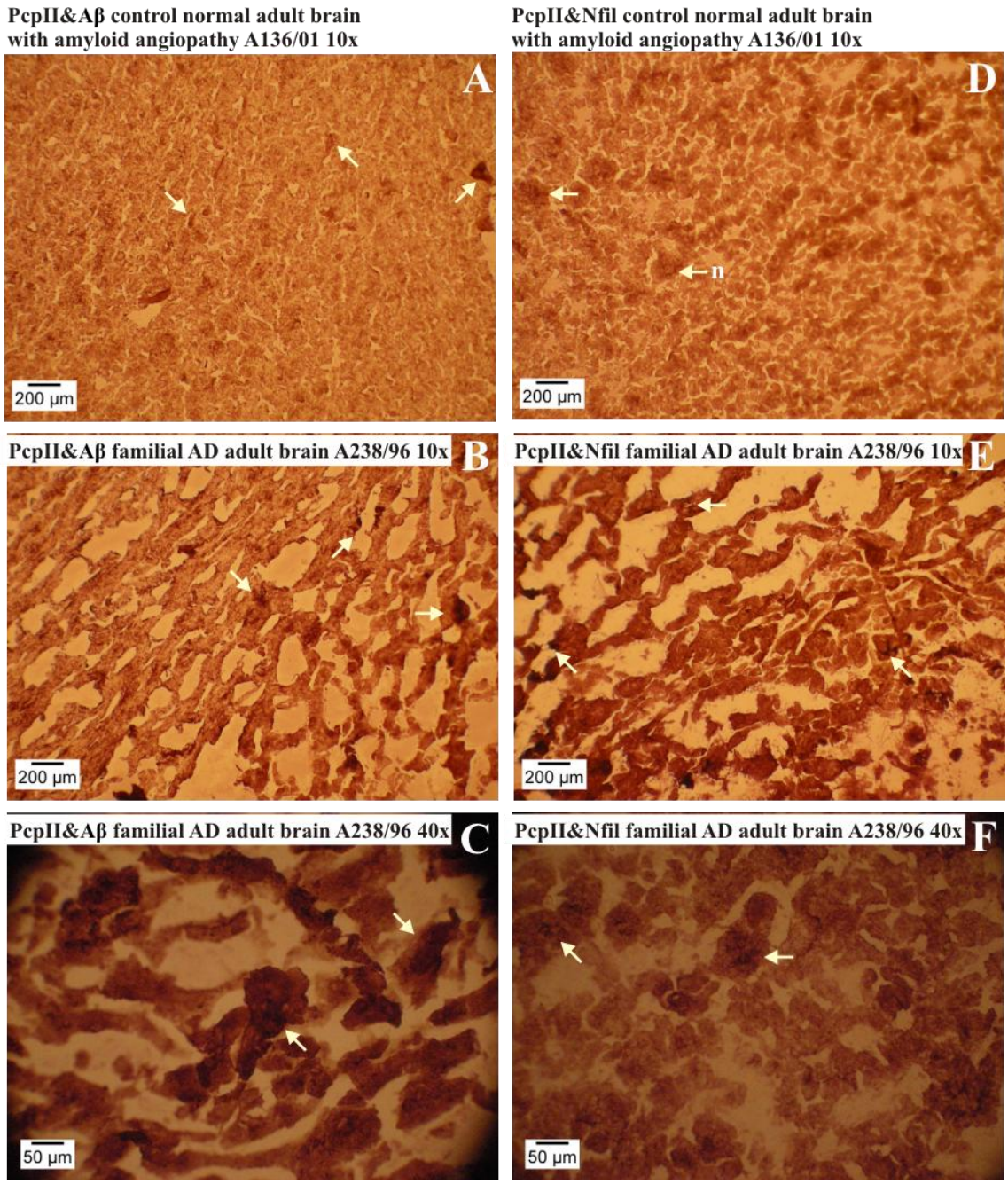

Figure 5.5. Double-immunostaining results of PcpII with Aβs (A – control, B and C – familial AD) and PcpII with neurofilaments (Nfil) (D – control, E and F – familial AD) in the cortical tissue sections. Magnification of each picture is shown in its heading. Dark brown or black colouration indicates localisation of PcpII and purple staining indicates localisation of Aβs or neurofilaments, respectively. White arrows point to the areas of the intense stainings, suggesting potential co-localisation of PcpII with either Aβs or neurofilaments; n stands for neurites.

The PcpII (dark brown or black) IHC co-staining results obtained for control sections for either Aβ (purple, figure 5.5 A,B,C) or neurofilaments (purple, figure 5.5 D,E,F) showed neglible level of the peptidase expression. Similarly to PcpI IHC results, a strong background staining was observed in all of the sections that hindered an accurate analysis, particularly for the Aβ and neurofilament antigens. There was a slightly higher level of black staining in AD sections in some patches overlaping with purple staining, which may suggest co-localisation of PcpII with amyloid peptides or, which is understood for this membrane-anchored ectoenzyme, with neurites. Concentrated and uneven distribution of the staining could suggest that all analysed antigens, as in case of PcpI, may be located within senile plaques, which are known to be composed of amyloid core, reactive microglia and dystrophic neuronal processes (Dickson, 1997). The increased level of PcpII in AD tissues is surprising, due to the fact that progressive neuronal loss and deterioration, observed in acute stages of the disorder, should rather result in down-regulation of the synthesis of this peptidase. This however, was not noticed in any of the analysed AD samples. The potential involvement of PcpII in degradation of the AβpGlu(3-40/42) or AβpGlu(11-40/42) peptides (1.1.3.3) still needs to be determined. Nonetheless, its narrow substrate specificity, which is limited to TRH, can be considered as a barrier preventing above peptides from being processed by this enzyme. The elevated level of PcpII in AD may have other implications. Studies showed that a depletion of TRH up-regulates the activity of glycogen synthetase kinase-3 (GSK-3β), which is essential for the phosphorylation of tau (Luo et al., 2002). The tau hyperphosphorylation in turn was observed to trigger axonal retraction in cultured neurons and gradual cell loss. Moreover, PcpII is an important control element of the mammalian regulatory system of hypothalamic/pituitary/thyroid axis, therefore uncontrolled activity of the enzyme could lead to deregulation of this pathway (Jeffcoate and Hutchinson, 1978; Wilk, 1986). Indeed clinical hypo- and hyperthyroidism are associated with an increased risk of AD (Tan et al., 2008).

The increased level of PcpI and, in lower degree, PcpII was observed in AD brain cortex tissue sections when compared with the control samples. This experiment however needs further optimisation mainly in the aspect of signal detection in order to prevent excessive background staining. It would be also advisable to employ an alternative immunofluorescence technique, where fluorescent labelling is used as a basis of the antigen detection and compare the results with those obtained for chromogenic

IHC. The role of both enzymes in the pathology is not well understood and still needs to be determined. PcpI in particular seems to be a good candidate for a study regarding its potential involvement in the degradation of pGlu-modified amyloid peptides, which were found in abundance in toxic AD lesions. PcpII in turn functions as a regulator of the TRH-mediated signalling system and is so far unknown in which way it is associated with Alzheimer's pathogenesis. A range of amyloid-degrading enzymes, such as neprilysin, endothelin converting enzyme or insulin-degrading enzyme are considered as therapeutic targets in neurodegeneration (Turner *et al.*, 2004; Nalivaeva *et al.*, 2008). The significance of both Pcp activities as tools for AD treatment is high due to the exceptional physiological properties of both enzymes.

5.3. Processing of pGlu-Aβ peptides by human PcpI

The abundance of the pGlu-modified Aβ peptides, being a major component of senile plaques found in AD brain, namely AβpGlu(3-40/42) and AβpGlu(11-40/42), may lead to the suggestion that a mechanism of their exposure to proteolytic degradation can be compromised. The Pcp activity, as yet, is the only identified means capable of the removal of the N-terminal pGlu protection from physiologically important biomolecules (1.2). Although numerous assays were conducted in order to determine substrate specificity of both PcpI and PcpII towards processing of the biologically important peptides, such as bombesin, neurotensin or LHRH, there is no reported study regarding its potential ability to degrade toxic pGlu-modified Aβs. The association of the progressive deposition of these peptides in AD brain and Pcp activity still needs to be investigated, nonetheless it was decided to qualitatively analyse if the AβpGlu(3-40/42) and AβpGlu(11-40/42) species can undergo proteolytic processing by human PcpI.

5.3.1. Materials and methods

The human PcpI activity towards degradation of pGlu-modified Aβs was assayed on the basis of the modified protocol by Dando and co-workers (Dando *et al.*, 2003). Synthetic AβpGlu(3-40), AβpGlu(3-42), AβpGlu(11-40) and AβpGlu(11-42) peptides were purchased from AnaSpec in a form of lyophilized material in serum vials. This was resuspended in 5% DMSO solution, according to manufacturer's instructions, in order to obtain a 10 mM final concentration and stored at -20°C. For the qualitative study, 25 µl of the 10 ng/µl PcpI in activity assay buffer (2.3.4) was individually mixed with 20 µM (final concentration) of each peptide in a total volume of 100 µl. Each of the reactions was conducted in triplicate and incubated at 37ºC for 1 hour. The negative control was prepared by the addition of acetic acid to the protein sample prior to mixing with the peptide solutions. The reaction was terminated by the addition of 10 µl of 1.5 M acetic acid. Analysis of the results was performed by mass spectrometry using a Q-TOF 6520 (Agilent) coupled to a HPLC-Chip 1200 interface system. The samples were loaded onto a micro C_{18} reverse phase analytical column (Agilent Protein Identification Chip) and eluted over 20 min using a methanol/water gradient with 0.1%

formic acid solution. Next monoisotopic masses of each individual substrate and product were calculated and used to obtain extracted ion chromatograms (EIC) to determine their presence in the sample solutions.

5.3.2. Results and discussion

5.3.2.1. Degradation of pGlu-modified Aβs by human PcpI

The mass spec analysis of the proteolytic cleavage of AβpGlu(3-40), AβpGlu(3-42), AβpGlu(11-40) and AβpGlu(11-42) peptides by PcpI showed that the desired product was only obtained for a degradation of the AβpGlu(3-40) variant (figure 5.6).

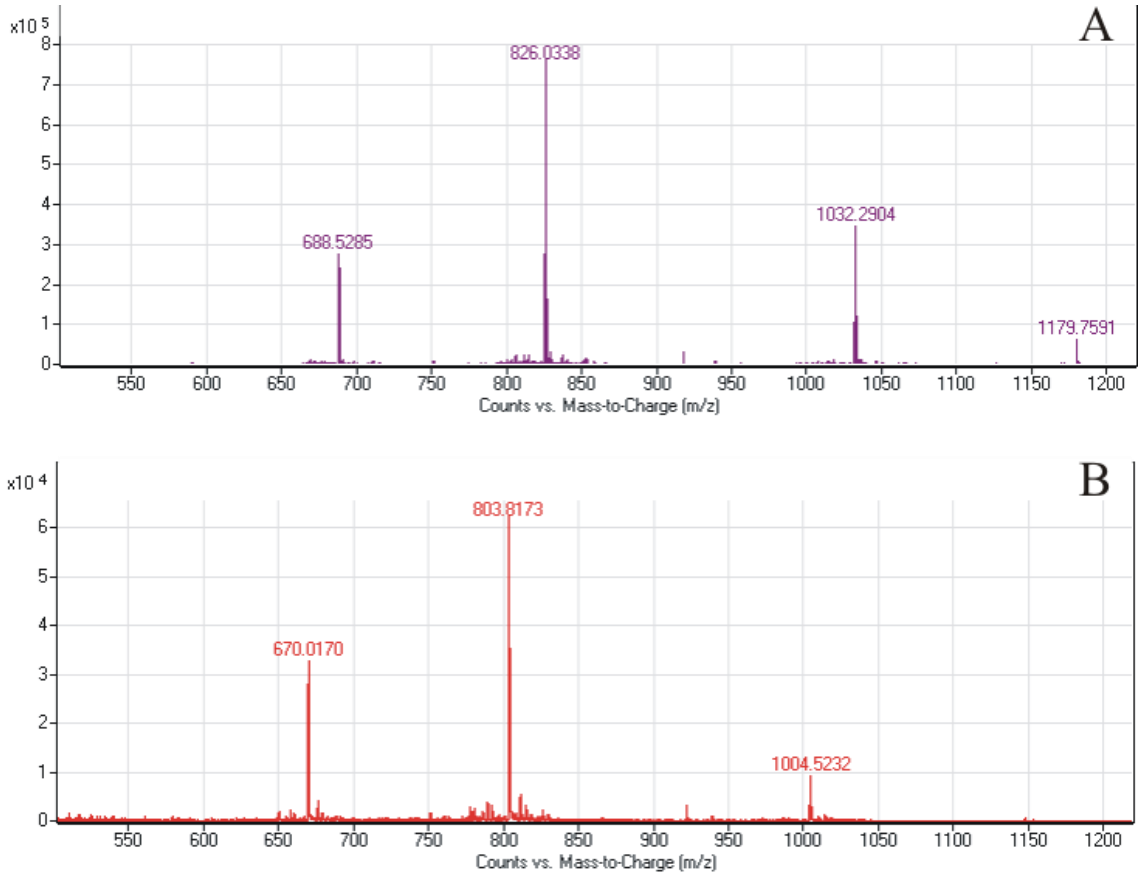

Figure 5.6. Mass spectrum for the proteolytic cleavage of AβpGlu(3-40) by PcpI. A top diagram (A) shows the characteristic spectrum obtained for the substrate and bottom one (B) – for product Aβ(4-40).

The spectra obtained for the other reactions – AβpGlu(3-42), AβpGlu(11-40) and AβpGlu(11-42) – did not confirm the presence of the desired cleavage products. However, the subsequent control analysis of the stock solutions of all of the above peptides revealed the charge state peaks characteristic for the product of the AβpGlu(3-40) degradation – Aβ(4-40) to be present in AβpGlu(3-42) and AβpGlu(11-42). Moreover, both stocks were cross-contaminated with AβGlu(3-40), which contains an N-terminal glutamic acid instead of pyroglutamyl group. There was no AβGlu(3-40) contamination and no Aβ(4-40) product in a stock of AβpGlu(3-40) or in a related negative control reaction sample, which could confirm that its degradation was catalysed by PcpI. Such findings may suggest that the peptides could undergo some kind of unspecific spontaneous disintegration or their synthesis was incomplete, hence the presence of a Aβ(4-40) contaminant, which lacks protecting N-terminal pGlu residue. It is also possible that the cyclisation of the N-terminal glutamic acid to pGlu was insufficient explaining the presence of AβGlu(3-40).

The unsuccessful processing of the shorter forms of Aβ, AβpGlu(11-40) and AβpGlu(11-42), may also lead to the conclusion that the peptides, due to their highly hydrophobic properties, can undergo a change in conformation or oligomerization. This in turn could hinder the access of the PcpI enzyme to the pGlu residue and thus prevent its removal. Such phenomenon can take place in the organisation of amyloid deposits, where the pGlu group may be not available for the enzymatic processing. Nonetheless positive results obtained for AβpGlu(3-40) confirmed the substrate specificity of the PcpI towards this group of peptides. It would be advisable to further optimize this assay as well as conduct similar qualitative analysis with PcpII, which was impossible here due to the lack of the enzyme preparation. The comparison of the results obtained for both enzymes could give an insight on their capability and effectiveness in degradation of pGlu-modified Aβs *in vivo* in AD pathology.

.

Chapter 6 – Summary, conclusions and future work

The experimental work conducted within this project was focused around the study of human PcpI, human PcpII and their potential relationship with an excessive production and deposition of the N-terminally pGlu-modified Aβ species in AD.

Human PcpI was successfully overexpressed in *E. coli* cells in the native and the recombinant form carrying N- or C-terminal His-tag. The production of these different enzyme variants was part of stability studies on the protein, which was observed to be extremely unstable *in vitro*. The initial approach, which aimed to overcome this problem, involved a variety of chemical additives or a change from Tris-HCl to K_2HPO_4/KH_2PO_4 based buffer in order to investigate how these alterations affect the protein behaviour (3.2.1.3.6). None of the above factors proved to be stabilising for the N-terminally His-tagged PcpI. The minor improvement in solubility was observed for 0.15 M NaCl and therefore it was included in purification buffers that were further used.

Due to the fact that the N-terminal His-tagged PcpI (6xHis-PcpI) was shown to be unstable in solution, two alternative variants of the enzyme were produced – native and C-terminally His-tagged (PcpI-6xHis). Several studies on the other proteins have been reported where the position of the affinity tag had an influence on protein folding and resulted in improved purification yields (3.2.1.4). The PcpI-6xHis variant was showed to be more stable than its N-terminally tagged counterpart, this was particularly observed during the protein concentration procedure. Additional work which aimed to identify the reasons of PcpI instability included performance of a thermofluor shift assay, site-directed mutagenesis of the non-catalytic cysteine residues and chemical modification of surface cysteines and lysines (3.3). The results of the screening for optimal buffer conditions using the thermofluor shift assay revealed a very destabilising effect of the Tris-HCl buffer used initially for PcpI. The Tris-HCl buffer was subsequently replaced by a zwitteronic HEPPS buffer, which provided the most stabilising environment for the peptidase as confirmed by the increased shift in melting temperature (3.3.1.2). The use of HEPPS buffer significantly improved the protein stability during the purification and concentration steps. This enabled both native PcpI and PcpI-6xHis proteins to be concentrated up to 50 mg/ml and used in crystallisation trials.

The site-directed mutagenesis study on all of the non-catalytic cysteine residues in human PcpI (3.3.2), suggested that at least some of these residues may have an important influence on protein function. Interesting results were obtained for the C107A variant, which was observed to be inactive and prone to dimerization. The C107 probably participates in the formation of a vicinal disulfide bridge with an adjacent C108 residue. Therefore, the above mutation could lead to an intermolecular cystine formation between the reactive C108 sulfhydryls. Moreover both residues with C99 and C102 are located within a Cys-rich loop, which could work as a functional subdomain. Such dense localisation of cysteines is typical for Zn-binding motifs. However the addition of $ZnCl_2$ to the protein-expressing culture (3.3.2.1.4) or the analysis of zinc acetate in the thermofluor shift assay (3.3.5.1) did not confirm any stabilising effect on the protein. Moreover, previous reports on the incubation of human PcpI with EDTA resulted in no change in activity, which indicates the absence of any metal ion being important for the protein function (Dando *et al.*, 2003).

Both native PcpI and PcpI-6xHis were subjected to an extensive crystallisation study in order to find optimal conditions for crystal nucleation and growth (3.4). The crystallisation experiments were conducted for all PcpI cysteine mutants as well as for the protein containing DTNB-modified surface cysteines or methylated surface lysines (3.3.3). This part of experimental studies proved to be extremely difficult with a few conditions that produced tiny crystals or crystalline precipitate. Nonetheless, small plate like crystals were produced for the PcpI-6xHis in the presence of the 2-pyrrolidone inhibitor in 0.1 M Bis-Tris pH 5.5 and 15% PEG3350. These crystals were shown to be protein and diffracted at a low resolution. This condition is useful as a starting point for a crystallisation optimisation procedure. The small crystals were also used for microseeding experiments. To date, these attempts have not yielded good quality crystals and further optimisation is necessary.

The part of the study on human PcpII involved attempts to express the protein in bacterial, insect and mammalian systems (4.2.1.2 and 4.2.1.3). The protein sequence was submitted to an online prediction server in order to identify putative disordered and globular regions that would help to establish domain boundaries. On the basis of this a series of truncated protein variants were cloned and tested for expression in specialised *E. coli* strains. However, an overexpression in the bacterial system was unsuccessful and this lead to subsequent overexpression trials which were conducted in insect *Sf*9 and VE-*Sf*9 and mammalian HEK 293T cells. This part of experimental work was

conducted in the OPPF laboratory (Research Complex at Harwell) and involved preparation of a range of pOPIN-based constructs, which allow for parallel protein expression screening in bacterial, insect and mammalian cell lines. The utilisation of baculovirus-mediated insect system was unsuccessful, however three of the constructs 8708, 8984 and 7465 (table 4.9) which were expressed in mammalian cell line yielded small levels of secreted PcpII/S62-H1024 protein. This result may be considered as a starting point for further optimisation of the overexpression conditions in order to obtain sufficient amount of the protein for structural studies and other applications.

Due to the lack of the structural information regarding PcpII, basic homology modelling of the putative catalytic domain was conducted using the structure of human ERAP1 as a template sharing 40% identity and 56% similarity (4.3.2.1). Additionally, docking simulations of TRH in the active site of the enzyme were performed to gain an insight into its probable binding mode. The modelling was successful, with the resulting structure having an RMSD of 1.33 Å to the template which indicates that the obtained structural fold is similar to that of ERAP1 conformation. The TRH docking results revealed the specific orientation of Tyr403 and Phe522 residues, which entrap the pGlu moiety through complex hydrogen bonding and hydrophobic interactions, and may be necessary for the proper orientation of the substrate in the active site. This experiment also showed the close interaction of the pGlu carbonyl oxygen with the catalytic Zn atom and important residues such as Ser268, Tyr527or Asp519, which may create hydrogen bonding with TRH residues . This could be essential for substrate recognition and correct orientation in relation to the catalytic moiety. Structural information gained from the three-dimensional PcpII model and, in particular, the structure of the active site could provide useful information which can be used to design further experiments such as site-directed mutagenesis and could aid in the search for potential enzyme inhibitors.

The final stage of this project was focused on the investigation of the involvement of PcpI and PcpII to AD pathogenesis. The IHC staining of both proteins was conducted in order to investigate any potential differences in their localisation and distribution between control and diseased cortical tissue sections (5.2). It could be suggested that the abundance of pGlu-modified Aβ species in AD brain may be a result of the decreased level of Pcp activity. Surprisingly, the immunostaining results indicated that the level of both PcpI and PcpII is increased in neurodegenerated tissue when compare to normal adult brain sections. Moreover the areas of stainings of both peptidases with either Aβ or neurofilaments showed their co-localisation in AD tissue, which probably is a result

of senile plaque deposition, where all four antigens could be detected. The distribution and amorphous staining of PcpI indicated that the protein may be over-expressed in reactive microglia, which were also found within amyloid plaques. The elevated level of PcpI may be associated with extensive proteolytic activity of microglial cells acting as macrophages and removing damaged biological material from the surrounding environment. In turn the increase in PcpII appearance could be a result of a deregulated hypothalamic/pituitary/thyroid system. A specific function of this peptidase relies on the regulation of the TRH neurotransmitter, therefore its up-regulated activity may subsequently have an effect on endocrine homeostasis and cell signalling. The IHC also revealed significant shrinkage of the cortical tissues progressing during AD development.

PcpI substrate specificity was tested against common pGlu-modified peptides, which were found in abundance in AD tissues as well as vascular and amyloid deposits (5.3). The AβpGlu(3-40), AβpGlu(3-42), AβpGlu(11-40) and AβpGlu(11-42) peptides were used as a substrates for PcpI in order to evaluate if they can be degraded by the enzyme. Positive results were obtained for AβpGlu(3-40) and the desired Aβ(4-40) product was confirmed by mass spectrometry analysis. The three other peptides failed the pGlu removal. However, analysis of the original stock material showed that all of them were contaminated with either Aβ(4-40) or AβGlu(3-40) species which may indicate spontaneous disintegration or incomplete synthesis. Therefore to analyse enzyme affinity towards the degradation of the remaining substrates, the procedure needs to be repeated on pure homogenous peptide samples. The other aspect of the possible failure in these reactions may also be due to the hydrophobic nature of all the peptides, which could spontaneously oligomerise or change conformation in a way that hinders accessibility of the pGlu residue for PcpI binding.

Future work on human PcpI should include further optimisation of crystallisation conditions already identified in initial screening, in order to yield good quality crystals for structural studies. Moreover, site-directed mutagenesis of chosen residues could prove to have a stabilising effect on the protein. Such an approach proved to be successful in the case of *B. amyloliquefaciens* PcpI, where artificial generation of the inter-subunit disulfide bridge in the position corresponding to the native bridges in *T. litoralis* and *P. furiosus* homologues, greatly increased its thermal stability (Kabashima *et al.*, 2001). Similarly, many prokaryotic Pcps possess Phe residue in a position of the conserved Tyr147 in the human enzyme. Interestingly, the residue is located in the substrate binding site and studies on human PcpI Y147F mutant confirmed it to be more thermostable (Mtawae *et al.*, 2008). It is worth investigating this and similar mutants in the context of their stability that could be also advantageous for structural studies.

Further study on human PcpII will include optimisation of its overexpression conditions in the mammalian cell system in order to produce sufficient amounts of the protein for a structural study. The full-length protein and its functional domains could also be tested for expression in alternative hosts such as COS or CHO cell lines. Consequently, new pOPIN-based constructs will be produced and used for expression screening of all PcpII variants. It would be advisable to conduct a wider study on the potential structural similarities between PcpI and PcpII.

An interesting observation is the potential structural and functional similarity between PcpI and PcpII. Correlations between both peptidases could be significant, for example the finding that PcpII is the only member of M1 metallopeptidase family, which possesses Cys in the conserved $HEXXHX_{18}E$ motif or that PcpI, in turn, contains a Cys-rich loop potentially able for Zn coordination. Moreover, prokaryotic Pcps display a different structure than that observed for other members of the C15 family. One example is the *T. litoralis* Pcp, which was observed to display similar scaffold to a zinc-dependent carboxypeptidase A from *Bos taurus* (PBD 2CTB) (Singleton *et al.*, 1999).

The IHC study on PcpI and PcpII level in AD tissues showed their up-regulated synthesis. Further studies of this phenomenon is of great interest as it may provide more information on the role of both enzymes in this neurodegenerative disorder and evaluate their potential use as a drug targets in AD treatment. An alternative

immunofluorescence staining method could result in better detection and help with the undesired background staining observed in the study. In order to confirm the exact localisation of both enzymes in tissue compartments, it is necessary to conduct a concurrent detection of antigens associated with microglia or neuronal loss. For the improvement of specificity and signal detection, it could be also advantageous to employ other anti-PcpI and anti-PcpII antibodies, when they become commercially available. Moreover, due to the fact that Pcp activity was seen to decrease with age in human cerebrospinal fluid (1.2.4.3) it is understood that any comparative staining should be conducted using age-matched controls.

Appendices

Appendix I. The map and cloning/expression region of pET-28a(+) vector

pET-28b(+) vector differs only by 1bp subtracted at position198 beyond *Bam*HI restriction site. Taken from www.merck-chemicals.co.uk.

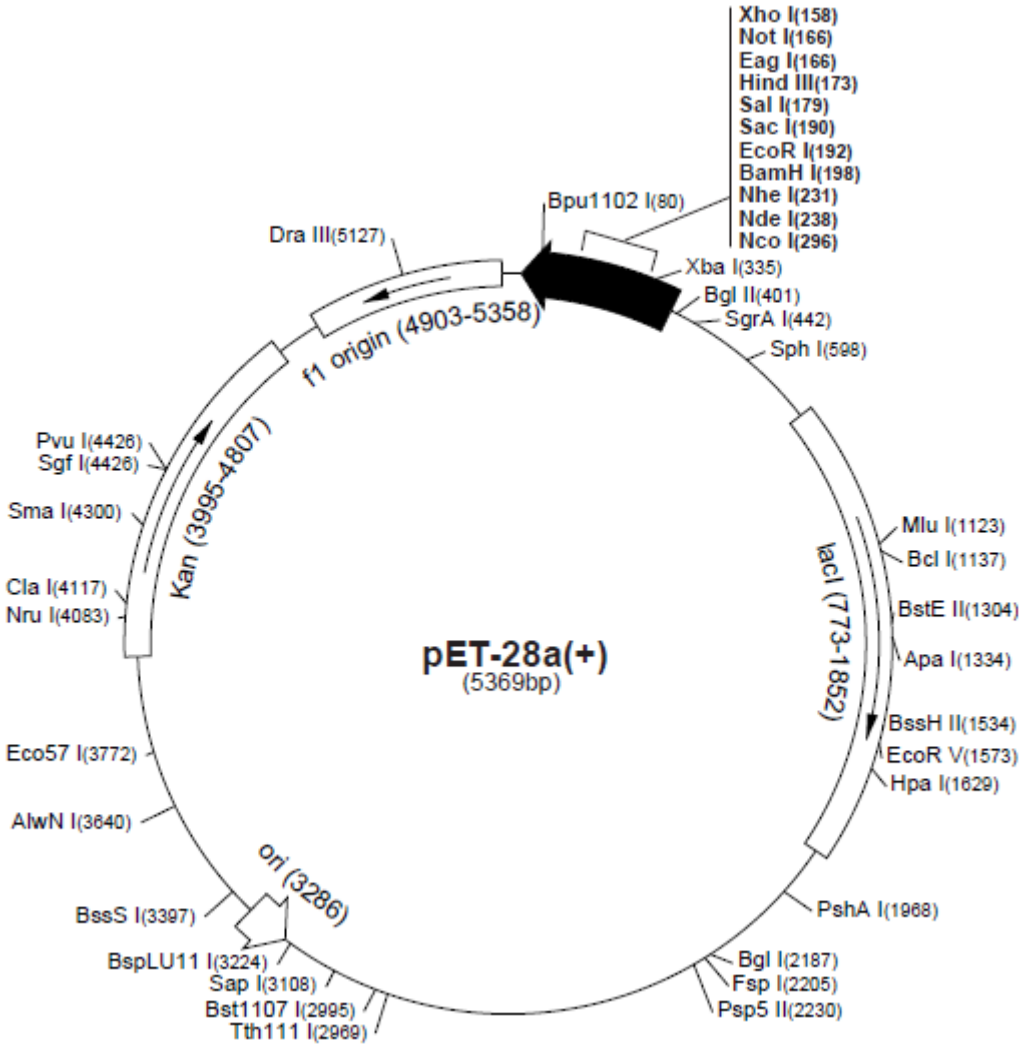

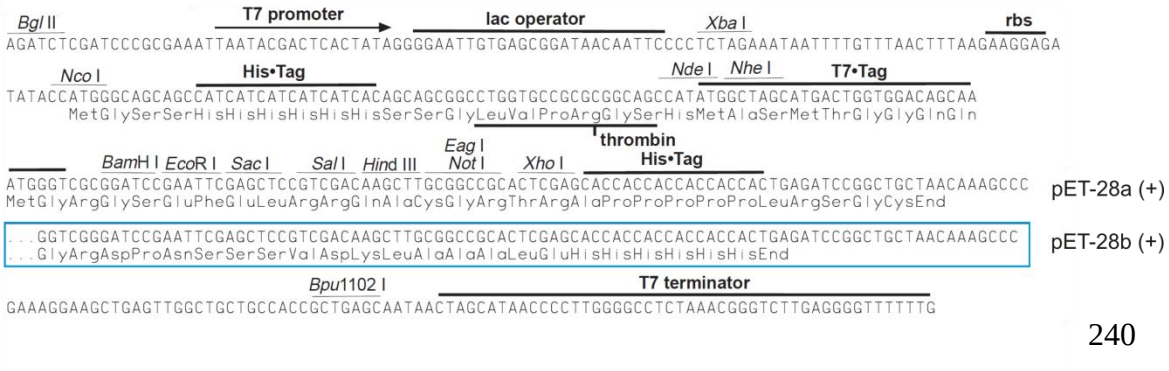

Appendix II. The map and cloning/expression region of pET-22b(+) vector

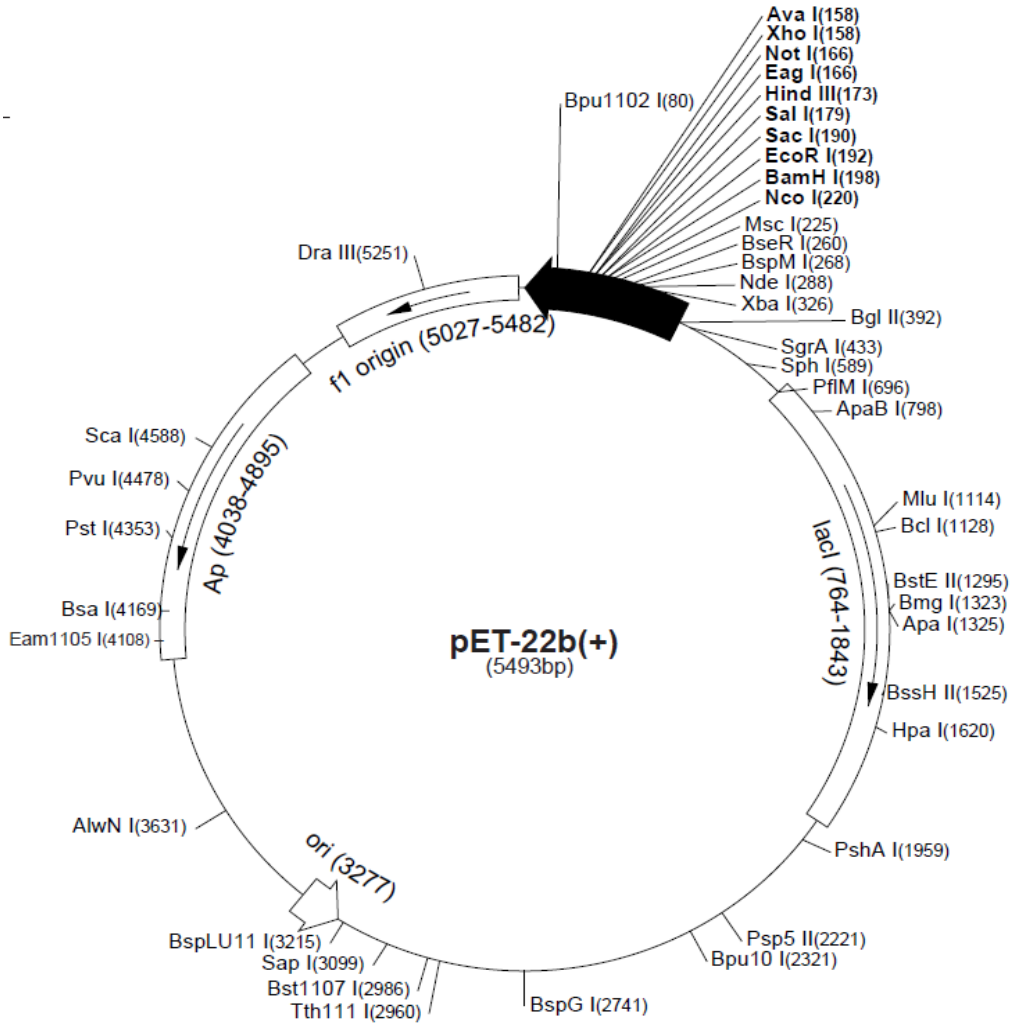

Taken from www.merck-chemicals.co.uk.

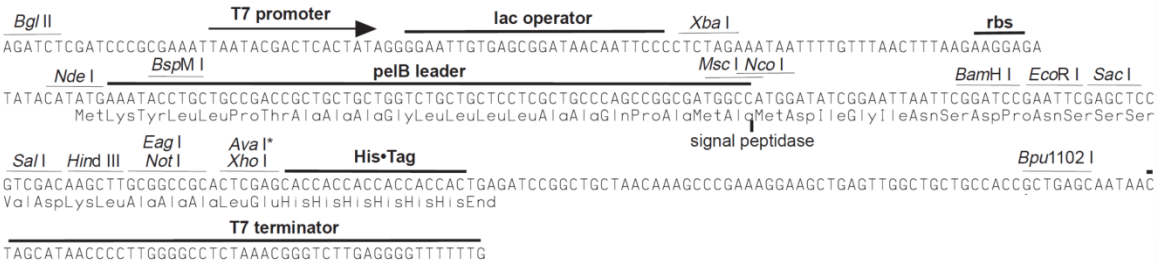

Appendix III. DNA sequencing results of PcpI

- the N-terminal His-tag motif is highlighted in green and the C-terminal His-tag motif is highlighted in orange
- TGA stop codon is highlighted in blue

DNA sequence:

ATGGGCAGCAGC**CATCATCATCATCATCAC**AGCAGCGGCCTGGTGCCGCGCGGCAGCCAT
ATGGAGCAGCCGAGGAAGGCGGTGGTAGTGACGGGATTTGGCCCTTTTGGGGAACACACCGTGA
ACGCCAGTTGGATTGCAGTTCAGGAGCTAGAAAAGCTAGGCCTTGGCGACAGCGTGGACCTGCA
TGTGTACGAGATTCCGGTTGAGTACCAAACAGTCCAGAGACTCATCCCCGCCCTGTGGGAGAAG
CACAGTCCACAGCTGGTGGTGCATGTGGGGGTGTCAGGCATGGCGACCACAGTCACACTGGAGA
AATGTGGACACAACAAGGGCTACAAGGGGCTGGACAACTGCCGCTTTTGCCCCGGCTCCCAGTG
CTGCGTGGAGGACGGGCCTGAAAGCATTGACTCCATCATCGACATGGATGCTGTGTGCAAGCGA
GTCACCACGTTGGGCCTGGATGTGTCGGTGACCATCTCGCAGGATGCCGGCAGATATCTCTGCG
ACTTTACCTACTACACCTCTTTGTACCAGAGTCACGGTCGATCAGCCTTCGTCCACGTGCCCCC
ACTGGGGAAGCCGTACAACGCGGACCAGCTGGGCAGGGCACTGAGAGCCATCATTGAGGAGATG
TTGGACCTCCTGGAGCAGTCAGAGGGCAAAATCAACTATTGCCACAAACACTGA
AAGCTTGCGGCCGCACTCGAG**CACCACCACCACCACCAC**TGA

Amino acid sequence:

MGSS**HHHHHH**SSGLVPRGSHMEQPRKAVVVTGFGPFGEHTVNASWIAVQELEKLGLGDS
VDLHVYEIPVEYQTVQRLIPALWEKHSPQLVVHVGVSGMATTVTLEKCGHNKGYKGLDN
CRFCPGSQCCVEDGPESIDSIIDMDAVCKRVTTLGLDVSVTISQDAGRYLCDFTYYTSL
YQSHGRSAFVHVPPLGKPYNADQLGRALRAIIEEMLDLLEQSEGKINYCHKH
KLAAALQ**HHHHHH**

Appendix IV. Calibration curve and chromatographic separation of the standard proteins on HiLoad™ 16/60 Superdex™ 200 column.

Taken from www.gelifesciences.com

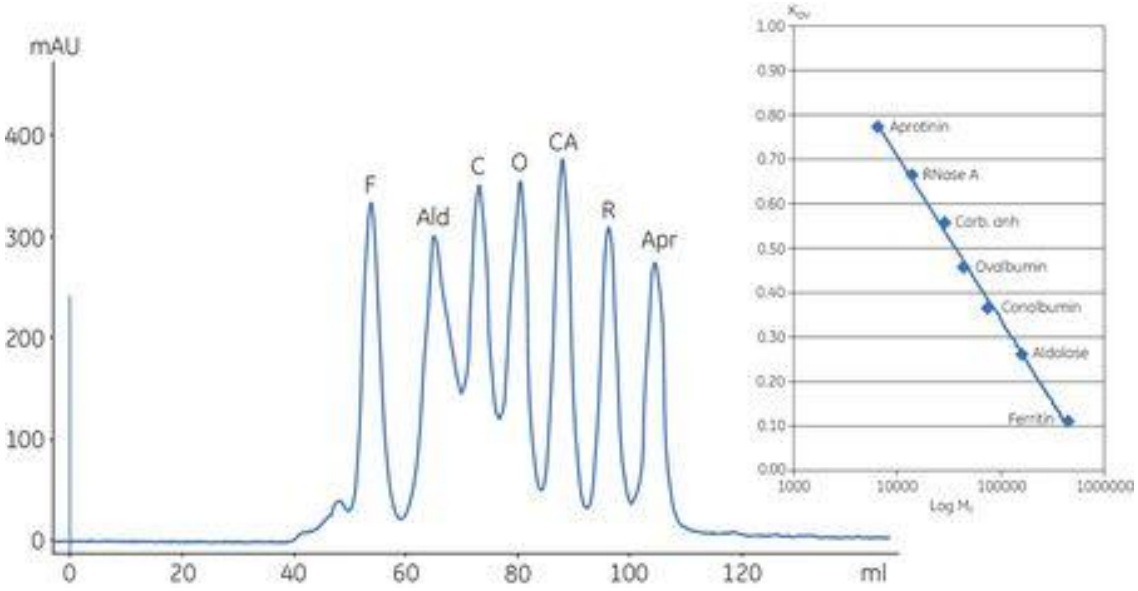

Protein standard	Abbr.	Molecular weight (kDa)
Aprotinin	Apr	6500
Ribonuclease A	R	13 700
Carbonic anhydrase	CA	29 000
Ovalbumin	O	43 000
Conalbumin	C	75 000
Aldolase	Ald	158 000
Ferritin	F	440 000

Appendix V. Standard curve for 7-amino-4-methyl coumarin (AMC) concentration.

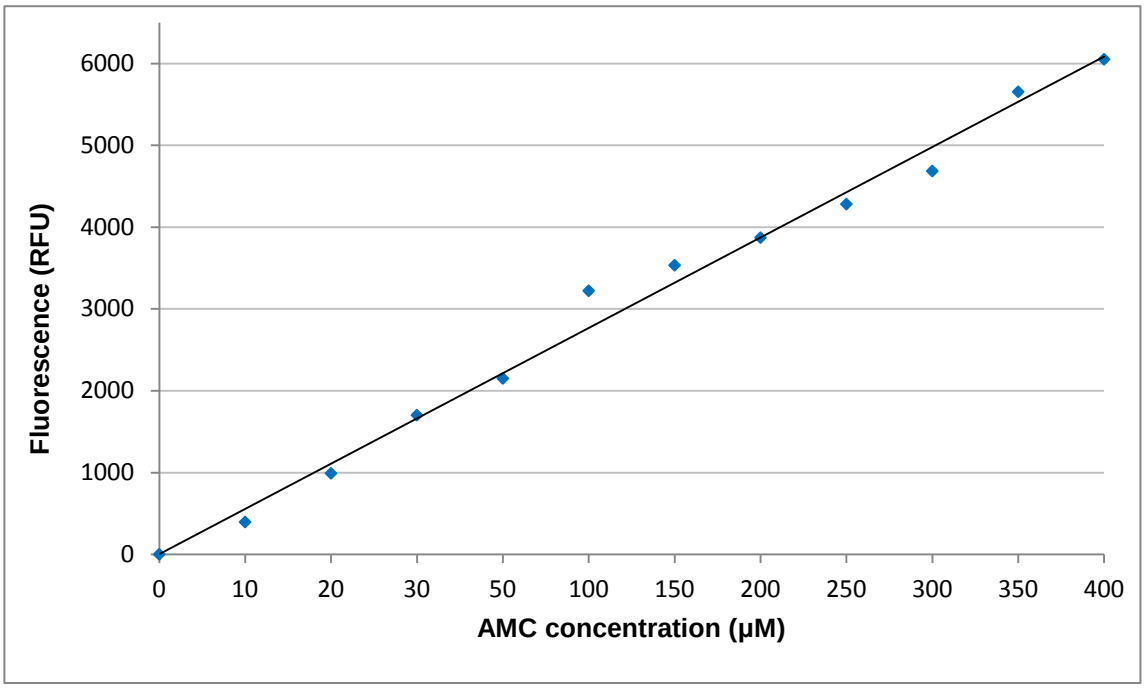

Appendix VI. A Ramachandran plot of the human PcpI model.

The plot was generated in RAMPAGE Ramachandran Plot server (Lovell *et al.*, 2003).

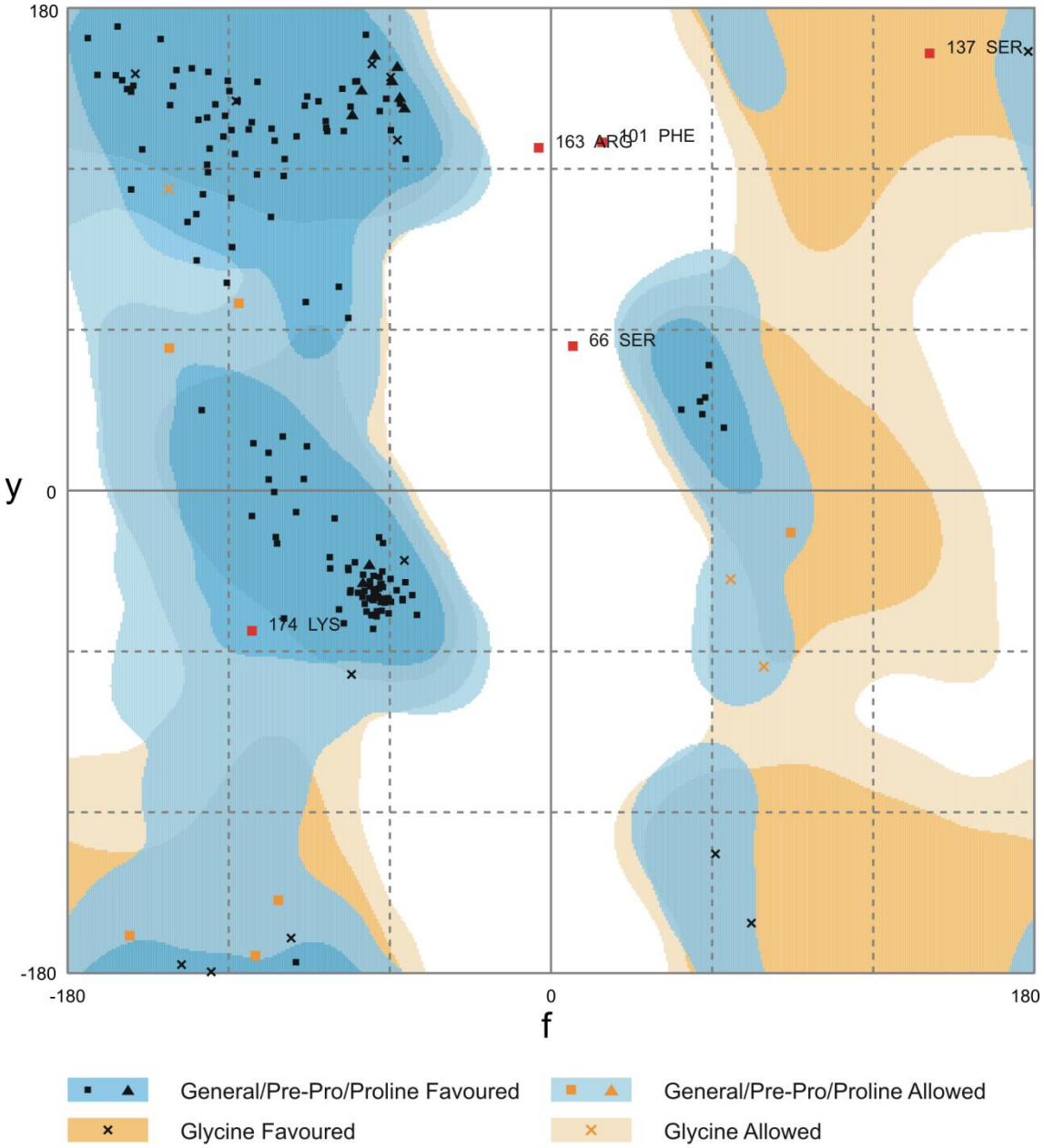

Number of residues in favoured region (~98.0% expected)	: 169 (92.3%)
Number of residues in allowed region (~2.0% expected)	: 9 (4.9%)
Number of residues in outlier region	: 5 (2.7%)

Appendix VII. Sequencing results of the PcpI cysteine mutants

```
C87A                MEQPRKAVVVTGFGPFGEHTVNASWIAVQELEKLGLGDSVDLHVYEIPVEYQTVQ  55
C99A                MEQPRKAVVVTGFGPFGEHTVNASWIAVQELEKLGLGDSVDLHVYEIPVEYQTVQ  55
C102A               MEQPRKAVVVTGFGPFGEHTVNASWIAVQELEKLGLGDSVDLHVYEIPVEYQTVQ  55
C107A               MEQPRKAVVVTGFGPFGEHTVNASWIAVQELEKLGLGDSVDLHVYEIPVEYQTVQ  55
C108A               MEQPRKAVVVTGFGPFGEHTVNASWIAVQELEKLGLGDSVDLHVYEIPVEYQTVQ  55
C126A               MEQPRKAVVVTGFGPFGEHTVNASWIAVQELEKLGLGDSVDLHVYEIPVEYQTVQ  55
C206A               MEQPRKAVVVTGFGPFGEHTVNASWIAVQELEKLGLGDSVDLHVYEIPVEYQTVQ  55
C99/102A            MEQPRKAVVVTGFGPFGEHTVNASWIAVQELEKLGLGDSVDLHVYEIPVEYQTVQ  55
C107/108A           MEQPRKAVVVTGFGPFGEHTVNASWIAVQELEKLGLGDSVDLHVYEIPVEYQTVQ  55
C99/102/107/108A    MEQPRKAVVVTGFGPFGEHTVNASWIAVQELEKLGLGDSVDLHVYEIPVEYQTVQ  55
CtA                 MEQPRKAVVVTGFGPFGEHTVNASWIAVQELEKLGLGDSVDLHVYEIPVEYQTVQ  55

C87A                RLIPALWEKHSPQLVVHVGVSGMATTVTLEKAGHNKGYKGLDNCRFCPGSQCCVE  110
C99A                RLIPALWEKHSPQLVVHVGVSGMATTVTLEKCGHNKGYKGLDNARFCPGSQCCVE  110
C102A               RLIPALWEKHSPQLVVHVGVSGMATTVTLEKCGHNKGYKGLDNCRFAPGSQCCVE  110
C107A               RLIPALWEKHSPQLVVHVGVSGMATTVTLEKCGHNKGYKGLDNCRFCPGSQACVE  110
C108A               RLIPALWEKHSPQLVVHVGVSGMATTVTLEKCGHNKGYKGLDNCRFCPGSQCAVE  110
C126A               RLIPALWEKHSPQLVVHVGVSGMATTVTLEKCGHNKGYKGLDNCRFCPGSQCCVE  110
C206A               RLIPALWEKHSPQLVVHVGVSGMATTVTLEKCGHNKGYKGLDNCRFCPGSQCCVE  110
C99/102A            RLIPALWEKHSPQLVVHVGVSGMATTVTLEKCGHNKGYKGLDNARFAPGSQCCVE  110
C107/108A           RLIPALWEKHSPQLVVHVGVSGMATTVTLEKCGHNKGYKGLDNCRFCPGSQAAVE  110
C99/102/107/108A    RLIPALWEKHSPQLVVHVGVSGMATTVTLEKCGHNKGYKGLDNARFAPGSQAAVE  110
CtA                 RLIPALWEKHSPQLVVHVGVSGMATTVTLEKAGHNKGYKGLDNARFAPGSQAAVE  110

C87A                DGPESIDSIIDMDAVCKRVTTLGLDVSVTISQDAGRYLCDFTYYTSLYQSHGRSA  165
C99A                DGPESIDSIIDMDAVCKRVTTLGLDVSVTISQDAGRYLCDFTYYTSLYQSHGRSA  165
C102A               DGPESIDSIIDMDAVCKRVTTLGLDVSVTISQDAGRYLCDFTYYTSLYQSHGRSA  165
C107A               DGPESIDSIIDMDAVCKRVTTLGLDVSVTISQDAGRYLCDFTYYTSLYQSHGRSA  165
C108A               DGPESIDSIIDMDAVCKRVTTLGLDVSVTISQDAGRYLCDFTYYTSLYQSHGRSA  165
C126A               DGPESIDSIIDMDAVAKRVTTLGLDVSVTISQDAGRYLCDFTYYTSLYQSHGRSA  165
C206A               DGPESIDSIIDMDAVCKRVTTLGLDVSVTISQDAGRYLCDFTYYTSLYQSHGRSA  165
C99/102A            DGPESIDSIIDMDAVCKRVTTLGLDVSVTISQDAGRYLCDFTYYTSLYQSHGRSA  165
C107/108A           DGPESIDSIIDMDAVCKRVTTLGLDVSVTISQDAGRYLCDFTYYTSLYQSHGRSA  165
C99/102/107/108A    DGPESIDSIIDMDAVCKRVTTLGLDVSVTISQDAGRYLCDFTYYTSLYQSHGRSA  165
CtA                 DGPESIDSIIDMDAVAKRVTTLGLDVSVTISQDAGRYLCDFTYYTSLYQSHGRSA  165

C87A                FVHVPPLGKPYNADQLGRALRAIIEEMLDLLEQSEGKINYCHKH  209
C99A                FVHVPPLGKPYNADQLGRALRAIIEEMLDLLEQSEGKINYCHKH  209
C102A               FVHVPPLGKPYNADQLGRALRAIIEEMLDLLEQSEGKINYCHKH  209
C107A               FVHVPPLGKPYNADQLGRALRAIIEEMLDLLEQSEGKINYCHKH  209
C108A               FVHVPPLGKPYNADQLGRALRAIIEEMLDLLEQSEGKINYCHKH  209
C126A               FVHVPPLGKPYNADQLGRALRAIIEEMLDLLEQSEGKINYCHKH  209
C206A               FVHVPPLGKPYNADQLGRALRAIIEEMLDLLEQSEGKINYAHKH  209
C99/102A            FVHVPPLGKPYNADQLGRALRAIIEEMLDLLEQSEGKINYCHKH  209
C107/108A           FVHVPPLGKPYNADQLGRALRAIIEEMLDLLEQSEGKINYCHKH  209
C99/102/107/108A    FVHVPPLGKPYNADQLGRALRAIIEEMLDLLEQSEGKINYCHKH  209
CtA                 FVHVPPLGKPYNADQLGRALRAIIEEMLDLLEQSEGKINYAHKH  209
```

Appendix VIII. DNA sequencing results of PcpII

DNA sequence:

ATGGGGGAAGACGACGCCGCGCTTCGGGCTGGCAGCAGGGGGCTCTCCGACCCGTGGGCAGACT
CAGTGGGAGTGCGACCCCGCACCACGGAGCGCCACATCGCCGTACACAAGCGGCTTGTGCTGGC
CTTCGCTGTGTCCCTCGTGGCATTGCTCGCGGTCACAATGCTCGCTGTGCTGCTCAGCCTGCGC
TTCGACGAGTGCGGGGCGAGTGCCACGCCAGGCGCCGACGGTGGCCCCTCAGGCTTTCCGGAGC
GCGGCGGCAACGGGAGCCTCCCTGGATCGGCCCGGCGCAACCACCACGCAGGCGGGGACTCCTG
GCAGCCCGAGGCGGGTGGGGTGGCCAGTCCGGGGACCACGTCGGCCCAGCCGCCGTCGGAGGAG
GAGCGGGAGCCGTGGGAGCCGTGGACGCAGCTGCGCCTGTCGGGCCACCTGAAGCCGCTGCACT
ACAATCTGATGCTCACCGCCTTCATGGAGAACTTCACCTTCTCCGGGGAGGTCAACGTGGAGAT
CGCGTGCCGGAACGCCACCCGCTACGTAGTGCTGCACGCTTCCCGAGTGGCGGTGGAGAAAGTG
CAGCTGGCCGAGGACCGGGCGTTCGGGGCTGTCCCTGTAGCCGGTTTTTTCCTCTACCCGCAAA
CCCAGGTCTTAGTGGTGGTGCTGAATAGGACACTGGACGCGCAGAGGAATTACAATCTGAAGAT
TATCTACAACGCGCTCATCGAGAATGAGCTCCTGGGCTTCTTCCGCAGCTCCTATGTGCTCCAC
GGGGAGAGAAGATTCCTTGGTGTTACTCAGTTTTCGCCTACACATGCCAGAAAGGCATTTCCTT
GTTTTGATGAGCCAATCTACAAGGCTACTTTCAAAATCAGCATCAAGCATCAAGCAACCTATTT
ATCTTTATCTAATATGCCAGTGGAAACTTCCGTGTTTGAGGAAGATGGATGGGTTACGGATCAC
TTTTCACAGACCCCTCTCATGTCCACATATTATTTAGCCTGGGCAATTTGCAACTTCACATACA
GAGAAACTACCACCAAGAGTGGGGTTGTAGTACGATTATATGCAAGACCTGATGCTATCAGAAG
AGGATCCGGGGACTATGCTCTCCATATAACAAAGAGATTAATAGAATTTTATGAAGACTACTTT
AAAGTGCCCTATTCCTTGCCAAAACTAGATCTTTTAGCTGTGCCTAAGCATCCGTATGCTGCTA
TGGAGAACTGGGGACTAAGTATTTTTGTGGAACAAAGAATACTGCTGGATCCCAGTGTTTCATC
TATTTCTTATTTGCTGGATGTCACCATGGTCATTGTTCATGAGATATGTCACCAGTGGTTTGGT
GACCTTGTGACGCCTGTGTGGTGGGAAGACGTGTGGCTGAAGGAAGGGTTTGCTCACTACTTTG
AATTTGTTGGTACAGACTACCTCTATCCTGGCTGGAACATGGAAAAGCAGAGGTTTCTGACCGA
TGTTCTGCATGAAGTGATGCTGCTGGACGGTTTGGCCAGTTCCCATCCAGTATCACAGGAAGTG
CTGCAGGCAACAGATATTGACAGGGTGTTTGACTGGATCGCATATAAAAAGGGTGCTGCTTTAA
TAAGAATGCTGGCTAATTTTATGGGCCATTCAGTTTTCCAGAGGGGTTTGCAAGATTATTTAAC
CATTCATAAGTATGGTAATGCAGCCAGAAATGATCTCTGGAATACATTATCGGAGGCTTTAAAA
AGAAATGGGAAATATGTAAATATACAAGAAGTAATGGATCAGTGGACACTCCAGATGGGTTATC
CTGTTATCACCATCTTGGGAAACACAACAGCAGAAAATAGAATAATAATTACCCAACAGCATTT
TATCTATGATATCAGTGCTAAAACTAAAGCACTTAAACTTCAGAATAACAGTTACCTGTGGCAG
ATTCCATTAACTATTGTGGTAGGAAATAGAAGCCATGTGTCTTCAGAAGCAATTATTTGGGTGT
CTAACAAATCAGAGCACCACAGAATAACTTATTTGGACAAAGGAAGCTGGCTGCTGGGGAACAT
CAATCAAACTGGCTATTTTAGAGTCAACTATGACCTAAGGAACTGGAGATTATTAATTGATCAA
TTAATCCGGAATCATGAGGTTCTTTCTGTCAGTAACCGAGCGGGCTTGATCGATGATGCCTTCA
GCCTAGCCAGGGCTGGCTATTTGCCTCAGAATATTCCTCTGGAGATTATCAGATACCTGTCTGA
GGAGAAGGATTTTCTTCCTTGGCATGCTGCCAGCCGAGCTCTTTATCCTCTAGATAAATTACTG
GACCGCATGGAAAACTACAACATTTTCAATGAATATATTTTAAAGCAAGTTGCAACAACATATA
TCAAGCTTGGGTGGCCGAAAAATAATTTTAATGGATCTCTTGTTCAAGCATCCTACCAACATGA
AGAACTACGTAGAGAAGTTATAATGCTGGCCTGCAGTTTTGGCAACAAGCACTGTCACCAACAG
GCATCAACACTTATTTCAGATTGGATTTCCAGCAACAGGAACAGAATACCACTAAATGTTAGAG
ACATCGTATACTGTACAGGAGTGTCACTACTGGATGAGGATGTCTGGGAATTCATATGGATGAA
ATTCCATTCCACCACAGCAGTTTCTGAGAAGAAAATATTATTGGAAGCCTTAACTTGCAGTGAT
GACAGGAATTTATTAAACAGGCTTCTAAATCTGTCACTGAATTCTGAGGTGGTGCTGGATCAAG
ATGCAATTGATGTCATAATCCATGTAGCTCGAAATCCACATGGTCGAGACCTTGCCTGGAAGTT
TTTCAGGGATAAATGGAAGATATTAAATACCAGGTATGGAGAAGCATTGTTTATGAATTCCAAA
CTCATCAGTGGTGTCACAGAATTTCTTAATACTGAAGGTGAACTCAAAGAGCTCAAGAACTTCA
TGAAAAACTATGATGGGGTAGCTGCTGCTTCTTTCTCACGAGCTGTGGAAACTGTCGAAGCCAA
TGTGCGCTGGAAAATGCTTTACCAAGACGAGCTTTTCCAATGGTTAGGAAAAGCTCTAAGACAC
TAA

Appendix VIII. DNA sequencing results of PcpII

Amino acid sequence:

MGEDDAALRAGSRGLSDPWADSVGVRPRTTERHIAVHKRLVLAFAVSLVALLAVTMLAV
LLSLRFDECGASATPGADGGPSGFPERGGNGSLPGSARRNHHAGGDSWQPEAGGVASPG
TTSAQPPSEEEREPWEPWTQLRLSGHLKPLHYNLMLTAFMENFTFSGEVNVEIACRNAT
RYVVLHASRVAVEKVQLAEDRAFGAVPVAGFFLYPQTQVLVVVLNRTLDAQRNYNLKII
YNALIENELLGFFRSSYVLHGERRFLGVTQFSPTHARKAFPCFDEPIYKATFKISIKHQ
ATYLSLSNMPVETSVFEEDGWVTDHFSQTPLMSTYYLAWAICNFTYRETTTKSGVVVRL
YARPDAIRRGSGDYALHITKRLIEFYEDYFKVPYSLPKLDLLAVPKHPYAAMENWGLSI
FVEQRILLDPSVSSISYLLDVTMVIVHEICHQWFGDLVTPVWWEDVWLKEGFAHYFEFV
GTDYLYPGWNMEKQRFLTDVLHEVMLLDGLASSHPVSQEVLQATDIDRVFDWIAYKKGA
ALIRMLANFMGHSVFQRGLQDYLTIHKYGNAARNDLWNTLSEALKRNGKYVNIQEVMDQ
WTLQMGYPVITILGNTTAENRIIITQQHFIYDISAKTKALKLQNNSYLWQIPLTIVVGN
RSHVSSEAIIWVSNKSEHHRITYLDKGSWLLGNINQTGYFRVNYDLRNWRLLIDQLIRN
HEVLSVSNRAGLIDDAFSLARAGYLPQNIPLEIIRYLSEEKDFLPWHAASRALYPLDKL
LDRMENYNIFNEYILKQVATTYIKLGWPKNNFNGSLVQASYQHEELRREVIMLACSFGN
KHCHQQASTLISDWISSNRNRIPLNVRDIVYCTGVSLLDEDVWEFIWMKFHSTTAVSEK
KILLEALTCSDDRNLLNRLLNLSLNSEVVLDQDAIDVIIHVARNPHGRDLAWKFFRDKW
KILNTRYGEALFMNSKLISGVTEFLNTEGELKELKNFMKNYDGVAAASFSRAVETVEAN
VRWKMLYQDELFQWLGKALRH

Appendix IX. DNA sequencing results of PcpII/L141-M541

- the N-terminal His-tag motif is highlighted in green

DNA sequence:

ATGGGCAGCAGC**CATCATCATCATCATCAC**AGCAGCGGCCTGGTGCCGCGCGGCAGCCATCTGT
CGGGCCACCTGAAGCCGCTGCACTACAATCTGATGCTCACCGCCTTCATGGAGAACTTCACCTT
CTCCGGGGAGGTCAACGTGGAGATCGCGTGCCGGAACGCCACCCGCTACGTAGTGCTGCACGCT
TCCCGAGTGGCGGTGGAGAAAGTGCAGCTGGCCGAGGACCGGGCGTTCGGGGCTGTCCCTGTAG
CCGGTTTTTTCCTCTACCCGCAAACCCAGGTCTTAGTGGTGGTGCTGAATAGGACACTGGACGC
GCAGAGGAATTACAATCTGAAGATTATCTACAACGCGCTCATCGAGAATGAGCTCCTGGGCTTC
TTCCGCAGCTCCTATGTGCTCCACGGGGAGAGAAGATTCCTTGGTGTTACTCAGTTTTCGCCTA
CACATGCCAGAAAGGCATTTCCTTGTTTTGATGAGCCAATCTACAAGGCTACTTTCAAAATCAG
CATCAAGCATCAAGCAACCTATTTATCTTTATCTAATATGCCAGTGGAAACTTCCGTGTTTGAG
GAAGATGGATGGGTTACGGATCACTTTTCACAGACCCCTCTCATGTCCACATATTATTTAGCCT
GGGCAATTTGCAACTTCACATACAGAGAAACTACCACCAAGAGTGGGGTTGTAGTACGATTATA
TGCAAGACCTGATGCTATCAGAAGAGGATCCGGGGACTATGCTCTCCATATAACAAAGAGATTA
ATAGAATTTTATGAAGACTACTTTAAAGTGCCCTATTCCTTGCCAAAACTAGATCTTTTAGCTG
TGCCTAAGCATCCGTATGCTGCTATGGAGAACTGGGGACTAAGTATTTTTGTGGAACAAAGAAT
ACTGCTGGATCCCAGTGTTTCATCTATTTCTTATTTGCTGGATGTCACCATGGTCATTGTTCAT
GAGATATGTCACCAGTGGTTTGGTGACCTTGTGACGCCTGTGTGGTGGGAAGACGTGTGGCTGA
AGGAAGGGTTTGCTCACTACTTTGAATTTGTTGGTACAGACTACCTCTATCCTGGCTGGAACAT
GGAAAAGCAGAGGTTTCTGACCGATGTTCTGCATGAAGTGATGCTGCTGGACGGTTTGGCCAGT
TCCCATCCAGTATCACAGGAAGTGCTGCAGGCAACAGATATTGACAGGGTGTTTGACTGGATCG
CATATAAAAAGGGTGCTGCTTTAATAAGAATGCTGGCTAATTTTATGTGA

Amino acid sequence:

MGSS**HHHHHH**SSGLVPRGSHMLSGHLKPLHYNLMLTAFMENFTFSGEVNVEIACRNATR
YVVLHASRVAVEKVQLAEDRAFGAVPVAGFFLYPQTQVLVVVLNRTLDAQRNYNLKIIY
NALIENELLGFFRSSYVLHGERRFLGVTQFSPTHARKAFPCFDEPIYKATFKISIKHQA
TYLSLSNMPVETSVFEEDGWVTDHFSQTPLMSTYYLAWAICNFTYRETTTKSGVVVRLY
ARPDAIRRGSGDYALHITKRLIEFYEDYFKVPYSLPKLDLLAVPKHPYAAMENWGLSIF
VEQRILLDPSVSSISYLLDVTMVIVHEICHQWFGDLVTPVWWEDVWLKEGFAHYFEFVG
TDYLYPGWNMEKQRFLTDVLHEVMLLDGLASSHPVSQEVLQATDIDRVFDWIAYKKGAA
LIRMLANFM

Appendix X. DNA sequencing results of PcpII/S62-G793

- the N-terminal His-tag motif is highlighted in green

DNA sequence:

ATGGGCAGCAGC**CATCATCATCATCATCAC**AGCAGCGGCCTGGTGCCGCGCGGCAGCCATAGCC
TGCGCTTCGACGAGTGCGGGGCGAGTGCCACGCCAGGCGCCGACGGTGGCCCCTCAGGCTTTCC
GGAGCGCGGCGGCAACGGGAGCCTCCCTGGATCGGCCCGGCGCAACCACCACGCAGGCGGGGAC
TCCTGGCAGCCCGAGGCGGGTGGGGTGGCCAGTCCGGGGACCACGTCGGCCCAGCCGCCGTCGG
AGGAGGAGCGGGAGCCGTGGGAGCCGTGGACGCAGCTGCGCCTGTCGGGCCACCTGAAGCCGCT
GCACTACAATCTGATGCTCACCGCCTTCATGGAGAACTTCACCTTCTCCGGGGAGGTCAACGTG
GAGATCGCGTGCCGGAACGCCACCCGCTACGTAGTGCTGCACGCTTCCCGAGTGGCGGTGGAGA
AAGTGCAGCTGGCCGAGGACCGGGCGTTCGGGGCTGTCCCTGTAGCCGGTTTTTTCCTCTACCC
GCAAACCCAGGTCTTAGTGGTGGTGCTGAATAGGACACTGGACGCGCAGAGGAATTACAATCTG
AAGATTATCTACAACGCGCTCATCGAGAATGAGCTCCTGGGCTTCTTCCGCAGCTCCTATGTGC
TCCACGGGGAGAGAAGATTCCTTGGTGTTACTCAGTTTTCGCCTACACATGCCAGAAAGGCATT
TCCTTGTTTTGATGAGCCAATCTACAAGGCTACTTTCAAAATCAGCATCAAGCATCAAGCAACC
TATTTATCTTTATCTAATATGCCAGTGGAAACTTCCGTGTTTGAGGAAGATGGATGGGTTACGG
ATCACTTTTCACAGACCCCTCTCATGTCCACATATTATTTAGCCTGGGCAATTTGCAACTTCAC
ATACAGAGAAACTACCACCAAGAGTGGGGTTGTAGTACGATTATATGCAAGACCTGATGCTATC
AGAAGAGGATCCGGGGACTATGCTCTCCATATAACAAAGAGATTAATAGAATTTTATGAAGACT
ACTTTAAAGTGCCCTATTCCTTGCCAAAACTAGATCTTTTAGCTGTGCCTAAGCATCCGTATGC
TGCTATGGAGAACTGGGGACTAAGTATTTTTGTGGAACAAAGAATACTGCTGGATCCCAGTGTT
TCATCTATTTCTTATTTGCTGGATGTCACCATGGTCATTGTTCATGAGATATGTCACCAGTGGT
TTGGTGACCTTGTGACGCCTGTGTGGTGGGAAGACGTGTGGCTGAAGGAAGGGTTTGCTCACTA
CTTTGAATTTGTTGGTACAGACTACCTCTATCCTGGCTGGAACATGGAAAAGCAGAGGTTTCTG
ACCGATGTTCTGCATGAAGTGATGCTGCTGGACGGTTTGGCCAGTTCCCATCCAGTATCACAGG
AAGTGCTGCAGGCAACAGATATTGACAGGGTGTTTGACTGGATCGCATATAAAAAGGGTGCTGC
TTTAATAAGAATGCTGGCTAATTTTATGGGCCATTCAGTTTTCCAGAGGGGTTTGCAAGATTAT
TTAACCATTCATAAGTATGGTAATGCAGCCAGAAATGATCTCTGGAATACATTATCGGAGGCTT
TAAAAAGAAATGGGAAATATGTAAATATACAAGAAGTAATGGATCAGTGGACACTCCAGATGGG
TTATCCTGTTATCACCATCTTGGGAAACACAACAGCAGAAAATAGAATAATAATTACCCAACAG
CATTTTATCTATGATATCAGTGCTAAAACTAAAGCACTTAAACTTCAGAATAACAGTTACCTGT
GGCAGATTCCATTAACTATTGTGGTAGGAAATAGAAGCCATGTGTCTTCAGAAGCAATTATTTG
GGTGTCTAACAAATCAGAGCACCACAGAATAACTTATTTGGACAAAGGAAGCTGGCTGCTGGGG
AACATCAATCAAACTGGCTATTTTAGAGTCAACTATGACCTAAGGAACTGGAGATTATTAATTG
ATCAATTAATCCGGAATCATGAGGTTCTTTCTGTCAGTAACCGAGCGGGCTTGATCGATGATGC
CTTCAGCCTAGCCAGGGCTGGCTATTTGCCTCAGAATATTCCTCTGGAGATTATCAGATACCTG
TCTGAGGAGAAGGATTTTCTTCCTTGGCATGCTGCCAGCCGAGCTCTTTATCCTCTAGATAAAT
TACTGGACCGCATGGAAAACTACAACATTTTCAATGAATATATTTTAAAGCAAGTTGCAACAAC
ATATATCAAGCTTGGGTAA

Appendix X. DNA sequencing results of PcpII/S62-G793

Amino acid sequence:

MGSS**HHHHHH**SSGLVPRGSHMSLRFDECGASATPGADGGPSGFPERGGNGSLPGSARRN
HHAGGDSWQPEAGGVASPGTTSAQPPSEEEREPWEPWTQLRLSGHLKPLHYNLMLTAFM
ENFTFSGEVNVEIACRNATRYVVLHASRVAVEKVQLAEDRAFGAVPVAGFFLYPQTQVL
VVVLNRTLDAQRNYNLKIIYNALIENELLGFFRSSYVLHGERRFLGVTQFSPTHARKAF
PCFDEPIYKATFKISIKHQATYLSLSNMPVETSVFEEDGWVTDHFSQTPLMSTYYLAWA
ICNFTYRETTTKSGVVVRLYARPDAIRRGSGDYALHITKRLIEFYEDYFKVPYSLPKLD
LLAVPKHPYAAMENWGLSIFVEQRILLDPSVSSISYLLDVTMVIVHEICHQWFGDLVTP
VWWEDVWLKEGFAHYFEFVGTDYLYPGWNMEKQRFLTDVLHEVMLLDGLASSHPVSQEV
LQATDIDRVFDWIAYKKGAALIRMLANFMGHSVFQRGLQDYLTIHKYGNAARNDLWNTL
SEALKRNGKYVNIQEVMDQWTLQMGYPVITILGNTTAENRIIITQQHFIYDISAKTKAL
KLQNNSYLWQIPLTIVVGNRSHVSSEAIIWVSNKSEHHRITYLDKGSWLLGNINQTGYF
RVNYDLRNWRLLIDQLIRNHEVLSVSNRAGLIDDAFSLARAGYLPQNIPLEIIRYLSEE
KDFLPWHAASRALYPLDKLLDRMENYNIFNEYILKQVATTYIKLG

Appendix XI. DNA sequencing results of PcpII/L141-H1024

- the N-terminal His-tag motif is highlighted in green

DNA sequence:

ATGGGCAGCAGC**CATCATCATCATCATCAC**AGCAGCGGCCTGGTGCCGCGCGGCAGCCATCTGT
CGGGCCACCTGAAGCCGCTGCACTACAATCTGATGCTCACCGCCTTCATGGAGAACTTCACCTT
CTCCGGGGAGGTCAACGTGGAGATCGCGTGCCGGAACGCCACCCGCTACGTAGTGCTGCACGCT
TCCCGAGTGGCGGTGGAGAAAGTGCAGCTGGCCGAGGACCGGGCGTTCGGGGCTGTCCCTGTAG
CCGGTTTTTTCCTCTACCCGCAAACCCAGGTCTTAGTGGTGGTGCTGAATAGGACACTGGACGC
GCAGAGGAATTACAATCTGAAGATTATCTACAACGCGCTCATCGAGAATGAGCTCCTGGGCTTC
TTCCGCAGCTCCTATGTGCTCCACGGGGAGAGAAGATTCCTTGGTGTTACTCAGTTTTCGCCTA
CACATGCCAGAAAGGCATTTCCTTGTTTTGATGAGCCAATCTACAAGGCTACTTTCAAAATCAG
CATCAAGCATCAAGCAACCTATTTATCTTTATCTAATATGCCAGTGGAAACTTCCGTGTTTGAG
GAAGATGGATGGGTTACGGATCACTTTTCACAGACCCCTCTCATGTCCACATATTATTTAGCCT
GGGCAATTTGCAACTTCACATACAGAGAAACTACCACCAAGAGTGGGGTTGTAGTACGATTATA
TGCAAGACCTGATGCTATCAGAAGAGGATCCGGGGACTATGCTCTCCATATAACAAAGAGATTA
ATAGAATTTTATGAAGACTACTTTAAAGTGCCCTATTCCTTGCCAAAACTAGATCTTTTAGCTG
TGCCTAAGCATCCGTATGCTGCTATGGAGAACTGGGGACTAAGTATTTTTGTGGAACAAAGAAT
ACTGCTGGATCCCAGTGTTTCATCTATTTCTTATTTGCTGGATGTCACCATGGTCATTGTTCAT
GAGATATGTCACCAGTGGTTTGGTGACCTTGTGACGCCTGTGTGGTGGGAAGACGTGTGGCTGA
AGGAAGGGTTTGCTCACTACTTTGAATTTGTTGGTACAGACTACCTCTATCCTGGCTGGAACAT
GGAAAAGCAGAGGTTTCTGACCGATGTTCTGCATGAAGTGATGCTGCTGGACGGTTTGGCCAGT
TCCCATCCAGTATCACAGGAAGTGCTGCAGGCAACAGATATTGACAGGGTGTTTGACTGGATCG
CATATAAAAAGGGTGCTGCTTTAATAAGAATGCTGGCTAATTTTATGGGCCATTCAGTTTTCCA
GAGGGGTTTGCAAGATTATTTAACCATTCATAAGTATGGTAATGCAGCCAGAAATGATCTCTGG
AATACATTATCGGAGGCTTTAAAAAGAAATGGGAAATATGTAAATATACAAGAAGTAATGGATC
AGTGGACACTCCAGATGGGTTATCCTGTTATCACCATCTTGGGAAACACAACAGCAGAAAATAG
AATAATAATTACCCAACAGCATTTTATCTATGATATCAGTGCTAAAACTAAAGCACTTAAACTT
CAGAATAACAGTTACCTGTGGCAGATTCCATTAACTATTGTGGTAGGAAATAGAAGCCATGTGT
CTTCAGAAGCAATTATTTGGGTGTCTAACAAATCAGAGCACCACAGAATAACTTATTTGGACAA
AGGAAGCTGGCTGCTGGGGAACATCAATCAAACTGGCTATTTTAGAGTCAACTATGACCTAAGG
AACTGGAGATTATTAATTGATCAATTAATCCGGAATCATGAGGTTCTTTCTGTCAGTAACCGAG
CGGGCTTGATCGATGATGCCTTCAGCCTAGCCAGGGCTGGCTATTTGCCTCAGAATATTCCTCT
GGAGATTATCAGATACCTGTCTGAGGAGAAGGATTTTCTTCCTTGGCATGCTGCCAGCCGAGCT
CTTTATCCTCTAGATAAATTACTGGACCGCATGGAAAACTACAACATTTTCAATGAATATATTT
TAAAGCAAGTTGCAACAACATATATCAAGCTTGGGTGGCCGAAAAATAATTTTAATGGATCTCT
TGTTCAAGCATCCTACCAACATGAAGAACTACGTAGAGAAGTTATAATGCTGGCCTGCAGTTTT
GGCAACAAGCACTGTCACCAACAGGCATCAACACTTATTTCAGATTGGATTTCCAGCAACAGGA
ACAGAATACCACTAAATGTTAGAGACATCGTATACTGTACAGGAGTGTCACTACTGGATGAGGA
TGTCTGGGAATTCATATGGATGAAATTCCATTCCACCACAGCAGTTTCTGAGAAGAAAATATTA
TTGGAAGCCTTAACTTGCAGTGATGACAGGAATTTATTAAACAGGCTTCTAAATCTGTCACTGA
ATTCTGAGGTGGTGCTGGATCAAGATGCAATTGATGTCATAATCCATGTAGCTCGAAATCCACA
TGGTCGAGACCTTGCCTGGAAGTTTTTCAGGGATAAATGGAAGATATTAAATACCAGGTATGGA
GAAGCATTGTTTATGAATTCCAAACTCATCAGTGGTGTCACAGAATTTCTTAATACTGAAGGTG
AACTCAAAGAGCTCAAGAACTTCATGAAAAACTATGATGGGGTAGCTGCTGCTTCTTTCTCACG
AGCTGTGGAAACTGTCGAAGCCAATGTGCGCTGGAAAATGCTTTACCAAGACGAGCTTTTCCAA
TGGTTAGGAAAAGCTCTAAGACACTAA

Appendix XI. DNA sequencing results of PcpII/L141-H1024

Amino acid sequence:

MGSS**HHHHHH**SSGLVPRGSHMASLSGHLKPLHYNLMLTAFMENFTFSGEVNVEIACRNA
TRYVVLHASRVAVEKVQLAEDRAFGAVPVAGFFLYPQTQVLVVVLNRTLDAQRNYNLKI
IYNALIENELLGFFRSSYVLHGERRFLGVTQFSPTHARKAFPCFDEPIYKATFKISIKH
QATYLSLSNMPVETSVFEEDGWVTDHFSQTPLMSTYYLAWAICNFTYRETTTKSGVVVR
LYARPDAIRRGSGDYALHITKRLIEFYEDYFKVPYSLPKLDLLAVPKHPYAAMENWGLS
IFVEQRILLDPSVSSISYLLDVTMVIVHEICHQWFGDLVTPVWWEDVWLKEGFAHYFEF
VGTDYLYPGWNMEKQRFLTDVLHEVMLLDGLASSHPVSQEVLQATDIDRVFDWIAYKKG
AALIRMLANFMGHSVFQRGLQDYLTIHKYGNAARNDLWNTLSEALKRNGKYVNIQEVMD
QWTLQMGYPVITILGNTTAENRIIITQQHFIYDISAKTKALKLQNNSYLWQIPLTIVVG
NRSHVSSEAIIWVSNKSEHHRITYLDKGSWLLGNINQTGYFRVNYDLRNWRLLIDQLIR
NHEVLSVSNRAGLIDDAFSLARAGYLPQNIPLEIIRYLSEEKDFLPWHAASRALYPLDK
LLDRMENYNIFNEYILKQVATTYIKLGWPKNNFNGSLVQASYQHEELRREVIMLACSFG
NKHCHQQASTLISDWISSNRNRIPLNVRDIVYCTGVSLLDEDVWEFIWMKFHSTTAVSE
KKILLEALTCSDDRNLLNRLLNLSLNSEVVLDQDAIDVIIHVARNPHGRDLAWKFFRDK
WKILNTRYGEALFMNSKLISGVTEFLNTEGELKELKNFMKNYDGVAAASFSRAVETVEA
NVRWKMLYQDELFQWLGKALRH

Appendix XII. List of pOPIN-based constructs and corresponding forward and reverse primer extensions for the In-Fusion™ cloning.

Vector	PCR insert	Forward primer extension	Reverse primer extension
pOPINE	PcpII/S62-H1024	AGGAGATATACCATG	GTGATGGTGATGTTT
pOPINE	PcpII/L141-H1024	AGGAGATATACCATG	GTGATGGTGATGTTT
pOPINF	PcpII	AAGTTCTGTTTCAGGGCCCG	ATGGTCTAGAAAGCTTTA
pOPINF	PcpII/S62-H1024	AAGTTCTGTTTCAGGGCCCG	ATGGTCTAGAAAGCTTTA
pOPINF	PcpII/L141-H1024	AAGTTCTGTTTCAGGGCCCG	ATGGTCTAGAAAGCTTTA
pOPING	PcpII/S62-H1024	GCGTAGCTGAAACCGGC	GTGATGGTGATGTTT
pOPING	PcpII/L141-H1024	GCGTAGCTGAAACCGGC	GTGATGGTGATGTTT
pOPINH	PcpII/S62-H1024	AAGTTCTGTTTCAGGGCCCG	ATGGTCTAGAAAGCTTTA
pOPINH	PcpII/L141-H1024	AAGTTCTGTTTCAGGGCCCG	ATGGTCTAGAAAGCTTTA
pOPINI	PcpII	ACCATCACAGCAGCGGC	ATGGTCTAGAAAGCTTTA
pOPINTTG	PcpII/S62-H1024	AAGTTCTGTTTCAGGGCCCG	ATGGTCTAGAAAGCTTTA
pOPINTTG	PcpII/L141-H1024	AAGTTCTGTTTCAGGGCCCG	ATGGTCTAGAAAGCTTTA
pOPINTTGNeo-3C-GFP-His	PcpII/S62-H1024	AAGTTCTGTTTCAGGGCCCG	ATGGTCTAGAAAGCTTTA
pOPINTTGNeo-3C-Halo7-His	PcpII/S62-H1024	AAGTTCTGTTTCAGGGCCCG	ATGGTCTAGAAAGCTTTA
pOPINTTGNeo-3C-CD4-His	PcpII/S62-H1024	GCGAACAGATCGGTGGT	ATGGTCTAGAAAGCTTTA
pOPINE-3C-GFP-His	PcpII/S62-H1024	AAGTTCTGTTTCAGGGCCCG	ATGGTCTAGAAAGCTTTA
pOPINE-3C-GFP-His	PcpII/L141-H1024	AAGTTCTGTTTCAGGGCCCG	ATGGTCTAGAAAGCTTTA
pOPINE-3C-Halo7-His	PcpII/S62-H1024	AGGAGATATACCATG	GTGATGGTGATGTT
pOPINE-3C-Halo7-His	PcpII/L141-H1024	AGGAGATATACCATG	GTGATGGTGATGTTT

Appendix XIII. A Ramachandran plot of the human PcpII model.

The plot was generated in RAMPAGE Ramachandran Plot server (Lovell *et al.*, 2003).

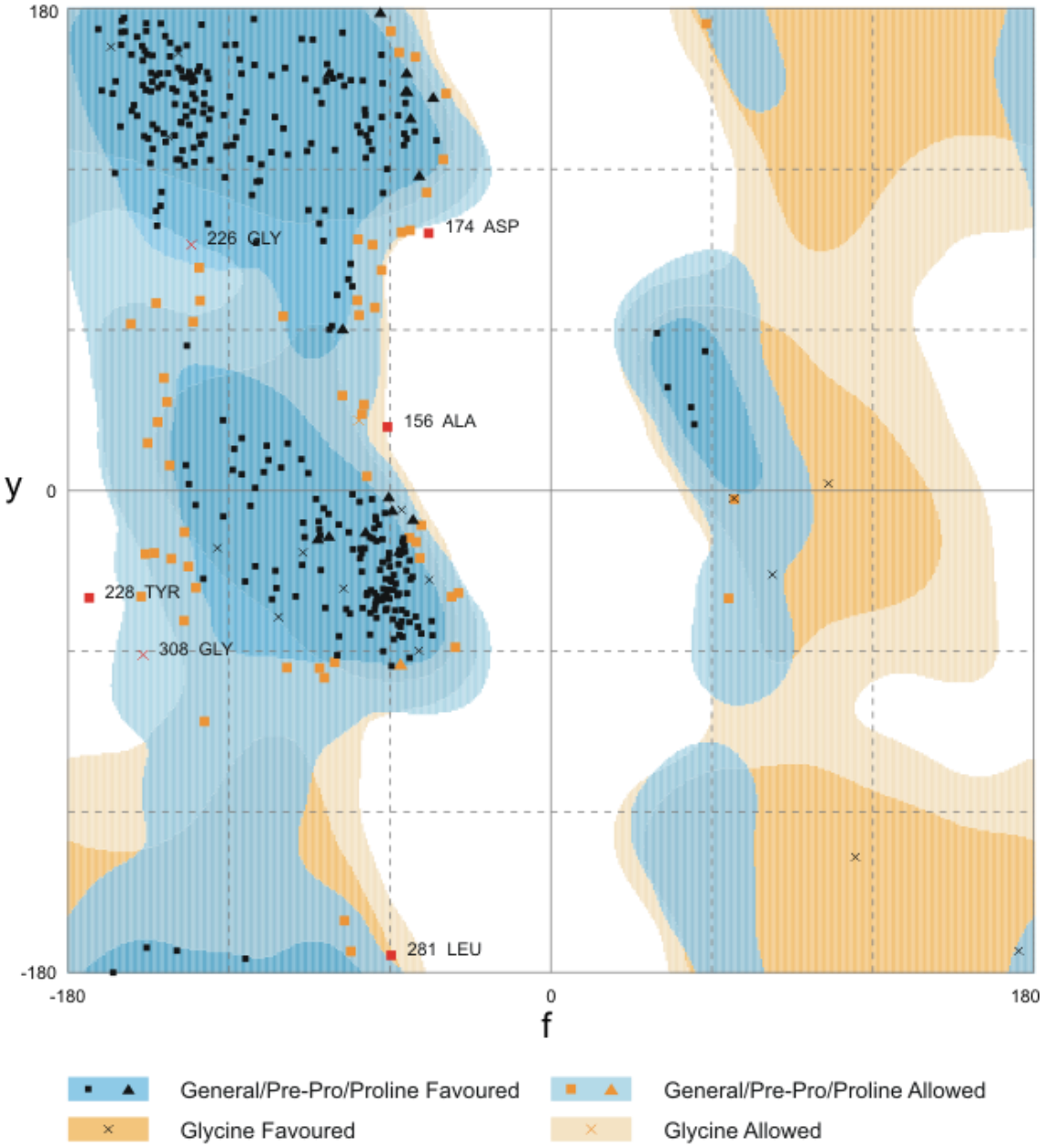

Number of residues in favoured region (~98.0% expected)	: 337 (84.5%)
Number of residues in allowed region (~2.0% expected)	: 56 (14.0%)
Number of residues in outlier region	: 6 (1.5%)

References

Abe, K., Fukuda, K., Tokui, T., 2004. Marginal involvement of pyroglutamyl aminopeptidase I in metabolism of thyrotropin-releasing hormone in rat brain. Biol Pharm Bull 27, 1197-1201.

Abe, K., Watanabe, N., Kosaka, T., Yamada, M., Tokui, T., Ikeda, T., 2003. Hydrolysis of synthetic substrate, L-pyroglutamyl p-nitroanilide is catalyzed solely by pyroglutamyl aminopeptidase I in rat liver cytosol. Biol Pharm Bull 26, 1528-1533.

Addlagatta, A., Gay, L., Matthews, B.W., 2006. Structure of aminopeptidase N from *Escherichia coli* suggests a compartmentalized, gated active site. Proc Natl Acad Sci U S A 103, 13339-13344.

ADI, 2010. World Alzheimer Report 2010. The global economic impact of dementia In: Wimo, A., Prince, M. (Eds.), World Alzheimer Report. Alzheimer's Disease International (ADI).

Albert, Z., Szewczuk, A., 1972. Pyrrolidonyl peptidase in some avian and rodent tissues. Histochemical localization and biochemical studies. Acta Histochem 44, 98-105.

Alonso, A.D., Grundke-Iqbal, I., Barra, H.S., Iqbal, K., 1997. Abnormal phosphorylation of tau and the mechanism of Alzheimer neurofibrillary degeneration: sequestration of microtubule-associated proteins 1 and 2 and the disassembly of microtubules by the abnormal tau. Proc Natl Acad Sci U S A 94, 298-303.

Alzheimer's Association, 2010. Alzheimer's Disease Facts and Figures. A Special Report on Race, Ethnicity and Alzheimer's Disease. Alzheimer's & Dementia 6.

Alzheimer, A., 1907. Uber eine eigenartige Erkankung der Hirnrinde (On an Unusual Illness of the Cerebral Cortex). Allgemeine Zeitschrift fur Psychiatrie und phychish-Gerichtliche Medizin 64, 146-148.

Anastasi, A., Erspamer, V., 1963. The isolation and amino acid sequence of eledoisin, the active endecapeptide of the posterior salivary glands of Eledone. Arch Biochem Biophys 101, 56-65.

Anastasi, A., Erspamer, V., Cei, J.M., 1964. Isolation and Amino Acid Sequence of Physalaemin, the Main Active Polypeptide of the Skin of Physalaemus Fuscumaculatus. Arch Biochem Biophys 108, 341-348.

Armentrout, R.W., Doolittle, R.F., 1969. Pyrrolidonecarboxylyl peptidase: stabilization and purification. Arch Biochem Biophys 132, 80-90.

Armstrong, R.A., Myers, D., Smith, C.U., 1991. Alzheimer's disease: size class frequency distribution of senile plaques: do they indicate when a brain tissue was affected? Neurosci Lett 127, 223-226.

Arnold, U., Schulenburg, C., Schmidt, D., Ulbrich-Hofmann, R., 2006. Contribution of structural peculiarities of onconase to its high stability and folding kinetics. Biochemistry 45, 3580-3587.

Asai, M., Iwata, N., Tomita, T., Iwatsubo, T., Ishiura, S., Saido, T.C., Maruyama, K., 2010. Efficient four-drug cocktail therapy targeting amyloid-beta peptide for Alzheimer's disease. J Neurosci Res 88, 3588-3597.

Awade, A., Cleuziat, P., Gonzales, T., Robert-Baudouy, J., 1992a. Characterization of the pcp gene encoding the pyrrolidone carboxyl peptidase of *Bacillus subtilis*. FEBS Lett 305, 67-73.

Awade, A., Gonzales, T., Cleuziat, P., Robert-Baudouy, J., 1992b. One step purification and characterization of the pyrrolidone carboxyl peptidase of *Streptococcus pyogenes* over-expressed in Escherichia coli. FEBS Lett 308, 70-74.

Awade, A.C., Cleuziat, P., Gonzales, T., Robert-Baudouy, J., 1994. Pyrrolidone carboxyl peptidase (Pcp): an enzyme that removes pyroglutamic acid (pGlu) from pGlu-peptides and pGlu-proteins. Proteins 20, 34-51.

Bachmann, C., Boulat, O., Meyrat, B.J., Colombo, J.P., Pilloud, P., 1994. Pitfalls in aminoacid and organic acid analysis: 3-hydroxypropionic aciduria. Eur J Pediatr 153, S23-26.

Balbach, J.J., Petkova, A.T., Oyler, N.A., Antzutkin, O.N., Gordon, D.J., Meredith, S.C., Tycko, R., 2002. Supramolecular structure in full-length Alzheimer's beta-amyloid fibrils: evidence for a parallel beta-sheet organization from solid-state nuclear magnetic resonance. Biophys J 83, 1205-1216.

Bancher, C., Brunner, C., Lassmann, H., Budka, H., Jellinger, K., Wiche, G., Seitelberger, F., Grundke-Iqbal, I., Iqbal, K., Wisniewski, H.M., 1989. Accumulation of abnormally phosphorylated tau precedes the formation of neurofibrillary tangles in Alzheimer's disease. Brain Res 477, 90-99.

Barnham, K.J., Kenche, V.B., Ciccotosto, G.D., Smith, D.P., Tew, D.J., Liu, X., Perez, K., Cranston, G.A., Johanssen, T.J., Volitakis, I., Bush, A.I., Masters, C.L., White, A.R., Smith, J.P., Cherny, R.A., Cappai, R., 2008. Platinum-based inhibitors of amyloid-beta as therapeutic agents for Alzheimer's disease. Proc Natl Acad Sci U S A 105, 6813-6818.

Barnham, K.J., McKinstry, W.J., Multhaup, G., Galatis, D., Morton, C.J., Curtain, C.C., Williamson, N.A., White, A.R., Hinds, M.G., Norton, R.S., Beyreuther, K., Masters, C.L., Parker, M.W., Cappai, R., 2003. Structure of the Alzheimer's disease amyloid precursor protein copper binding domain. A regulator of neuronal copper homeostasis. J Biol Chem 278, 17401-17407.

Barrett, A.J., McDonald, J.K., 1986. Mammalian proteases : a glossary and bibliography. Vol.2, Exopeptidases. Academic, London.

Barrett, A.J., Rawlings, N.D., Woessner, J.F., 1998. Handbook of proteolytic enzymes. Academic Press, San Diego ; London.

Battistoni, A., Carri, M.T., Mazzetti, A.P., Rotilio, G., 1992. Temperature-dependent protein folding in vivo--lower growth temperature increases yield of two genetic

variants of *Xenopus laevis* Cu,Zn superoxide dismutase in Escherichia coli. Biochem Biophys Res Commun 186, 1339-1344.

Bauer, K., 1987. Adenohypophyseal degradation of thyrotropin releasing hormone regulated by thyroid hormones. Nature 330, 375-377.

Bauer, K., 1988. Degradation and biological inactivation of thyrotropin releasing hormone (TRH): regulation of the membrane-bound TRH-degrading enzyme from rat anterior pituitary by estrogens and thyroid hormones. Biochimie 70, 69-74.

Bauer, K., 1994. Purification and characterization of the thyrotropin-releasing-hormone-degrading ectoenzyme. Eur J Biochem 224, 387-396.

Bauer, K., Carmeliet, P., Schulz, M., Baes, M., Denef, C., 1990. Regulation and cellular localization of the membrane-bound thyrotropin-releasing hormone-degrading enzyme in primary cultures of neuronal, glial and adenohypophyseal cells. Endocrinology 127, 1224-1233.

Bauer, K., Kleinkauf, H., 1980. Catabolism of thyroliberin by rat adenohypophyseal tissue extract. Eur J Biochem 106, 107-117.

Bauer, K., Nowak, P., Kleinkauf, H., 1981. Specificity of a serum peptidase hydrolyzing thyroliberin at pyroglutamyl-histidine bone. Eur J Biochem 118, 173-176.

Bauvois, C., Jacquamet, L., Huston, A.L., Borel, F., Feller, G., Ferrer, J.L., 2008. Crystal structure of the cold-active aminopeptidase from *Colwellia psychrerythraea*, a close structural homologue of the human bifunctional leukotriene A4 hydrolase. J Biol Chem 283, 23315-23325.

Behl, M., Zhang, Y., Zheng, W., 2009. Involvement of insulin-degrading enzyme in the clearance of beta-amyloid at the blood-CSF barrier: Consequences of lead exposure. Cerebrospinal Fluid Res 6, 11.

Bennett, B.D., Babu-Khan, S., Loeloff, R., Louis, J.C., Curran, E., Citron, M., Vassar, R., 2000. Expression analysis of BACE2 in brain and peripheral tissues. J Biol Chem 275, 20647-20651.

Berg, J.M., 1990. Zinc fingers and other metal-binding domains. Elements for interactions between macromolecules. J Biol Chem 265, 6513-6516.

Berger, I., Fitzgerald, D.J., Richmond, T.J., 2004. Baculovirus expression system for heterologous multiprotein complexes. Nat Biotechnol 22, 1583-1587.

Berrow, N.S., Alderton, D., Owens, R.J., 2009. The precise engineering of expression vectors using high-throughput In-Fusion PCR cloning. Methods Mol Biol 498, 75-90.

Berrow, N.S., Alderton, D., Sainsbury, S., Nettleship, J., Assenberg, R., Rahman, N., Stuart, D.I., Owens, R.J., 2007. A versatile ligation-independent cloning method suitable for high-throughput expression screening applications. Nucleic Acids Res 35, e45.

Bickeboller, H., Campion, D., Brice, A., Amouyel, P., Hannequin, D., Didierjean, O., Penet, C., Martin, C., Perez-Tur, J., Michon, A., Dubois, B., Ledoze, F., Thomas-Anterion, C., Pasquier, F., Puel, M., Demonet, J.F., Moreaud, O., Babron, M.C.,

Meulien, D., Guez, D., Chartier-Harlin, M.C., Frebourg, T., Agid, Y., Martinez, M., Clerget-Darpoux, F., 1997. Apolipoprotein E and Alzheimer disease: genotype-specific risks by age and sex. Am J Hum Genet 60, 439-446.

Bird, T.D., 2008. Genetic aspects of Alzheimer disease. Genet Med 10, 231-239.

Birks, J., 2006. Cholinesterase inhibitors for Alzheimer's disease. Cochrane Database Syst Rev, CD005593.

Blake, C.C., Ghosh, M., Harlos, K., Avezoux, A., Anthony, C., 1994. The active site of methanol dehydrogenase contains a disulphide bridge between adjacent cysteine residues. Nat Struct Biol 1, 102-105.

Blennow, K., de Leon, M.J., Zetterberg, H., 2006. Alzheimer's disease. Lancet 368, 387-403.

Blocq, P., Marinesco, G., 1892. Sur les lésions et la pathogénie de l'épilepsie dite essentielle. La Semaine Medicale 12, 445-446.

Bohme, L., Bar, J.W., Hoffmann, T., Manhart, S., Ludwig, H.H., Rosche, F., Demuth, H.U., 2008. Isoaspartate residues dramatically influence substrate recognition and turnover by proteases. Biol Chem 389, 1043-1053.

Borchelt, D.R., Thinakaran, G., Eckman, C.B., Lee, M.K., Davenport, F., Ratovitsky, T., Prada, C.M., Kim, G., Seekins, S., Yager, D., Slunt, H.H., Wang, R., Seeger, M., Levey, A.I., Gandy, S.E., Copeland, N.G., Jenkins, N.A., Price, D.L., Younkin, S.G., Sisodia, S.S., 1996. Familial Alzheimer's disease-linked presenilin 1 variants elevate Abeta1-42/1-40 ratio in vitro and in vivo. Neuron 17, 1005-1013.

Bordji, K., Becerril-Ortega, J., Nicole, O., Buisson, A., 2010. Activation of extrasynaptic, but not synaptic, NMDA receptors modifies amyloid precursor protein expression pattern and increases amyloid-ss production. J Neurosci 30, 15927-15942.

Boyett, K.W., DiCarlo, G., Jantzen, P.T., Jackson, J., O'Leary, C., Wilcock, D., Morgan, D., Gordon, M.N., 2003. Increased fibrillar beta-amyloid in response to human clq injections into hippocampus and cortex of APP+PS1 transgenic mice. Neurochem Res 28, 83-93.

Braak, H., Braak, E., 1991. Neuropathological stageing of Alzheimer-related changes. Acta Neuropathol 82, 239-259.

Braak, H., Braak, E., 1997. Frequency of stages of Alzheimer-related lesions in different age categories. Neurobiol Aging 18, 351-357.

Bradford, M.M., 1976. A rapid and sensitive method for the quantitation of microgram quantities of protein utilizing the principle of protein-dye binding. Anal Biochem 72, 248-254.

Browne, P., O'Cuinn, G., 1983. An evaluation of the role of a pyroglutamyl peptidase, a post-proline cleaving enzyme and a post-proline dipeptidyl amino peptidase, each purified from the soluble fraction of guinea-pig brain, in the degradation of thyroliberin in vitro. Eur J Biochem 137, 75-87.

Budimir, A., 2011. Metal ions, Alzheimer's disease and chelation therapy. Acta Pharm 61, 1-14.

Burdick, D., Soreghan, B., Kwon, M., Kosmoski, J., Knauer, M., Henschen, A., Yates, J., Cotman, C., Glabe, C., 1992. Assembly and aggregation properties of synthetic Alzheimer's A4/beta amyloid peptide analogs. J Biol Chem 267, 546-554.

Bush, A.I., Pettingell, W.H., Multhaup, G., d Paradis, M., Vonsattel, J.P., Gusella, J.F., Beyreuther, K., Masters, C.L., Tanzi, R.E., 1994. Rapid induction of Alzheimer A beta amyloid formation by zinc. Science 265, 1464-1467.

Butterfield, D.A., Boyd-Kimball, D., 2004. Amyloid beta-peptide(1-42) contributes to the oxidative stress and neurodegeneration found in Alzheimer disease brain. Brain Pathol 14, 426-432.

Buxbaum, J.D., Liu, K.N., Luo, Y., Slack, J.L., Stocking, K.L., Peschon, J.J., Johnson, R.S., Castner, B.J., Cerretti, D.P., Black, R.A., 1998. Evidence that tumor necrosis factor alpha converting enzyme is involved in regulated alpha-secretase cleavage of the Alzheimer amyloid protein precursor. J Biol Chem 273, 27765-27767.

Cai, H., Wang, Y., McCarthy, D., Wen, H., Borchelt, D.R., Price, D.L., Wong, P.C., 2001. BACE1 is the major beta-secretase for generation of Abeta peptides by neurons. Nat Neurosci 4, 233-234.

Caille, I., Allinquant, B., Dupont, E., Bouillot, C., Langer, A., Muller, U., Prochiantz, A., 2004. Soluble form of amyloid precursor protein regulates proliferation of progenitors in the adult subventricular zone. Development 131, 2173-2181.

Capecchi, J.T., Loudon, G.M., 1985. Substrate specificity of pyroglutamylaminopeptidase. J Med Chem 28, 140-143.

Caporaso, G.L., Takei, K., Gandy, S.E., Matteoli, M., Mundigl, O., Greengard, P., De Camilli, P., 1994. Morphologic and biochemical analysis of the intracellular trafficking of the Alzheimer beta/A4 amyloid precursor protein. J Neurosci 14, 3122-3138.

Carmichael, O.T., Kuller, L.H., Lopez, O.L., Thompson, P.M., Dutton, R.A., Lu, A., Lee, S.E., Lee, J.Y., Aizenstein, H.J., Meltzer, C.C., Liu, Y., Toga, A.W., Becker, J.T., 2007. Ventricular volume and dementia progression in the Cardiovascular Health Study. Neurobiol Aging 28, 389-397.

Carrera, M.P., Ramirez-Exposito, M.J., Valenzuela, M.T., Garcia, M.J., Mayas, M.D., Arias de Saavedra, J.M., Sanchez, R., Perez, M.C., Martinez-Martos, J.M., 2005. Pyrrolidon carboxypeptidase activities in the hypothalamus-pituitary-thyroid and hypothalamus-pituitary-ovary axes of rats with mammary gland cancer induced by N-methyl nitrosourea. Horm Metab Res 37, 74-78.

Carugo, O., Cemazar, M., Zahariev, S., Hudaky, I., Gaspari, Z., Perczel, A., Pongor, S., 2003. Vicinal disulfide turns. Protein Eng 16, 637-639.

Casas, C., Sergeant, N., Itier, J.M., Blanchard, V., Wirths, O., van der Kolk, N., Vingtdeux, V., van de Steeg, E., Ret, G., Canton, T., Drobecq, H., Clark, A., Bonici, B., Delacourte, A., Benavides, J., Schmitz, C., Tremp, G., Bayer, T.A., Benoit, P., Pradier, L., 2004. Massive CA1/2 neuronal loss with intraneuronal and N-terminal truncated

Abeta42 accumulation in a novel Alzheimer transgenic model. Am J Pathol 165, 1289-1300.

Castano, E.M., Prelli, F., Wisniewski, T., Golabek, A., Kumar, R.A., Soto, C., Frangione, B., 1995. Fibrillogenesis in Alzheimer's disease of amyloid beta peptides and apolipoprotein E. Biochem J 306 (Pt 2), 599-604.

Casteels, P., Ampe, C., Jacobs, F., Tempst, P., 1993. Functional and chemical characterization of Hymenoptaecin, an antibacterial polypeptide that is infection-inducible in the honeybee (*Apis mellifera*). J Biol Chem 268, 7044-7054.

Castellano, J.M., Kim, J., Stewart, F.R., Jiang, H., DeMattos, R.B., Patterson, B.W., Fagan, A.M., Morris, J.C., Mawuenyega, K.G., Cruchaga, C., Goate, A.M., Bales, K.R., Paul, S.M., Bateman, R.J., Holtzman, D.M., 2011. Human apoE Isoforms Differentially Regulate Brain Amyloid-β Peptide Clearance. Science Translational Medicine 3, 89ra57.

Cemazar, M., Zahariev, S., Lopez, J.J., Carugo, O., Jones, J.A., Hore, P.J., Pongor, S., 2003. Oxidative folding intermediates with nonnative disulfide bridges between adjacent cysteine residues. Proc Natl Acad Sci U S A 100, 5754-5759.

Cetin, F., Dincer, S., 2007. The effect of intrahippocampal beta amyloid (1-42) peptide injection on oxidant and antioxidant status in rat brain. Ann N Y Acad Sci 1100, 510-517.

Charli, J.L., Mendez, M., Joseph-Bravo, P., Wilk, S., 1987. Specific inhibitors of pyroglutamyl peptidase I and prolyl endopeptidase do not change the in vitro release of TRH or its content in rodent brain. Neuropeptides 9, 373-378.

Chavez-Gutierrez, L., Bourdais, J., Aranda, G., Vargas, M.A., Matta-Camacho, E., Ducancel, F., Segovia, L., Joseph-Bravo, P., Charli, J.L., 2005. A truncated isoform of pyroglutamyl aminopeptidase II produced by exon extension has dominant-negative activity. J Neurochem 92, 807-817.

Chavez-Gutierrez, L., Matta-Camacho, E., Osuna, J., Horjales, E., Joseph-Bravo, P., Maigret, B., Charli, J.L., 2006. Homology modeling and site-directed mutagenesis of pyroglutamyl peptidase II. Insights into omega-versus aminopeptidase specificity in the M1 family. J Biol Chem 281, 18581-18590.

Chayen, N.E., 1997. The role of oil in macromolecular crystallization. Structure 5, 1269-1274.

Chayen, N.E., 1998. Comparative studies of protein crystallization by vapour-diffusion and microbatch techniques. Acta Crystallogr D Biol Crystallogr 54, 8-15.

Chayen, N.E., Saridakis, E., 2008. Protein crystallization: from purified protein to diffraction-quality crystal. Nat Methods 5, 147-153.

Chen, W.T., Liao, Y.H., Yu, H.M., Cheng, I.H., Chen, Y.R., 2011. Distinct effects of Zn2+, Cu2+, Fe3+, and Al3+ on amyloid-beta stability, oligomerization, and aggregation: amyloid-beta destabilization promotes annular protofibril formation. J Biol Chem 286, 9646-9656.

Chen, Y.Z., 2004. APP induces neuronal apoptosis through APP-BP1-mediated downregulation of beta-catenin. Apoptosis 9, 415-422.

Cherny, R.A., Atwood, C.S., Xilinas, M.E., Gray, D.N., Jones, W.D., McLean, C.A., Barnham, K.J., Volitakis, I., Fraser, F.W., Kim, Y., Huang, X., Goldstein, L.E., Moir, R.D., Lim, J.T., Beyreuther, K., Zheng, H., Tanzi, R.E., Masters, C.L., Bush, A.I., 2001. Treatment with a copper-zinc chelator markedly and rapidly inhibits beta-amyloid accumulation in Alzheimer's disease transgenic mice. Neuron 30, 665-676.

Choi, N.S., Hahm, J.H., Maeng, P.J., Kim, S.H., 2005. Comparative study of enzyme activity and stability of bovine and human plasmins in electrophoretic reagents, beta-mercaptoethanol, DTT, SDS, Triton X-100, and urea. J Biochem Mol Biol 38, 177-181.

Chyung, A.S., Greenberg, B.D., Cook, D.G., Doms, R.W., Lee, V.M., 1997. Novel beta-secretase cleavage of beta-amyloid precursor protein in the endoplasmic reticulum/intermediate compartment of NT2N cells. J Cell Biol 138, 671-680.

Cirrito, J.R., Deane, R., Fagan, A.M., Spinner, M.L., Parsadanian, M., Finn, M.B., Jiang, H., Prior, J.L., Sagare, A., Bales, K.R., Paul, S.M., Zlokovic, B.V., Piwnica-Worms, D., Holtzman, D.M., 2005. P-glycoprotein deficiency at the blood-brain barrier increases amyloid-beta deposition in an Alzheimer disease mouse model. J Clin Invest 115, 3285-3290.

Cleuziat, P., Awade, A., Robert-Baudouy, J., 1992. Molecular characterization of pcp, the structural gene encoding the pyrrolidone carboxylyl peptidase from *Streptococcus pyogenes*. Mol Microbiol 6, 2051-2063.

Colciaghi, F., Borroni, B., Pastorino, L., Marcello, E., Zimmermann, M., Cattabeni, F., Padovani, A., Di Luca, M., 2002. [alpha]-Secretase ADAM10 as well as [alpha]APPs is reduced in platelets and CSF of Alzheimer disease patients. Mol Med 8, 67-74.

Connelly, S., 2006. Studies on pyroglutamyl carboxyl peptidase enzymes and cholinesterase inhibitors: implications for Alzheimer's disease. PhD Thesis. University of Exeter.

Coons, A.H., Creech, H.J., Jones, R.N., 1941. Immunological properties of an antibody containing a fluorescent group. Proc Soc Exp Biol Med 47, 200-202.

Cork, L.C., 1990. Neuropathology of Down syndrome and Alzheimer disease. Am J Med Genet Suppl 7, 282-286.

Costa, N.J., Dahm, C.C., Hurrell, F., Taylor, E.R., Murphy, M.P., 2003. Interactions of mitochondrial thiols with nitric oxide. Antioxid Redox Signal 5, 291-305.

Cras, P., Smith, M.A., Richey, P.L., Siedlak, S.L., Mulvihill, P., Perry, G., 1995. Extracellular neurofibrillary tangles reflect neuronal loss and provide further evidence of extensive protein cross-linking in Alzheimer disease. Acta Neuropathol 89, 291-295.

Creemers, J.W., Ines Dominguez, D., Plets, E., Serneels, L., Taylor, N.A., Multhaup, G., Craessaerts, K., Annaert, W., De Strooper, B., 2001. Processing of beta-secretase by furin and other members of the proprotein convertase family. J Biol Chem 276, 4211-4217.

Cruz, C., Charli, J.L., Vargas, M.A., Joseph-Bravo, P., 1991. Neuronal localization of pyroglutamate aminopeptidase II in primary cultures of fetal mouse brain. J Neurochem 56, 1594-1601.

Cummins, P.M., O'Connor, B., 1996. Bovine brain pyroglutamyl aminopeptidase (type-1): purification and characterisation of a neuropeptide-inactivating peptidase. Int J Biochem Cell Biol 28, 883-893.

Cummins, P.M., O'Connor, B., 1998. Pyroglutamyl peptidase: an overview of the three known enzymatic forms. Biochim Biophys Acta 1429, 1-17.

Cynis, H., Scheel, E., Saido, T.C., Schilling, S., Demuth, H.U., 2008. Amyloidogenic processing of amyloid precursor protein: evidence of a pivotal role of glutaminyl cyclase in generation of pyroglutamate-modified amyloid-beta. Biochemistry 47, 7405-7413.

Cynis, H., Schilling, S., Bodnar, M., Hoffmann, T., Heiser, U., Saido, T.C., Demuth, H.U., 2006. Inhibition of glutaminyl cyclase alters pyroglutamate formation in mammalian cells. Biochim Biophys Acta 1764, 1618-1625.

Czajkowski, C., Karlin, A., 1995. Structure of the nicotinic receptor acetylcholine-binding site. Identification of acidic residues in the delta subunit within 0.9 nm of the 5 alpha subunit-binding. J Biol Chem 270, 3160-3164.

Czekay, G., Bauer, K., 1993. Identification of the thyrotropin-releasing-hormone-degrading ectoenzyme as a metallopeptidase. Biochem J 290 (Pt 3), 921-926.

D'Amico, S., Feller, G., 2009. A nondetergent sulfobetaine improves protein unfolding reversibility in microcalorimetric studies. Anal Biochem 385, 389-391.

D'Andrea, M.R., Cole, G.M., Ard, M.D., 2004. The microglial phagocytic role with specific plaque types in the Alzheimer disease brain. Neurobiol Aging 25, 675-683.

D'Andrea, M.R., Nagele, R.G., 2002. MAP-2 immunolabeling can distinguish diffuse from dense-core amyloid plaques in brains with Alzheimer's disease. Biotech Histochem 77, 95-103.

D'Andrea, M.R., Nagele, R.G., Wang, H.Y., Peterson, P.A., Lee, D.H., 2001. Evidence that neurones accumulating amyloid can undergo lysis to form amyloid plaques in Alzheimer's disease. Histopathology 38, 120-134.

D'Arcy, A., Mac Sweeney, A., Stihle, M., Haber, A., 2003. The advantages of using a modified microbatch method for rapid screening of protein crystallization conditions. Acta Crystallogr D Biol Crystallogr 59, 396-399.

D'Arrigo, C., Tabaton, M., Perico, A., 2009. N-terminal truncated pyroglutamyl beta amyloid peptide Abetapy3-42 shows a faster aggregation kinetics than the full-length Abeta1-42. Biopolymers 91, 861-873.

Dando, P.M., Fortunato, M., Strand, G.B., Smith, T.S., Barrett, A.J., 2003. Pyroglutamyl-peptidase I: cloning, sequencing, and characterisation of the recombinant human enzyme. Protein Expr Purif 28, 111-119.

Danielsson, J., Andersson, A., Jarvet, J., Graslund, A., 2006. 15N relaxation study of the amyloid beta-peptide: structural propensities and persistence length. Magn Reson Chem 44 Spec No, S114-121.

Davey, F.R., Busch, G.J., 1970. Immunohistochemistry of glomerulonephritis using horseradish peroxidase and fluorescein-labeled antibody: a comparison of two technics. Am J Clin Pathol 53, 531-536.

Davis, D.G., Schmitt, F.A., Wekstein, D.R., Markesbery, W.R., 1999. Alzheimer neuropathologic alterations in aged cognitively normal subjects. J Neuropathol Exp Neurol 58, 376-388.

de Gandarias, J.M., Irazusta, J., Silio, M., Gil, J., Saitua, N., Casis, L., 1998. Soluble and membrane-bound pyroglutamyl-peptidase I activity in the developing cerebellum and brain cortex. Int J Dev Biol 42, 103-106.

de Lamotte, F., Duviau, M.P., Sanier, C., Thai, R., Poncet, J., Bieysse, D., Breton, F., Pujade-Renaud, V., 2007. Purification and characterization of cassiicolin, the toxin produced by *Corynespora cassiicola*, causal agent of the leaf fall disease of rubber tree. J Chromatogr B Analyt Technol Biomed Life Sci 849, 357-362.

De Strooper, B., 2010. Proteases and proteolysis in Alzheimer disease: a multifactorial view on the disease process. Physiol Rev 90, 465-494.

Delaere, P., Duyckaerts, C., Masters, C., Beyreuther, K., Piette, F., Hauw, J.J., 1990. Large amounts of neocortical beta A4 deposits without neuritic plaques nor tangles in a psychometrically assessed, non-demented person. Neurosci Lett 116, 87-93.

Devanand, D.P., Pradhaban, G., Liu, X., Khandji, A., De Santi, S., Segal, S., Rusinek, H., Pelton, G.H., Honig, L.S., Mayeux, R., Stern, Y., Tabert, M.H., de Leon, M.J., 2007. Hippocampal and entorhinal atrophy in mild cognitive impairment: prediction of Alzheimer disease. Neurology 68, 828-836.

DeWitt, D.A., Perry, G., Cohen, M., Doller, C., Silver, J., 1998. Astrocytes regulate microglial phagocytosis of senile plaque cores of Alzheimer's disease. Exp Neurol 149, 329-340.

Dickerson, B.C., Stoub, T.R., Shah, R.C., Sperling, R.A., Killiany, R.J., Albert, M.S., Hyman, B.T., Blacker, D., Detoledo-Morrell, L., 2011. Alzheimer-signature MRI biomarker predicts AD dementia in cognitively normal adults. Neurology 76, 1395-1402.

Dickson, D.W., 1997. The pathogenesis of senile plaques. J Neuropathol Exp Neurol 56, 321-339.

Dickson, D.W., Crystal, H.A., Mattiace, L.A., Masur, D.M., Blau, A.D., Davies, P., Yen, S.H., Aronson, M.K., 1992. Identification of normal and pathological aging in prospectively studied nondemented elderly humans. Neurobiol Aging 13, 179-189.

Dominguez, D., Tournoy, J., Hartmann, D., Huth, T., Cryns, K., Deforce, S., Serneels, L., Camacho, I.E., Marjaux, E., Craessaerts, K., Roebroek, A.J., Schwake, M., D'Hooge, R., Bach, P., Kalinke, U., Moechars, D., Alzheimer, C., Reiss, K., Saftig, P., De Strooper, B., 2005. Phenotypic and biochemical analyses of BACE1- and BACE2-deficient mice. J Biol Chem 280, 30797-30806.

Dominy, B.N., Perl, D., Schmid, F.X., Brooks, C.L., 3rd, 2002. The effects of ionic strength on protein stability: the cold shock protein family. J Mol Biol 319, 541-554.

Doolittle, R.F., Armentrout, R.W., 1968. Pyrrolidonyl peptidase. An enzyme for selective removal of pyrrolidonecarboxylic acid residues from polypeptides. Biochemistry 7, 516-521.

Drago, D., Bettella, M., Bolognin, S., Cendron, L., Scancar, J., Milacic, R., Ricchelli, F., Casini, A., Messori, L., Tognon, G., Zatta, P., 2008. Potential pathogenic role of beta-amyloid(1-42)-aluminum complex in Alzheimer's disease. Int J Biochem Cell Biol 40, 731-746.

Drew, S.C., Masters, C.L., Barnham, K.J., 2010. Alzheimer's Abeta peptides with disease-associated N-terminal modifications: influence of isomerisation, truncation and mutation on Cu2+ coordination. PLoS One 5, e15875.

Dulbecco, R., Freeman, G., 1959. Plaque production by the polyoma virus. Virology 8, 396-397.

Dunham, J.H., Meyer, R.C., Garcia, E.L., Hall, R.A., 2009. GPR37 surface expression enhancement via N-terminal truncation or protein-protein interactions. Biochemistry 48, 10286-10297.

Duyckaerts, C., Delatour, B., Potier, M.C., 2009. Classification and basic pathology of Alzheimer disease. Acta Neuropathol 118, 5-36.

Ebe, T., 2007. [Green fluorescent protein as a marker gene expression]. Tanpakushitsu Kakusan Koso 52, 1766-1767.

Edman, P., Begg, G., 1967. A protein sequenator. Eur J Biochem 1, 80-91.

Ellman, G.L., 1959. Tissue sulfhydryl groups. Arch Biochem Biophys 82, 70-77.

Engst, S., Miller, S.M., 1999. Alternative routes for entry of HgX2 into the active site of mercuric ion reductase depend on the nature of the X ligands. Biochemistry 38, 3519-3529.

Enzinger, C., Fazekas, F., Matthews, P.M., Ropele, S., Schmidt, H., Smith, S., Schmidt, R., 2005. Risk factors for progression of brain atrophy in aging: six-year follow-up of normal subjects. Neurology 64, 1704-1711.

Ericsson, U.B., Hallberg, B.M., Detitta, G.T., Dekker, N., Nordlund, P., 2006. Thermofluor-based high-throughput stability optimization of proteins for structural studies. Anal Biochem 357, 289-298.

Eschenfeldt, W.H., Maltseva, N., Stols, L., Donnelly, M.I., Gu, M., Nocek, B., Tan, K., Kim, Y., Joachimiak, A., 2010. Cleavable C-terminal His-tag vectors for structure determination. J Struct Funct Genomics 11, 31-39.

Escobedo, M., Cravioto, J., 1973. Studies on the malabsorption syndromes. Inhibition of (Na+-K+) ATPase of small intestine microvilli by pyrrolidone carboxylic acid. Clin Chim Acta 49, 147-151.

Evnouchidou, I., Momburg, F., Papakyriakou, A., Chroni, A., Leondiadis, L., Chang, S.C., Goldberg, A.L., Stratikos, E., 2008. The internal sequence of the peptide-substrate determines its N-terminus trimming by ERAP1. PLoS One 3, e3658.

Expert-Bezancon, N., Rabilloud, T., Vuillard, L., Goldberg, M.E., 2003. Physical-chemical features of non-detergent sulfobetaines active as protein-folding helpers. Biophys Chem 100, 469-479.

Facklam, R., Pigott, N., Franklin, R., Elliott, J., 1995. Evaluation of three disk tests for identification of enterococci, leuconostocs, and pediococci. J Clin Microbiol 33, 885-887.

Faivre-Bauman, A., Loudes, C., Barret, A., Tixier-Vidal, A., Bauer, K., 1986. Possible role of neuropeptide degrading enzymes on thyroliberin secretion in fetal hypothalamic cultures grown in serum free medium. Neuropeptides 7, 125-138.

Fath-Goodin, A., Kroemer, J., Martin, S., Reeves, K., Webb, B.A., 2006. Polydnavirus genes that enhance the baculovirus expression vector system. Adv Virus Res 68, 75-90.

Feng, Y., Wang, X.P., Yang, S.G., Wang, Y.J., Zhang, X., Du, X.T., Sun, X.X., Zhao, M., Huang, L., Liu, R.T., 2009. Resveratrol inhibits beta-amyloid oligomeric cytotoxicity but does not prevent oligomer formation. Neurotoxicology 30, 986-995.

Fiala, M., 2010. Re-balancing of inflammation and abeta immunity as a therapeutic for Alzheimer's disease-view from the bedside. CNS Neurol Disord Drug Targets 9, 192-196.

Flood, J.F., Roberts, E., Sherman, M.A., Kaplan, B.E., Morley, J.E., 1994. Topography of a binding site for small amnestic peptides deduced from structure-activity studies: relation to amnestic effect of amyloid beta protein. Proc Natl Acad Sci U S A 91, 380-384.

Francis, P.T., Palmer, A.M., Snape, M., Wilcock, G.K., 1999. The cholinergic hypothesis of Alzheimer's disease: a review of progress. J Neurol Neurosurg Psychiatry 66, 137-147.

Furukawa, K., Sopher, B.L., Rydel, R.E., Begley, J.G., Pham, D.G., Martin, G.M., Fox, M., Mattson, M.P., 1996. Increased activity-regulating and neuroprotective efficacy of alpha-secretase-derived secreted amyloid precursor protein conferred by a C-terminal heparin-binding domain. J Neurochem 67, 1882-1896.

Gallagher, S.P., O'Connor, B., 1998. A study of a highly specific pyroglutamyl aminopeptidase type-II from the membrane fraction of bovine brain. Int J Biochem Cell Biol 30, 115-133.

Gallagher, S.P., O'Leary, R.M., O'Connor, B., 1997. The development of two fluorimetric assays for the determination of pyroglutamyl aminopeptidase type-II activity. Anal Biochem 250, 1-9.

Garat, B., Miranda, J., Charli, J.L., Joseph-Bravo, P., 1985. Presence of a membrane bound pyroglutamyl amino peptidase degrading thyrotropin releasing hormone in rat brain. Neuropeptides 6, 27-40.

Gasteiger, E., Gattiker, A., Hoogland, C., Ivanyi, I., Appel, R.D., Bairoch, A., 2003. ExPASy: The proteomics server for in-depth protein knowledge and analysis. Nucleic Acids Res 31, 3784-3788.

Gatta, V., Drago, D., Fincati, K., Valenti, M.T., Dalle Carbonare, L., Sensi, S.L., Zatta, P., 2011. Microarray analysis on human neuroblastoma cells exposed to aluminum, beta(1-42)-amyloid or the beta(1-42)-amyloid aluminum complex. PLoS One 6, e15965.

Ghiso, J., Calero, M., Matsubara, E., Governale, S., Chuba, J., Beavis, R., Wisniewski, T., Frangione, B., 1997. Alzheimer's soluble amyloid beta is a normal component of human urine. FEBS Lett 408, 105-108.

Ghosh, S., Thakur, M.K., 2008. PS1 expression is downregulated by gonadal steroids in adult mouse brain. Neurochem Res 33, 365-369.

Giasson, B.I., Forman, M.S., Higuchi, M., Golbe, L.I., Graves, C.L., Kotzbauer, P.T., Trojanowski, J.Q., Lee, V.M., 2003. Initiation and synergistic fibrillization of tau and alpha-synuclein. Science 300, 636-640.

Gilbert, J.B., Price, V.E., Greenstein, J.P., 1949. Effect of anions on the non-enzymatic desamidation of glutamine. J Biol Chem 180, 209-218.

Giulian, D., Haverkamp, L.J., Yu, J., Karshin, W., Tom, D., Li, J., Kazanskaia, A., Kirkpatrick, J., Roher, A.E., 1998. The HHQK domain of beta-amyloid provides a structural basis for the immunopathology of Alzheimer's disease. J Biol Chem 273, 29719-29726.

Glenner, G.G., Wong, C.W., 1984. Alzheimer's disease: initial report of the purification and characterization of a novel cerebrovascular amyloid protein. Biochem Biophys Res Commun 120, 885-890.

Goate, A., Chartier-Harlin, M.C., Mullan, M., Brown, J., Crawford, F., Fidani, L., Giuffra, L., Haynes, A., Irving, N., James, L., et al., 1991. Segregation of a missense mutation in the amyloid precursor protein gene with familial Alzheimer's disease. Nature 349, 704-706.

Goedert, M., Spillantini, M.G., Jakes, R., Rutherford, D., Crowther, R.A., 1989. Multiple isoforms of human microtubule-associated protein tau: sequences and localization in neurofibrillary tangles of Alzheimer's disease. Neuron 3, 519-526.

Goetz, I.E., Weinstein, C., Roberts, E., 1973. Inhibition of growth of hamster tumor cells in vitro by pyrrolidone carboxylic acid in a glutamine-dependent system. In Vitro 8, 279-282.

Golovanov, A.P., Hautbergue, G.M., Wilson, S.A., Lian, L.Y., 2004. A simple method for improving protein solubility and long-term stability. J Am Chem Soc 126, 8933-8939.

Gomez-Isla, T., Hollister, R., West, H., Mui, S., Growdon, J.H., Petersen, R.C., Parisi, J.E., Hyman, B.T., 1997. Neuronal loss correlates with but exceeds neurofibrillary tangles in Alzheimer's disease. Ann Neurol 41, 17-24.

Gomez-Isla, T., Price, J.L., McKeel, D.W., Jr., Morris, J.C., Growdon, J.H., Hyman, B.T., 1996. Profound loss of layer II entorhinal cortex neurons occurs in very mild Alzheimer's disease. J Neurosci 16, 4491-4500.

Gomez-Ramos, A., Diaz-Hernandez, M., Rubio, A., Miras-Portugal, M.T., Avila, J., 2008. Extracellular tau promotes intracellular calcium increase through M1 and M3 muscarinic receptors in neuronal cells. Mol Cell Neurosci 37, 673-681.

Gonzales, T., Robert-Baudouy, J., 1994. Characterization of the pcp gene of *Pseudomonas fluorescens* and of its product, pyrrolidone carboxyl peptidase (Pcp). J Bacteriol 176, 2569-2576.

Good, N.E., Winget, G.D., Winter, W., Connolly, T.N., Izawa, S., Singh, R.M., 1966. Hydrogen ion buffers for biological research. Biochemistry 5, 467-477.

Gordon, D.J., Sciarretta, K.L., Meredith, S.C., 2001. Inhibition of beta-amyloid(40) fibrillogenesis and disassembly of beta-amyloid(40) fibrils by short beta-amyloid congeners containing N-methyl amino acids at alternate residues. Biochemistry 40, 8237-8245.

Gouras, G.K., Xu, H., Gross, R.S., Greenfield, J.P., Hai, B., Wang, R., Greengard, P., 2000. Testosterone reduces neuronal secretion of Alzheimer's beta-amyloid peptides. Proc Natl Acad Sci U S A 97, 1202-1205.

Graeber, M.B., Streit, W.J., 1990. Microglia: immune network in the CNS. Brain Pathol 1, 2-5.

Graham, F.L., Smiley, J., Russell, W.C., Nairn, R., 1977. Characteristics of a human cell line transformed by DNA from human adenovirus type 5. J Gen Virol 36, 59-74.

Green, B.D., Mooney, M.H., Gault, V.A., Irwin, N., Bailey, C.J., Harriott, P., Greer, B., O'Harte, F.P., Flatt, P.R., 2004. N-terminal His(7)-modification of glucagon-like peptide-1(7-36) amide generates dipeptidyl peptidase IV-stable analogues with potent antihyperglycaemic activity. J Endocrinol 180, 379-388.

Greenfield, J.P., Leung, L.W., Cai, D., Kaasik, K., Gross, R.S., Rodriguez-Boulan, E., Greengard, P., Xu, H., 2002. Estrogen lowers Alzheimer beta-amyloid generation by stimulating trans-Golgi network vesicle biogenesis. J Biol Chem 277, 12128-12136.

Greenfield, J.P., Tsai, J., Gouras, G.K., Hai, B., Thinakaran, G., Checler, F., Sisodia, S.S., Greengard, P., Xu, H., 1999. Endoplasmic reticulum and trans-Golgi network generate distinct populations of Alzheimer beta-amyloid peptides. Proc Natl Acad Sci U S A 96, 742-747.

Grignon, Y., Duyckaerts, C., Bennecib, M., Hauw, J.J., 1998. Cytoarchitectonic alterations in the supramarginal gyrus of late onset Alzheimer's disease. Acta Neuropathol 95, 395-406.

Grundke-Iqbal, I., Iqbal, K., Quinlan, M., Tung, Y.C., Zaidi, M.S., Wisniewski, H.M., 1986. Microtubule-associated protein tau. A component of Alzheimer paired helical filaments. J Biol Chem 261, 6084-6089.

Guilloteau, J.P., Fromage, N., Ries-Kautt, M., Reboul, S., Bocquet, D., Dubois, H., Faucher, D., Colonna, C., Ducruix, A., Becquart, J., 1996. Purification, stabilization, and crystallization of a modular protein: Grb2. Proteins 25, 112-119.

Guillozet, A.L., Weintraub, S., Mash, D.C., Mesulam, M.M., 2003. Neurofibrillary Tangles, Amyloid, and Memory in Aging and Mild Cognitive Impairment. Arch Neurol 60, 729-736.

Gutowski, N.J., Newcombe, J., Cuzner, M.L., 1999. Tenascin-R and C in multiple sclerosis lesions: relevance to extracellular matrix remodelling. Neuropathol Appl Neurobiol 25, 207-214.

Guy, J.E., Isupov, M.N., Littlechild, J.A., 2003. The structure of an alcohol dehydrogenase from the hyperthermophilic archaeon *Aeropyrum pernix*. J Mol Biol 331, 1041-1051.

Haaijman, J.J., Coolen, J., Krose, C.J., Pronk, G.J., Ming, Z.F., 1986. Fluorescein and tetramethyl rhodamine as haptens in enzyme immunohistochemistry. Histochemistry 84, 363-370.

Haass, C., Hung, A.Y., Schlossmacher, M.G., Oltersdorf, T., Teplow, D.B., Selkoe, D.J., 1993. Normal cellular processing of the beta-amyloid precursor protein results in the secretion of the amyloid beta peptide and related molecules. Ann N Y Acad Sci 695, 109-116.

Haass, C., Lemere, C.A., Capell, A., Citron, M., Seubert, P., Schenk, D., Lannfelt, L., Selkoe, D.J., 1995. The Swedish mutation causes early-onset Alzheimer's disease by beta-secretase cleavage within the secretory pathway. Nat Med 1, 1291-1296.

Haitinger, L., 1882. Vorläufige Mittheilung über Glutaminsäure und Pyrrol. Monatshefte für Chemie 3, 228-229.

Hamilton, R.L., 2000. Lewy bodies in Alzheimer's disease: a neuropathological review of 145 cases using alpha-synuclein immunohistochemistry. Brain Pathol 10, 378-384.

Hammond, C.J., Hallock, L.R., Howanski, R.J., Appelt, D.M., Little, C.S., Balin, B.J., 2010. Immunohistological detection of *Chlamydia pneumoniae* in the Alzheimer's disease brain. BMC Neurosci 11, 121.

Hanahan, D., 1983. Studies on transformation of *Escherichia coli* with plasmids. J Mol Biol 166, 557-580.

Hanahan, D., Jessee, J., Bloom, F.R., 1991. Plasmid transformation of *Escherichia coli* and other bacteria. Methods Enzymol 204, 63-113.

Hardy, J., Allsop, D., 1991. Amyloid deposition as the central event in the aetiology of Alzheimer's disease. Trends Pharmacol Sci 12, 383-388.

Hardy, J., Selkoe, D.J., 2002. The amyloid hypothesis of Alzheimer's disease: progress and problems on the road to therapeutics. Science 297, 353-356.

Harigaya, Y., Saido, T.C., Eckman, C.B., Prada, C.M., Shoji, M., Younkin, S.G., 2000. Amyloid beta protein starting pyroglutamate at position 3 is a major component of the

amyloid deposits in the Alzheimer's disease brain. Biochem Biophys Res Commun 276, 422-427.

Harkany, T., Abraham, I., Laskay, G., Timmerman, W., Jost, K., Zarandi, M., Penke, B., Nyakas, C., Luiten, P.G., 1999. Propionyl-IIGL tetrapeptide antagonizes beta-amyloid excitotoxicity in rat nucleus basalis. Neuroreport 10, 1693-1698.

Harrison, R.L., Jarvis, D.L., 2006. Protein N-glycosylation in the baculovirus-insect cell expression system and engineering of insect cells to produce "mammalianized" recombinant glycoproteins. Adv Virus Res 68, 159-191.

Hartlage-Rubsamen, M., Morawski, M., Waniek, A., Jager, C., Zeitschel, U., Koch, B., Cynis, H., Schilling, S., Schliebs, R., Demuth, H.U., Rossner, S., 2011. Glutaminyl cyclase contributes to the formation of focal and diffuse pyroglutamate (pGlu)-Abeta deposits in hippocampus via distinct cellular mechanisms. Acta Neuropathol 121, 705-719.

Hassell, A.M., An, G., Bledsoe, R.K., Bynum, J.M., Carter, H.L., 3rd, Deng, S.J., Gampe, R.T., Grisard, T.E., Madauss, K.P., Nolte, R.T., Rocque, W.J., Wang, L., Weaver, K.L., Williams, S.P., Wisely, G.B., Xu, R., Shewchuk, L.M., 2007. Crystallization of protein-ligand complexes. Acta Crystallogr D Biol Crystallogr 63, 72-79.

Hayashi, M.A., Camargo, A.C., 2005. The Bradykinin-potentiating peptides from venom gland and brain of *Bothrops jararaca* contain highly site specific inhibitors of the somatic angiotensin-converting enzyme. Toxicon 45, 1163-1170.

He, W., Barrow, C.J., 1999. The A beta 3-pyroglutamyl and 11-pyroglutamyl peptides found in senile plaque have greater beta-sheet forming and aggregation propensities in vitro than full-length A beta. Biochemistry 38, 10871-10877.

Hendriks, L., van Duijn, C.M., Cras, P., Cruts, M., Van Hul, W., van Harskamp, F., Warren, A., McInnis, M.G., Antonarakis, S.E., Martin, J.J., et al., 1992. Presenile dementia and cerebral haemorrhage linked to a mutation at codon 692 of the beta-amyloid precursor protein gene. Nat Genet 1, 218-221.

Hilbich, C., Kisters-Woike, B., Reed, J., Masters, C.L., Beyreuther, K., 1992. Substitutions of hydrophobic amino acids reduce the amyloidogenicity of Alzheimer's disease beta A4 peptides. J Mol Biol 228, 460-473.

Hinkle, P.M., Tashjian, A.H., Jr., 1973. Receptors for thyrotropin-releasing hormone in prolactin producing rat pituitary cells in culture. J Biol Chem 248, 6180-6186.

Hook, V., Toneff, T., Bogyo, M., Greenbaum, D., Medzihradszky, K.F., Neveu, J., Lane, W., Hook, G., Reisine, T., 2005. Inhibition of cathepsin B reduces beta-amyloid production in regulated secretory vesicles of neuronal chromaffin cells: evidence for cathepsin B as a candidate beta-secretase of Alzheimer's disease. Biol Chem 386, 931-940.

Horsthemke, B., Leblanc, P., Kordon, C., Wattiaux-De Coninck, S., Wattiaux, R., Bauer, K., 1984. Subcellular distribution of particle-bound neutral peptidases capable of hydrolyzing gonadoliberin, thyroliberin, enkephalin and substance P. Eur J Biochem 139, 315-320.

Hosoda, R., Saido, T.C., Otvos, L., Jr., Arai, T., Mann, D.M., Lee, V.M., Trojanowski, J.Q., Iwatsubo, T., 1998. Quantification of modified amyloid beta peptides in Alzheimer disease and Down syndrome brains. J Neuropathol Exp Neurol 57, 1089-1095.

Hsu, S.M., Soban, E., 1982. Color modification of diaminobenzidine (DAB) precipitation by metallic ions and its application for double immunohistochemistry. J Histochem Cytochem 30, 1079-1082.

Hu, X., Hicks, C.W., He, W., Wong, P., Macklin, W.B., Trapp, B.D., Yan, R., 2006. Bace1 modulates myelination in the central and peripheral nervous system. Nat Neurosci 9, 1520-1525.

Hughes, E., Burke, R.M., Doig, A.J., 2000. Inhibition of toxicity in the beta-amyloid peptide fragment beta –(25-35) using N-methylated derivatives: a general strategy to prevent amyloid formation. J Biol Chem 275, 25109-25115.

Huse, J.T., Pijak, D.S., Leslie, G.J., Lee, V.M., Doms, R.W., 2000. Maturation and endosomal targeting of beta-site amyloid precursor protein-cleaving enzyme. The Alzheimer's disease beta-secretase. J Biol Chem 275, 33729-33737.

Imahori, K., Hoshi, M., Ishiguro, K., Sato, K., Takahashi, M., Shiurba, R., Yamaguchi, H., Takashima, A., Uchida, T., 1998. Possible role of tau protein kinases in pathogenesis of Alzheimer's disease. Neurobiol Aging 19, S93-98.

Imahori, K., Uchida, T., 1997. Physiology and pathology of tau protein kinases in relation to Alzheimer's disease. J Biochem 121, 179-188.

Iqbal, K., Grundke-Iqbal, I., Zaidi, T., Merz, P.A., Wen, G.Y., Shaikh, S.S., Wisniewski, H.M., Alafuzoff, I., Winblad, B., 1986. Defective brain microtubule assembly in Alzheimer's disease. Lancet 2, 421-426.

Iqbal, K., Liu, F., Gong, C.X., Grundke-Iqbal, I., 2010. Tau in Alzheimer disease and related tauopathies. Curr Alzheimer Res 7, 656-664.

Iqbal, K., Wisniewski, H.M., Shelanski, M.L., Brostoff, S., Liwnicz, B.H., Terry, R.D., 1974. Protein changes in senile dementia. Brain Res 77, 337-343.

Irwin, N., Green, B.D., Gault, V.A., Greer, B., Harriott, P., Bailey, C.J., Flatt, P.R., O'Harte, F.P., 2005. Degradation, insulin secretion, and antihyperglycemic actions of two palmitate-derivitized N-terminal pyroglutamyl analogues of glucose-dependent insulinotropic polypeptide. J Med Chem 48, 1244-1250.

Isaac, R.E., Bland, N.D., Shirras, A.D., 2009. Neuropeptidases and the metabolic inactivation of insect neuropeptides. Gen Comp Endocrinol 162, 8-17.

Ito, K., Inoue, T., Takahashi, T., Huang, H.S., Esumi, T., Hatakeyama, S., Tanaka, N., Nakamura, K.T., Yoshimoto, T., 2001. The mechanism of aubstrate eecognition of pyroglutamyl-peptidase I from *Bacillus amyloliquefaciens* as determined by X-ray crystallography and site-directed mutagenesis. J Biol Chem 276, 18557-18562.

Ito, K., Nakajima, Y., Onohara, Y., Takeo, M., Nakashima, K., Matsubara, F., Ito, T., Yoshimoto, T., 2006. Crystal structure of aminopeptidase N (proteobacteria alanyl aminopeptidase) from *Escherichia coli* and conformational change of methionine 260 involved in substrate recognition. J Biol Chem 281, 33664-33676.

Iwatsubo, T., Saido, T.C., Mann, D.M., Lee, V.M., Trojanowski, J.Q., 1996. Full-length amyloid-beta (1-42(43)) and amino-terminally modified and truncated amyloid-beta 42(43) deposit in diffuse plaques. Am J Pathol 149, 1823-1830.

Jarrett, J.T., Berger, E.P., Lansbury, P.T., Jr., 1993. The carboxy terminus of the beta amyloid protein is critical for the seeding of amyloid formation: implications for the pathogenesis of Alzheimer's disease. Biochemistry 32, 4693-4697.

Jeffcoate, S.L., Hutchinson, J.S.M., 1978. The endocrine hypothalamus. Academic Press, London.

Jiang, J.W., Zheng, S.S., Xue, F., Gao, L.H., Jiang, G.P., Xie, H.Y., 2006. Enteral feeding of glycyl-glutamine dipeptide improves the structure and absorptive function of the small intestine after allogenetic liver transplantation in rats. Hepatobiliary Pancreat Dis Int 5, 199-204.

Johnston, J.A., Liu, W.W., Todd, S.A., Coulson, D.T., Murphy, S., Irvine, G.B., Passmore, A.P., 2005. Expression and activity of beta-site amyloid precursor protein cleaving enzyme in Alzheimer's disease. Biochem Soc Trans 33, 1096-1100.

Kabashima, T., Li, Y., Kanada, N., Ito, K., Yoshimoto, T., 2001. Enhancement of the thermal stability of pyroglutamyl peptidase I by introduction of an intersubunit disulfide bond. Biochim Biophys Acta 1547, 214-220.

Kang, J., Lemaire, H.G., Unterbeck, A., Salbaum, J.M., Masters, C.L., Grzeschik, K.H., Multhaup, G., Beyreuther, K., Muller-Hill, B., 1987. The precursor of Alzheimer's disease amyloid A4 protein resembles a cell-surface receptor. Nature 325, 733-736.

Karas, G.B., Scheltens, P., Rombouts, S.A., Visser, P.J., van Schijndel, R.A., Fox, N.C., Barkhof, F., 2004. Global and local gray matter loss in mild cognitive impairment and Alzheimer's disease. Neuroimage 23, 708-716.

Kawas, C.H., Corrada, M.M., 2006. Alzheimer's and dementia in the oldest-old: a century of challenges. Curr Alzheimer Res 3, 411-419.

Kayed, R., Jackson, G.R., 2009. Prefilament tau species as potential targets for immunotherapy for Alzheimer disease and related disorders. Curr Opin Immunol 21, 359-363.

Kelly, J.A., Loscher, C.E., Gallagher, S., O'Connor, B., 1997. Degradation of pyroglutamyl-phenylalanyl-proline amide by a pyroglutamyl aminopeptidase purified from membrane fractions of bovine brain. Biochem Soc Trans 25, 114S.

Kilbane, Z., Vaas, P.R., Cuiv, P.O., O'Connor, B., 2007. Cloning and heterologous expression of bovine pyroglutamyl peptidase type-1 in *Escherichia coli*: purification, biochemical and kinetic characterisation. Mol Cell Biochem 297, 189-197.

Kim, B.M., Schultz, L.W., Raines, R.T., 1999. Variants of ribonuclease inhibitor that resist oxidation. Protein Sci 8, 430-434.

Kim, H.J., Chae, S.C., Lee, D.K., Chromy, B., Lee, S.C., Park, Y.C., Klein, W.L., Krafft, G.A., Hong, S.T., 2003. Selective neuronal degeneration induced by soluble oligomeric amyloid beta protein. Faseb J 17, 118-120.

Kim, J., Onstead, L., Randle, S., Price, R., Smithson, L., Zwizinski, C., Dickson, D.W., Golde, T., McGowan, E., 2007. Abeta40 inhibits amyloid deposition in vivo. J Neurosci 27, 627-633.

Kim, W., Hecht, M.H., 2005. Sequence determinants of enhanced amyloidogenicity of Alzheimer A{beta}42 peptide relative to A{beta}40. J Biol Chem 280, 35069-35076.

Kinsella, K.G., 1992. Changes in life expectancy 1900-1990. Am J Clin Nutr 55, 1196S-1202S.

Kirkland, T.A., Adler, M., Bauman, J.G., Chen, M., Haeggstrom, J.Z., King, B., Kochanny, M.J., Liang, A.M., Mendoza, L., Phillips, G.B., Thunnissen, M., Trinh, L., Whitlow, M., Ye, B., Ye, H., Parkinson, J., Guilford, W.J., 2008. Synthesis of glutamic acid analogs as potent inhibitors of leukotriene A4 hydrolase. Bioorg Med Chem 16, 4963-4983.

Kirschner, D.A., Abraham, C., Selkoe, D.J., 1986. X-ray diffraction from intraneuronal paired helical filaments and extraneuronal amyloid fibers in Alzheimer disease indicates cross-beta conformation. Proc Natl Acad Sci U S A 83, 503-507.

Kochan, G., Krojer, T., Harvey, D., Fischer, R., Chen, L., Vollmar, M., von Delft, F., Kavanagh, K.L., Brown, M.A., Bowness, P., Wordsworth, P., Kessler, B.M., Oppermann, U., 2011. Crystal structures of the endoplasmic reticulum aminopeptidase-1 (ERAP1) reveal the molecular basis for N-terminal peptide trimming. Proc Natl Acad Sci U S A 108, 7745-7750.

Kochan, G., Tyborowska, J., Szewczyk, B., 1993. Expression of animal virus genes using baculovirus AcNPV. Acta Biochim Pol 40, 1-3.

Koedam, E.L., Lauffer, V., van der Vlies, A.E., van der Flier, W.M., Scheltens, P., Pijnenburg, Y.A., 2010. Early-versus late-onset Alzheimer's disease: more than age alone. J Alzheimers Dis 19, 1401-1408.

Kohsaka, S., Hamanoue, M., Nakajima, K., 1996. Functional implication of secretory proteases derived from microglia in the central nervous system. Keio J Med 45, 263-269.

Kokkoni, N., Stott, K., Amijee, H., Mason, J.M., Doig, A.J., 2006. N-Methylated peptide inhibitors of beta-amyloid aggregation and toxicity. Optimization of the inhibitor structure. Biochemistry 45, 9906-9918.

Koo, E.H., Squazzo, S.L., 1994. Evidence that production and release of amyloid beta-protein involves the endocytic pathway. J Biol Chem 269, 17386-17389.

Krieger, E., Nabuurs, S.B., Vriend, G., 2003. Homology modeling. Methods Biochem Anal 44, 509-523.

Kril, J.J., Patel, S., Harding, A.J., Halliday, G.M., 2002. Neuron loss from the hippocampus of Alzheimer's disease exceeds extracellular neurofibrillary tangle formation. Acta Neuropathol 103, 370-376.

Kuda, T., Shoji, M., Arai, H., Kawashima, S., Saido, T.C., 1997. Reduction of plasma glutamyl aminopeptidase activity in sporadic Alzheimer's disease. Biochem Biophys Res Commun 231, 526-530.

Kumar, A., Moody, L., Olaivar, J.F., Lewis, N.A., Khade, R.L., Holder, A.A., Zhang, Y., Rangachari, V., 2010. Inhibition of Abeta42 peptide aggregation by a binuclear ruthenium(II)-platinum(II) complex: Potential for multi-metal organometallics as anti-amyloid agents. ACS Chem Neurosci 2010, 691-701.

Kumar, S., Tsai, C.J., Nussinov, R., 2000. Factors enhancing protein thermostability. Protein Eng 13, 179-191.

Kuo, Y.M., Emmerling, M.R., Woods, A.S., Cotter, R.J., Roher, A.E., 1997. Isolation, chemical characterization, and quantitation of A beta 3-pyroglutamyl peptide from neuritic plaques and vascular amyloid deposits. Biochem Biophys Res Commun 237, 188-191.

Kwiatkowska, J., Torain, B., Glenner, G.G., 1974. A pyrrolidonecarboxylate peptidase from the particulate fraction of *Klebsiella cloacae*. Purification of the stable enzyme and its use in releasing the NH2 terminus from pyrrolidonecarboxylyl peptides and proteins. J Biol Chem 249, 7729-7736.

Kyrieleis, O.J., Goettig, P., Kiefersauer, R., Huber, R., Brandstetter, H., 2005. Crystal structures of the tricorn interacting factor F3 from *Thermoplasma acidophilum*, a zinc aminopeptidase in three different conformations. J Mol Biol 349, 787-800.

Laemmli, U.K., 1970. Cleavage of structural proteins during the assembly of the head of bacteriophage T4. Nature 227, 680-685.

Larkin, M.A., Blackshields, G., Brown, N.P., Chenna, R., McGettigan, P.A., McWilliam, H., Valentin, F., Wallace, I.M., Wilm, A., Lopez, R., Thompson, J.D., Gibson, T.J., Higgins, D.G., 2007. Clustal W and Clustal X version 2.0. Bioinformatics 23, 2947-2948.

Larner, A.J., 1999. Hypothesis: amyloid beta-peptides truncated at the N-terminus contribute to the pathogenesis of Alzheimer's disease. Neurobiol Aging 20, 65-69.

Laskay, G., Zarandi, M., Varga, J., Jost, K., Fonagy, A., Torday, C., Latzkovits, L., Penke, B., 1997. A putative tetrapeptide antagonist prevents beta-amyloid-induced long-term elevation of [Ca2+]i in rat astrocytes. Biochem Biophys Res Commun 235, 479-481.

Lautenschlager, N.T., Martins, R.N., 2005. Common versus uncommon causes of dementia. Int Psychogeriatr 17 Suppl 1, S27-34.

Lawson, L.J., Perry, V.H., Dri, P., Gordon, S., 1990. Heterogeneity in the distribution and morphology of microglia in the normal adult mouse brain. Neuroscience 39, 151-170.

Le Saux, O., Robert-Baudouy, J., 1997. Pyroglutamic acid and iron regulate the expression of the pcp gene in *Pseudomonas fluorescens* MFO. FEMS Microbiol Lett 155, 209-215.

Lee, C.Y., Landreth, G.E., 2010. The role of microglia in amyloid clearance from the AD brain. J Neural Transm 117, 949-960.

Lei, S.P., Lin, H.C., Wang, S.S., Callaway, J., Wilcox, G., 1987. Characterization of the *Erwinia carotovora* pelB gene and its product pectate lyase. J Bacteriol 169, 4379-4383.

Lemere, C.A., Masliah, E., 2010. Can Alzheimer disease be prevented by amyloid-beta immunotherapy? Nat Rev Neurol 6, 108-119.

Leone, J.W., Hampton, B., Fowler, E., Moyer, M., Krishna, R.G., Chin, C.C., 2011. Removal of N-terminal blocking groups from proteins. Curr Protoc Protein Sci Chapter 11, Unit11 17.

Levy, E., Carman, M.D., Fernandez-Madrid, I.J., Power, M.D., Lieberburg, I., van Duinen, S.G., Bots, G.T., Luyendijk, W., Frangione, B., 1990. Mutation of the Alzheimer's disease amyloid gene in hereditary cerebral hemorrhage, Dutch type. Science 248, 1124-1126.

Li, H.L., Wang, H.H., Liu, S.J., Deng, Y.Q., Zhang, Y.J., Tian, Q., Wang, X.C., Chen, X.Q., Yang, Y., Zhang, J.Y., Wang, Q., Xu, H., Liao, F.F., Wang, J.Z., 2007. Phosphorylation of tau antagonizes apoptosis by stabilizing beta-catenin, a mechanism involved in Alzheimer's neurodegeneration. Proc Natl Acad Sci U S A 104, 3591-3596.

Liao, Y.D., Wang, S.C., Leu, Y.J., Wang, C.F., Chang, S.T., Hong, Y.T., Pan, Y.R., Chen, C., 2003. The structural integrity exerted by N-terminal pyroglutamate is crucial for the cytotoxicity of frog ribonuclease from *Rana pipiens*. Nucleic Acids Res 31, 5247-5255.

Lichty, J.J., Malecki, J.L., Agnew, H.D., Michelson-Horowitz, D.J., Tan, S., 2005. Comparison of affinity tags for protein purification. Protein Expr Purif 41, 98-105.

Lin, H., Bhatia, R., Lal, R., 2001. Amyloid beta protein forms ion channels: implications for Alzheimer's disease pathophysiology. Faseb J 15, 2433-2444.

Lin, S.Y., Duan, K.J., Lin, T.C., 1995. Direct or indirect skin lipid-ordering effect of pyrrolidone carboxylate sodium after topical treatment with penetration enhancers. Biomed Mater Eng 5, 9-20.

Linding, R., Russell, R.B., Neduva, V., Gibson, T.J., 2003. GlobPlot: Exploring protein sequences for globularity and disorder. Nucleic Acids Res 31, 3701-3708.

Lippa, C.F., Schmidt, M.L., Lee, V.M., Trojanowski, J.Q., 1999. Antibodies to alpha-synuclein detect Lewy bodies in many Down's syndrome brains with Alzheimer's disease. Ann Neurol 45, 353-357.

Littlechild, J.A., Guy, J., Connelly, S., Mallett, L., Waddell, S., Rye, C.A., Line, K., Isupov, M., 2007. Natural methods of protein stabilization: thermostable biocatalysts. Biochem Soc Trans 35, 1558-1563.

Liu, B., Moloney, A., Meehan, S., Morris, K., Thomas, S.E., Serpell, L.C., Hider, R., Marciniak, S.J., Lomas, D.A., Crowther, D.C., 2011. Iron promotes the toxicity of amyloid beta peptide by impeding its ordered aggregation. J Biol Chem 286, 4248-4256.

Lorenzo, A., Yuan, M., Zhang, Z., Paganetti, P.A., Sturchler-Pierrat, C., Staufenbiel, M., Mautino, J., Vigo, F.S., Sommer, B., Yankner, B.A., 2000. Amyloid beta interacts with the amyloid precursor protein: a potential toxic mechanism in Alzheimer's disease. Nat Neurosci 3, 460-464.

Los, G.V., Wood, K., 2007. The HaloTag: a novel technology for cell imaging and protein analysis. Methods Mol Biol 356, 195-208.

Love, S., Miners, S., Palmer, J., Chalmers, K., Kehoe, P., 2009. Insights into the pathogenesis and pathogenicity of cerebral amyloid angiopathy. Front Biosci 14, 4778-4792.

Lovell, S.C., Davis, I.W., Arendall, W.B., 3rd, de Bakker, P.I., Word, J.M., Prisant, M.G., Richardson, J.S., Richardson, D.C., 2003. Structure validation by Calpha geometry: phi,psi and Cbeta deviation. Proteins 50, 437-450.

Lu, D.C., Shaked, G.M., Masliah, E., Bredesen, D.E., Koo, E.H., 2003. Amyloid beta protein toxicity mediated by the formation of amyloid-beta protein precursor complexes. Ann Neurol 54, 781-789.

Luo, L., Yano, N., Mao, Q., Jackson, I.M., Stopa, E.G., 2002. Thyrotropin releasing hormone (TRH) in the hippocampus of Alzheimer patients. J Alzheimers Dis 4, 97-103.

Luo, Y., Bolon, B., Kahn, S., Bennett, B.D., Babu-Khan, S., Denis, P., Fan, W., Kha, H., Zhang, J., Gong, Y., Martin, L., Louis, J.C., Yan, Q., Richards, W.G., Citron, M., Vassar, R., 2001. Mice deficient in BACE1, the Alzheimer's beta-secretase, have normal phenotype and abolished beta-amyloid generation. Nat Neurosci 4, 231-232.

Ma, J., Yee, A., Brewer, H.B., Jr., Das, S., Potter, H., 1994. Amyloid-associated proteins alpha 1-antichymotrypsin and apolipoprotein E promote assembly of Alzheimer beta-protein into filaments. Nature 372, 92-94.

Maas, S., 1999. Efficient and rapid procedure for blue-white screening of recombinant bacterial clones. Biotechniques 27, 1126-1128.

Mackenzie, I.R., 1994. Senile plaques do not progressively accumulate with normal aging. Acta Neuropathol 87, 520-525.

Mackenzie, I.R., Hao, C., Munoz, D.G., 1995. Role of microglia in senile plaque formation. Neurobiol Aging 16, 797-804.

Mann, D.M., Yates, P.O., 1986. Neurotransmitter deficits in Alzheimer's disease and in other dementing disorders. Hum Neurobiol 5, 147-158.

Mantle, D., Lauffart, B., Perry, E.K., Perry, R.H., 1989. Comparison of major cortical aminopeptidase activity in normal brain and brain from patients with Alzheimer's disease. J Neurol Sci 89, 227-234.

Marsischky, G., LaBaer, J., 2004. Many paths to many clones: a comparative look at high-throughput cloning methods. Genome Res 14, 2020-2028.

Martinez, J.M., Ramirez, M.J., Prieto, I., Petzelt, C., Hermoso, F., Alba, F., Arias Saavedra, J.M., Ramirez, M., 1999. Human serum pyroglutamyl-beta-naphthylamide hydrolyzing activity during development and aging. Arch Gerontol Geriatr 28, 31-36.

Marty, J.P., 2002. [NMF and cosmetology of cutaneous hydration]. Ann Dermatol Venereol 129, 131-136.

Mattson, M.P., 1997. Cellular actions of beta-amyloid precursor protein and its soluble and fibrillogenic derivatives. Physiol Rev 77, 1081-1132.

Mattson, M.P., Cheng, B., Davis, D., Bryant, K., Lieberburg, I., Rydel, R.E., 1992. beta-Amyloid peptides destabilize calcium homeostasis and render human cortical neurons vulnerable to excitotoxicity. J Neurosci 12, 376-389.

Mawuenyega, K.G., Sigurdson, W., Ovod, V., Munsell, L., Kasten, T., Morris, J.C., Yarasheski, K.E., Bateman, R.J., 2010. Decreased clearance of CNS beta-amyloid in Alzheimer's disease. Science 330, 1774.

Mayeux, R., Tang, M.X., Jacobs, D.M., Manly, J., Bell, K., Merchant, C., Small, S.A., Stern, Y., Wisniewski, H.M., Mehta, P.D., 1999. Plasma amyloid beta-peptide 1-42 and incipient Alzheimer's disease. Ann Neurol 46, 412-416.

Maynard, C.J., Cappai, R., Volitakis, I., Cherny, R.A., White, A.R., Beyreuther, K., Masters, C.L., Bush, A.I., Li, Q.X., 2002. Overexpression of Alzheimer's disease amyloid-beta opposes the age-dependent elevations of brain copper and iron. J Biol Chem 277, 44670-44676.

McAllister, C., Long, J., Bowers, A., Walker, A., Cao, P., Honda, S., Harada, N., Staufenbiel, M., Shen, Y., Li, R., 2010. Genetic targeting aromatase in male amyloid precursor protein transgenic mice down-regulates beta-secretase (BACE1) and prevents Alzheimer-like pathology and cognitive impairment. J Neurosci 30, 7326-7334.

McGowan, S., Porter, C.J., Lowther, J., Stack, C.M., Golding, S.J., Skinner-Adams, T.S., Trenholme, K.R., Teuscher, F., Donnelly, S.M., Grembecka, J., Mucha, A., Kafarski, P., Degori, R., Buckle, A.M., Gardiner, D.L., Whisstock, J.C., Dalton, J.P., 2009. Structural basis for the inhibition of the essential *Plasmodium falciparum* M1 neutral aminopeptidase. Proc Natl Acad Sci U S A 106, 2537-2542.

Menendez-Gonzalez, M., Perez-Pinera, P., Martinez-Rivera, M., Calatayud, M.T., Blazquez Menes, B., 2005. APP processing and the APP-KPI domain involvement in the amyloid cascade. Neurodegener Dis 2, 277-283.

Mi, W., Li, L., Su, X.D., 2008. 5,5′-Dithio-bis(2-nitrobenzoic acid) modification of cysteine improves the crystal quality of human chloride intracellular channel protein 2. Biochem Biophys Res Commun 368, 919-922.

Michikawa, M., Fan, Q.W., Isobe, I., Yanagisawa, K., 2000. Apolipoprotein E exhibits isoform-specific promotion of lipid efflux from astrocytes and neurons in culture. J Neurochem 74, 1008-1016.

Miller, D.L., Papayannopoulos, I.A., Styles, J., Bobin, S.A., Lin, Y.Y., Biemann, K., Iqbal, K., 1993. Peptide compositions of the cerebrovascular and senile plaque core amyloid deposits of Alzheimer's disease. Arch Biochem Biophys 301, 41-52.

Minicozzi, V., Stellato, F., Comai, M., Serra, M.D., Potrich, C., Meyer-Klaucke, W., Morante, S., 2008. Identifying the minimal copper- and zinc-binding site sequence in amyloid-beta peptides. J Biol Chem 283, 10784-10792.

Minniti, A.N., Rebolledo, D.L., Grez, P.M., Fadic, R., Aldunate, R., Volitakis, I., Cherny, R.A., Opazo, C., Masters, C., Bush, A.I., Inestrosa, N.C., 2009. Intracellular

amyloid formation in muscle cells of Abeta-transgenic *Caenorhabditis elegans*: determinants and physiological role in copper detoxification. Mol Neurodegener 4, 2.

Mirzaei, M., Jardin, B., Elias, C.B., Prakash, S., 2008. Expression and production of human interleukin-7 in insect cells using baculovirus expression vector system (BEVS). Appl Biochem Biotechnol 151, 93-103.

Miyakawa, T., Shimoji, A., Kuramoto, R., Higuchi, Y., 1982. The relationship between senile plaques and cerebral blood vessels in Alzheimer's disease and senile dementia. Morphological mechanism of senile plaque production. Virchows Arch B Cell Pathol Incl Mol Pathol 40, 121-129.

Mohamed, A., Posse de Chaves, E., 2011. Abeta internalization by neurons and glia. Int J Alzheimers Dis 2011, 127984.

Monsuur, A.J., Stepniak, D., Diosdado, B., Wapenaar, M.C., Mearin, M.L., Koning, F., Wijmenga, C., 2006. Genetic and functional analysis of pyroglutamyl-peptidase I in coeliac disease. Eur J Gastroenterol Hepatol 18, 637-644.

Morley, J.E., Farr, S.A., Banks, W.A., Johnson, S.N., Yamada, K.A., Xu, L., 2010. A physiological role for amyloid-beta protein:enhancement of learning and memory. J Alzheimers Dis 19, 441-449.

Moss, J., Bundgaard, H., 1992. Prodrugs of peptides. 19. Protection of the pyroglutamyl residue against pyroglutamyl aminopeptidase by N-acyloxymethylation and other means. Acta Pharm Nord 4, 301-308.

Moya, K.L., Benowitz, L.I., Schneider, G.E., Allinquant, B., 1994. The amyloid precursor protein is developmentally regulated and correlated with synaptogenesis. Dev Biol 161, 597-603.

Mtawae, K., O'Connor, B., Ó'Fagain, C. (Eds.), 2008. Stability and Kinetic Studies on recombinant human Pyroglutamyl Peptidase I and a single site variant, Y147F. In Biotechnology: Research ,Technology & Applications. Nova Science Publishers.

Mudge, A.W., Fellows, R.E., 1973. Bovine pituitary pyrrolidonecarboxylyl peptidase. Endocrinology 93, 1428-1434.

Mulczyk, M., Szewczuk, A., 1970. Pyrrolidonyl peptidase in bacteria: a new colorimetric test for differentiation of enterobacteriaceae. J Gen Microbiol 61, 9-13.

Mulczyk, M., Szewczuk, A., 1972. Pyrrolidonyl peptidase activity: a simple test for differentiating staphylococci. J Gen Microbiol 70, 383-384.

Mullan, M., Crawford, F., Axelman, K., Houlden, H., Lilius, L., Winblad, B., Lannfelt, L., 1992. A pathogenic mutation for probable Alzheimer's disease in the APP gene at the N-terminus of beta-amyloid. Nat Genet 1, 345-347.

Mungas, D., Reed, B.R., Jagust, W.J., DeCarli, C., Mack, W.J., Kramer, J.H., Weiner, M.W., Schuff, N., Chui, H.C., 2002. Volumetric MRI predicts rate of cognitive decline related to AD and cerebrovascular disease. Neurology 59, 867-873.

Munoz, D.G., Feldman, H., 2000. Causes of Alzheimer's disease. Cmaj 162, 65-72.

Munoz, D.G., Woulfe, J., Kertesz, A., 2007. Argyrophilic thorny astrocyte clusters in association with Alzheimer's disease pathology in possible primary progressive aphasia. Acta Neuropathol 114, 347-357.

Muraki, M., 2008. Improved secretion of human Fas ligand extracellular domain by N-terminal part truncation in *Pichia pastoris* and preparation of the N-linked carbohydrate chain trimmed derivative. Protein Expr Purif 60, 205-213.

Murdoch, B.E., 2010. Acquired speech and language disorders : a neuroanatomical and functional neurological approach. Wiley-Blackwell ; Chichester : John Wiley [distributor], Hoboken, N.J.

Nagele, R.G., D'Andrea, M.R., Lee, H., Venkataraman, V., Wang, H.Y., 2003. Astrocytes accumulate A beta 42 and give rise to astrocytic amyloid plaques in Alzheimer disease brains. Brain Res 971, 197-209.

Nalivaeva, N.N., Fisk, L.R., Belyaev, N.D., Turner, A.J., 2008. Amyloid-degrading enzymes as therapeutic targets in Alzheimer's disease. Curr Alzheimer Res 5, 212-224.

Namba, Y., Tomonaga, M., Kawasaki, H., Otomo, E., Ikeda, K., 1991. Apolipoprotein E immunoreactivity in cerebral amyloid deposits and neurofibrillary tangles in Alzheimer's disease and kuru plaque amyloid in Creutzfeldt-Jakob disease. Brain Res 541, 163-166.

Navarrete Santos, A., Wulfanger, J., Helbing, G., Blosz, T., Langner, J., Riemann, D., 2002. Two C-terminal cysteines are necessary for proper folding of the peptidase neprilysin/CD10. Biochem Biophys Res Commun 295, 423-427.

Nettleship, J.E., Assenberg, R., Diprose, J.M., Rahman-Huq, N., Owens, R.J., 2010. Recent advances in the production of proteins in insect and mammalian cells for structural biology. J Struct Biol 172, 55-65.

Nettleship, J.E., Rahman-Huq, N., Owens, R.J., 2009. The production of glycoproteins by transient expression in Mammalian cells. Methods Mol Biol 498, 245-263.

Newman, J., 2004. Novel buffer systems for macromolecular crystallization. Acta Crystallogr D Biol Crystallogr 60, 610-612.

Niedziela-Majka, A., Rymarczyk, G., Kochman, M., Ozyhar, A., 1998. GST-Induced dimerization of DNA-binding domains alters characteristics of their interaction with DNA. Protein Expr Purif 14, 208-220.

Niesen, F.H., Berglund, H., Vedadi, M., 2007. The use of differential scanning fluorimetry to detect ligand interactions that promote protein stability. Nat Protoc 2, 2212-2221.

Nikolaev, A., McLaughlin, T., O'Leary, D.D., Tessier-Lavigne, M., 2009. APP binds DR6 to trigger axon pruning and neuron death via distinct caspases. Nature 457, 981-989.

Niwa, K., Porter, V.A., Kazama, K., Cornfield, D., Carlson, G.A., Iadecola, C., 2001. A beta-peptides enhance vasoconstriction in cerebral circulation. Am J Physiol Heart Circ Physiol 281, H2417-2424.

Nordberg, A., 1996. Application of PET in dementia disorders. Acta Neurol Scand Suppl 168, 71-76.

Nordberg, A., Rinne, J.O., Kadir, A., Langstrom, B., 2010. The use of PET in Alzheimer disease. Nat Rev Neurol 6, 78-87.

O'Connor, B., O'Cuinn, G., 1984. Localization of a narrow-specificity thyroliberin hydrolyzing pyroglutamate aminopeptidase in synaptosomal membranes of guinea-pig brain. Eur J Biochem 144, 271-278.

O'Cuinn, G., O'Connor, B., Elmore, M., 1990. Degradation of thyrotropin-releasing hormone and luteinising hormone-releasing hormone by enzymes of brain tissue. J Neurochem 54, 1-13.

O'Harte, F.P., Gault, V.A., Parker, J.C., Harriott, P., Mooney, M.H., Bailey, C.J., Flatt, P.R., 2002. Improved stability, insulin-releasing activity and antidiabetic potential of two novel N-terminal analogues of gastric inhibitory polypeptide: N-acetyl-GIP and pGlu-GIP. Diabetologia 45, 1281-1291.

O'Leary, R.M., O'Connor, B., 1995. A study of a synaptosomal thyrotropin releasing hormone-inactivating pyroglutamate aminopeptidase from bovine brain. Int J Biochem Cell Biol 27, 881-890.

Odagaki, Y., Hayashi, A., Okada, K., Hirotsu, K., Kabashima, T., Ito, K., Yoshimoto, T., Tsuru, D., Sato, M., Clardy, J., 1999. The crystal structure of pyroglutamyl peptidase I from *Bacillus amyloliquefaciens* reveals a new structure for a cysteine protease. Structure 7, 399-411.

Ogasahara, K., Khechinashvili, N.N., Nakamura, M., Yoshimoto, T., Yutani, K., 2001. Thermal stability of pyrrolidone carboxyl peptidases from the hyperthermophilic Archaeon, *Pyrococcus furiosus*. Eur J Biochem 268, 3233-3242.

Ohno, M., Cole, S.L., Yasvoina, M., Zhao, J., Citron, M., Berry, R., Disterhoft, J.F., Vassar, R., 2007. BACE1 gene deletion prevents neuron loss and memory deficits in 5XFAD APP/PS1 transgenic mice. Neurobiol Dis 26, 134-145.

Ohno, M., Sametsky, E.A., Younkin, L.H., Oakley, H., Younkin, S.G., Citron, M., Vassar, R., Disterhoft, J.F., 2004. BACE1 deficiency rescues memory deficits and cholinergic dysfunction in a mouse model of Alzheimer's disease. Neuron 41, 27-33.

Ohsawa, I., Takamura, C., Morimoto, T., Ishiguro, M., Kohsaka, S., 1999. Amino-terminal region of secreted form of amyloid precursor protein stimulates proliferation of neural stem cells. Eur J Neurosci 11, 1907-1913.

Opazo, C., Huang, X., Cherny, R.A., Moir, R.D., Roher, A.E., White, A.R., Cappai, R., Masters, C.L., Tanzi, R.E., Inestrosa, N.C., Bush, A.I., 2002. Metalloenzyme-like activity of Alzheimer's disease beta-amyloid. Cu-dependent catalytic conversion of dopamine, cholesterol, and biological reducing agents to neurotoxic H(2)O(2). J Biol Chem 277, 40302-40308.

Orlowski, M., Meister, A., 1971. Partial reactions catalyzed by –glutamylcysteine synthetase and evidence for an activated glutamate intermediate. J Biol Chem 246, 7095-7105.

Oshimura, E., Abe, H., Oota, R., 2007. Hair and amino acids: the interactions and the effects. J Cosmet Sci 58, 347-357.

Oubridge, C., Ito, N., Teo, C.H., Fearnley, I., Nagai, K., 1995. Crystallisation of RNA-protein complexes. II. The application of protein engineering for crystallisation of the U1A protein-RNA complex. J Mol Biol 249, 409-423.

Pace, C.N., Trevino, S., Prabhakaran, E., Scholtz, J.M., 2004. Protein structure, stability and solubility in water and other solvents. Philos Trans R Soc Lond B Biol Sci 359, 1225-1234; discussion 1234-1225.

Panchal, M., Loeper, J., Cossec, J.C., Perruchini, C., Lazar, A., Pompon, D., Duyckaerts, C., 2010. Enrichment of cholesterol in microdissected Alzheimer's disease senile plaques as assessed by mass spectrometry. J Lipid Res 51, 598-605.

Pantoliano, M.W., Petrella, E.C., Kwasnoski, J.D., Lobanov, V.S., Myslik, J., Graf, E., Carver, T., Asel, E., Springer, B.A., Lane, P., Salemme, F.R., 2001. High-density miniaturized thermal shift assays as a general strategy for drug discovery. J Biomol Screen 6, 429-440.

Papadopoulos, T., Heuer, H., Bauer, K., 2000. Analysis of the thyrotropin-releasing hormone-degrading ectoenzyme by site-directed mutagenesis of cysteine residues. Cys68 is involved in disulfide-linked dimerization. Eur J Biochem 267, 2617-2623.

Papadopoulos, T., Kelly, J.A., Bauer, K., 2001. Mutational analysis of the thyrotropin-releasing hormone-degrading ectoenzyme. similarities and differences with other members of the M1 family of aminopeptidases and thermolysin. Biochemistry 40, 9347-9355.

Park, C.B., Lee, S.B., Ryu, D.D., 2001. L-pyroglutamate spontaneously formed from L-glutamate inhibits growth of the hyperthermophilic archaeon *Sulfolobus solfataricus*. Appl Environ Microbiol 67, 3650-3654.

Park, C.B., Ryu, D.D., Lee, S.B., 2003. Inhibitory effect of L-pyroglutamate on extremophiles: correlation with growth temperature and pH. FEMS Microbiol Lett 221, 187-190.

Pederzolli, C.D., Sgaravatti, A.M., Braum, C.A., Prestes, C.C., Zorzi, G.K., Sgarbi, M.B., Wyse, A.T., Wannmacher, C.M., Wajner, M., Dutra-Filho, C.S., 2007. 5-Oxoproline reduces non-enzymatic antioxidant defenses in vitro in rat brain. Metab Brain Dis 22, 51-65.

Peillon, F., Le Dafniet, M., Pagesy, P., Li, J.Y., Benlot, C., Brandi, A.M., Joubert, D., 1991. Neuropeptides of anterior pituitary origin. Autocrine or paracrine functions? Pathol Res Pract 187, 577-580.

Perlman, J.H., Thaw, C.N., Laakkonen, L., Bowers, C.Y., Osman, R., Gershengorn, M.C., 1994. Hydrogen bonding interaction of thyrotropin-releasing hormone (TRH) with transmembrane tyrosine 106 of the TRH receptor. J Biol Chem 269, 1610-1613.

Petkova, A.T., Ishii, Y., Balbach, J.J., Antzutkin, O.N., Leapman, R.D., Delaglio, F., Tycko, R., 2002. A structural model for Alzheimer's beta –amyloid fibrils based on experimental constraints from solid state NMR. Proc Natl Acad Sci U S A 99, 16742-16747.

Pezzini, A., Del Zotto, E., Volonghi, I., Giossi, A., Costa, P., Padovani, A., 2009. Cerebral amyloid angiopathy: a common cause of cerebral hemorrhage. Curr Med Chem 16, 2498-2513.

Piccini, A., Russo, C., Gliozzi, A., Relini, A., Vitali, A., Borghi, R., Giliberto, L., Armirotti, A., D'Arrigo, C., Bachi, A., Cattaneo, A., Canale, C., Torrassa, S., Saido, T.C., Markesbery, W., Gambetti, P., Tabaton, M., 2005. beta-amyloid is different in normal aging and in Alzheimer disease. J Biol Chem 280, 34186-34192.

Plant, L.D., Boyle, J.P., Smith, I.F., Peers, C., Pearson, H.A., 2003. The production of amyloid beta peptide is a critical requirement for the viability of central neurons. J Neurosci 23, 5531-5535.

Plant, L.D., Webster, N.J., Boyle, J.P., Ramsden, M., Freir, D.B., Peers, C., Pearson, H.A., 2006. Amyloid beta peptide as a physiological modulator of neuronal 'A'-type K+ current. Neurobiol Aging 27, 1673-1683.

Poduslo, J.F., Gilles, E.J., Ramakrishnan, M., Howell, K.G., Wengenack, T.M., Curran, G.L., Kandimalla, K.K., 2010. HH domain of Alzheimer's disease Abeta provides structural basis for neuronal binding in PC12 and mouse cortical/hippocampal neurons. PLoS One 5, e8813.

Polak, J.M., Van Noorden, S., 2003. Introduction to immunocytochemistry. BIOS Scientific Publishers, Oxford.

Popescu, A., Lippa, C.F., Lee, V.M., Trojanowski, J.Q., 2004. Lewy bodies in the amygdala: increase of alpha-synuclein aggregates in neurodegenerative diseases with tau-based inclusions. Arch Neurol 61, 1915-1919.

Prasad, C., 1987. Activation/inactivation of rat tissue pyroglutamate aminopeptidase by disulfide bond-reducing agents. Neuropeptides 9, 211-215.

Proteau, A., Shi, R., Cygler, M., 2010. Application of dynamic light scattering in protein crystallization. Curr Protoc Protein Sci Chapter 17, Unit 17 10.

Puzzo, D., Privitera, L., Leznik, E., Fa, M., Staniszewski, A., Palmeri, A., Arancio, O., 2008. Picomolar amyloid-beta positively modulates synaptic plasticity and memory in hippocampus. J Neurosci 28, 14537-14545.

Qian, W., Yin, X., Hu, W., Shi, J., Gu, J., Grundke-Iqbal, I., Iqbal, K., Gong, C.X., Liu, F., 2011. Activation of protein phosphatase 2B and hyperphosphorylation of Tau in Alzheimer's disease. J Alzheimers Dis 23, 617-627.

Quist, A., Doudevski, I., Lin, H., Azimova, R., Ng, D., Frangione, B., Kagan, B., Ghiso, J., Lal, R., 2005. Amyloid ion channels: a common structural link for protein-misfolding disease. Proc Natl Acad Sci U S A 102, 10427-10432.

Raina, A.K., Hochman, A., Zhu, X., Rottkamp, C.A., Nunomura, A., Siedlak, S.L., Boux, H., Castellani, R.J., Perry, G., Smith, M.A., 2001. Abortive apoptosis in Alzheimer's disease. Acta Neuropathol 101, 305-310.

Rajendran, L., Honsho, M., Zahn, T.R., Keller, P., Geiger, K.D., Verkade, P., Simons, K., 2006. Alzheimer's disease beta-amyloid peptides are released in association with exosomes. Proc Natl Acad Sci U S A 103, 11172-11177.

Ramirez-Exposito, M.J., Robert-Baudouy, J., Mayas, M.D., Garcia, M.J., Ramirez, M., Martinez-Martos, J.M., 2001. Acetylcholinesterase inhibitor SDZ ENA 713 (Rivastigmine) increases brain pyrrolidone carboxyl peptidase activity. Eur Neuropsychopharmacol 11, 381-383.

Ramos-Vara, J.A., 2005. Technical aspects of immunohistochemistry. Vet Pathol 42, 405-426.

Rawlings, N.D., Barrett, A.J., 1995. Evolutionary families of metallopeptidases. Methods Enzymol 248, 183-228.

Rawlings, N.D., Barrett, A.J., Bateman, A., 2010. MEROPS: the peptidase database. Nucleic Acids Res 38, D227-233.

Ray, K., Hines, C.S., Rodgers, D.W., 2002. Mapping sequence differences between thimet oligopeptidase and neurolysin implicates key residues in substrate recognition. Protein Sci 11, 2237-2246.

Rayment, I., 1997. Reductive alkylation of lysine residues to alter crystallization properties of proteins. Methods Enzymol 276, 171-179.

Rayment, I., Rypniewski, W.R., Schmidt-Base, K., Smith, R., Tomchick, D.R., Benning, M.M., Winkelmann, D.A., Wesenberg, G., Holden, H.M., 1993. Three-dimensional structure of myosin subfragment-1: a molecular motor. Science 261, 50-58.

Razak, K., Newland, A.C., 1992. Induction of CD13 expression on fresh myeloid leukaemia: correlation of CD13 expression with aminopeptidase-N activity. Leuk Res 16, 625-630.

Richards, F.M., 1997. Protein stability: still an unsolved problem. Cell Mol Life Sci 53, 790-802.

Ring, S., Weyer, S.W., Kilian, S.B., Waldron, E., Pietrzik, C.U., Filippov, M.A., Herms, J., Buchholz, C., Eckman, C.B., Korte, M., Wolfer, D.P., Muller, U.C., 2007. The secreted beta-amyloid precursor protein ectodomain APPs alpha is sufficient to rescue the anatomical, behavioral, and electrophysiological abnormalities of APP-deficient mice. J Neurosci 27, 7817-7826.

Roberts, S.B., Ripellino, J.A., Ingalls, K.M., Robakis, N.K., Felsenstein, K.M., 1994. Non-amyloidogenic cleavage of the beta-amyloid precursor protein by an integral membrane metalloendopeptidase. J Biol Chem 269, 3111-3116.

Rogan, S., Lippa, C.F., 2002. Alzheimer's disease and other dementias: a review. Am J Alzheimers Dis Other Demen 17, 11-17.

Rogers, J., Strohmeyer, R., Kovelowski, C.J., Li, R., 2002. Microglia and inflammatory mechanisms in the clearance of amyloid beta peptide. Glia 40, 260-269.

Rohan de Silva, H.A., Jen, A., Wickenden, C., Jen, L.S., Wilkinson, S.L., Patel, A.J., 1997. Cell-specific expression of beta-amyloid precursor protein isoform mRNAs and proteins in neurons and astrocytes. Brain Res Mol Brain Res 47, 147-156.

Roitt, I.M., Delves, P.J., 2001. Roitt's essential immunology. Blackwell Science, Oxford.

Rozenfeld, R., Muller, L., El Messari, S., Llorens-Cortes, C., 2004. The C-terminal domain of aminopeptidase A is an intramolecular chaperone required for the correct folding, cell surface expression, and activity of this monozinc aminopeptidase. J Biol Chem 279, 43285-43295.

Rozengurt, E., 2002. Neuropeptides as growth factors for normal and cancerous cells. Trends Endocrinol Metab 13, 128-134.

Rudberg, P.C., Tholander, F., Andberg, M., Thunnissen, M.M., Haeggstrom, J.Z., 2004. Leukotriene A4 hydrolase: identification of a common carboxylate recognition site for the epoxide hydrolase and aminopeptidase substrates. J Biol Chem 279, 27376-27382.

Russo, C., Schettini, G., Saido, T.C., Hulette, C., Lippa, C., Lannfelt, L., Ghetti, B., Gambetti, P., Tabaton, M., Teller, J.K., 2000. Presenilin-1 mutations in Alzheimer's disease. Nature 405, 531-532.

Russo, C., Violani, E., Salis, S., Venezia, V., Dolcini, V., Damonte, G., Benatti, U., D'Arrigo, C., Patrone, E., Carlo, P., Schettini, G., 2002. Pyroglutamate-modified amyloid beta-peptides--AbetaN3(pE)--strongly affect cultured neuron and astrocyte survival. J Neurochem 82, 1480-1489.

Saido, T.C., 2000. Involvement of polyglutamine endolysis followed by pyroglutamate formation in the pathogenesis of triplet repeat/polyglutamine-expansion diseases. Med Hypotheses 54, 427-429.

Saido, T.C., Iwatsubo, T., Mann, D.M., Shimada, H., Ihara, Y., Kawashima, S., 1995. Dominant and differential deposition of distinct beta-amyloid peptide species, A beta N3(pE), in senile plaques. Neuron 14, 457-466.

Saido, T.C., Yamao-Harigaya, W., Iwatsubo, T., Kawashima, S., 1996. Amino- and carboxyl-terminal heterogeneity of beta-amyloid peptides deposited in human brain. Neurosci Lett 215, 173-176.

Sambrook, J., Fritsch, E.F., Maniatis, T., 1989. Molecular cloning. Cold Spring Harbor Laboratory Press, Cold Spring Harbor, N.Y.

Sanan, D.A., Weisgraber, K.H., Russell, S.J., Mahley, R.W., Huang, D., Saunders, A., Schmechel, D., Wisniewski, T., Frangione, B., Roses, A.D., et al., 1994. Apolipoprotein E associates with beta amyloid peptide of Alzheimer's disease to form novel monofibrils. Isoform apoE4 associates more efficiently than apoE3. J Clin Invest 94, 860-869.

Sanchez, B., Alba, F., Luna, J.D., Martinez, J.M., Prieto, I., Ramirez, M., 1996. Pyroglutamyl peptidase I levels and their left-right distribution in the rat retina and hypothalamus are influenced by light-dark conditions. Brain Res 731, 254-257.

Sandbrink, R., Hartmann, T., Masters, C.L., Beyreuther, K., 1996. Genes contributing to Alzheimer's disease. Mol Psychiatry 1, 27-40.

Sanger, F., Thompson, E.O., Kitai, R., 1955. The amide groups of insulin. Biochem J 59, 509-518.

Scahill, R.I., Frost, C., Jenkins, R., Whitwell, J.L., Rossor, M.N., Fox, N.C., 2003. A longitudinal study of brain volume changes in normal aging using serial registered magnetic resonance imaging. Arch Neurol 60, 989-994.

Scheuner, D., Eckman, C., Jensen, M., Song, X., Citron, M., Suzuki, N., Bird, T.D., Hardy, J., Hutton, M., Kukull, W., Larson, E., Levy-Lahad, E., Viitanen, M., Peskind, E., Poorkaj, P., Schellenberg, G., Tanzi, R., Wasco, W., Lannfelt, L., Selkoe, D., Younkin, S., 1996. Secreted amyloid beta-protein similar to that in the senile plaques of Alzheimer's disease is increased in vivo by the presenilin 1 and 2 and APP mutations linked to familial Alzheimer's disease. Nat Med 2, 864-870.

Schilling, S., Appl, T., Hoffmann, T., Cynis, H., Schulz, K., Jagla, W., Friedrich, D., Wermann, M., Buchholz, M., Heiser, U., von Horsten, S., Demuth, H.U., 2008a. Inhibition of glutaminyl cyclase prevents pGlu-Abeta formation after intracortical/hippocampal microinjection in vivo/in situ. J Neurochem 106, 1225-1236.

Schilling, S., Hoffmann, T., Manhart, S., Hoffmann, M., Demuth, H.U., 2004. Glutaminyl cyclases unfold glutamyl cyclase activity under mild acid conditions. FEBS Lett 563, 191-196.

Schilling, S., Lauber, T., Schaupp, M., Manhart, S., Scheel, E., Bohm, G., Demuth, H.U., 2006. On the seeding and oligomerization of pGlu-amyloid peptides (in vitro). Biochemistry 45, 12393-12399.

Schilling, S., Manhart, S., Hoffmann, T., Ludwig, H.H., Wasternack, C., Demuth, H.U., 2003. Substrate specificity of glutaminyl cyclases from plants and animals. Biol Chem 384, 1583-1592.

Schilling, S., Zeitschel, U., Hoffmann, T., Heiser, U., Francke, M., Kehlen, A., Holzer, M., Hutter-Paier, B., Prokesch, M., Windisch, M., Jagla, W., Schlenzig, D., Lindner, C., Rudolph, T., Reuter, G., Cynis, H., Montag, D., Demuth, H.U., Rossner, S., 2008b. Glutaminyl cyclase inhibition attenuates pyroglutamate Abeta and Alzheimer's disease-like pathology. Nat Med 14, 1106-1111.

Schlenzig, D., Manhart, S., Cinar, Y., Kleinschmidt, M., Hause, G., Willbold, D., Funke, S.A., Schilling, S., Demuth, H.U., 2009. Pyroglutamate formation influences solubility and amyloidogenicity of amyloid peptides. Biochemistry 48, 7072-7078.

Schmitmeier, S., Thole, H., Bader, A., Bauer, K., 2002. Purification and characterization of the thyrotropin-releasing hormone (TRH)-degrading serum enzyme and its identification as a product of liver origin. Eur J Biochem 269, 1278-1286.

Schomburg, L., Bauer, K., 1995. Thyroid hormones rapidly and stringently regulate the messenger RNA levels of the thyrotropin-releasing hormone (TRH) receptor and the TRH-degrading ectoenzyme. Endocrinology 136, 3480-3485.

Schomburg, L., Turwitt, S., Prescher, G., Lohmann, D., Horsthemke, B., Bauer, K., 1999. Human TRH-degrading ectoenzyme cDNA cloning, functional expression, genomic structure and chromosomal assignment. Eur J Biochem 265, 415-422.

Schott, J.M., Price, S.L., Frost, C., Whitwell, J.L., Rossor, M.N., Fox, N.C., 2005. Measuring atrophy in Alzheimer disease: a serial MRI study over 6 and 12 months. Neurology 65, 119-124.

Selkoe, D.J., 1993. Physiological production of the beta-amyloid protein and the mechanism of Alzheimer's disease. Trends Neurosci 16, 403-409.

Selkoe, D.J., 2001. Alzheimer's disease: genes, proteins, and therapy. Physiol Rev 81, 741-766.

Seltzer, B., Sherwin, I., 1983. A comparison of clinical features in early- and late-onset primary degenerative dementia. One entity or two? Arch Neurol 40, 143-146.

Seubert, P., Vigo-Pelfrey, C., Esch, F., Lee, M., Dovey, H., Davis, D., Sinha, S., Schlossmacher, M., Whaley, J., Swindlehurst, C., et al., 1992. Isolation and quantification of soluble Alzheimer's beta-peptide from biological fluids. Nature 359, 325-327.

Sevalle, J., Amoyel, A., Robert, P., Fournie-Zaluski, M.C., Roques, B., Checler, F., 2009. Aminopeptidase A contributes to the N-terminal truncation of amyloid beta-peptide. J Neurochem 109, 248-256.

Shaw, P.J., Ince, P.G., Falkous, G., Mantle, D., 1996. Cytoplasmic, lysosomal and matrix protease activities in spinal cord tissue from amyotrophic lateral sclerosis (ALS) and control patients. J Neurol Sci 139 Suppl, 71-75.

Shimada, Y., Nakamura, M., Naito, Y., Nomura, K., Ohno-Iwashita, Y., 1999. C-terminal amino acid residues are required for the folding and cholesterol binding property of perfringolysin O, a pore-forming cytolysin. J Biol Chem 274, 18536-18542.

Shimizu, T., Watanabe, A., Ogawara, M., Mori, H., Shirasawa, T., 2000. Isoaspartate formation and neurodegeneration in Alzheimer's disease. Arch Biochem Biophys 381, 225-234.

Shrestha, B., Smee, C., Gileadi, O., 2008. Baculovirus expression vector system: an emerging host for high-throughput eukaryotic protein expression. Methods Mol Biol 439, 269-289.

Sidera, C., Liu, C., Austen, B., 2002. Pro-domain removal in ASP-2 and the cleavage of the amyloid precursor are influenced by pH. BMC Biochem 3, 25.

Sigman, J.A., Sharky, M.L., Walsh, S.T., Pabon, A., Glucksman, M.J., Wolfson, A.J., 2003. Involvement of surface cysteines in activity and multimer formation of thimet oligopeptidase. Protein Eng 16, 623-628.

Sigurdsson, E.M., Permanne, B., Soto, C., Wisniewski, T., Frangione, B., 2000. In vivo reversal of amyloid-beta lesions in rat brain. J Neuropathol Exp Neurol 59, 11-17.

Silva, A.R., Silva, C.G., Ruschel, C., Helegda, C., Wyse, A.T., Wannmacher, C.M., Wajner, M., Dutra-Filho, C.S., 2001. L-pyroglutamic acid inhibits energy production and lipid synthesis in cerebral cortex of young rats in vitro. Neurochem Res 26, 1277-1283.

Singleton, M., Isupov, M., Littlechild, J., 1999. X-ray structure of pyrrolidone carboxyl peptidase from the hyperthermophilic archaeon *Thermococcus litoralis*. Structure 7, 237-244.

Sinha, S., Anderson, J.P., Barbour, R., Basi, G.S., Caccavello, R., Davis, D., Doan, M., Dovey, H.F., Frigon, N., Hong, J., Jacobson-Croak, K., Jewett, N., Keim, P., Knops, J., Lieberburg, I., Power, M., Tan, H., Tatsuno, G., Tung, J., Schenk, D., Seubert, P., Suomensaari, S.M., Wang, S., Walker, D., Zhao, J., McConlogue, L., John, V., 1999. Purification and cloning of amyloid precursor protein beta-secretase from human brain. Nature 402, 537-540.

Sisodia, S.S., 1992. Beta-amyloid precursor protein cleavage by a membrane-bound protease. Proc Natl Acad Sci U S A 89, 6075-6079.

Small, D.H., Clarris, H.L., Williamson, T.G., Reed, G., Key, B., Mok, S.S., Beyreuther, K., Masters, C.L., Nurcombe, V., 1999. Neurite-outgrowth regulating functions of the amyloid protein precursor of Alzheimer's disease. J Alzheimers Dis 1, 275-285.

Soba, P., Eggert, S., Wagner, K., Zentgraf, H., Siehl, K., Kreger, S., Lower, A., Langer, A., Merdes, G., Paro, R., Masters, C.L., Muller, U., Kins, S., Beyreuther, K., 2005. Homo- and heterodimerization of APP family members promotes intercellular adhesion. Embo J 24, 3624-3634.

Sokabe, M., Kawamura, T., Sakai, N., Yao, M., Watanabe, N., Tanaka, I., 2002. The X-ray crystal structure of pyrrolidone-carboxylate peptidase from hyperthermophilic archaea *Pyrococcus horikoshii*. J Struct Funct Genomics 2, 145-154.

Solans, A., Estivill, X., de La Luna, S., 2000. A new aspartyl protease on 21q22.3, BACE2, is highly similar to Alzheimer's amyloid precursor protein beta-secretase. Cytogenet Cell Genet 89, 177-184.

Soto, C., Kascsak, R.J., Saborio, G.P., Aucouturier, P., Wisniewski, T., Prelli, F., Kascsak, R., Mendez, E., Harris, D.A., Ironside, J., Tagliavini, F., Carp, R.I., Frangione, B., 2000. Reversion of prion protein conformational changes by synthetic beta-sheet breaker peptides. Lancet 355, 192-197.

Soto, C., Sigurdsson, E.M., Morelli, L., Kumar, R.A., Castano, E.M., Frangione, B., 1998. Beta-sheet breaker peptides inhibit fibrillogenesis in a rat brain model of amyloidosis: implications for Alzheimer's therapy. Nat Med 4, 822-826.

Spadaro, D., Yun, B.W., Spoel, S.H., Chu, C., Wang, Y.Q., Loake, G.J., 2010. The redox switch: dynamic regulation of protein function by cysteine modifications. Physiol Plant 138, 360-371.

Spadiut, O., Olsson, L., Brumer, H., 3rd, 2010. A comparative summary of expression systems for the recombinant production of galactose oxidase. Microb Cell Fact 9, 68.

Spignoli, G., Magnani, M., Giovannini, M.G., Pepeu, G., 1987. Effect of pyroglutamic acid stereoisomers on ECS and scopolamine-induced memory disruption and brain acetylcholine levels in the rat. Pharmacol Res Commun 19, 901-912.

Stadelmann, C., Deckwerth, T.L., Srinivasan, A., Bancher, C., Bruck, W., Jellinger, K., Lassmann, H., 1999. Activation of caspase-3 in single neurons and autophagic granules of granulovacuolar degeneration in Alzheimer's disease. Evidence for apoptotic cell death. Am J Pathol 155, 1459-1466.

Stellwagen, E., Prantner, J.D., Stellwagen, N.C., 2008. Do zwitterions contribute to the ionic strength of a solution? Anal Biochem 373, 407-409.

Stoltenberg, M., Bush, A.I., Bach, G., Smidt, K., Larsen, A., Rungby, J., Lund, S., Doering, P., Danscher, G., 2007. Amyloid plaques arise from zinc-enriched cortical layers in APP/PS1 transgenic mice and are paradoxically enlarged with dietary zinc deficiency. Neuroscience 150, 357-369.

Strittmatter, W.J., Saunders, A.M., Schmechel, D., Pericak-Vance, M., Enghild, J., Salvesen, G.S., Roses, A.D., 1993. Apolipoprotein E: high-avidity binding to beta-amyloid and increased frequency of type 4 allele in late-onset familial Alzheimer disease. Proc Natl Acad Sci U S A 90, 1977-1981.

Styner, M., Lieberman, J.A., McClure, R.K., Weinberger, D.R., Jones, D.W., Gerig, G., 2005. Morphometric analysis of lateral ventricles in schizophrenia and healthy controls regarding genetic and disease-specific factors. Proc Natl Acad Sci U S A 102, 4872-4877.

Suen, C.S., Wilk, S., 1989. Regulation of thyrotropin releasing hormone degrading enzymes in rat brain and pituitary by L-3,5,3′-triiodothyronine. J Neurochem 52, 884-888.

Summers, M.D., Anderson, D.L., 1972. Granulosis virus deoxyribonucleic acid: a closed, double-stranded molecule. J Virol 9, 710-713.

Szewczuk, A., Kwiatkowska, J., 1970. Pyrrolidonyl peptidase in animal, plant and human tissues. Occurrence and some properties of the enzyme. Eur J Biochem 15, 92-96.

Tamboli, I.Y., Barth, E., Christian, L., Siepmann, M., Kumar, S., Singh, S., Tolksdorf, K., Heneka, M.T., Lutjohann, D., Wunderlich, P., Walter, J., 2010. Statins promote the degradation of extracellular amyloid {beta}-peptide by microglia via stimulation of exosome-associated insulin-degrading enzyme (IDE) secretion. J Biol Chem 285, 37405-37414.

Tan, Z.S., Beiser, A., Vasan, R.S., Au, R., Auerbach, S., Kiel, D.P., Wolf, P.A., Seshadri, S., 2008. Thyroid function and the risk of Alzheimer disease: the Framingham Study. Arch Intern Med 168, 1514-1520.

Tanaka, H., Chinami, M., Mizushima, T., Ogasahara, K., Ota, M., Tsukihara, T., Yutani, K., 2001. X-ray crystalline structures of pyrrolidone carboxyl peptidase from a hyperthermophile, *Pyrococcus furiosus*, and its cys-free mutant. J Biochem 130, 107-118.

Taylor, W.L., Dixon, J.E., 1978. Characterization of a pyroglutamate aminopeptidase from rat serum that degrades thyrotropin-releasing hormone. J Biol Chem 253, 6934-6940.

Teipel, S.J., Flatz, W.H., Heinsen, H., Bokde, A.L., Schoenberg, S.O., Stockel, S., Dietrich, O., Reiser, M.F., Moller, H.J., Hampel, H., 2005. Measurement of basal forebrain atrophy in Alzheimer's disease using MRI. Brain 128, 2626-2644.

Thal, D.R., Capetillo-Zarate, E., Schultz, C., Rub, U., Saido, T.C., Yamaguchi, H., Haass, C., Griffin, W.S., Del Tredici, K., Braak, H., Ghebremedhin, E., 2005. Apolipoprotein E co-localizes with newly formed amyloid beta-protein (Abeta) deposits

lacking immunoreactivity against N-terminal epitopes of Abeta in a genotype-dependent manner. Acta Neuropathol 110, 459-471.

Thal, D.R., Griffin, W.S., de Vos, R.A., Ghebremedhin, E., 2008. Cerebral amyloid angiopathy and its relationship to Alzheimer's disease. Acta Neuropathol 115, 599-609.

Thal, D.R., Rub, U., Orantes, M., Braak, H., 2002. Phases of A beta-deposition in the human brain and its relevance for the development of AD. Neurology 58, 1791-1800.

Thal, L.J., Kantarci, K., Reiman, E.M., Klunk, W.E., Weiner, M.W., Zetterberg, H., Galasko, D., Pratico, D., Griffin, S., Schenk, D., Siemers, E., 2006. The role of biomarkers in clinical trials for Alzheimer disease. Alzheimer Dis Assoc Disord 20, 6-15.

Thomas, P., Smart, T.G., 2005. HEK293 cell line: a vehicle for the expression of recombinant proteins. J Pharmacol Toxicol Methods 51, 187-200.

Thompson, P.M., Dutton, R.A., Hayashi, K.M., Lu, A., Lee, S.E., Lee, J.Y., Lopez, O.L., Aizenstein, H.J., Toga, A.W., Becker, J.T., 2006. 3D mapping of ventricular and corpus callosum abnormalities in HIV/AIDS. Neuroimage 31, 12-23.

Thompson, P.M., Hayashi, K.M., De Zubicaray, G.I., Janke, A.L., Rose, S.E., Semple, J., Hong, M.S., Herman, D.H., Gravano, D., Doddrell, D.M., Toga, A.W., 2004. Mapping hippocampal and ventricular change in Alzheimer disease. Neuroimage 22, 1754-1766.

Tjernberg, L.O., Naslund, J., Lindqvist, F., Johansson, J., Karlstrom, A.R., Thyberg, J., Terenius, L., Nordstedt, C., 1996. Arrest of beta-amyloid fibril formation by a pentapeptide ligand. J Biol Chem 271, 8545-8548.

Tolnay, M., Probst, A., 1999. REVIEW: tau protein pathology in Alzheimer's disease and related disorders. Neuropathol Appl Neurobiol 25, 171-187.

Tomaselli, S., Esposito, V., Vangone, P., van Nuland, N.A., Bonvin, A.M., Guerrini, R., Tancredi, T., Temussi, P.A., Picone, D., 2006. The alpha-to-beta conformational transition of Alzheimer's Abeta-(1-42) peptide in aqueous media is reversible: a step by step conformational analysis suggests the location of beta conformation seeding. Chembiochem 7, 257-267.

Tritsch, G.L., Moore, G.E., 1962. Spontaneous decomposition of glutamine in cell culture media. Exp Cell Res 28, 360-364.

Trivedi, S., Gehlot, H.S., Rao, S.R., 2006. Protein thermostability in Archaea and Eubacteria. Genet Mol Res 5, 816-827.

Trojanowski, J.Q., Lee, V.M., 1995. Phosphorylation of paired helical filament tau in Alzheimer's disease neurofibrillary lesions: focusing on phosphatases. Faseb J 9, 1570-1576.

Tsuru, D., Fujiwara, K., Kado, K., 1978. Purification and characterization of L-pyrrolidonecarboxylate peptidase from *Bacillus amyloiliquefaciens*. J Biochem 84, 467-476.

Tsuru, D., Sakabe, K., Yoshimoto, T., Fujiwara, K., 1982. Pyroglutamyl peptidase from chicken liver: purification and some properties. J Pharmacobiodyn 5, 859-868.

Turner, A.J., Fisk, L., Nalivaeva, N.N., 2004. Targeting amyloid-degrading enzymes as therapeutic strategies in neurodegeneration. Ann N Y Acad Sci 1035, 1-20.

Tyler, S.J., Dawbarn, D., Wilcock, G.K., Allen, S.J., 2002. alpha- and beta-secretase: profound changes in Alzheimer's disease. Biochem Biophys Res Commun 299, 373-376.

Uchihara, T., Duyckaerts, C., Lazarini, F., Mokhtari, K., Seilhean, D., Amouyel, P., Hauw, J.J., 1996. Inconstant apolipoprotein E (ApoE)-like immunoreactivity in amyloid beta protein deposits: relationship with *apoε* genotype in aging brain and Alzheimer's disease. Acta Neuropathol 92, 180-185.

Uhlhaas, S., Lange, H., 1988. Striatal deficiency of L-pyroglutamic acid in Huntington's disease is accompanied by increased plasma levels. Brain Res 457, 196-199.

Uliana, J.A., Doolittle, R.F., 1969. Pyrrolidonecarboxylyl peptidase: studies on the specificity of the enzyme. Arch Biochem Biophys 131, 561-565.

Vadakkadathmeethal, K., Felczak, A., Davignon, I., Collins, J., Sunahara, R.K., 2005. Cloning and characterization of the G protein betagamma subunits from *Trichoplusia ni* (High Five cells). Insect Biochem Mol Biol 35, 333-345.

Vagenende, V., Yap, M.G., Trout, B.L., 2009. Mechanisms of protein stabilization and prevention of protein aggregation by glycerol. Biochemistry 48, 11084-11096.

Valdivia, A., Irazusta, J., Fernandez, D., Mugica, J., Ochoa, C., Casis, L., 2004. Pyroglutamyl peptidase I and prolyl endopeptidase in human semen: increased activity in necrozoospermia. Regul Pept 122, 79-84.

Vallee, B.L., Auld, D.S., 1990. Zinc coordination, function, and structure of zinc enzymes and other proteins. Biochemistry 29, 5647-5659.

Van Craenenbroeck, K., Vanhoenacker, P., Haegeman, G., 2000. Episomal vectors for gene expression in mammalian cells. Eur J Biochem 267, 5665-5678.

van den Burg, B., Eijsink, V.G., 2002. Selection of mutations for increased protein stability. Curr Opin Biotechnol 13, 333-337.

Van der Werf, P., Orlowski, M., Meister, A., 1971. Enzymatic conversion of 5-oxo-L-proline (L-pyrrolidone carboxylate) to L-glutamate coupled with cleavage of adenosine triphosphate to adenosine diphosphate, a reaction in the –glutamyl cycle. Proc Natl Acad Sci U S A 68, 2982-2985.

Vargas, M.A., Cisneros, M., Herrera, J., Joseph-Bravo, P., Charli, J.L., 1992. Regional distribution of pyroglutamyl peptidase II in rabbit brain, spinal cord, and organs. Peptides 13, 255-260.

Vasina, J.A., Baneyx, F., 1997. Expression of aggregation-prone recombinant proteins at low temperatures: a comparative study of the *Escherichia coli cspA* and *tac* promoter systems. Protein Expr Purif 9, 211-218.

Vassar, R., 2002. Beta-secretase (BACE) as a drug target for Alzheimer's disease. Adv Drug Deliv Rev 54, 1589-1602.

Vassar, R., Bennett, B.D., Babu-Khan, S., Kahn, S., Mendiaz, E.A., Denis, P., Teplow, D.B., Ross, S., Amarante, P., Loeloff, R., Luo, Y., Fisher, S., Fuller, J., Edenson, S., Lile, J., Jarosinski, M.A., Biere, A.L., Curran, E., Burgess, T., Louis, J.C., Collins, F., Treanor, J., Rogers, G., Citron, M., 1999. Beta-secretase cleavage of Alzheimer's amyloid precursor protein by the transmembrane aspartic protease BACE. Science 286, 735-741.

Vassar, R., Kovacs, D.M., Yan, R., Wong, P.C., 2009. The beta-secretase enzyme BACE in health and Alzheimer's disease: regulation, cell biology, function, and therapeutic potential. J Neurosci 29, 12787-12794.

von Bernhardi, R., Tichauer, J.E., Eugenin, J., 2010. Aging-dependent changes of microglial cells and their relevance for neurodegenerative disorders. J Neurochem 112, 1099-1114.

Vuillard, L., Marret, N., Rabilloud, T., 1995. Enhancing protein solubilization with nondetergent sulfobetaines. Electrophoresis 16, 295-297.

Walter, T.S., Meier, C., Assenberg, R., Au, K.F., Ren, J., Verma, A., Nettleship, J.E., Owens, R.J., Stuart, D.I., Grimes, J.M., 2006. Lysine methylation as a routine rescue strategy for protein crystallization. Structure 14, 1617-1622.

Wang, D., Chalk, J.B., Rose, S.E., de Zubicaray, G., Cowin, G., Galloway, G.J., Barnes, D., Spooner, D., Doddrell, D.M., Semple, J., 2002a. MR image-based measurement of rates of change in volumes of brain structures. Part II: application to a study of Alzheimer's disease and normal aging. Magn Reson Imaging 20, 41-48.

Wang, H.Y., D'Andrea, M.R., Nagele, R.G., 2002b. Cerebellar diffuse amyloid plaques are derived from dendritic Abeta42 accumulations in Purkinje cells. Neurobiol Aging 23, 213-223.

Wang, X., Connor, M., Smith, R., Maciejewski, M.W., Howden, M.E., Nicholson, G.M., Christie, M.J., King, G.F., 2000. Discovery and characterization of a family of insecticidal neurotoxins with a rare vicinal disulfide bridge. Nat Struct Biol 7, 505-513.

Warburg, O., Christian, W., 1942. Isolation and crystallization of enolase. Biochem. Z. 310, 384-421.

Waxman, E.A., Lynch, D.R., 2005. N-methyl-D-aspartate receptor subtype mediated bidirectional control of p38 mitogen-activated protein kinase. J Biol Chem 280, 29322-29333.

Weber, R.E., 1992. Use of ionic and zwitterionic (Tris/BisTris and HEPES) buffers in studies on hemoglobin function. J Appl Physiol 72, 1611-1615.

Weidemann, A., Eggert, S., Reinhard, F.B., Vogel, M., Paliga, K., Baier, G., Masters, C.L., Beyreuther, K., Evin, G., 2002. A novel epsilon-cleavage within the transmembrane domain of the Alzheimer amyloid precursor protein demonstrates homology with Notch processing. Biochemistry 41, 2825-2835.

Weller, R.O., Boche, D., Nicoll, J.A., 2009. Microvasculature changes and cerebral amyloid angiopathy in Alzheimer's disease and their potential impact on therapy. Acta Neuropathol 118, 87-102.

White, A.R., Reyes, R., Mercer, J.F., Camakaris, J., Zheng, H., Bush, A.I., Multhaup, G., Beyreuther, K., Masters, C.L., Cappai, R., 1999. Copper levels are increased in the cerebral cortex and liver of APP and APLP2 knockout mice. Brain Res 842, 439-444.

Wilcock, D.M., Gharkholonarehe, N., Van Nostrand, W.E., Davis, J., Vitek, M.P., Colton, C.A., 2009. Amyloid reduction by amyloid-beta vaccination also reduces mouse tau pathology and protects from neuron loss in two mouse models of Alzheimer's disease. J Neurosci 29, 7957-7965.

Wilk, S., 1986. Neuropeptide-specific peptidases: does brain contain a specific TRH-degrading enzyme? Life Sci 39, 1487-1492.

Wilk, S., Wilk, E.K., 1989. Pyroglutamyl peptidase II, a thyrotropin releasing hormone degrading enzyme: purification and specificity studies of the rabbit brain enzyme. Neurochem Int 15, 81-89.

Willis, M.S., Hogan, J.K., Prabhakar, P., Liu, X., Tsai, K., Wei, Y., Fox, T., 2005. Investigation of protein refolding using a fractional factorial screen: a study of reagent effects and interactions. Protein Sci 14, 1818-1826.

Willliams, T.L., Johnson, B.R., Urbanc, B., Jenkins, T.A., Connell, S.D., Serpell, L.C., 2011. Alzheimer's Ab42 oligomers but not fibrils simultaneously bind to and cause damage to ganglioside containing lipid membranes. Biochem J.

Winkler, J., Thal, L.J., Gage, F.H., Fisher, L.J., 1998. Cholinergic strategies for Alzheimer's disease. J Mol Med 76, 555-567.

Winstead, J.A., Wold, F., 1964. Studies on Rabbit Muscle Enolase. Chemical Evidence for Two Polypeptide Chains in the Active Enzyme. Biochemistry 3, 791-795.

Wirths, O., Bethge, T., Marcello, A., Harmeier, A., Jawhar, S., Lucassen, P.J., Multhaup, G., Brody, D.L., Esparza, T., Ingelsson, M., Kalimo, H., Lannfelt, L., Bayer, T.A., 2010. Pyroglutamate Abeta pathology in APP/PS1KI mice, sporadic and familial Alzheimer's disease cases. J Neural Transm 117, 85-96.

Wisniewski, T., Castano, E.M., Golabek, A., Vogel, T., Frangione, B., 1994. Acceleration of Alzheimer's fibril formation by apolipoprotein E in vitro. Am J Pathol 145, 1030-1035.

Wisniewski, T., Ghiso, J., Frangione, B., 1997. Biology of A beta amyloid in Alzheimer's disease. Neurobiol Dis 4, 313-328.

Wisniewski, T., Sadowski, M., 2008. Preventing beta-amyloid fibrillization and deposition: beta-sheet breakers and pathological chaperone inhibitors. BMC Neurosci 9 Suppl 2, S5.

Woestenenk, E.A., Hammarstrom, M., van den Berg, S., Hard, T., Berglund, H., 2004. His tag effect on solubility of human proteins produced in *Escherichia coli*: a comparison between four expression vectors. J Struct Funct Genomics 5, 217-229.

Wood, P.L., 2003. Neuroinflammation : mechanisms and management. Humana ; Abingdon : Marston, Totowa, N.J.

Wozniak, M.A., Itzhaki, R.F., Shipley, S.J., Dobson, C.B., 2007. *Herpes simplex* virus infection causes cellular beta-amyloid accumulation and secretase upregulation. Neurosci Lett 429, 95-100.

Wozniak, M.A., Mee, A.P., Itzhaki, R.F., 2009. *Herpes simplex* virus type 1 DNA is located within Alzheimer's disease amyloid plaques. J Pathol 217, 131-138.

Wu, Z., Li, M., Zhao, C., Zhou, J., Chang, Y., Li, X., Gao, P., Lu, X., Li, Y., Xu, G., 2010. Urinary metabonomics study in a rat model in response to protein-energy malnutrition by using gas chromatography-mass spectrometry and liquid chromatography-mass spectrometry. Mol Biosyst 6, 2157-2163.

Xiang, L., Ishii, T., Hosoda, K., Kamiya, A., Enomoto, M., Nameki, N., Inoue, Y., Kubota, K., Kohno, T., Wakamatsu, K., 2008. Interaction of anti-aggregation agent dimethylethylammonium propane sulfonate with acidic fibroblast growth factor. J Magn Reson 194, 147-151.

Xu, H., Gouras, G.K., Greenfield, J.P., Vincent, B., Naslund, J., Mazzarelli, L., Fried, G., Jovanovic, J.N., Seeger, M., Relkin, N.R., Liao, F., Checler, F., Buxbaum, J.D., Chait, B.T., Thinakaran, G., Sisodia, S.S., Wang, R., Greengard, P., Gandy, S., 1998. Estrogen reduces neuronal generation of Alzheimer beta-amyloid peptides. Nat Med 4, 447-451.

Yamaguchi, H., Morimatsu, M., Hirai, S., Takahashi, K., 1987. Alzheimer's neurofibrillary tangles are penetrated by astroglial processes and appear eosinophilic in their final stages. Acta Neuropathol 72, 214-217.

Yan, R., Munzner, J.B., Shuck, M.E., Bienkowski, M.J., 2001. BACE2 functions as an alternative alpha-secretase in cells. J Biol Chem 276, 34019-34027.

Yang, L.B., Lindholm, K., Yan, R., Citron, M., Xia, W., Yang, X.L., Beach, T., Sue, L., Wong, P., Price, D., Li, R., Shen, Y., 2003. Elevated beta-secretase expression and enzymatic activity detected in sporadic Alzheimer disease. Nat Med 9, 3-4.

Yao, Z.X., Papadopoulos, V., 2002. Function of beta-amyloid in cholesterol transport: a lead to neurotoxicity. Faseb J 16, 1677-1679.

Yasojima, K., McGeer, E.G., McGeer, P.L., 2001. Relationship between beta amyloid peptide generating molecules and neprilysin in Alzheimer disease and normal brain. Brain Res 919, 115-121.

Yazawa, H., Yu, Z.X., Takeda, Le, Y., Gong, W., Ferrans, V.J., Oppenheim, J.J., Li, C.C., Wang, J.M., 2001. Beta amyloid peptide (Abeta42) is internalized via the G-protein-coupled receptor FPRL1 and forms fibrillar aggregates in macrophages. Faseb J 15, 2454-2462.

Yoshimoto, T., Shimoda, T., Kitazono, A., Kabashima, T., Ito, K., Tsuru, D., 1993. Pyroglutamyl peptidase gene from *Bacillus amyloliquefaciens*: cloning, sequencing, expression, and crystallization of the expressed enzyme. J Biochem 113, 67-73.

Yu, L., Aa, J., Xu, J., Sun, M., Qian, S., Cheng, L., Yang, S., Shi, R., 2011. Metabolomic phenotype of gastric cancer and precancerous stages based on gas chromatography time-of-flight mass spectrometry. J Gastroenterol Hepatol 26, 1290-1297.

Yun, E.Y., Goo, T.W., Kim, S.W., Choi, K.H., Hwang, J.S., Kang, S.W., Kwon, O.Y., 2005. Galatosylation and sialylation of mammalian glycoproteins produced by baculovirus-madiated gene expression in insect cells. Biotechnol Lett 27, 1035-1039.

Zhang, R.M., Snyder, G.H., 1989. Dependence of formation of small disulfide loops in two-cysteine peptides on the number and types of intervening amino acids. J Biol Chem 264, 18472-18479.

Zhao, G., Mao, G., Tan, J., Dong, Y., Cui, M.Z., Kim, S.H., Xu, X., 2004. Identification of a new presenilin-dependent zeta-cleavage site within the transmembrane domain of amyloid precursor protein. J Biol Chem 279, 50647-50650.

Zhao, G., Tan, J., Mao, G., Cui, M.Z., Xu, X., 2007. The same gamma-secretase accounts for the multiple intramembrane cleavages of APP. J Neurochem 100, 1234-1246.

Zhao, M., Su, J., Head, E., Cotman, C.W., 2003. Accumulation of caspase cleaved amyloid precursor protein represents an early neurodegenerative event in aging and in Alzheimer's disease. Neurobiol Dis 14, 391-403.